International
Progress Report

IPR-02-45

Äspö Hard Rock Laboratory

Impact of the tunnel construction on the groundwater system at Äspö

Task 5. Äspö Task Force on groundwater flow and transport of solutes

Urban Svensson
Computer-aided Fluid Engineering AB

Marcus Laaksoharju
GeoPoint AB

Ioana Gurban
DE&S

January 2002

Svensk Kärnbränslehantering AB
Swedish Nuclear Fuel
and Waste Management Co
Box 5864
SE-102 40 Stockholm Sweden
Tel +46 8 459 84 00
Fax +46 8 661 57 19

Äspö Hard Rock
Laboratory

Report no.	No.
IPR-02-45	F65K
Author	Date
Svensson, Laaksoharju, Gurban	02-01-10
Checked by	Date
Peter Wikberg	02-01-20
Approved	Date
Christer Svemar	02-11-19

Äspö Hard Rock Laboratory

Impact of the tunnel construction on the groundwater system at Äspö

Task 5. Äspö Task Force on groundwater flow and transport of solutes

Urban Svensson
Computer-aided Fluid Engineering AB

Marcus Laaksoharju
GeoPoint AB

Ioana Gurban
DE&S

January 2002

Keywords: Groundwater flow, solute transport, coupled hydrogeochemistry, chemistry, mixing, Äspö, Task 5

FOREWORD

This report summarises the work by the SKB modelling group, performed within Task #5. For a general background and objectives of the project, see Wikberg (1998). The report is made up of four parts with the following titles and authors:

Part I. Impact of the tunnel construction on the groundwater system at Äspö – Executive summary. U. Svensson and M. Laaksoharju.

Part II. M3 predictions of the groundwater chemical changes associated with the construction of the Äspö HRL. M. Laaksoharju, and I. Gurban.

Part III. The origin and composition of groundwater leaking into the Äspö tunnel. U. Svensson.

Part IV. Modelling Questionnaire for Task #5. U. Svensson and M. Laaksoharju.

ABSTRACT

Characterisation of a site for nuclear waste disposal normally involves development of hydrodynamical and hydrochemical numerical models. These models, and the basic data sets, are however in most cases developed independently, and may even be inconsistent. This report describes an attempt to integrate hydrological and hydrochemical information and modelling concepts.

The key element in this integration is the obtained chemistry calculated as mixing portions of water types by using a new modelling technique. This concept can be used in both hydrochemical and hydrogeological modelling of a site. The groundwater at Äspö is modelled to consist of a complex mixture of the water types: Meteoric (precipitation water), Baltic (seawater), Glacial (meltwater from the last glaciation) and Äspö Brine (old highly saline groundwater). The hydrochemical analysis, and model, gives the spatial and temporal distributions of these four water types. In the hydrodynamical model it is also possible to calculate the distribution of water types, for example by solving a number of advection/diffusion equations, provided that initial and boundary conditions are available (these are derived from field data by the hydrochemical analysis). The results from the hydrodynamical model, in particular path lines and flow velocities, can in turn be used in the hydrochemical analysis, as the transport aspect is normally missing in these models. From this brief description it is clear that an integrated view, based on both hydrogeological and hydrochemical information from a specific site, can and ought to be established.

The project was carried out along the lines indicated above and a number of comparisons and integrated evaluations were carried out. In this process both the hydrochemical and hydrodynamical models were “exposed in a new light”, stimulating new developments and improvements. An improved understanding of the studied site was also obtained in this process.

The general conclusion of the study is that the integrated view and evaluation, based on both hydrochemical and hydrogeological information, is of great value in a site investigation. The hydrodynamical models are constrained by new data sets and information and the hydrochemical models can benefit from the information concerning path lines and transport velocity.

ABSTRACT (Swedish)

Hydrodynamiska och hydrokemiska numeriska modeller utgör väsentliga redskap vid platsundersökningar för kärnbränsleförvar. Modellerna, och grundläggande fältdata, utvecklas dock ofta oberoende av varandra och är ibland direkt motstridiga. I denna rapport beskrivs ett försök att förbättra situationen genom att integrera båda typerna av modeller, koncept och databaser.

Det viktigaste elementet i denna integration är transformeringen av uppmätt grundvattenkemi till beräknade blandningsproportioner av olika vattentyper. Denna transformering görs med hjälp av ny modelleringsteknik och resultaten kan användas både i hydrokemiska och hydrogeologiska platsspecifika modelleringar. Grundvattnen i Äspö har modellerats som bestående av en komplex blandning av följande vattentyper: Meteoriskt (från nederbörd), Baltiskt (från Östersjön), Glacialt (från senaste istiden) och Äspö Brine (gammalt, mycket salt grundvatten). Den hydrokemiska modellen och analysen ger den rumsliga och tidsmässiga fördelningen av dessa fyra vattentyper. En hydrodynamisk modell kan också beräkna fördelningen av vattentyper, t.ex. genom att lösa en serie advektions/diffusions ekvationer. Resultaten från den hydrodynamiska modellen, speciellt strömlinjer och flödeshastigheter kan också direkt användas i den hydrokemiska modellen, eftersom transportmekanismer ofta behandlas alltför enkelt, eller negligeras, i dessa modeller. Från denna översiktliga beskrivning står det klart att en integrerad platsanalys kan och bör ge ett mer komplett beslutsunderlag.

Projektet genomfördes i stort enligt de ovan beskrivna riktlinjerna; ett antal jämförelser och samordnade analyser gav nya krav och aspekter på båda typerna av modeller. En fördjupad förståelse av processerna i undersökningsområdet erhölls även.

Den generella slutsatsen från studien är att platsundersökningar, och olika numeriska modeller, kan bli mer tillförlitliga om ett integrerat synsätt på hydrokemi och hydrogeologi tillämpas. Hydrodynamiska modeller kan testas/verifieras mot hydrokemiska data och hydrokemiska modeller kan göras mer realistiska med avseende på transportmekanismer.

TABLE OF CONTENTS

Part I

IMPACT OF THE TUNNEL CONSTRUCTION ON THE GROUNDWATER SYSTEM AT ÄSPÖ

- EXECUTIVE SUMMARY

Urban Svensson* and Marcus Laaksoharju**

*Computer-aided Fluid Engineering AB and**GeoPoint AB

1 INTRODUCTION

Characterisation of a site for nuclear fuel waste disposal typically involves taking thousands of measurements and developing site-specific models in each of several scientific disciplines, such as hydrogeology and hydrochemistry. Numerical hydrodynamic models utilise these field measurements in the development of new concepts and in the calibration of the models. However, hydrochemical models do not normally consider the geohydrological data and the geohydrologist is often not familiar with the hydrochemical data sets. These models are usually independent of each other, and are sometimes even inconsistent. Combining such models into a defensible, self-consistent understanding of the site characteristics has been problematic, and presenting this understanding in a clear and concise manner to stakeholders has proven to be difficult. This has motivated SKB to initiate a modelling task with the following general objective: "Develop a procedure for integration of hydrological and hydrochemical information and modelling concepts". The background and detailed information for this modelling task, called Task #5, is given in Wikberg (1998).

If such an integration can be accomplished successfully, it is anticipated that the following benefits will result.

- Geohydrological models will be constrained by a new data set. If, as an example, the model can not produce any Meteoric water at a certain depth and the hydrochemical data indicates that there is a certain fraction of this water type at this depth, then we have to revise the model.

- Hydrochemical models generally focus on the effects from reactions on the obtained groundwater, rather than the effects from transport. An integrated modelling approach can describe flow directions and hence help to understand the origin of the groundwater, the turn over time of the groundwater system can indicate the age of the groundwater, and knowing the flow rate can be used to indicate the reaction rate. The obtained groundwater chemistry is a result of reactions and transport, therefore only an integrated description can be used to correctly describe the measurements.

The main obstacle for such an integration is perhaps "cultural", meaning that chemists and hydrologists do not have a common language. This problem was realised when the task was initiated and a solution was provided; the obtained hydrochemistry was calculated with the computer code M3 (Multivariate Mixing and Mass balance model (Laaksoharju et al., 1999; and Part II in this report) and presented as mixing portions of four water types: Meteoric (precipitation water), Baltic (sea water), Glacial (meltwater from the last glaciation) and Äspö Brine (old highly saline groundwater) rather than using chemical constituents. The concept of mixing portions can be said to be the main integration tool, as it resolves the "cultural" problem mentioned above.

The main objective of the study is, as mentioned, to develop a procedure for the integration of hydrological and hydrochemical information and modelling concepts. More refined objectives will be defined in the parts of this report dealing with the hydrochemistry and the hydrogeology of the site. In this executive summary the basic methods will be outlined, some sample results shown and, in particular, the results of the study will be discussed and summarized.

The site in question is the Äspö Hard Rock Laboratory (HRL) on the east coast of Sweden, described in detail in Rhén et al. (1997). Extensive data sets, both hydrochemical and hydrogeological, are available, covering both the time prior to, during and after the construction of the laboratory.

In Task #5, it is the evolution of the groundwater composition during the construction phase of the Äspö HRL that is in focus.

2 METHOD

Hydrochemistry

M3 is an interpretative technique that performs a cluster analysis (using multivariate principal component analysis) to identify waters of different origins, infer the mixing ratio of these end-members to reproduce each sample's chemistry, identify any deviations between the chemical measurements of each sample and the theoretical chemistry from the mixing calculation, interpret these deviations as resulting from interactions with the solid minerals, and interpret the spatial distribution of these reactions (mass-balance reactions). As mixing of different groundwater types from various identified sources (i.e. end-members) can also be handled by hydrodynamic models, this provides an excellent opportunity to mathematically interface hydrochemistry with hydrogeology. The key element in the integration scheme is the definition of mixing portions of the four water types. It is thus of crucial importance that this is a realistic and adequate starting point.

When modelling with M3, the risk of conceptual errors occurs when making assumptions such as "groundwater composition is a good tracer for the flow system" (which is generally the case). The water composition may not necessarily be a unique tracer without a point source, such as labelled water in a tracer test. The accuracy is therefore much lower in M3 modelling than in a tracer test. On the other hand the site scale changes are better traced in groundwater samples than by using fracture specific tracer tests. Another assumption in M3 is that all the reference waters are mixed. This is necessary in order to construct an ideal mixing model and to be able to compare all the samples collected at a site. In reality there are physical hindrances such as depth or geological structures, which may prevent mixing from occurring, and therefore not every end-member necessarily contributes to every water sample taken. Generally, three reference waters dominate in the M3 calculations and the other ones are close to or below the detection limit for the method (a mixing portion of <10%). Uncertainty can occur from selecting the wrong number and type of end-members. Other uncertainties in M3 can be due to sampling errors, analytical errors, conceptual errors and methodological errors. These difficulties are handled in M3 by stating the uncertainty in the method as ±0.1 mixing units and the detection limit for the method as <10% of a mixing portion.

M3 calculations, together with visualisation of major groundwater changes, were used as background information for the groundwater modelling performed within Task #5. The modelling was used, for example, to constrain boundary conditions and to check the consistency between models. An example is the consistency check between the SKB hydrodynamic modelling and the chemical modelling with M3. The consistency check was done by comparing cutting planes corresponding to the main fracture zones produced by the two individual models. The salinity distribution obtained by the two approaches was compared for the following fracture zones: NE1, NE2, NE3, NNW1, NNW2, NNW3, NNW4, NNW5, NNW6, NNW7, NNW8, EW1N, EW1S, EW3, EW7, EN4N, EN4S, NW1 and SFZ11 (for details see Part II of this report). The Cl content and the mixing portion calculations along the Äspö HRL tunnel seemed to agree fairly well.

Hydrogeology

In the geohydrological model, the four water types will be tracked during the construction phase of the tunnel. This calls for initial and boundary conditions. The approach adopted can be summarised as follows:

- t ground level, it was assumed that 100% Meteoric water is found on land and 100% Baltic water below the Baltic Sea.
- At vertical and bottom boundaries the water composition was estimated from field data. In the calibration process, these compositions were fine-tuned. Transient boundary conditions for pressure and salinity were obtained from a regional model.
- Initial water composition in the domain was calculated, as a steady state distribution. The calculated distribution was compared with field data.

An advection/diffusion equation for each water type is solved, subject to the initial and boundary conditions outlined above. Also the Darcian flow equations and the mass and salinity equations were solved at each time step, providing the flow field for the advection/diffusion equations. A novel feature of the flow model, which is of the continuum type, is that the conductivity and porosity fields were determined from a fracture network. Another novel feature of the flow model concerns the unsaturated zone. The method developed allows for a realistic fixed flux at the upper boundary. For natural conditions most of this flux finds its way to the sea, while a large fraction contributes to the tunnel inflow, when present.

The calculated distributions were evaluated against the hydrochemical data by point-by-point comparisons for initial conditions, tunnel front at 3170 metres and completed tunnel (time 1996-05). In the calibration of the model, the water compositions at the vertical and bottom boundaries were fine-tuned. A fair agreement with measured data (trends, averages and point to point comparisons) was achieved.

Project strategy

Before Task #5 started a flow chart describing the interaction between the chemistry and hydrology models was presented, see Figure 1. As can be seen, it was suggested that the exercise should be performed in two steps, with a consistency check as the final event in both steps. The main check was the chemical composition, or mixing ratios, in control points (CP), but also the general characteristics of the flow, pressure, salinity, water type, etc. distributions should be evaluated.

The actual work followed the flow chart, with only minor modifications, the first step model is in Part III called Model99. The flow chart given in Figure 2 shows how the two model developments actually interacted. As can be seen the flow model was established without direct reference to chemical compositions (salinity data were however used). When the distributions of various water types were calculated, boundary conditions were formulated from measured compositions. It should be emphasised that the initial distributions were calculated from these boundary conditions, assuming steady state conditions; the interpolated mixing proportions were only used for a comparison (visual) between the two models. In the calibration phase as many points as possible, within the domain, were used but, once again, only data from borehole

sections were used. The calibrated model was then used for predictions of the water compositions in tunnel section 2 900 – 3 600 metres and also for an analysis of the origin of the water entering the tunnel, using a backtracking technique.

The two steps in the model development, both followed the flow chart in Figure 2. The first consistency check resulted in the following conclusion:

– Model99 is in fair agreement with field data, still the model needs to be improved conceptually with respect to conductivity, porosity and connectivity fields.

This conclusion stemmed from a discussion about "storage of water for long time periods in a continuum model", as the chemical data indicated that Glacial water had been stored for 12 000 years, or more, at a depth of a few hundred metres below Äspö. A major development, concerned with the generation of the above mentioned fields, was undertaken, see Part III for details.

The final model can not be claimed to be in better agreement with field data, but it is sounder conceptually and more carefully calibrated. It has the potential to store water for very long time periods.

An important part of the project strategy is the prediction of water composition in control points ahead of tunnel front 2 900 metres. Measured data for these points were not available to the modelling teams until after the predictions had been delivered.

A careful evaluation of the achievements of Task #5 is of course also a part of the project strategy. The discussion and conclusion sections of this executive summary (see also Part II and III) provide some input to such an evaluation, but the main evaluation is performed by an external review of the project.

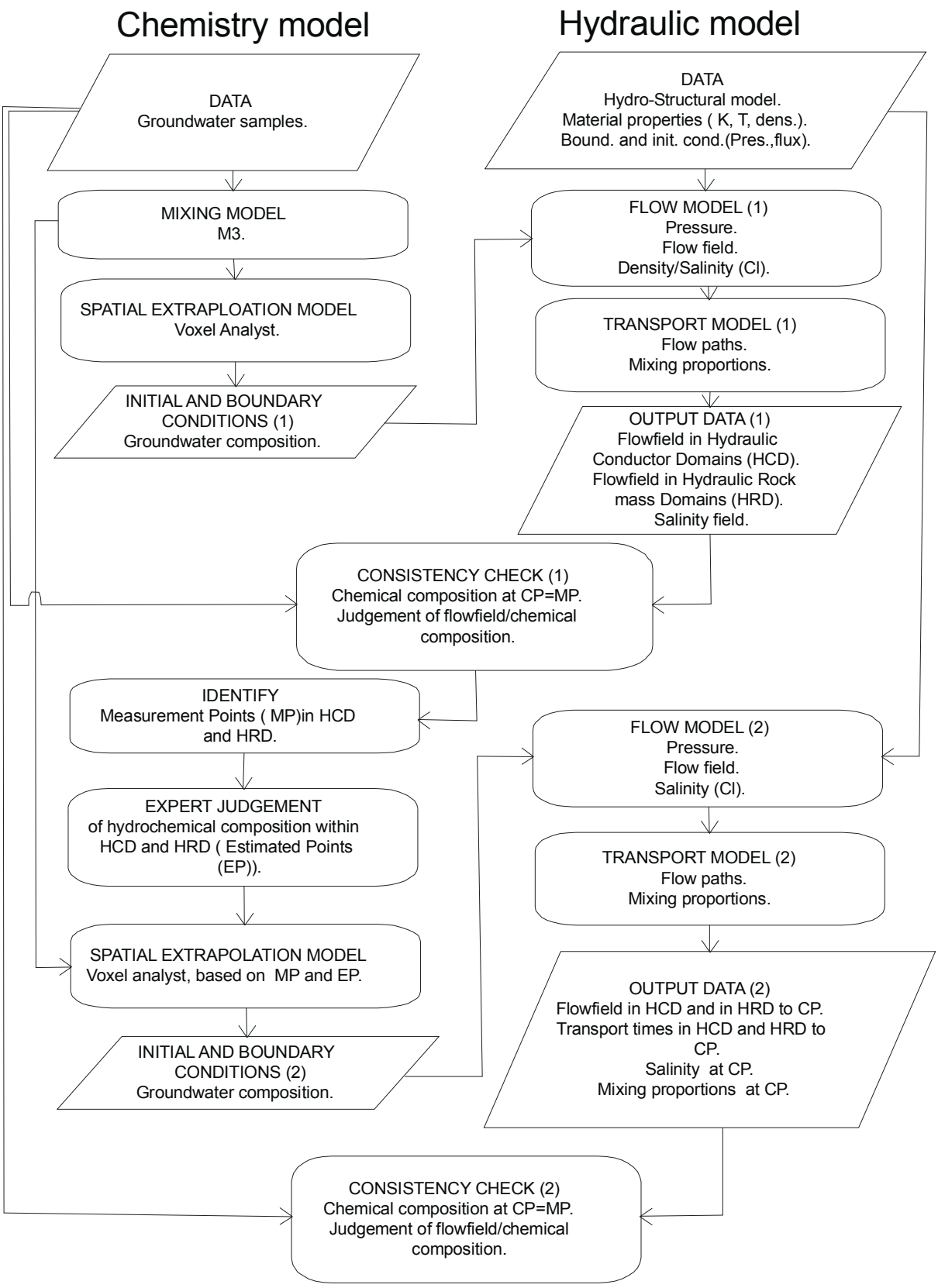

Figure 1. *Suggested flow chart, and work plan, for the model integration in* Task #5 *(CP=control point).*

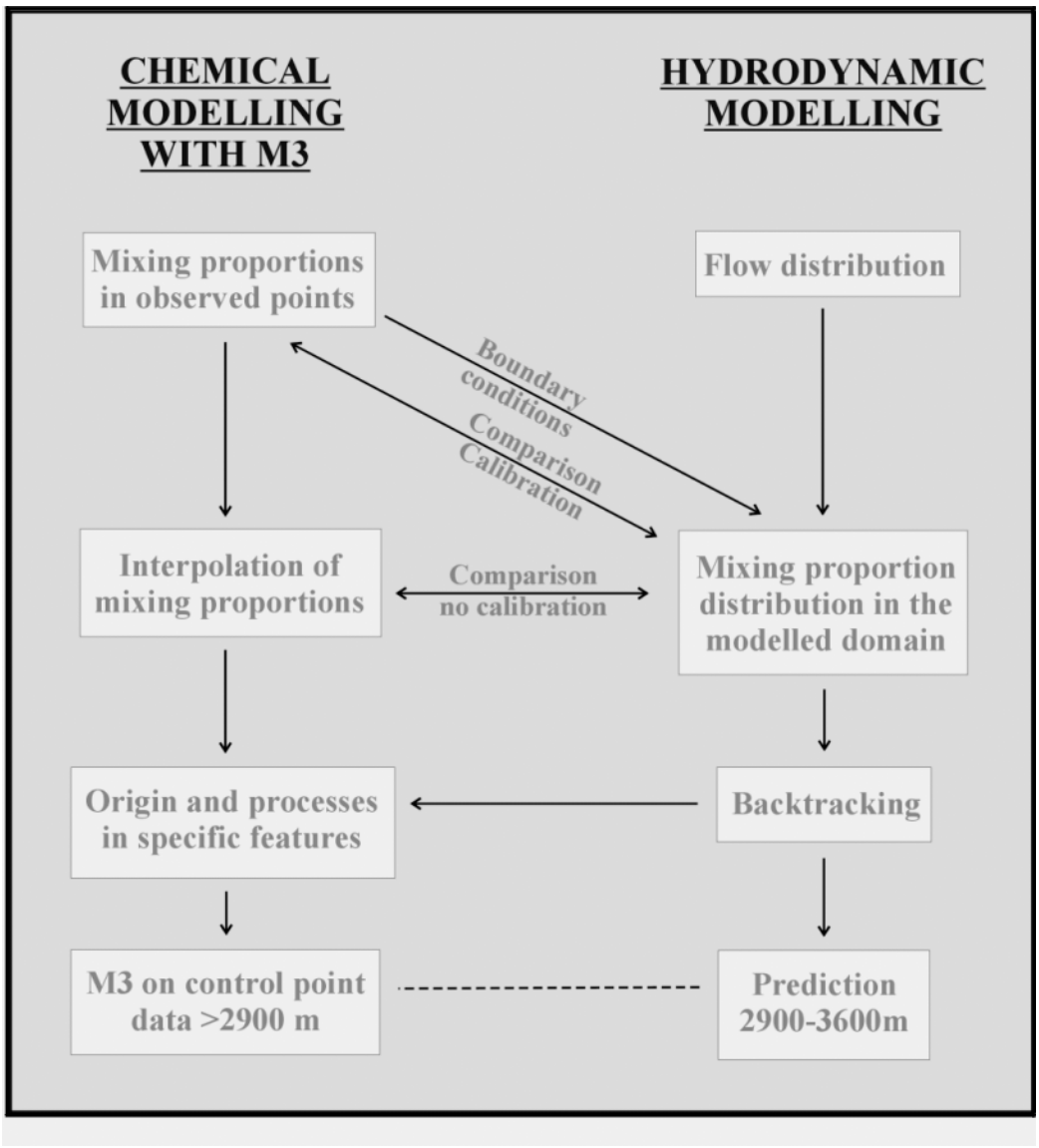

Figure 2. *Illustration of the integration between the M3 model and the SKB hydrodynamic model. The same integration scheme was used for both steps in the development.*

3 MAIN RESULTS

In the specification of requested results from the modelling exercises, comparisons of water mixing fractions (measured and calculated) in a number of control points are in focus. Also the flow paths to these control points were requested, in order to get a deeper understanding of the origin of water leaking into the tunnel. The presentation of these results is given in Part II and III of this report; here only some highlights are given.

In Figure 3, the evolution of the water composition in control point SA2074 (which is close to tunnel coordinate 2074 metres) is given. It is seen that the numerical model predicts a decrease of the Glacial component, with time. This is a typical trend found also in the M3 mixing calculations based on the field measurements (Gurban et al., 1998 and Figure 4-13 in Part II). From the hydrological model it was also estimated how much of the water found in a control point, that originates from outside the domain, i.e. is supplied from the boundary conditions. In Figure 3, the fraction coming from the boundaries is also given.

Next some results that illustrate the transient response, due to the excavation of the tunnel, will be discussed. The change in the water composition as predicted by the hydrological model is shown in Figures 4 and 5. The initial conditions (Figure 4) were calculated as a steady state situation, with boundary conditions estimated from field data. When the tunnel has been excavated to a length of 3170 metres (Figure 5) it is found that a much more irregular distribution is predicted. Note also the upconing of Äspö Brine below the tunnel. A more detailed study of the upconing process is presented in Figure 6. It was found that the numerical model predicts an increase in salinity, in fair agreement with the measured increase. As this simulation requires that a correct transport velocity is calculated, it demonstrates an important feature of the model.

One part of the consistency test and the integration between the chemical and hydrodynamic modelling was the particle tracking. As an example of this work the result from the SKB particle tracking model is combined with the result from the M3 mixing and mass balance calculations to analyse the flow paths to the control points SA2074 and SA2783, see Figure 7. The result indicates that the mixing calculations can be used to compare and integrate the results from the particle tracking, since both are independent modelling tools describing the possible origin and flow paths of the groundwater; The particle tracking indicates the flow paths while the M3 modelling indicates the mixing situation and the reactions taking place along the flow paths.

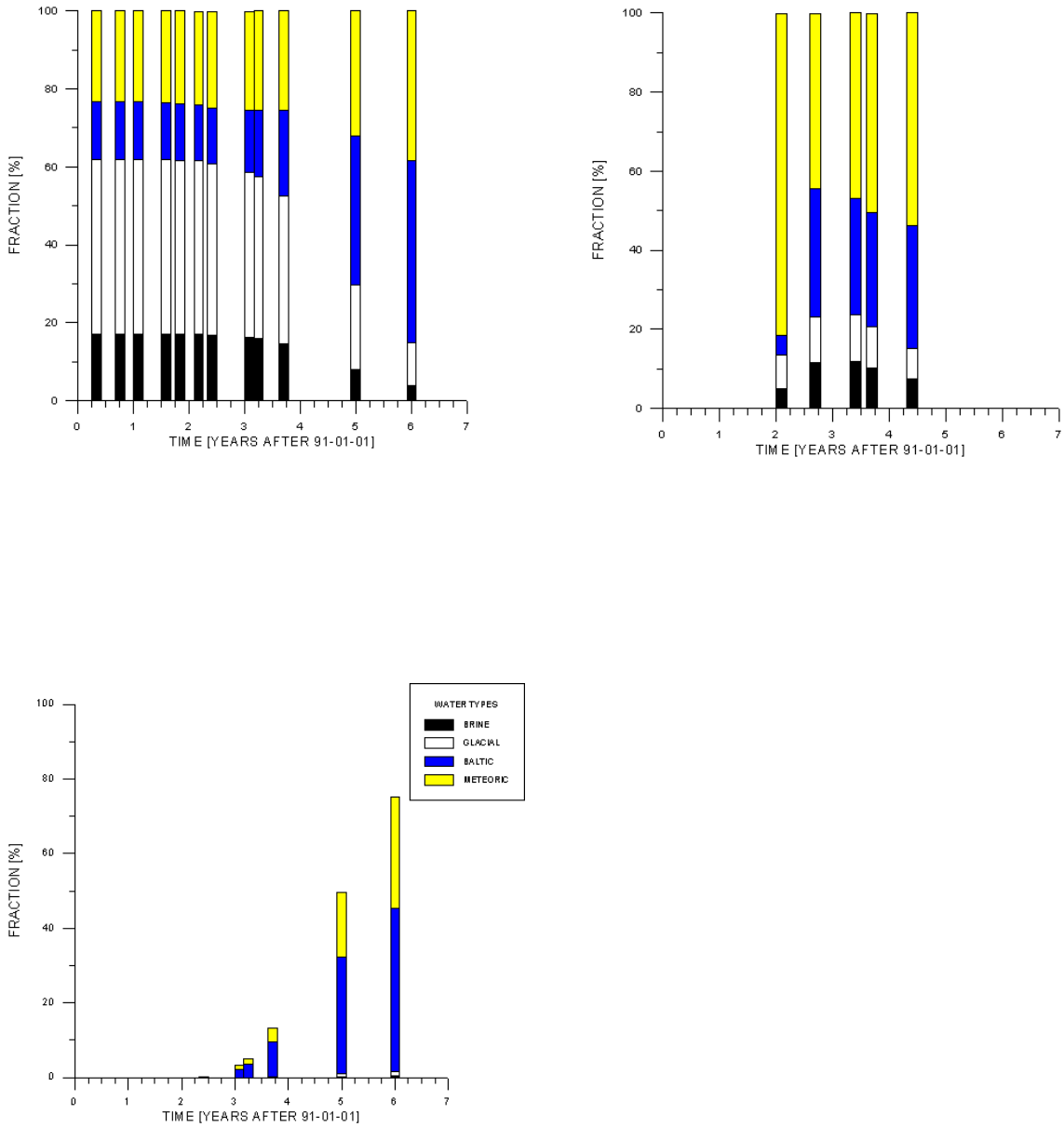

Figure 3. *Water composition in control point SA2074 as a function of time. Measured (top right) and simulated (top left) composition and fraction coming from the domain boundaries. Time for tunnel passing the point: 2.09.*

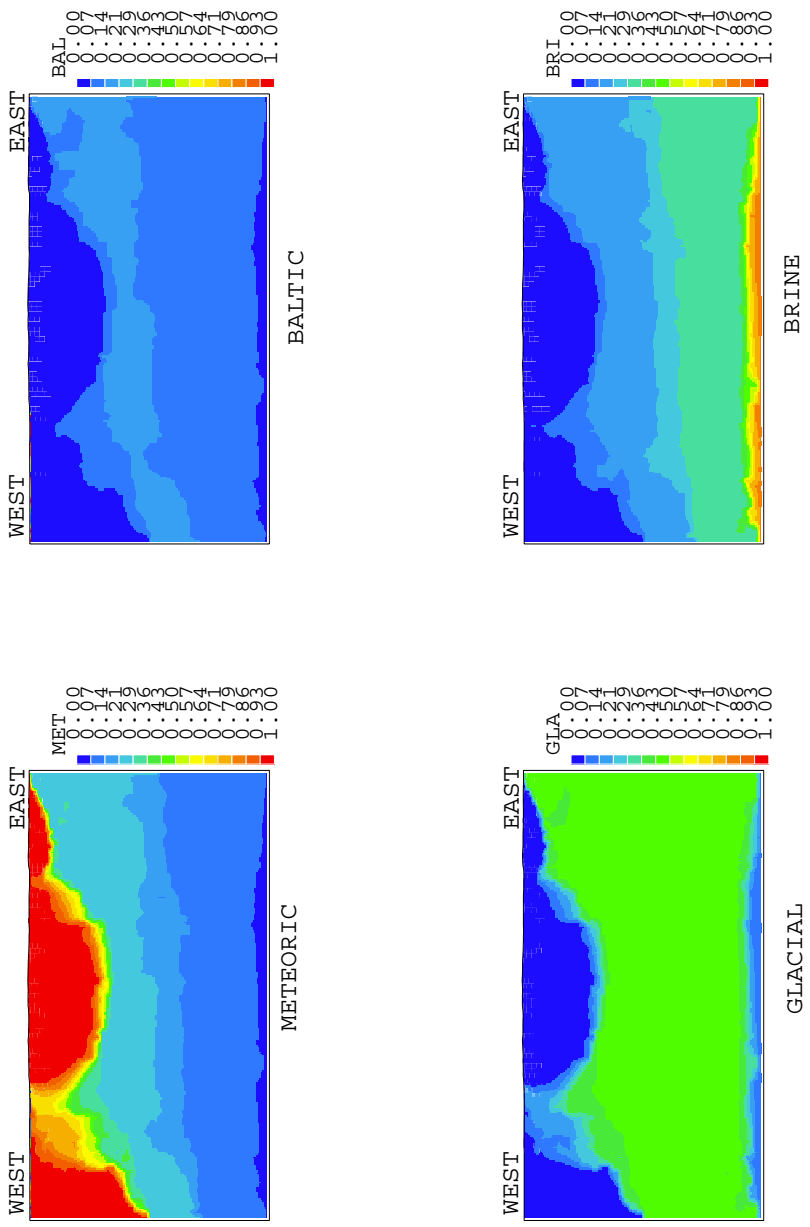

Figure 4. *Vertical sections through the centre of the spiral part of the tunnel, showing the simulated initial distributions of various water types.*

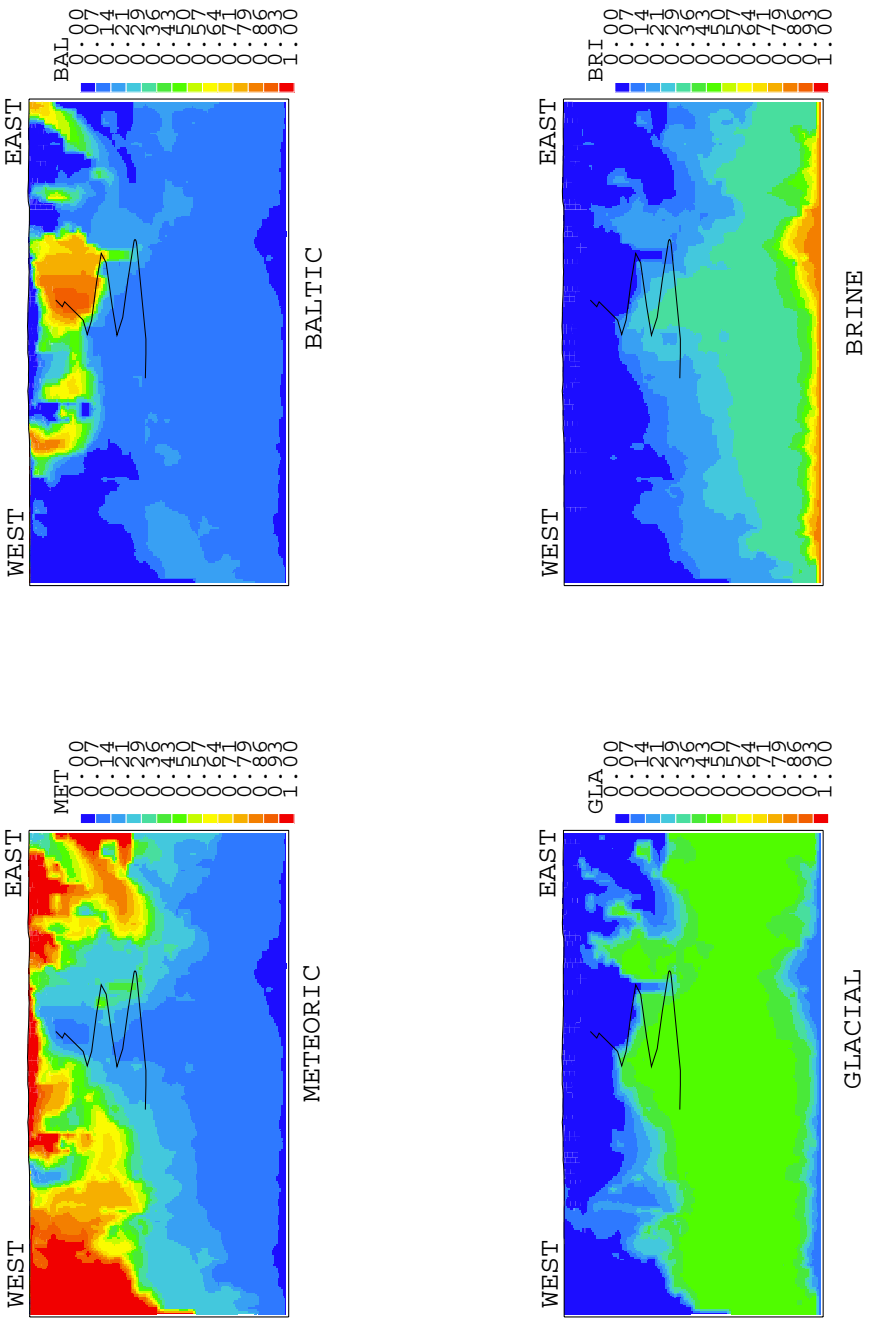

Figure 5. *Vertical sections through the centre of the spiral part of the tunnel, showing the simulated distributions of various water types. Tunnel front position: 3 170 metres.*

These examples illustrate quite well the type of comparisons and analysis that have been at the heart of Task #5. Apart from direct integration of results, the individual models have also been developed during the project. For the hydrological model the main development concerns the specification of the conductivity and porosity fields. The new algorithm for the unsaturated zone is also considered to be essential, both for the present project and for future modelling tasks. The hydrochemical modelling part of the project showed an additional need for explanations of the M3 model, the modelling, the uncertainty and the assumptions used in the modelling.

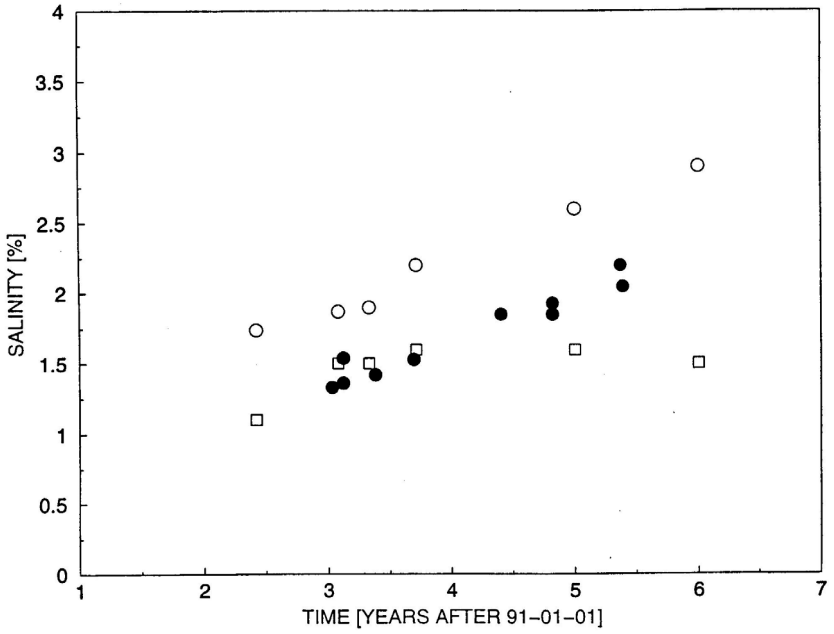

Figure 6. *The upconing process. Salinity as a function of time at a depth of 370 metres.*

- *Field data (SA2783 and SA2880)*

○ *Simulated maximum salinity at a depth of 370 metres.*

□ *Simulated salinity at tunnel coordinate 2 800 metres.*

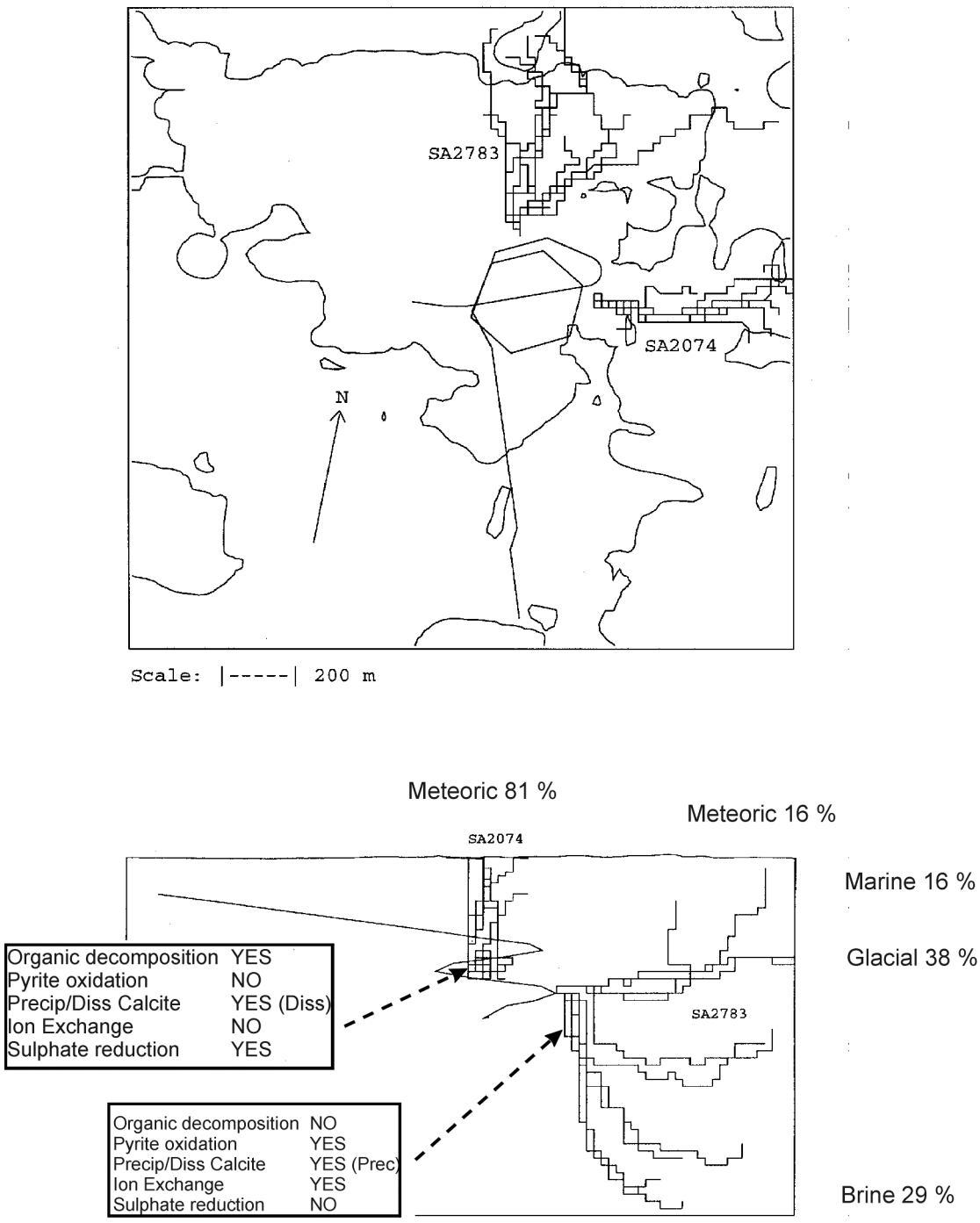

Figure 7. *The result from the Particle Tracking model shown as flow-lines is combined with the M3 mixing (see percentage values for each reference water) and mass balance calculations. The results from the mass balance calculations (boxed in) are used to indicate major reactions that may modify the groundwater composition at the control points SA2074 and SA2783.*

4 DISCUSSION

Lessons learned

Since this is a pilot exercise, –to integrate hydrochemical and geohydrological information, one should not expect that the present study can provide the final solutions to the problems encountered in such an integration. If we instead consider the study as a step towards a useful approach or method, it is relevant to discuss what lessons have been learned. If this view is adopted the following topics are relevant:

- **Glacial water.** Field data indicates that Glacial water may dominate the water composition at a depth of a few hundred metres below Äspö. The fact that this water has been stored in the rock for 12 000 years (or more), brings up questions about flow paths, connectivity and storage volumes. As the present generation of continuum models will have problems with long time storage of a certain water type, one can conclude that the study points to a need for further development of ways to generate realistic conductivity and porosity fields.

- **Four water types.** From the hydrogeological point of view, the presentation of the hydrochemistry as a mixture of four water types is convenient (rather than dealing with chemical constituents).

- **Chemistry and transport**. From the hydrochemical point of view the evolution of the groundwater composition is strongly related to the present and past flow conditions. The results from the hydrodynamic models give the flow direction and turnover time of the groundwater, which can be used as an independent or integrated part in the hydrochemical modelling/evaluation.

- **Method for comparison**. In the present study the focus has been on point-by-point comparisons of measured and simulated water compositions. The hydrological model does however predict fields with high spatial variability. If this is correct, point-by-point comparisons are uncertain, which is also demonstrated in a sensitivity study, and other ways for comparisons may need to be considered (trends, averages, overall site description, etc).

- **Boundary conditions.** Predicting the evolution of the groundwater chemistry requires boundary conditions. The hydrological model, with its present kinematic porosity field, predicts that water from outside the domain will reach the tunnel during the construction period. If this is correct, it is improved knowledge about the water composition outside the computational domain that can reduce one of the main uncertainties in the simulations.

- **Groundwater sampling.** The Task #5 exercise showed that groundwater chemistry is an effective tracer for the present and paleo hydrodynamical changes. The groundwater sampling campaign has therefore to be planned to reflect these changes. There is a need for more samples taken in time series and simultaneous collection of data from several, or all sampling locations. Few but well planned site scale sampling campaigns with simultaneous sampling from several or all boreholes can be used to produce dynamic “snap shots” of the hydrochemical/hydrodynamic changes. Task #5 data often lacked long time series and simultaneously collected samples, which made the modelling and interpolation difficult.

Implications for groundwater modelling

It is not to be expected that all groundwater modelling projects can utilise the integration strategy used in Task #5. It is therefore of interest to discuss how less ambitious schemes may serve both hydrological and chemical model developments and applications. The following is suggested:

Hydrological models. Consider the Äspö HRL and how the set-up/calibration/application of a hydrological model can be improved/constrained by chemical data sets. Depending on the circumstances one may choose one of the following (in order of complexity) strategies.

1) **Utilise the salinity data only.** As the water below Äspö is density stratified it is probably necessary to include the salinity balance in most model studies. It is however possible to make more extensive use of these data sets, than is normally done. Some suggestions:

- Study the time history of the upconing. Can be used for a calibration of kinematic porosity as the travel time is proportional to this parameter.

- For natural conditions the fresh water lens below Äspö has a thickness of about 150 metres in the central part of Äspö. The transition to saltier water below this depth is gradual. Why is it gradual? For steady state conditions the hydrodynamical model predicts a fairly sharp interface. Is the gradual transition due to seasonal and yearly fluctuations in the groundwater table, pushing the fresh water lens up and down?

- Simulate, and compare with measurements, the time history of the salinity of all inflows to the tunnel. The variation in time is an indication from where the water originates.

2) **Hydrochemical observations.** Use the chemical data sets to establish a number of hydrochemical signatures, or "hard facts", that can be used to constrain the hydrological model; some examples include:

- For natural conditions, find the maximum penetration depth of Meteoric water. The hard fact could be formulated as "during the last hundred years no precipitation on Äspö has penetrated deeper than 300 metres". Flow paths, originating from ground level on Äspö, calculated by the hydrological model, should then be checked against this "signature from the chemistry".

- During the construction of the tunnel, Äspö Brine water may reach the tunnel level. Is it possible to establish where and when this old water type first enters the tunnel? If so, we have another useful signature from chemistry to test our model against.

- For present day conditions, i.e. with completed tunnel, it is of interest to determine the fraction of the total inflow to the tunnel that comes from recent precipitation. Is the precipitation on Äspö large enough to support this, or can we conclude that there must be another source (for example the Laxemar area)? If so, the hydrological model must be able to show flow paths from this additional source.

- The presence of Glacial water is another signature from the chemistry that can be used to test the porosity and connectivity structure of a model. Can a certain water type be stored for 12 000 years?

These examples of "hard facts from chemistry" should be seen as possible, and not as existing, facts. Some work is of course needed to establish a reliable and documented set of hydrochemical signatures that can be used as hard facts.

3) **Task #5 type approach.** This is the most complete, and also most expensive, approach. In this approach the spatial distributions of hydrochemical fields, including boundary conditions, form the basis for the comparisons.

Hydrochemical models. In the future the hydrochemical modelling should be performed in close collaboration with the hydrogeological modelling at an early stage of the site investigation programme. The construction of a feasible conceptual model (present and paleo flow model) for the site is needed in both types of modelling and with input from both hydrogeology and hydrochemistry. A predictive modelling of a new site should be performed and gradually updated when new data are available. Such exercises will reveal areas where more data and more accurate modelling should be implemented. The results from the hydrochemical models should be developed further and be presented more like the results from the hydrogeological modelling (e.g. flow lines based on hydrochemical modelling) in order to ease the comparison. The calculations of the uncertainties of the used models can be improved.

5 CONCLUSIONS

Findings from the modelling exercise

The objective of Task #5 is to develop a procedure for integration of hydrochemical and hydrogeological information and modelling concepts. As a general conclusion, this has been achieved technically, meaning that all requested results have been produced and a fair agreement between measurements and simulations have been demonstrated. Some more specific conclusions are:

- The Task #5 exercise has shown that the often difficult task of integrating chemistry in the hydrodynamic models can be overcome by the concept of mixing portions. The new concept is that the obtained chemical composition is used to construct an ideal mixing model of the site. The mixing portions divide the obtained groundwater composition in portions of origin from selected reference waters or end-members. The mixing portions can be used to compare/integrate/support the results from hydrodynamic models.

- A flow model can be used to calculate the effects from reactions by using the mixing portions to calculate the contribution from the reference waters and compare these with the measured groundwater constituents. A deviation indicates a gain/loss which can be due to reactions.

- The M3 code can be used to construct a mixing model for a site and to trace the major reactions altering the groundwater composition. The M3 modelling is independent from hydrogeological data and models but the mixing portions can be used to compare and integrate the models.

- Having repeated sampling with a time series the relative hydrodynamic changes can be described by means of mixing portions and short-term predictions of the future groundwater changes can be performed.

- The hydrological model predicts an evolution of the water composition during the construction phase of the tunnel that is in fair agreement with mixing portion calculations based on field data, in terms of averages and trends.

- During the Task #5 exercise some shortcomings, concerning the porosity field, in the hydrological model were detected. Generally, the hydrochemical data set provides a new test bench for the hydrological model.

- The uncertainties in M3 mixing calculations can be due to sampling errors, analytical errors, conceptual errors and methodological errors. These difficulties are handled in M3 by stating the uncertainty in the method as ±0.1 mixing units and the detection limit for the method as <10% of a mixing portion. The need for uncertainty ranges in M3 calculations was brought in focus during the TASK#5 exercise.

Site understanding

The modelling results presented do give a certain description and understanding of the evaluation of the groundwater composition during the construction of the Äspö HRL. The main features of this description are:

- The atmospheric pressure in the tunnel generates high pressure gradients close to the tunnel with an inflow of water as a result (see Figure 4-5, 4-6 in Part II). The low pressure around the tunnel is reflected at ground level, see Figure 6-1 (Part III). However, on the regional scale the Äspö HRL is perhaps best considered as a "point sink" that draws water from all directions.

- Starting with water from above, one can show that the Meteoric water from Äspö is not enough to explain the fraction of Meteoric water in the inflows to the tunnel. Probably, Meteoric water from the Laxemar area is providing a substantial part, see Figure 6-18 in Part III and also Figure 4-6 in Part II.

- The horizontal flow towards the tunnel can be expected to follow the selective withdrawal principle, meaning that water from a certain density interval is mainly contributing to the inflow. This suggestion was given in Svensson (1997a), where also an illustration can be found. The withdrawn water is replaced with water from above. This leads us to expect that the Glacial water in the domain should steadily be replaced by Meteoric and Baltic waters. The decrease in Glacial water can be found in both measurements and simulations, see Tables 5-3 and 5-5 (Part III).

- Water with higher salinity, than is found at the level of the Äspö HRL under natural conditions, is found in the central part of the tunnel spiral. This is an indication of a water transport from below the tunnel level, the so called upconing process. Field data on the salinity variation with time at tunnel position 2800 metres can be found in Figure 6, where also simulation results are presented. It is interesting to note that the simulated maximum salinity continues to rise also after the tunnel was completed, which is at time 3.7 years in Figure 6. The salinity field is hence not in a steady state at time 97-01-01, which is the date the simulation was carried out to. The upconing can also be seen in Figure 6-18 in Part III and in Figure 4-6 in Part II, where it is found that water with a high fraction of Äspö Brine is found in the spiral part of the tunnel. As the transient salinity field affects the flow and pressure distributions, it is an indication that steady state site scale models can be questioned.

More examples could be given, but it is clear that the integrated modelling approach has contributed to a better understanding of the site.

Part II

TASK#5: M3 PREDICTIONS OF THE GROUNDWATER CHEMICAL CHANGES ASSOCIATED WITH THE CONSTRUCTION OF THE ÄSPÖ HRL

M. Laaksoharju* and I. Gurban**

***Geopoint AB, Stockholm**

****Duke Engineering and Services, Ottawa**

1 INTRODUCTION

The aim of Task #5 is to compare and ultimately to integrate hydrochemistry and hydrogeology. The modelling approach could be used for any future repository site investigation and evaluation, especially in a crystalline bedrock environment.

The aims of Part II of this report are: (i) to describe the M3 model for statistical interpretation of hydrochemical data and the uncertainties in using it to quantify the reference water components in groundwater samples; (ii) to present the results of using M3 on the graphically-interpolated hydrochemical data from the Äspö Hard Rock Laboratory (HRL) that form the basis for Task #5; (iii) to examine the trends of changes over time in reference water mixing proportions along the tunnel and to assess the linearity of these changes and the viability of extrapolating to predict the trends of future short term changes; and (iiii) compare and integrate those results with the hydrodynamic modelling presented in Part III of this report.

As output from this task, we provide the following:

a) Background information and boundary conditions for Task#5 modelling in the form of M3 groundwater mixing proportions calculated with the M3 Multivariate Mixing and Mass balance calculation tool and visualisations of the groundwater compositions and mixing proportions with the Voxel Analyst graphical tool.

b) M3 interpretation of the changes in the chemistry of groundwater caused by the tunnel construction at the Äspö HRL.

c) Estimations of changes over time in groundwater mixing proportions at calibration Control Points (CP) with HRL tunnel positions <2900m and using these changes to estimate changes at prediction CPs with tunnel positions at >2900m.

d) Comparison of the results of the chemical mixing and reaction modelling using M3 with hydrodynamic modelling.

2 BRIEF DESCRIPTION OF THE SITE AND GROUNDWATERS

The underground experimental Äspö Hard Rock Laboratory (HRL) (Figure 2-1), in south-east Sweden was initiated by the Swedish Nuclear Fuel and Waste Management Company (SKB). This site is an important test and research facility which is used as part of the Swedish programme to dispose of spent nuclear fuel in crystalline bedrock.

Boreholes drilled from the surface at the Äspö site consist of percussion drilled boreholes to a depth of around 100m and deep core drilled boreholes with an approximate depth of 1000m; one cored borehole from the nearby Laxemar site on the mainland reaches a depth of around 1700m. Probe boreholes drilled along and into the bedrock from the HRL tunnel wall generally have a length of 20m. The total length of the tunnel is approximately 3600m and the tunnel spiral reaches a maximum depth of 450m.

The boreholes at the Äspö site have been used for more than 10 years for various investigations such as: hydrogeochemical (Smellie and Laaksoharju, 1992; Banwart et al. 1993; Banwart ed., 1995; Nilsson, 1995; Laaksoharju et al. 1995; Laaksoharju and Skårman 1995; Smellie et al., 1995, Laaksoharju and Wallin (eds.), 1997; Laaksoharju et al., 1999a), hydrogeological (Rhén et al., 1993; 1994; Rhén and Stanfors, 1993) and geological (Stanfors et al., 1992; 1993 a,b; 1994).

The present day conditions at Äspö consist of a thin lens of meteoric fresh water to a depth of 250m and a saline water consisting of a proportion of present and ancient Baltic Sea water and glacial melt water to a depth of 400-600 metres. Below this level the saline water still contains a proportion of glacial water and, in addition, a proportion of increasingly deep Äspö brine water of which a large portion has not been in contact with the atmosphere for millions of years (Laaksoharju et al., 1999a). During the HRL tunnel construction changes occurred in the composition of the water flowing into the tunnel at different locations. The variation in, in for example, salinity was however relatively small, while the variation in the mixing proportions of the different reference waters varied considerably. The effects from different pre- and post-glacial events have affected the groundwater composition at Äspö. (Laaksoharju and Wallin (eds.), 1997).

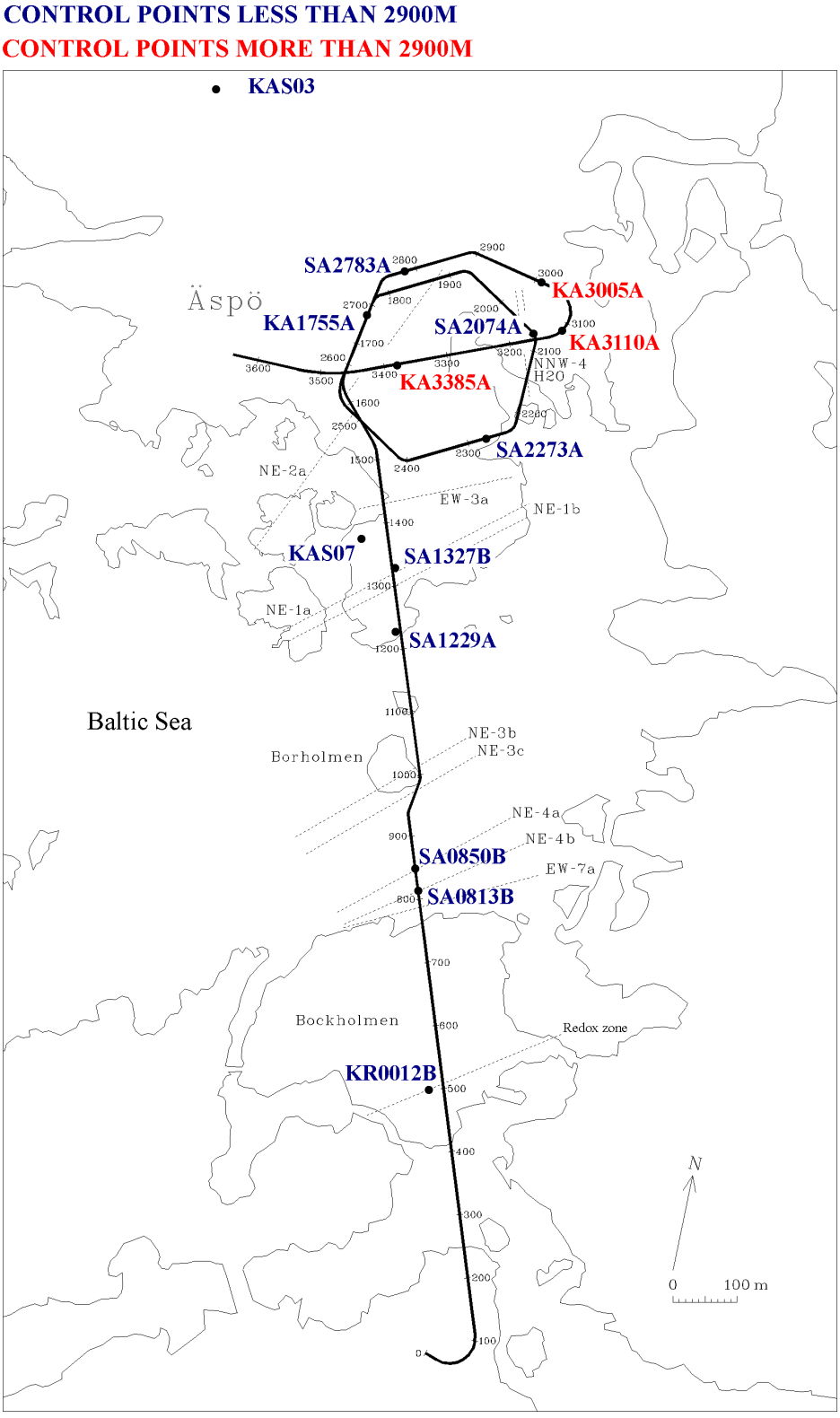

Figure 2-1: *Location and outline of the Äspö Hard Rock Laboratory in relation to the major fracture zones. The control points (CP) are selected groundwater samples used in the modelling. The control points >2900m are used for predictions*

3 DATA, STRATEGY AND TOOLS USED FOR CALCULATIONS AND PREDICTIONS

3.1 DATA USED

Data used in this task are contained in the data set that has been distributed within Task #5 (see Figure 3-1). They are the compositions of groundwater samples from boreholes in the vicinity of the tunnel, taken both before and after construction of the tunnel, plus time series samples of water inflows to the tunnel. Compositions of groundwater samples from boreholes have been used to estimate compositions at points along the tunnel by using the Voxel Analyst graphical interpolation tool. The results of this modelling are reported by Gurban et al. (1998). Time series samples of inflows are divided into data for Control Points (CP) at tunnel positions <2900m which have been used for calibration of rates of change over time, and data for CPs at tunnel positions >2900m which are compared with compositions that have been predicted from the trends at the calibration CPs.

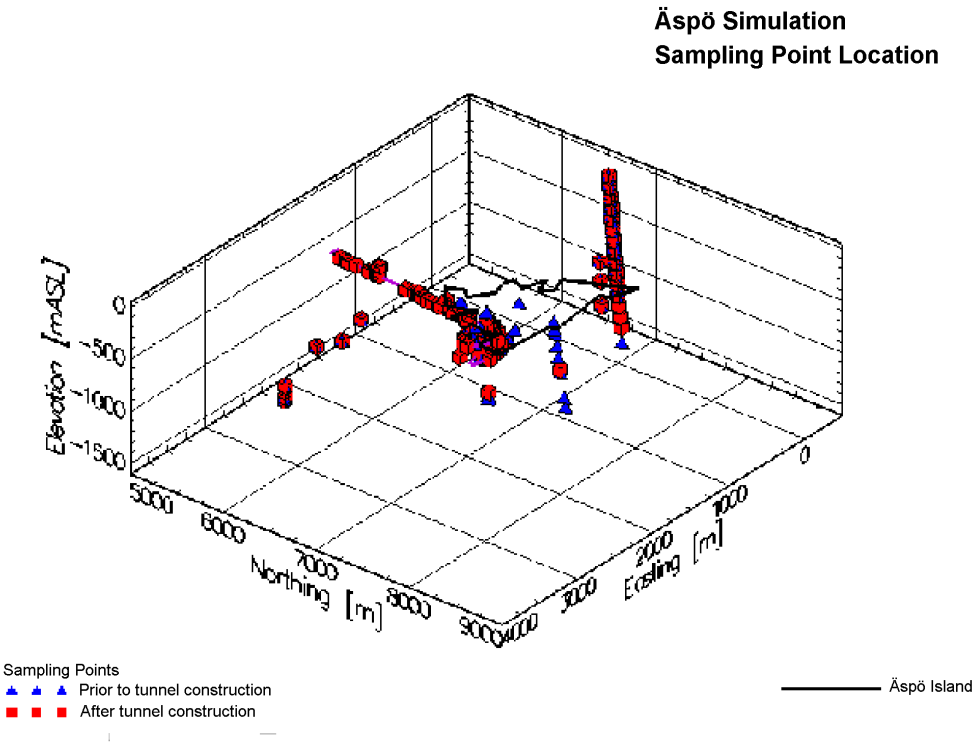

Figure 3-1: *Visualisation of the sampling points available for Task#5 modelling reflecting the groundwater condition prior to and after the Äspö HRL tunnel construction. The contour of the Äspö island is shown in the figure (for orientation see Figure 2-1).*

3.2 STRATEGY

The strategy employed was to:

- Use statistical analysis with 'M3' software (see Section 4) of the Task #5 hydrochemical data set to deduce a number of 'reference waters'. These reference waters are component water masses with distinct sources and compositions, the mixing of which can account for the compositions of the sampled groundwaters.

- Calculate the mixing proportions between the reference waters in each water sample. Groundwater samples prior to tunnel construction came from boreholes in the area around the site of the Äspö HRL; additional groundwater samples were obtained from inflows to the tunnel during and after construction. Use the M3 mixing proportions and the assumed compositions of each of the reference waters to reconstruct compositions for each water sample. Cross-plots of these reconstructed concentrations versus measured concentrations for each solute show which of the solutes are affected by water-rock reaction, i.e. are non-conservative.

- Use variations in M3 mixing proportions to represent the changes in groundwater chemistry caused by tunnel construction. The distributions at points in time of conservative solutes and of mixing proportions of each of the reference waters are displayed graphically using an interpolation and contouring routine in Voxel Analyst software.

- Interpolate values for conservative solute concentrations and reference water mixing proportions in specific major fracture zones, using Voxel Analyst. These data are required by the hydrodynamic modelling teams in Task #5.

- Examine directions of change over time in the M3 principal components for tunnel inflows. Calculate average rates of change in the mixing proportions of reference waters for inflows at each Control Point at <2900m. Assign an average rate of change in mixing proportions for each dominant water type. Test the linearity of changes in mixing by comparing forward predictions from initial values, using the average rates of change, with observed compositions for most recent samples in time series.

- Use these average rates of change for each water type at <2900m to predict inflow water compositions at >2900m, using initial water compositions derived by spatial interpolation of borehole water compositions prior to tunnel construction. Compare M3-predicted concentrations of conservative solutes and proportions of reference waters with M3 analyses of actual water samples and also with simple Voxel Analyst interpolations.

- Compare the results of the chemical mixing and reaction modelling with the hydrodynamic modelling.

3.3 M3 MODEL

In the following sections the M3 model is described, the uncertainty of the modelling is discussed and the reactions considered in the present Task #5 modelling are listed.

3.3.1 M3 MODEL DESCRIPTION

A new method named Multivariate Mixing and Mass balance calculations (abbreviated to M3) has been developed (Laaksoharju et. al., 1999b). M3 modelling uses a statistical method to analyse variations in groundwater compositions so that the mixing components, their proportions, and chemical reactions are revealed. The method quantifies the contribution to hydrochemical variations by mixing of groundwater masses in a flow system by comparing groundwater compositions to identified reference waters. Subsequently, contributions to variations in non-conservative solutes from reactions are calculated. The modelling assumes the following: 1) chemical composition is a good tracer for the evolution by mixing and reactions of a groundwater, 2) the compositions of groundwaters being studied are predominantly determined by mixing of a number of chemically-distinct water types or 'reference waters', 3) groundwaters

represented in the data set of compositions have evolved by similar mixing and reaction processes. The features of the model are:

- It is a mathematical tool which can be used to evaluate groundwater field data, to help construct a conceptual model for the site and to support expert judgement for site characterisation;

- It uses the entire hydrochemical data set to construct a model of geochemical evolution, in contrast to a thermodynamic model that simulates reactions or predicts the reaction potential for a single water composition;

- The results of mixing calculations can be integrated with hydrodynamic models, either as a calibration tool or to define boundary conditions;

- Experience has shown that to construct a mixing model based on physical understanding often requires more information than available especially at site scale. M3 results can provide additional information of the major flow paths, flow directions and residence times of the different groundwater types which can be valuable in transport modelling;

- The numerical results of the modelling can be visualised and presented for non-expert use;

The M3 modelling approach differs from geochemical equilibrium/mass transfer modelling in that it operates by statistical analysis of a set of multiple groundwater compositions for the studied region, whereas mass transfer modelling simulates changes for individual water samples. M3 modelling interprets compositional variations for groundwaters in a given region dominantly in terms of mixing between different groundwater masses; water-rock reactions are inferred by deviations from expected mixing trends for specific solutes. On the other hand, mass transfer modelling simulates the evolution from one water composition to another in terms of detailed geochemical reactions, on which mixing of another water composition might be superimposed. M3 mass-balance calculations have been compared with results from geochemical modelling with the NETPATH code but the results are comparable only when the mixing model is the same and when employing the same reference waters. Such comparisons can only be performed at a local 'one-dimensional' scale since NETPATH uses only one conservative tracer solute (e.g. chloride) in mixing calculations.

Although the M3 model is fairly new, several test cases have been modelled such as: Sweden (SKB sites), Canada (Cigar Lake), Finland (Palmottu) and Gabon (Oklo) (see Laaksoharju, 1999c).

Mixing calculations with M3 interpret a groundwater system in terms of a spatial arrangement of mixing proportions and predominance of the various reference waters. The number of reference waters that can reasonably be inferred is generally restricted by the data variability existing in the studied groundwater system. The spatial relationships of these component water masses may be related to water movements in the system over time, thus the information can be integrated with hydrodynamic models, by defining boundary conditions and as a calibration tool to constrain directions and magnitudes of flow. This is how M3 has been used in Task #5. In order to model the

mixing changes in the dynamic system, i.e. prior to and after tunnel construction at the Äspö HRL, time series data have been used. Simultaneous sampling from several points at different times has resulted in a series of "snapshots" of the groundwater evolution over the time since tunnel construction.

The computer code M3 runs as a toolbox under the Windows program Matlab 5.3 or higher. The model consists of 3 steps where the first step is a standard principal component analysis, followed by calculations of mixing proportions, and finally mass balance calculations as described below. As an example, Figure 3-2 shows the modelling steps applied to the Äspö Hard Rock Laboratory data. M3 modelling always follows the same procedure:

(1) Principal Component Analysis (PCA)

A standard multivariate technique called Principal Component Analysis (PCA) is used for the clustering of the data in order to summarise the information and to construct an *ideal mixing model* for the site. The starting point is the measurement of various chemical variables for a number of groundwater samples ("variables 1, 2, 3…….n" in Figure 3-2a). Generally the major solutes Cl, Ca, Na, Mg, K, SO_4 and HCO_3 in combination with the isotopes δ^2H, $\delta^{18}O$ and ^3H are measured. If there is a lack of isotope data the modelling can still be performed but generally with a lower resolution if the isotopes contain unique information concerning groundwater sources and the flow system. By using PCA the samples can be visualised as corresponding to points in a multi-dimensional space where the number of dimensions equals the number of different constituents (Figure 3-2b). The PCA rotates the coordinate system in this space to find the optimum orientation to display the largest possible resolution of the different point clusters.

The PCA analysis is carried out on standardised data. The standardised value of each concentration measurement is obtained by subtracting the mean and dividing by the standard deviation. The PCA effectively reduces the large data matrix to two or more smaller matrices which accounts for most of the information within the original data. The two or more resulting data matrices consist of principal component (PC) scores and loadings. The PC scores (S) are linear combinations of the standardised data (x) with the loadings (l) as the coefficients:

$$S_{n,c} = \sum x_{n,p} l_{p,c}$$

where n is the groundwater sample, p is the particular chemical measurement and c is the principal component. The PC scores therefore contain information on all the chemical variables combined into a single number, with the loadings indicating the relative contribution each variable makes to that score. PCA aims to describe as much as possible of the information from the hydrochemical variables in the first equation (called the first principal component). As much as possible of the remaining information is described by the second principal component. For the Äspö data set the first two principal components describe 70% of the information in the data set.

The third or fourth principal components contain information that is less useful in terms of mixing and reactions, depending on the complexity of the examined data and the chosen variables. If the first two principal components contain most of the information, an x, y scatter plot can be drawn (Figure 3-2c), where x is the equation for the first principal component and y the equation for the second principal component. The loadings for the different elements are in this example:

PC1=-0.25[Na]-0.08[K]-0.23[Ca]-0.05[Mg]+0.11[HCO3]-0.24[Cl]-0.23[SO4]+0.08[3H]-0.03[2H]+0.01[180]

PC2=-0.04[Na]-0.23[K]+0.05[Ca]-0.24[Mg]+0.16[HCO3]+0.02[Cl]+0.02[SO4]-0.10[3H]-0.27[2H]-0.29[180]

In order to ease comparisons, the loadings for the different variables are normalised in M3 since this is how eigenvectors are generally presented. The elements are centre scaled before eigenvalues and eigenvectors are calculated.

The PC-plot is used to visualise the clustering of the data as well as to identify reference waters (Figure 3-2d). Reference waters are water compositions that are selected as the component waters from which the sampled groundwaters can be derived by mixing. A reference groundwater can be any water composition but generally extreme waters or end-members such as rainwater or deep water are assigned. There are no limitations concerning how many reference waters can be selected in the modelling, but the general rule is to use as few as possible to describe the observed variations. In theory the obtained water composition can be dedicated to only a few or to several reference waters since the sum of the mixing proportions always add up to 100%. The number of reference waters can also be guided by the type of modelling to be performed or by a conceptual model of the site. The selection of end-members or reference waters typically involves the following steps:

- Construction of an independent palaeohydrogeological and present-day conceptual model for the site to suggest which type of water (glacial meltwater, seawater, meteoric waters) may have entered the bedrock.

- The distribution of the samples in the PCA is used to guide the minimum number and type of reference waters needed to explain the observations. This is generally an iterative process where different options are tested. New reference water compositions guided by the conceptual model may be inserted to describe the observations. The scale (e.g. fracture scale or site scale) of the modelling determines which samples are to be included in the PCA and hence the number of end-members needed for the modelling.

- Testing of the mixing model to see how well it predicts conservative variables such as chloride, oxygen-18 and deuterium. Depending on the outcome of this test a decision is made to reject or accept the model. If rejected, the scale of modelling is changed by deleting measurements and end-members. If the model is acceptable, an uncertainty range is calculated from the deviation of the water conservative elements.

- Feasibility testing using different mixing proportions of the reference waters to reproduce the observed groundwater composition to build confidence in the modelling. Include simple tests where say 50% meteoric water is mixed with 50% brine water to test that the water composition plots half way between the reference waters in the PCA.

Lines are drawn in the PC-plot between the reference waters so that a polygon is formed. The polygon defines the observations which can be described by the selected reference waters. By definition, samples inside the polygon can be described by the selected reference waters.

(2) *Calculations of Mixing Proportions*

The mixing proportions describe the contributions of each reference water composition to the observed water (Figure 3-2e). They are inversely proportional to the distance of a sample to the selected reference waters in the plot. On a two-dimensional surface, a mathematically unique solution is only obtained from mixing proportions containing a maximum of three reference waters. If there are more than three reference waters, a centre point P is created at the weight point of the polygon. By using this centre point, mixing proportions can be assigned when there are more than three reference waters in a two-dimensional plot (Laaksoharju et al., 1999b). For a polygon containing, say, five reference waters, M3 would suggest that a sample plotting at the centre point consists of 20% of each reference water.

(3) *Mass Balance Calculations to Estimate Non-Conservative Behaviour*

The mixing proportions estimated from M3 are used to recalculate concentrations for the individual variables, assuming conservative mixing between reference waters. Deviation between calculated and measured values indicates that there is a source or sink due to reaction. Mass balance calculations are then used to quantify gains or losses due to these reactions (e.g. for HCO_3 in Figure 3-2f).

Reactions can modify water compositions to the extent that a new reference water is indicated in the PC-plot. For example, reduction of sulphate in sea water leads to an additional reference water called ‘Altered Marine’ water at Äspö (see Figure 3-2d-f). If such a ‘reacted reference water’ is used in the mixing calculations, only reactions or mixing not contained in the reference water composition are modelled.

a)

Sample no	Variable 1	Variable 2	Variable 3	Variable 4	Variable 5
1	8500	45.5	19300	2.12	14.1
2	613	2.4	162	21	61
3	1960	95	93.7	234	90
4	11.5	2.3	15.4	1.9	63
5	2140	35.1	504	195	760
6	3020	7.3	4380	49.5	11
7	0	0	0	0	3
8	3179.8	154.1	152.0	379.6	146.0
9	0	0	0	2	7
10	2144	91.8	103	258	793
11	2320	26	818	217	227
12	2250	28	741	244	219
13	335	14	80	36	235
14	336	12	87	39	235
15	228	4	27	4	373

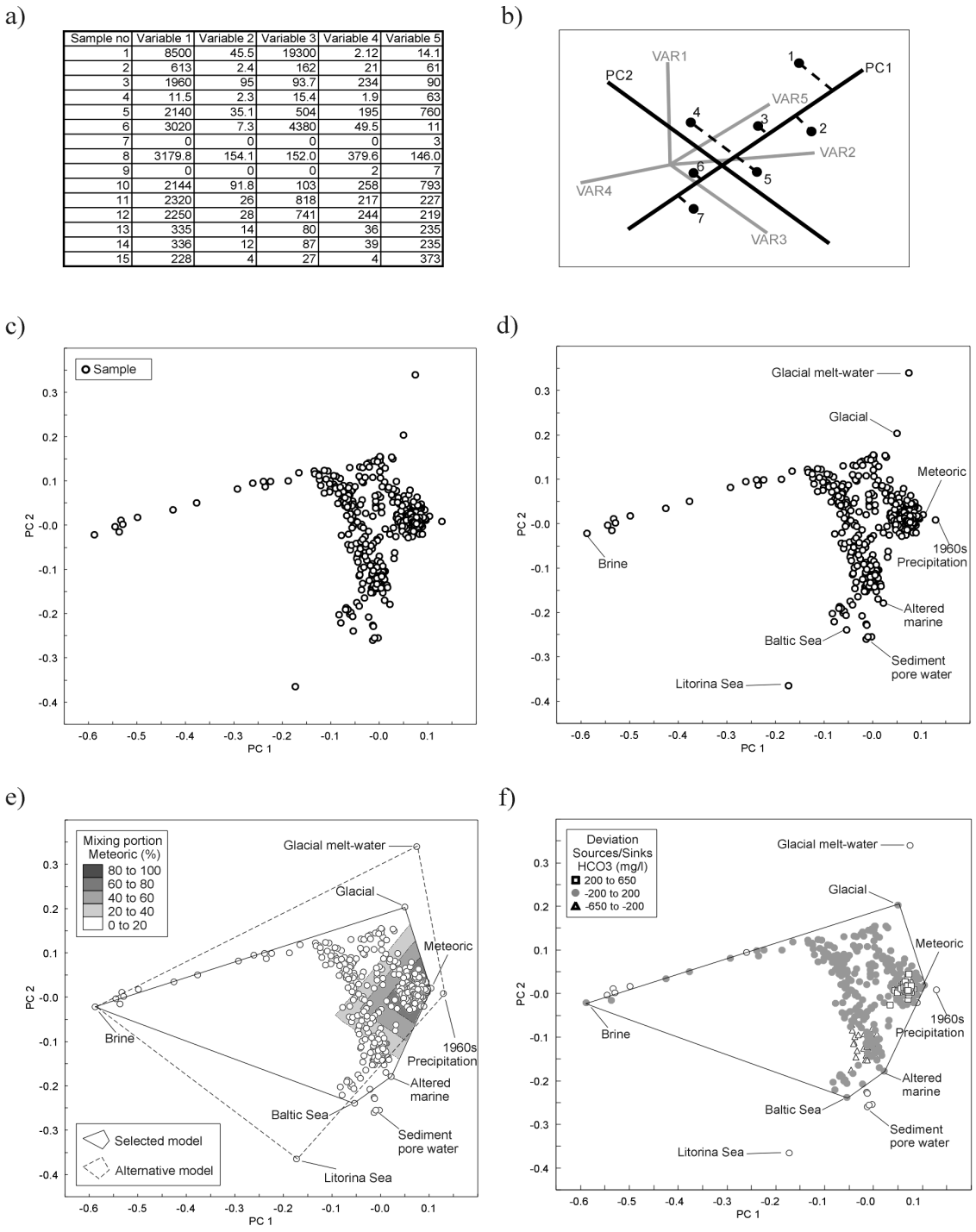

Figure 3-2: *A schematic visualisation of the different steps in the M3 modelling; a) Data table containing groundwater compositions. b) The principle for principal component analysis; seven groundwater samples and their location in the multivariate space (VAR1-VAR5) and their projection on the principal component 1 (PC1) are shown. Principal component analysis is used to obtain the maximum resolution of the data set. c) The result of the principal component analysis showing principal components 1 and 2. d) Selection of possible reference waters - the other groundwaters are compared to these, e) Mixing calculations – the linear distance of a sample to the reference waters e.g. the proportions of Meteoric water (%) are calculated in the figure for the selected ideal mixing model; the alternative model uses a new set of reference waters. f) Mass balance calculations – the sources and sinks (mg/l) of carbonate (HCO_3) are shown which cannot be accounted for by using the ideal mixing model. The M3 model is applied to data from the Äspö Hard Rock Laboratory for Task#5; a reduced data set was used due to problems with the tritium analyses. The PC-plot for Task#5 data has therefore a different appearance, see Figure 4-1.*

3.3.2 UNCERTAINTIES IN THE M3 MODELLING

When constructing a M3 mixing model a stepwise approach is suggested starting with conservative tracers and then including non-conservative tracers. The effect of the analytical and method uncertainties on the modelling should be evaluated. The complexity of the site and the scale (site or local) of the modelling should, together with palaeo/present hydrodynamic modelling, indicate the complexity and the numbers of reference waters needed in the modelling. The layout of the PCA generally sets constraints for the modelling and the number of possible reference waters is generally restricted by the data variability obtained at the site. The outcome of the mixing modelling can be compared with the results from hydrodynamic modelling. For example, the mixing proportion calculations can be evaluated by using an independent flow model to estimate mixing fluxes, or the mixing proportions can be used to calibrate the initial and boundary conditions and compositions for a transient flow model (as has been done in Task#5). The mass-balance calculations should be supported by independent measurements (e.g. microbes that can indicate sulphate reduction, organic decomposition or iron reduction) or by additional geochemical modelling. The results and the relevance of the different models should always be critically reviewed at all steps of the modelling. It is important to note that the M3 model deals only with water quality information; no space or time constraints, geological or hydrogeological information are included in the model.

The following are sources of uncertainties in using M3:

1) Input hydrochemical data errors originating as sampling errors caused by the effects from drilling, borehole activities, extensive pumping, hydraulic short-circuiting of the borehole and uplifting of water which changes the in-situ pH and Eh conditions of the sample, or as analytical errors.

2) Conceptual errors such as wrong general assumptions, selecting wrong type/number of end-members and mixing samples that are not mixed.

3) Methodological errors such as oversimplification, bias or non-linearity in the model, and the systematic uncertainty which is attributable to the use of the centre point to create a solution for the mixing model.

The effects from sampling errors are difficult to estimate since essentially there is no in-situ sample from undisturbed conditions. Labelled drilling water indicates generally a less than 1% contamination from drilling fluids in the samples. Borehole activities and short-circuiting of the borehole may cause unnatural mixing of the groundwater. Figure 4-1 shows an extreme case of how the groundwater composition in the borehole can change in the open hole compared with water from sampling of discrete fractures (Laaksoharju 1999c). In this particular case the dilution during drilling was more than 10,000 mg/l Cl and the groundwater level in the borehole was lowered 50-100m. These changes may therefore also affect groundwater in fractures although the changes are likely to be less severe. For example, changing the pumping rate during sampling can considerably alter the groundwater composition by ± 2000 mg/l Cl (Laaksoharju, 1999c).

Pumping out of the water can cause super saturation of, e.g. calcite, which may change the Ca and HCO_3 content in the sample. The uncertainty from sampling errors has been estimated/modelled to be in most of the cases in the order of ±10% from the undisturbed 'real' values. Analytical errors for different elements vary but extensive comparison between different laboratories generally indicate a deviation of 1-5% in the values (Laaksoharju, 1999c). Uncertainties in analytical data account for variability of up to ±10% in the calculated mixing proportions, and overall mixing proportions of less than 10% can be regarded as potentially insignificant.

An example of a conceptual error is assuming that the groundwater composition is a good tracer for the flow system. The water composition is not necessarily a tracer of mixing directly related to flow since there is not a point source as there is when labelled water is used in a tracer test.

Another source of uncertainty in the mixing model is the loss of information in using only the first two principal components. The third principal component gathers generally around 10% of the groundwater information compared with the first and second principal components which contain around 70% of the information. A sample could appear to be closer to a reference water in the 2D surface than in a 3D surface involving the third principal component.

The necessity of using the centre point in the M3 model for more than three reference waters increases the uncertainty in the modelled mixture. For example, a sample plotting at the centre point will have an uncertainty of 20% in the proportion of each reference water, since some of the reference waters could be absent from the mixture rather than being present at 20%. In reality not every reference water necessarily contributes to every water sample taken. In the present case, three reference waters dominate in the M3 calculations and the other ones are close to or under 10% which is regarded as the 'detection limit'.

Uncertainty in mixing calculations is smaller near the boundary of the PCA polygon and larger near the centre. Based on averaging over the polygon, the uncertainty range is ±10% at a confidence level of 90%. Substantially larger uncertainties therefore apply to 10% of the samples.

Further methodological errors are introduced when mixing proportions from M3 calculations are used directly in hydrodynamic modelling, because transport equations of mixing fractions are non-linear. To avoid this additional source of error, it has been suggested that principal components 1 and 2 should be used directly in the transport calculations, transferring the results into mixing proportions (Peter Jackson, per. comm. 2001).

In summary, uncertainty arising from conceptual and methodological errors can be potentially far greater than that from sampling or analytical uncertainties. More detailed discussions of various M3 issues are presented in Appendix 3.

3.3.3 REACTIONS CONSIDERED IN M3 MODELLING

In theory thousands of chemical reactions could be written involving the water, solids and gases in a regional groundwater system such as that at the Äspö site. There are eight main categories of reactions and processes that control the chemistry of most groundwaters: precipitation-dissolution, acid-base, complexation, substitution-hydrolysis, oxidation-reduction, ion-filtration-osmosis, dissolution and exsolution of gases and sorption/desorption. Worldwide site modelling has revealed that the actual number of reactions that dominate the groundwater chemistry is quite small such as (Alley, 1993):

1) Introduction of CO_2 gas in the unsaturated zone
2) Dissolution of calcite and dolomite, and precipitation of calcite
3) Cation exchange
4) Oxidation of iron containing minerals, pyrite and organic matter
5) Reduction of oxygen, nitrate, and sulphate, with production of sulphide
6) Reductive production of methane
7) Dissolution of gypsum, anhydrite and halite
8) Incongruent dissolution of primary silicates with formation of clays

Since the Task #5 modelling of Äspö aims to describe the groundwater changes due to the tunnel construction, this added a constraint in the modelling, namely to focus on fast reactions. The relatively low temperature (at -200m = 11°C; the gradient is 1.6°C per 100m) of the groundwater hinders equilibrium being established between groundwater and fracture minerals. However, recent research has shown that microbes mediate in many reactions that otherwise would not take place. Organic material (CH_2O) generally plays an important role in these kinds of biological processes. The processes that could influence groundwater compositions in the timescale of HRL construction at the Äspö site are biological processes, redox reactions, calcite dissolution/precipitation and ion exchange.

The following six reactions have been considered, with comments on the qualitative outcomes of mixing and mass balance modelling with M3:

1) *Organic decomposition:* This reaction is detected in the unsaturated zone associated with Meteoric water. This process consumes oxygen and adds reducing capacity to the groundwater according to the reaction: $O_2 + CH_2O \rightarrow CO_2 + H_2O$. M3 reports a gain of HCO_3 as a result of this reaction.

2) *Organic redox reactions:* An important redox reaction is reduction of iron III minerals through oxidation of organic matter: $4Fe(III) + CH_2O + H_2O \rightarrow 4Fe^{2+} + 4H^+ + CO_2$. M3 reports a gain of Fe and HCO_3 as a result of this reaction. This reaction takes place in the shallow part of the bedrock associated with influx of Meteoric water.

3) *Inorganic redox reaction:* An example of an important inorganic redox reaction is sulphide oxidation in the soil and the fracture minerals containing pyrite according to the reaction: $HS^- + 2O_2 \rightarrow SO_4^{2-} + H^+$. M3 reports a gain of SO_4 as a result of this reaction. This reaction takes place in the shallow part of the bedrock associated with influx of Meteoric water.

4) *Dissolution and precipitation of calcite:* There is generally a dissolution of calcite in the upper part and precipitation in the lower part of the bedrock according to the reaction: $CO_2 + CaCO_3 \rightarrow Ca^{2+} + 2HCO_3^-$. M3 reports a gain or a loss of Ca and HCO_3 as a result of this reaction. This reaction can take place in any groundwater type.

5) *Ion exchange:* Cation exchange with Na/Ca is a common reaction in groundwater according to the reaction: $Na_2X_{(s)} + Ca^{2+} \rightarrow CaX_{(s)} + 2Na^+$, where X is a solid substrate such as a clay mineral. M3 reports a change in the Na/Ca ratios as a result of this reaction. This reaction can take place in any groundwater type.

6) *Sulphate reduction:* Microbes can reduce sulphate to sulphide using organic substances in natural groundwater as reducing agents according to the reaction: $SO_4^{2-} + 2(CH_2O) + OH^- \rightarrow HS^- + 2HCO_3^- + H_2O$. This reaction is of importance since it may cause corrosion of the copper capsules. Vigorous sulphate reduction is generally detected in association with marine sediments that provide the organic material and the favourable salinity interval for the microbes. M3 reports a loss of SO_4 and a gain of HCO_3 as a result of this reaction. This reaction modifies the seawater composition by increasing the HCO_3 content and decreasing the SO_4 content.

3.4 VISUALISATION TOOL

Voxel Analyst software is used to interpolate and visualise hydrochemical data and modelled mixing proportions of reference waters. It is a general-purpose data visualisation and analysis tool for attributes within a 3-dimensional volume data set. For Task #5 the modelled volume is: Xmin = -300, Xmax = 3450.44, Ymin = 5600, Ymax = 8121, Zmin = -1500, Zmax = 20, all these being in metres.

3.5 BOUNDARY AND INITIAL COMPOSITIONS

For interpolation the observations shown in Figure 3-1 are used, together with added points in the corners and at the surface to represent boundary conditions. The added values are from observations located close to the corners and representing the appropriate depths. For the boundary conditions at the surface, either rainwater or seawater were used to reflect the changes of the geography at the site. The composition and the distribution of the added points are listed and visualised by Gurban et al. (1998). The coordinates for the vertical cutting planes are:

1) X= 2200.3; Y= 5600; and X=2200.3; Y=8121 (along the tunnel)

2) X= -300; Y= 7560.8; and X=3450.44; Y= 7560.8

In order to constrain the hydrodynamic models used in Task #5, the distribution of Cl and M3 mixing portions along fracture zones at Äspö was required. As an example, the distributions of the Cl and mixing portions along the major fracture zones NE1, NE2, NE3, EW3 and NNW4, prior to tunnel construction are visualised in Figures 4-8 to 4-12. The depth extension of the model is 1500m and the cutting plane represents the intersection of the fracture zone defined by Rhén et al., 1997.

4 RESULTS OF THE M3 CALCULATIONS

4.1 SELECTION OF REFERENCE WATERS FOR M3 MODELLING

Using the variables Na, K, Ca, Mg, Cl, HCO_3, SO_4, ^2H, ^3H and ^{18}O in the PCA analysis, four reference groundwaters were chosen: Brine, Glacial, Meteoric and Marine.

The reference waters were selected so that most of the samples are inside the polygon. To keep the hydrodynamic simulations simple, more complex reference waters such as Litorina Sea water (old Baltic Sea water) and Modified Sea water (sea water modified by sulphate reduction) were excluded from the calculations. The closer to the reference water a groundwater plots, the more of that type of water the sample contains. The interpreted M3 mixing proportions were used by the modelling teams in Task #5. This simplification effectively introduces a conceptual uncertainty as described above in Section 3.3.2, especially for groundwaters such as locations under the sea. The selected reference waters for the current M3 modelling used within Task #5 are (for analytical composition see Gurban et al. 1998):

- *Meteoric: represents precipitation in the 1960's and infiltration water*
- *Baltic Sea water: represents modern Sea water from Baltic Sea*
- *Brine water: represents deep (1700m) groundwater from KLX02 at Laxemar.*
- *Glacial water: represents meltwater from the last glaciation ca. 10 000 years ago.*

The definition and usage of the term 'brine' needs some clarification. In some literature the definition of 'brine' is a water with a "considerably higher salinity" (Alley, 1993) than seawater which contains ~20,000 mg/l Cl. The brine sample from Äspö (47,200 mg/l, Cl) meets that requirement. However, in many international publications a lower limit of 100,000 TDS (~60,000 mg/l, Cl) is used for brine. The "Äspö brine" is therefore more dilute compared with some definitions. In the following text the term 'Brine' refers always to the Äspö brine salinity of 47,200 mg/l Cl.

The selected reference waters for the current modelling are shown in Figure 4-1 in relation to the groundwaters sampled in boreholes at Äspö. The uncertainty range when adding/removing 10% of the contribution from the reference waters for one sample (in red) is shown in Figure 4-1.

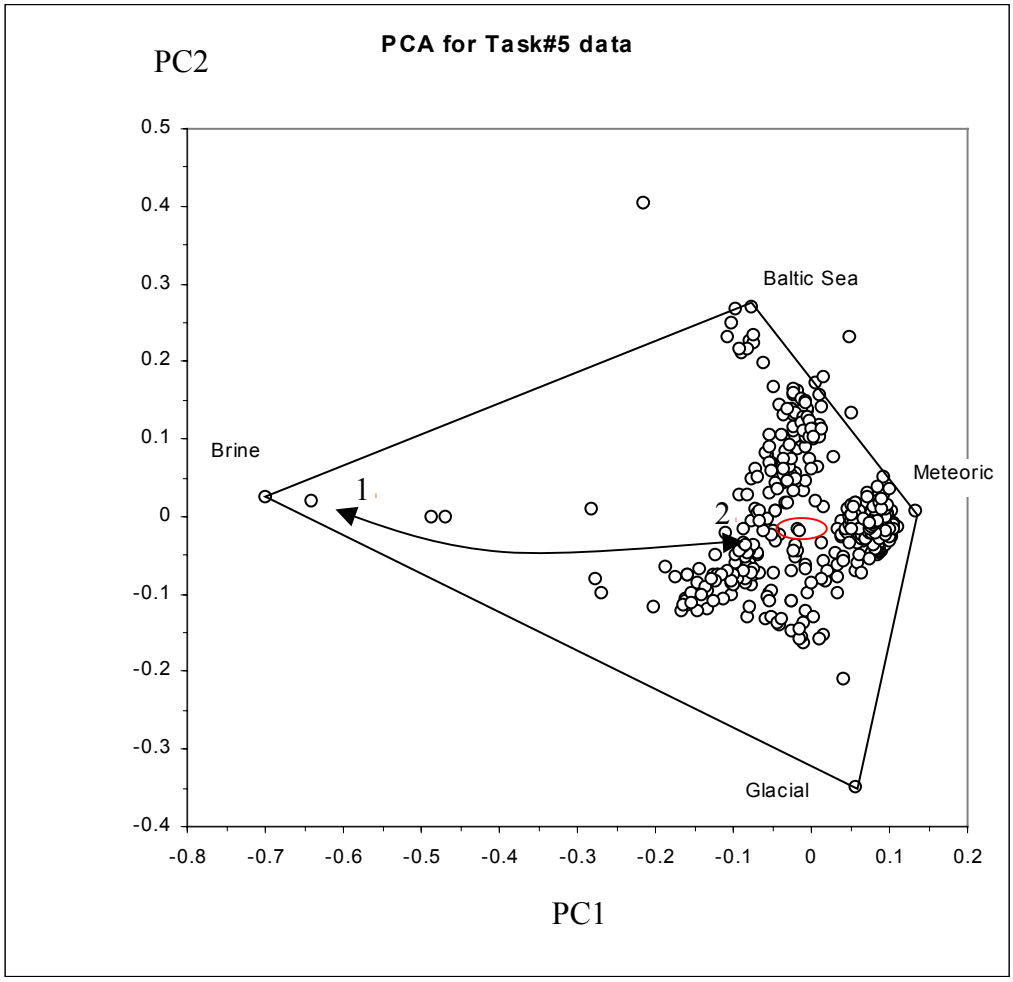

Figure 4-1: *PCA plot used as a basis for the M3 calculations. The reference waters for the groundwater modelling are shown and the polygon defines the samples that can be modelled by the selected reference waters. The arrow illustrates the magnitude of groundwater changes in the fracture (1) versus the groundwater changes in the borehole during drilling (2). The changes are due to mixing in the open borehole during drilling. The sampling was performed at a depth of 1420m-1705m at KLX02 (Laaksoharju 1999c) in the Laxemar area close to Äspö. The changes are extreme in this particular case due to borehole activities at great depth which increase the potential for disturbances at fractures prior to sampling. Mixing tends to make a greater impact on groundwater samples than, for example, analytical uncertainties (see Appendix 3). Repeated sampling from isolated fractures during 1993 and 1999 indicate that the fracture specific water at Laxemar is however not affected considerably by the open hole effects. The plot (red circle) is also used to illustrate how much the effect from the general uncertainty of ±10% is (calculated by adding/removing 10% contribution from the reference samples to the obtained groundwater composition at the sample SA1420A). The uncertainty range covers generally the uncertainty of the groundwater composition from drilling, sampling, chemical analysis and modelling. The equations for the first and second principal components are listed at the axes showing the loadings for the different elements. The first and second principal components summarise 72% of the total information content in the variables.*

4.2 TESTING THE VALIDITY OF THE SELECTED MODEL

The aim of the example below is to show how the validity of the selected mixing model can be tested. Knowing the mixing proportions and the compositions for the reference waters (Brine, Glacial, Meteoric and Baltic Sea), concentrations of individual solutes can be calculated for all water samples. The predicted new groundwater solute values are compared with measured values in Figure 4-2. A deviation for the conservative elements indicates errors in the model, however if this mean deviation is not larger than 10% from measured values, the model is considered validated and can be used for mass-balance calculations.

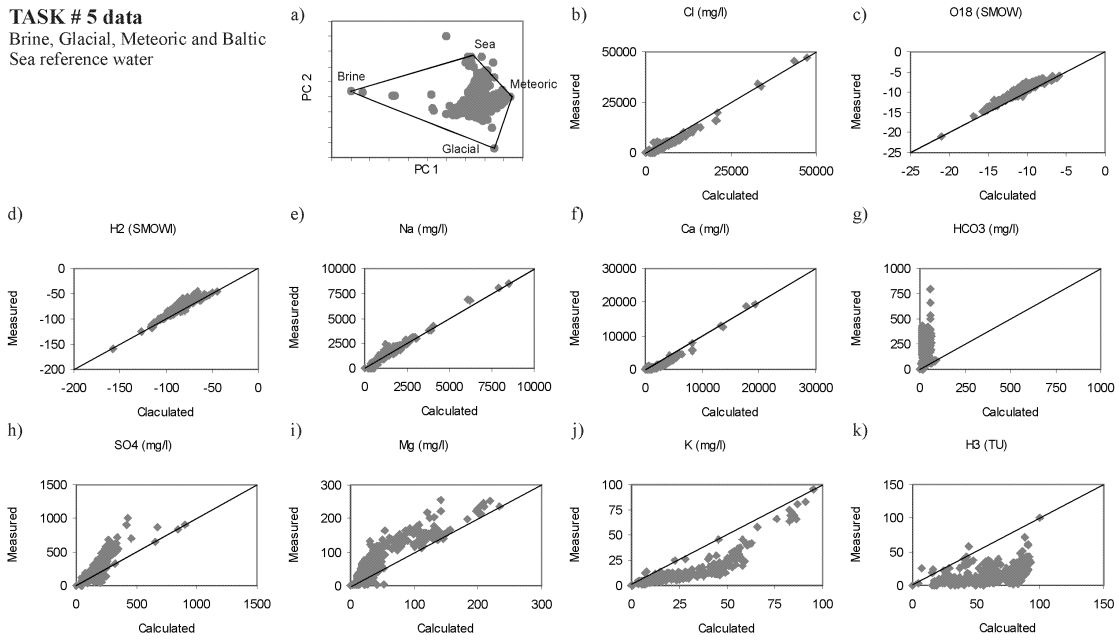

Figure 4-2: *The Task#5 groundwater is modelled to be a mixture of Brine, Glacial, Meteoric and Baltic Sea reference waters as shown in the PCA (Figure a). The calculated values based on the mixing proportions and the element contribution from reference waters are compared with measured values for different groundwater constituents (Figures b-k). If the value is on the line the predicted and measured values coincide, if the value is above/under the line there is a deviation between the measured and predicted values. A deviation from the line for the water conservative elements such as Cl, oxygen-18 (^{18}O) and deuterium (^{2}H) indicates scatter in the model. A deviation for a reactive element such as carbonate (HCO_3) can indicate gain (values over the line) or losses (values under the line) associated with reactions.*

Calculated values for the water conservative elements (Figures 4.2b-d) agree rather well with the measured values. This can be used as an indication that the selected reference waters describe the mixing of groundwater masses at the Äspö site scale satisfactorily. The calculated values for the reactive elements such as bicarbonate (HCO_3), sulphate (SO_4), magnesium (Mg) and potassium (K) deviate from the measured values which can be associated with water rock interactions. The loss of tritium (^{3}H) could be due to radioactive decay indicating age differences between recent groundwaters in the mixtures and in the relevant reference water, i.e. meteoric water; unfortunately the tritium measurements are uncertain for some of the samples due to analytical problems.

4.3 CHANGES IN THE GROUNDWATER COMPOSITION DUE TO THE TUNNEL CONSTRUCTION

Groundwater compositions prior to and after HRL tunnel construction are shown as 3D visualisations with Voxel Analyst for the conservative tracers Cl, oxygen-18, and of M3 mixing proportions and measured versus M3 modelled carbonate values (Figure 4-3 to 4-7). Meteoric (from the surface), Baltic sea (from the sea), Glacial (from depth) and Brine waters (from depth) have been drawn towards the tunnel.

Figure 4-7 shows that there has been a gain of carbonate. The increase under land is associated with decomposition of organic matter and calcite dissolution but under the sea the increase is due to sulphate reduction (see 3.3.3).

In order to help constrain and validate the hydrodynamic models used in Task#5, the distribution of Cl and M3 mixing proportions along fracture zones at Äspö were required. As an example, the distributions of the Cl and mixing proportions along the major fracture zones NE1, NE2, NE3, EW3 and NNW4, prior to tunnel construction are visualised in Figures 4-8 to 4-12. The depth extension of the model is 1500m and the cutting plane represents the intersection of the fractured zone defined by Rhén et al., 1997.

The temporal and spatial changes of groundwater compositions along the course of the tunnel are traced on PC-plots in Figures 4-13, 4-14 and 4-15. The *first sample* refers to the first sample in the time series sampled from a borehole at the Äspö site, and the *last sample* refers to the last sample in the time series sampled from the same borehole. The length of the time series can vary from some months to years (Gurban et al., 1998).

From Figure 4-13 the following conclusions are drawn: a) When the first sample is dominated by meteoric water the last sample is as well. b) Although some samples migrate towards a more marine signature, samples with a marine origin seem to move to a less marine signature. c) Glacial water samples seem to change to a composition with less glacial water. d) Saline groundwater seems to have a higher brine component in the last sample. The general trend is that the waters tend to be more mixed with time and move therefore towards the centre of the plot. Figures 4-14 and 4-15 show a similar trend where the tunnel construction seems to induce more mixed water. The water that is pumped out from the tunnel has a Cl concentration of around 6000 mg/l which coincides with the Cl concentration obtained for samples close to the centre of the plot.

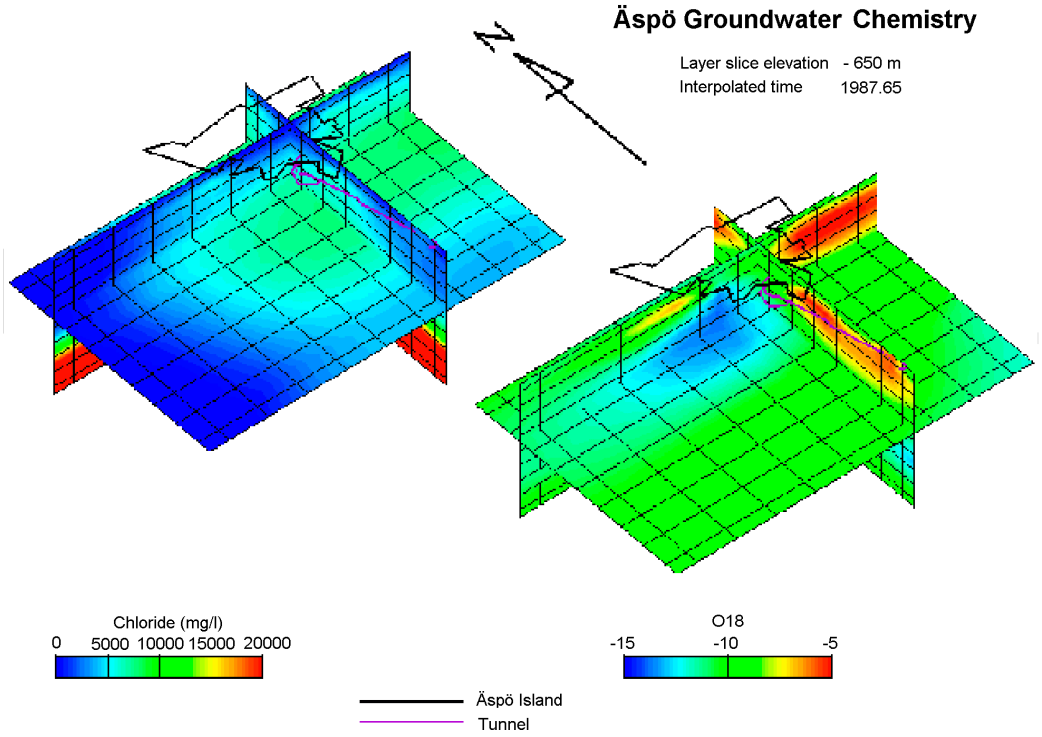

Figure 4-3: *The result of the interpolation of water conservative tracers Cl and oxygen-18 prior to the Äspö HRL tunnel construction (1987). The contour of Äspö island and the planned extension of the HRL tunnel are shown (for orientation see Figure 2-1). The horizontal cutting plane is at –650m depth.*

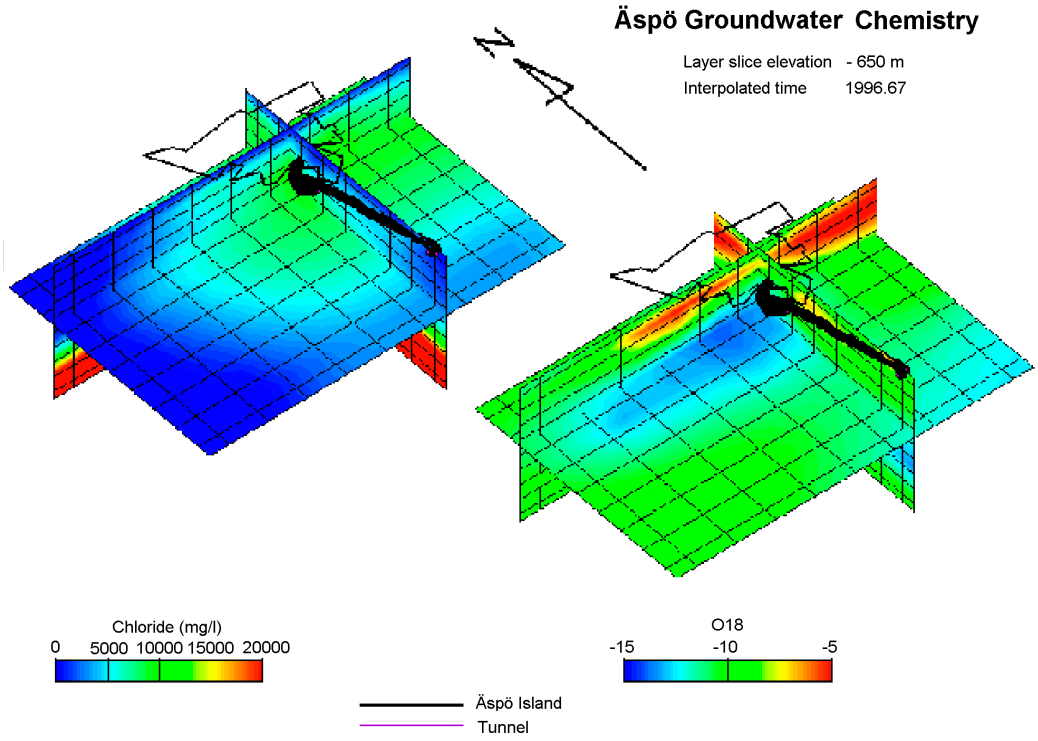

Figure 4-4: *The result of the interpolation of water conservative tracers Cl and oxygen-18 after the Äspö HRL tunnel construction (1996). The contour of Äspö island and the extension of the HRL tunnel are shown (for orientation see Figure 2-1). The horizontal cutting plane is at –650m depth.*

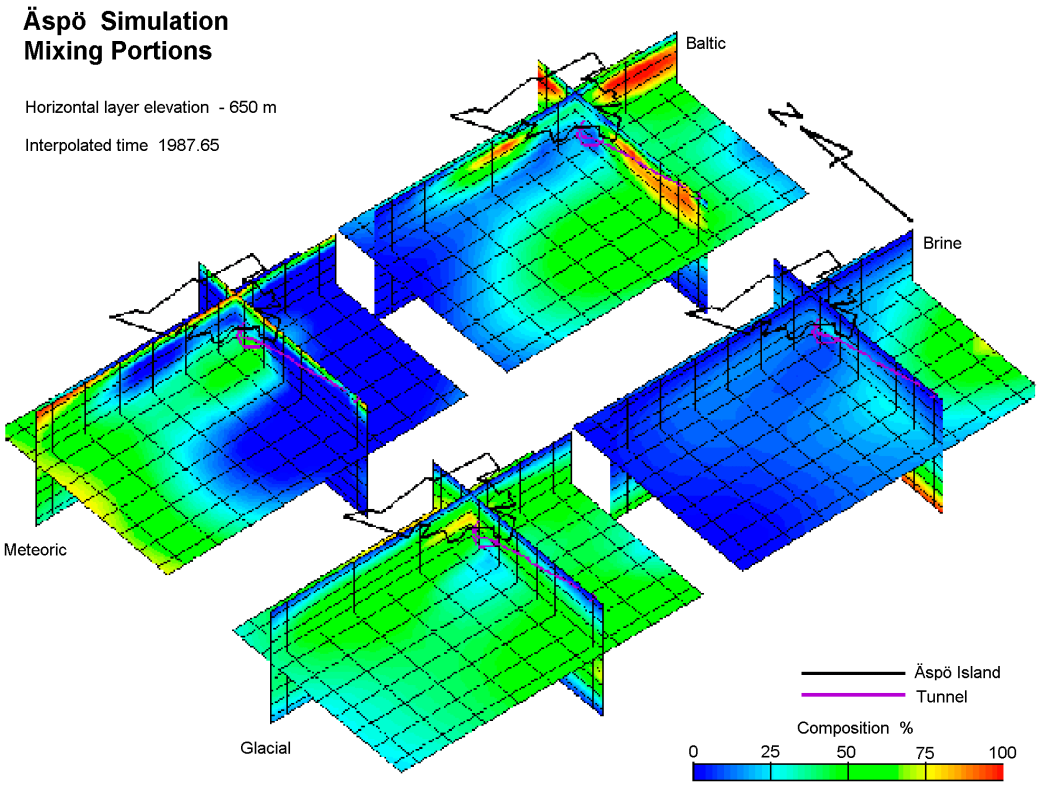

Figure 4-5: *The result of the interpolation of M3 mixing proportion calculations (Composition %) for Meteoric, Glacial, Baltic and Brine waters prior to the Äspö HRL tunnel construction (1987). The contour of Äspö island and the planned extension of the HRL tunnel are shown (for orientation see Figure 2-1). The horizontal cutting plane is at –650m depth.*

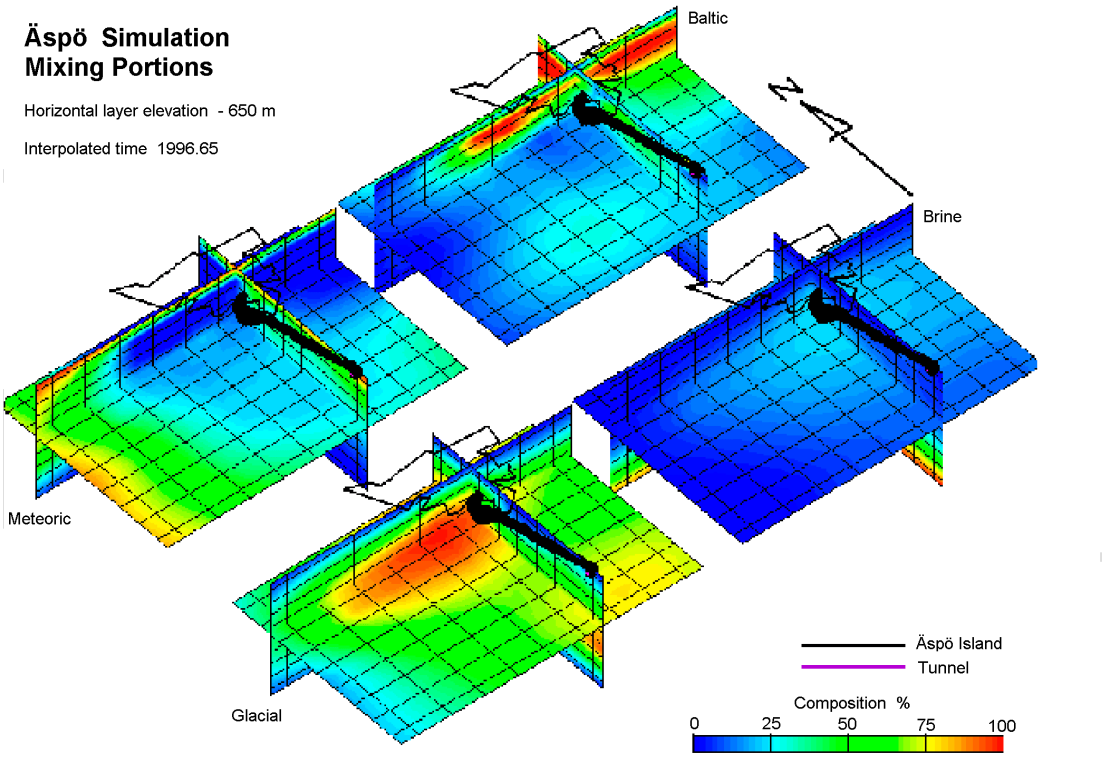

Figure 4-6: *The result of the interpolation of M3 mixing proportion calculations (Composition %) for Meteoric, Glacial, Baltic and Brine waters after the Äspö HRL tunnel construction (1996). The contour of Äspö island and the extension of the HRL tunnel are shown (for orientation see Figure 2-1). The horizontal cutting plane is at –650m depth.*

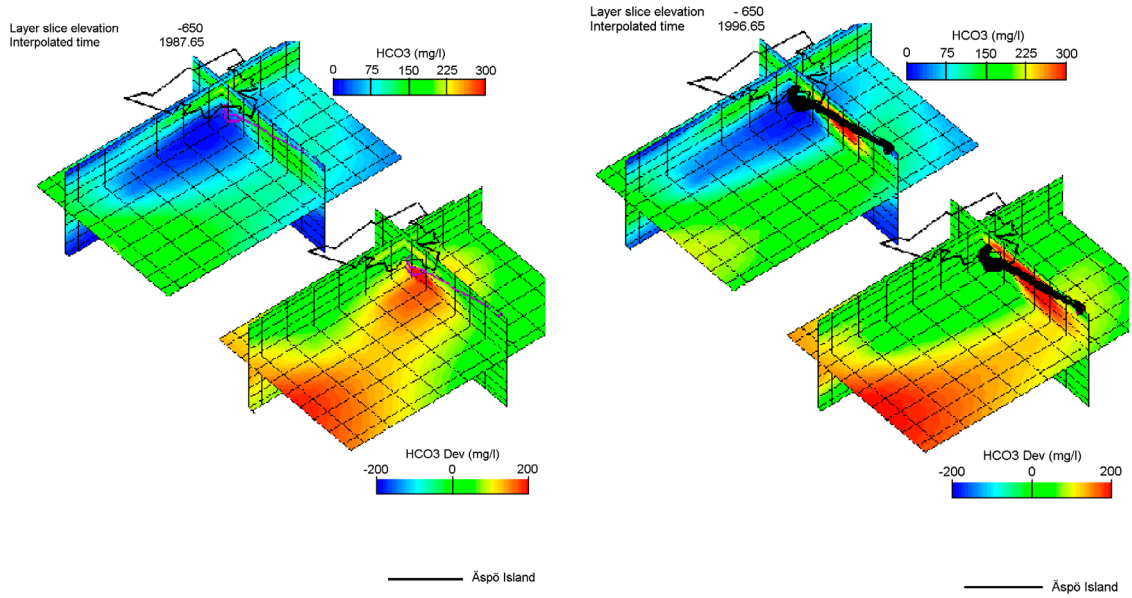

Figure 4-7: *The M3 modelled carbonate (HCO_3) values are compared in the left figure prior to (1987) and in the right figure after (1996) the HRL tunnel construction. The modelled values (deviation = measured values – predicted values) for carbonate show an increasing gain of carbonate associated with the HRL tunnel construction not accounted for by mixing. The increase under land is associated with decomposition of organic matter and calcite dissolution but under the sea the increase is due to sulphate reduction. The contour of Äspö island and the extension of the HRL tunnel are shown (for orientation see Figure 2-1). The horizontal cutting plane is at –650m depth.*

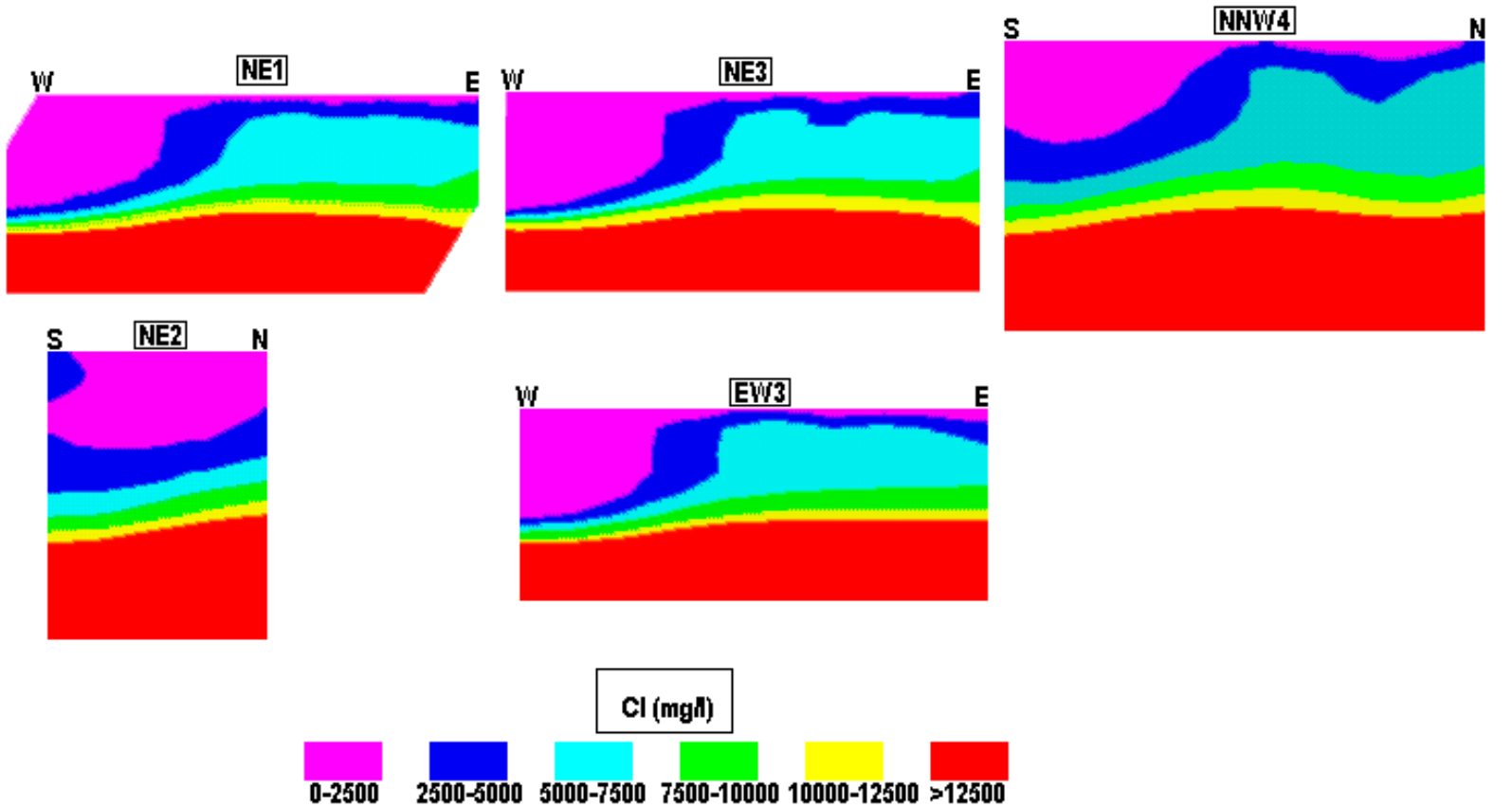

Figure 4-8: *Based on groundwater conditions prior to the HRL tunnel construction (undisturbed conditions), the Cl content (mg/l) along the fracture zones NE-1, NE-3, NNW4, NE2 and EW-3 is shown (for orientation see Figure2-1).*

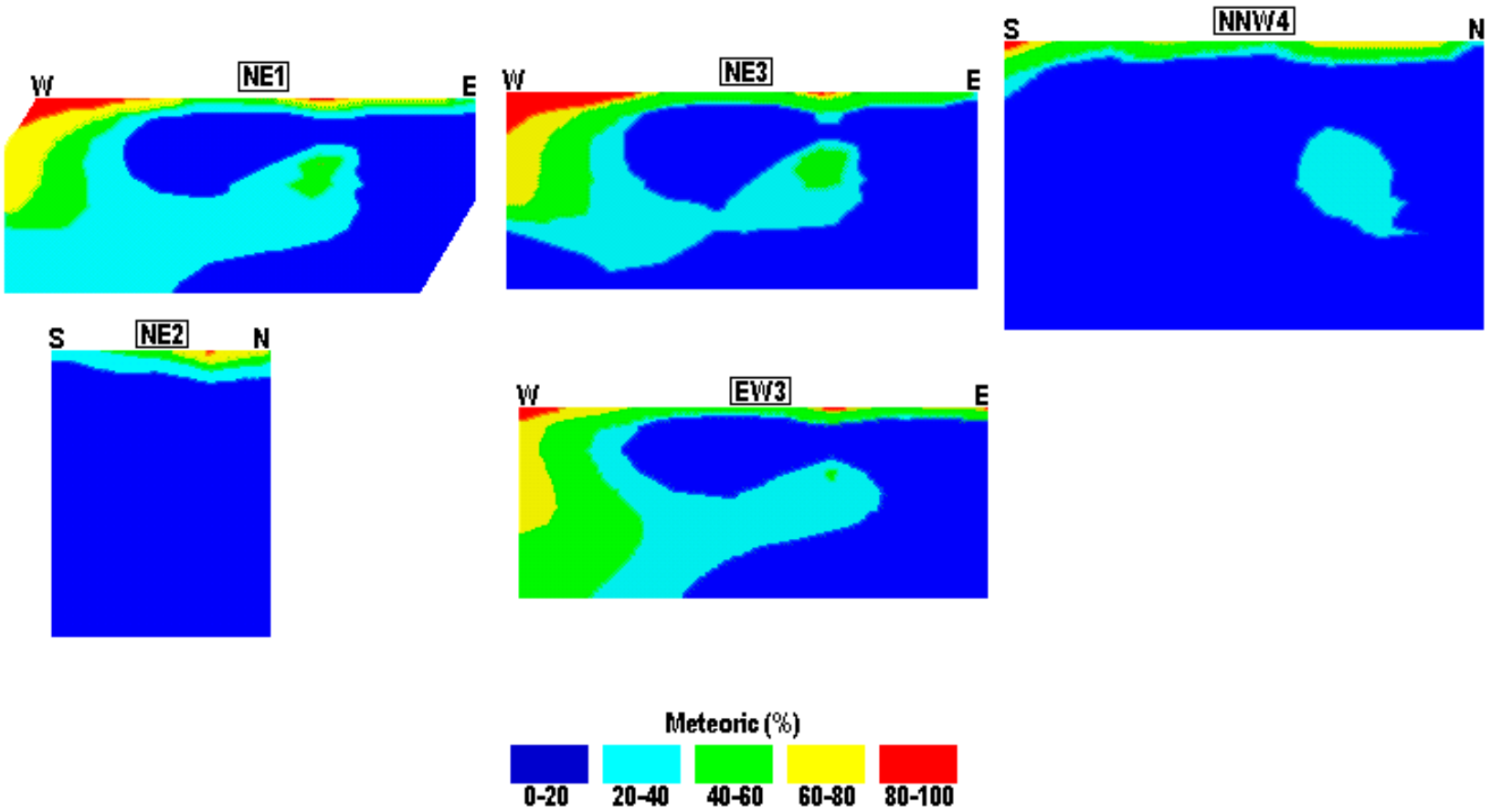

Figure 4-9: *Based on groundwater conditions prior to the HRL tunnel construction (undisturbed conditions), the mixing proportion of Meteoric water (%) along the fracture zones NE-1, NE-3, NNW4, NE2 and EW-3 is shown (for orientation see Figure 2-1).*

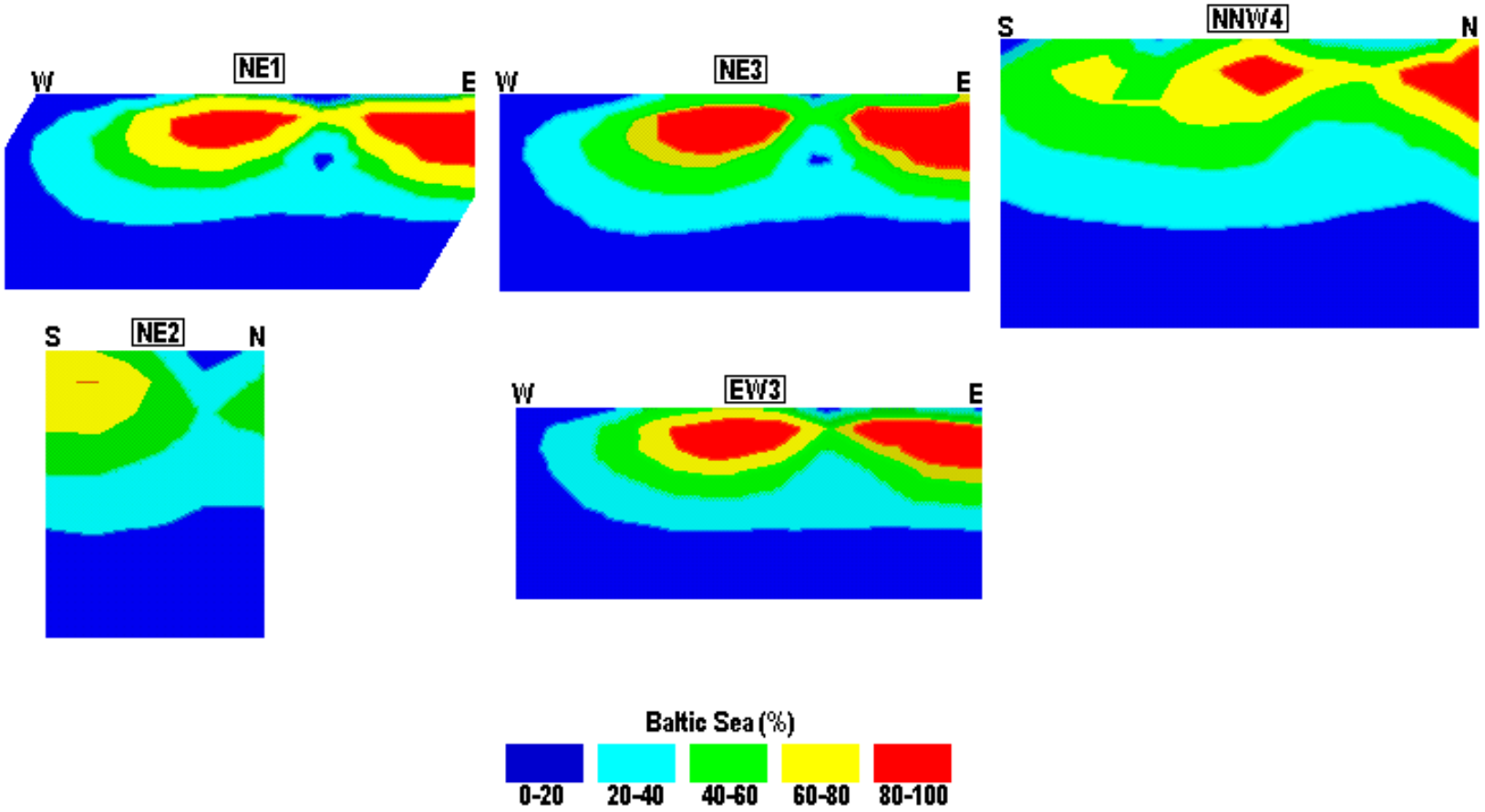

Figure 4-10: *Based on groundwater conditions prior to the HRL tunnel construction (undisturbed conditions), the mixing proportion of Baltic Sea water (%) along the fracture zones NE-1, NE-3, NNW4, NE2 and EW-3 is shown (for orientation see Figure 2-1*

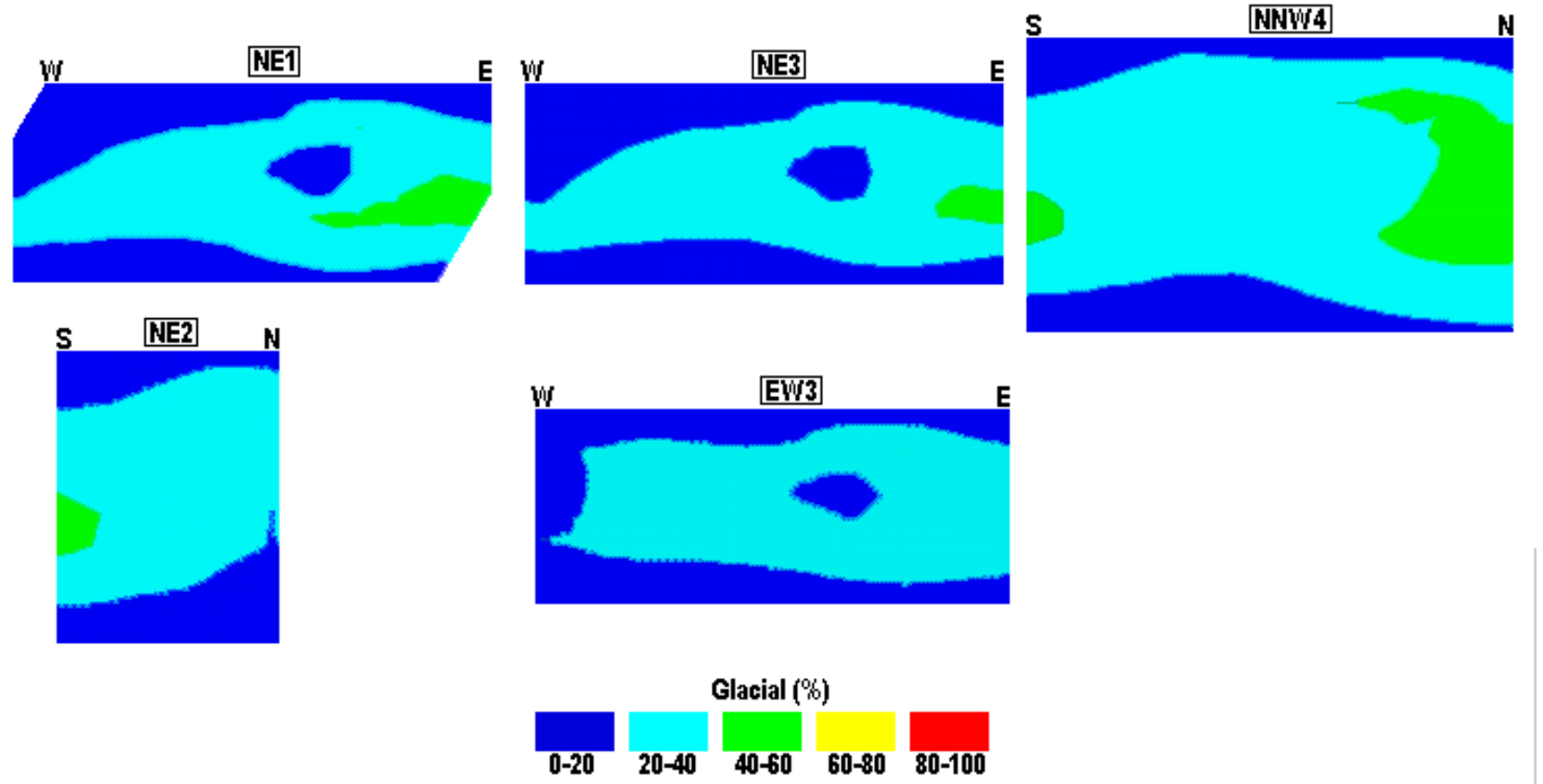

Figure 4-11: *Based on groundwater conditions prior to the HRL tunnel construction (undisturbed conditions), the mixing proportion of Glacial water (%) along the fracture zones NE-1, NE-3, NNW4, NE2 and EW-3 is shown (for orientation see Figure 2-1).*

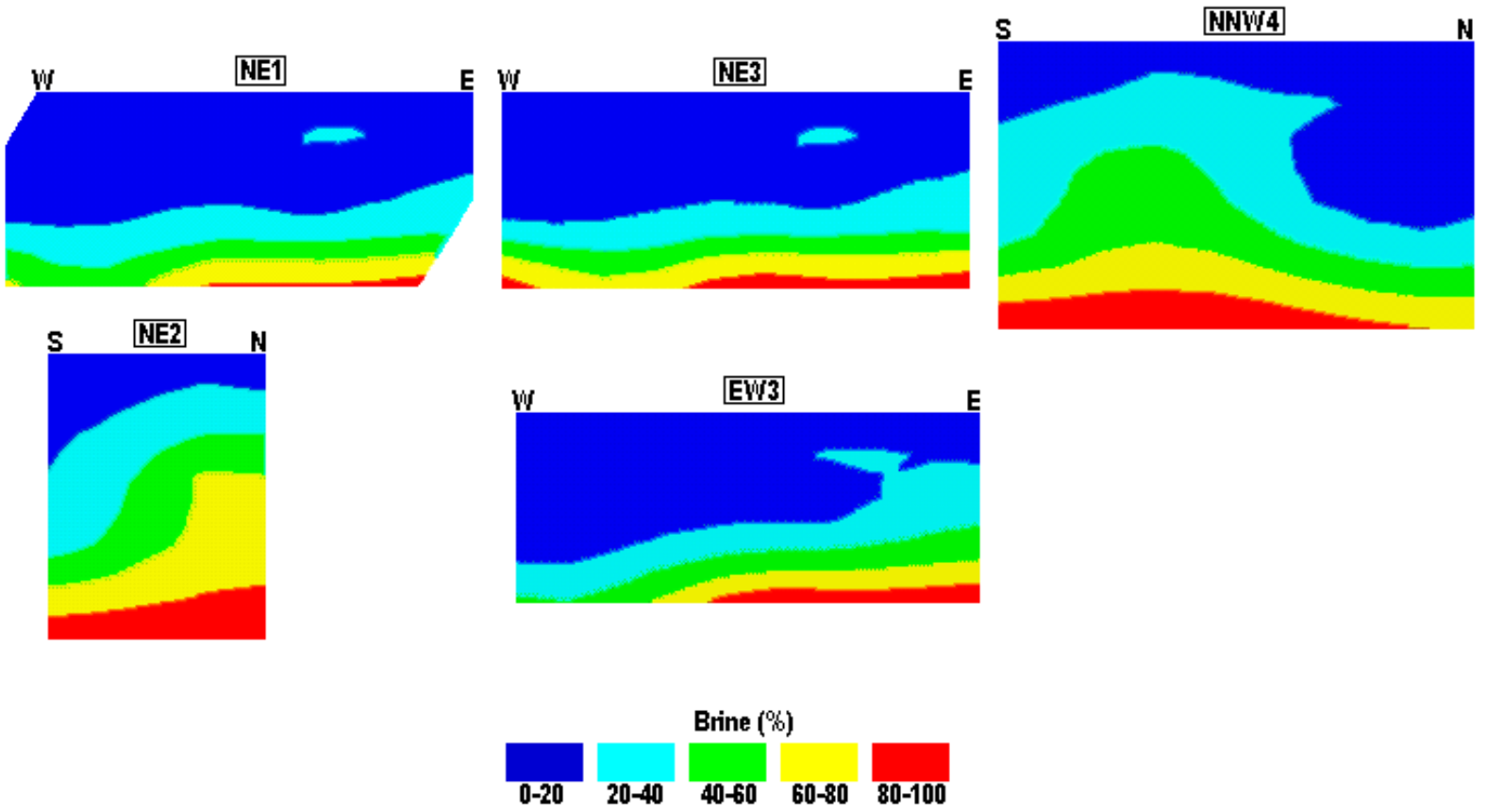

Figure 4-12: *Based on groundwater conditions prior to the HRL tunnel construction (undisturbed conditions), the mixing proportion of Brine water (%) along the fracture zones NE-1, NE-3, NNW4, NE2 and EW-3 is shown (for orientation see Figure 2-1).*

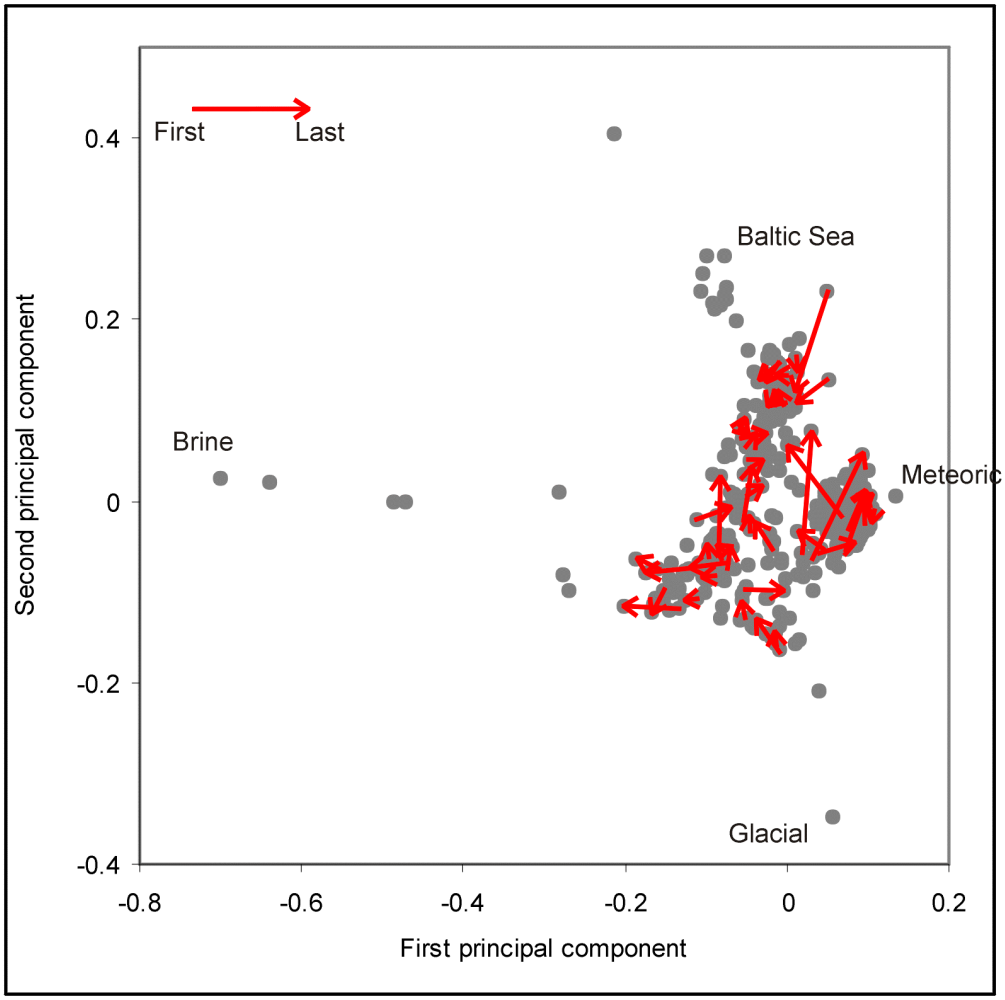

Figure 4-13: *PCA plot used to show the changes in the groundwater composition due to the tunnel construction. First refers to the first sample taking from the time series, Last refers to the last sample of that time series. Note that the arrows represent simplifications of the real development which often is non-linear.*

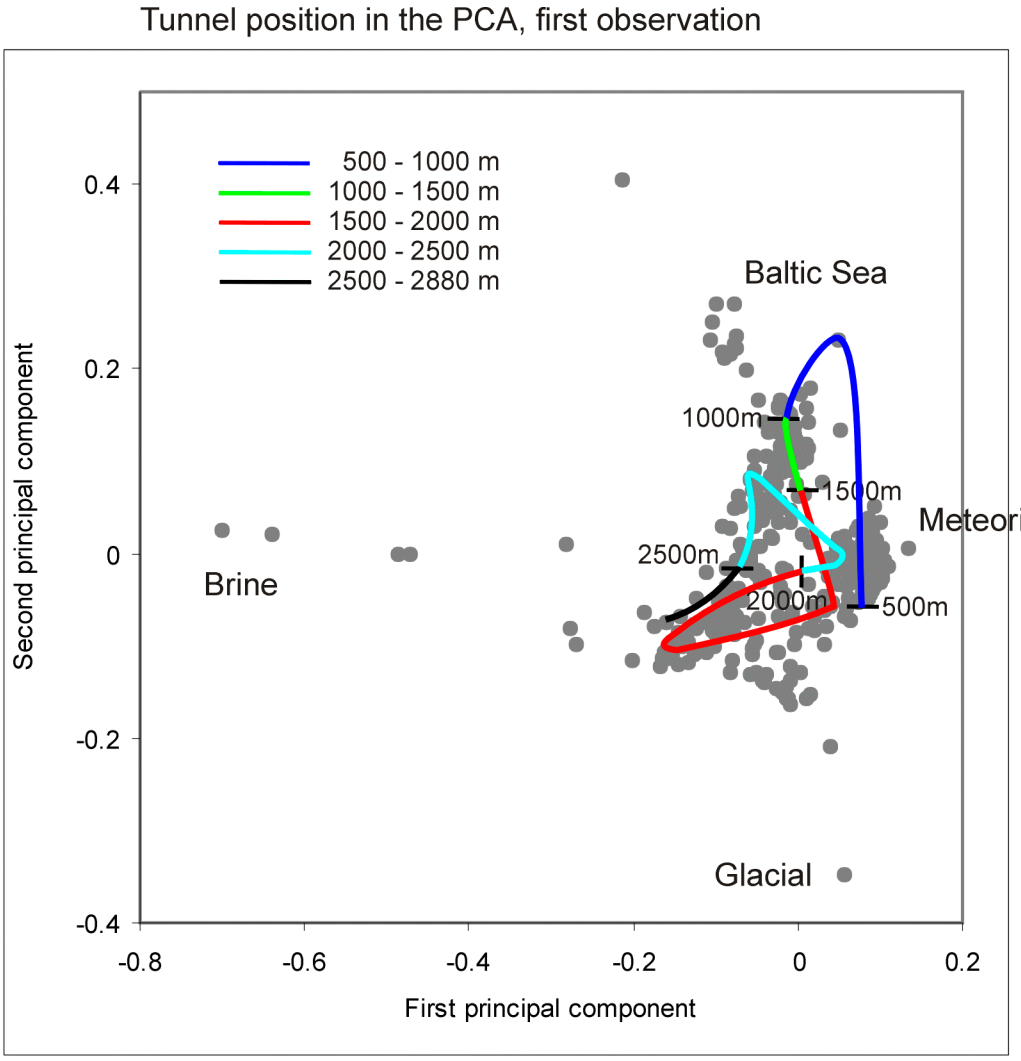

Figure 4-14: *PCA plot used to show the general (simplified) changes in groundwater composition in the samples along the tunnel for the first sample in the time series. The tunnel length and the orientation is shown in Figure 2-1. The 500-1000m tunnel section shows that the groundwater changes from meteoric towards a marine signature due to the fact that the tunnel starts under the land and continues under the sea. The 1000-2000m tunnel section shows a change from marine to meteoric, glacial, brine signature and then back to a meteoric signature due to the fact that this section starts under the sea and then continues under the land of Äspö and ends in the first tunnel spiral. The 2000-2880m section represents the end of the first and the beginning of the second spiral of the tunnel. The water types change from meteoric to marine and then towards a more brine signature. The reason for the groundwater changes along the tunnel is that the tunnel penetrates different fracture zones located under land, sea and at great depth, which contain different groundwater signatures and hence are reflected in the PC-plot. The variations can only be described by simultaneous changes of all variables as result of mixing and evolution of the water. Non-systematic changes such as analytical errors in some variables do not significantly move the position of the points in the PC-plot (see Appendix 3).*

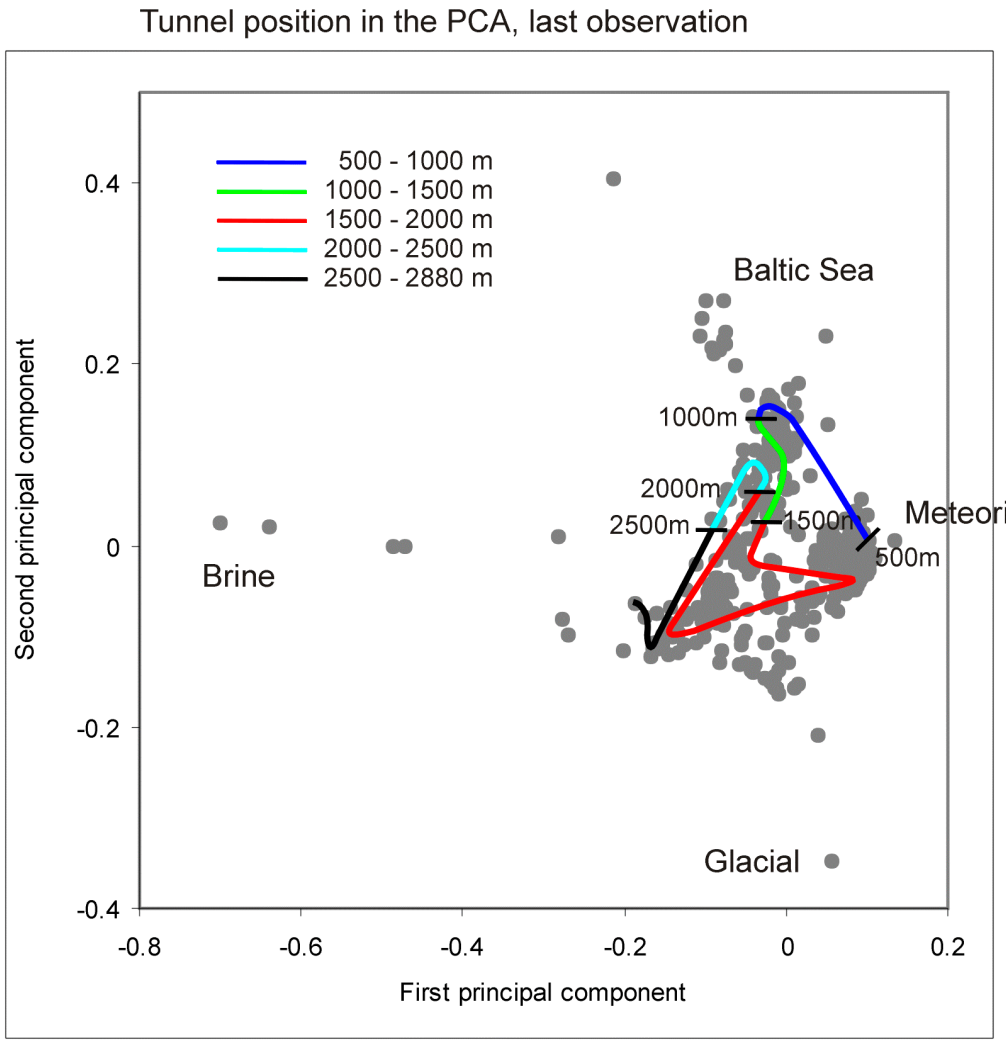

Figure 4-15: *PCA plot used to show the general (simplified) changes in groundwater composition in the samples along the tunnel for the last sample in the time series. The tunnel length and the orientation are shown in Figure 2-1. The 500-1000m tunnel section shows that the groundwater changes from meteoric towards a marine signature due to the fact that the tunnel starts under the land and then continues under the sea. The 1000-2000m tunnel section shows a change from marine to meteoric, glacial, brine signature and then back to marine signature due to the fact that this section starts under the sea and then continues under the land of Äspö and ends in the first tunnel spiral. Note that the water type at about 2000m has changed from meteoric in the initial samples (Fig. 4-14) to marine/Baltic in the last samples, showing that intrusion of Baltic water is a dominant process here. The 2000-2880m section represents the end of the first and the beginning of the second spiral of the tunnel. The water types change from marine towards a more brine signature. The reason for the groundwater changes along the tunnel is that the tunnel penetrates different fracture zones located under land, sea and at great depth, which contain different groundwater signatures and hence are reflected in the PC-plot. The variations can only be described by simultaneous changes of all variables as result of mixing and evolution of the water (see Appendix 3). Comparing with Figure 4-14 (first samples) the waters in this plot show less variation but also a tendency to be pulled towards the centre of the plot. The reason is that these samples are more mixed than the first collected samples in Figure 4-14. The most mixed waters occur in the centre of the plot.*

5 PREDICTIVE MODEL CONSTRUCTION

5.1 MIXING PROPORTIONS AND GEOMETRY

In order to be able to relate the groundwater changes to locations in the Äspö site, depth (Figure 5-1) and x-y co-ordinates (Figures 5-2 and 5-3) were plotted versus calculated changes in mixing proportions. A systematic change might indicate a correlation which could be used for predicting future changes.

Figures 5-1, 5-2 and 5-3 show a complex relation between the changes in mixing proportions and location, indicating the complexity of the changes due to the tunnel construction. This approach was not used further in developing a method to extrapolate mixing changes over time.

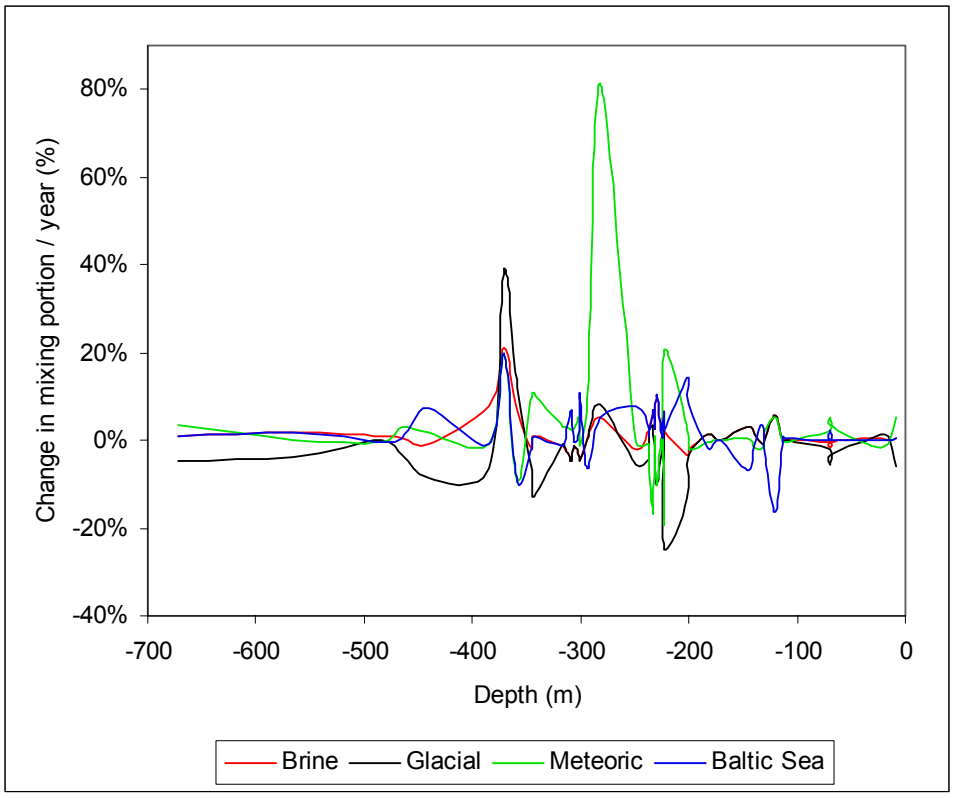

Figure 5-1: *Plot of depth versus calculated changes in mixing proportions between the first and last sample in the time series from Äspö. The calculations were made for changes in Brine, Baltic Sea, Glacial and Meteoric water portions.*

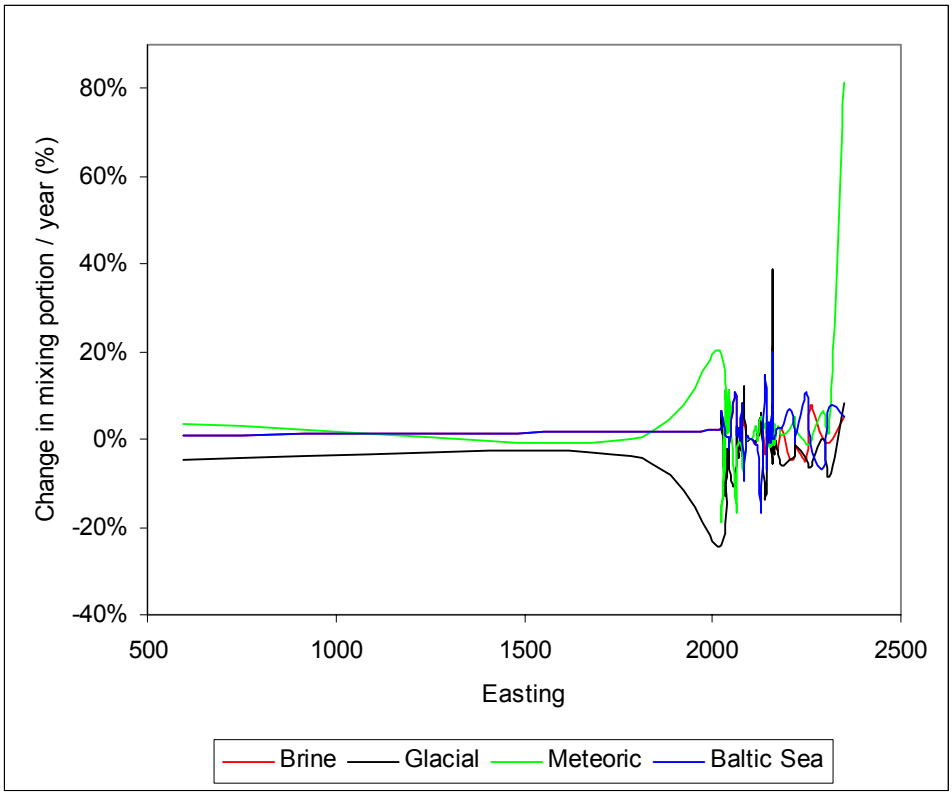

Figure 5-2: *Plot of x co-ordinates (easting) versus the calculated changes in mixing proportions between the first and last sample in the time series from Äspö. The calculations were made for changes in Brine, Baltic Sea, Glacial and Meteoric water portions.*

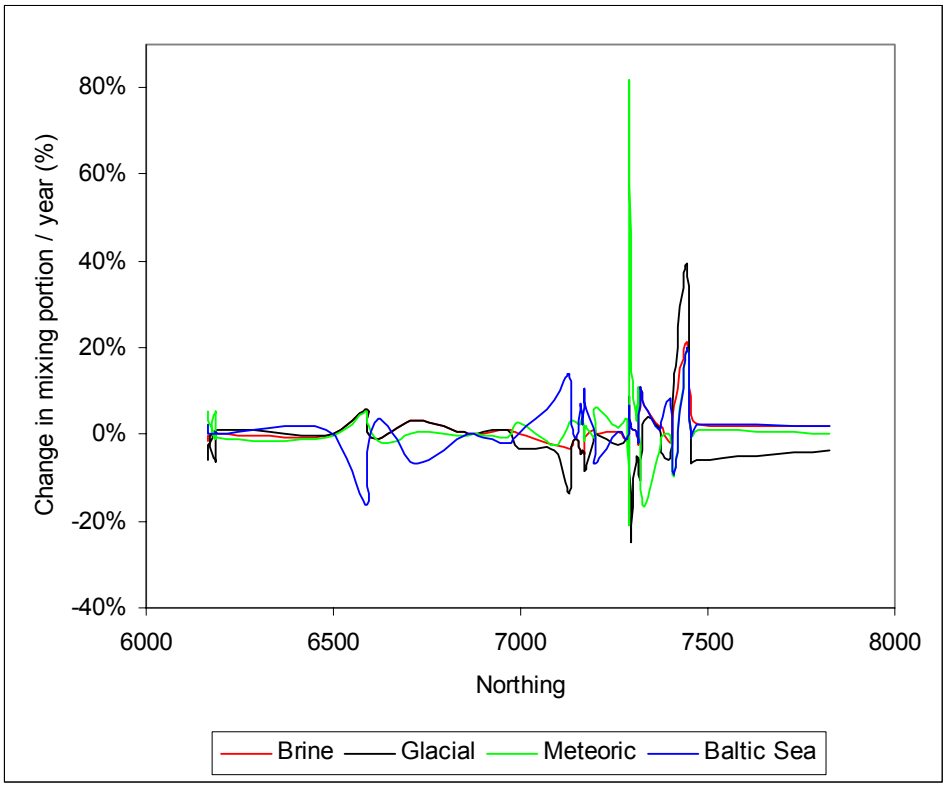

***Figure 5-3**: Plot of y co-ordinates (northing) versus the calculated changes in mixing proportions between the first and last sample in the time series from Äspö. The calculations were made for changes in Brine, Baltic Sea, Glacial and Meteoric water portions.*

5.2 MIXING PROPORTIONS AND HYDRAULIC PARAMETERS

The possibility of correlation between hydraulic parameters and water composition was investigated. This was done by checking both the hydraulic properties and the groundwater compositions for a number of sampled sections. The hydraulic parameters investigated were the hydraulic conductivity K (m/s) and the transmissivity T (m^2/s).

As an example, Figure 5-4 shows the hydraulic conductivity plotted versus the mixing proportions; no correlation between the K and mixing proportions is observed. The explanation could be that the hydraulic parameters do not reflect a large hydraulic variety of the sampled sections, and also that the mixing proportions reflect processes in the whole rock domain.

Another way of studying this was to superimpose a hydrodynamic parameter (K or T) on the PCA chemical data plot. No specific correlation or trends were observed between the chemical parameters and the hydraulic conductivity, as seen in Figure 5-5.

Finally, the changes in the mixing proportion per year were compared with the transmissivity and conductivity values respectively. As seen in Figure 5-6 there were no specific trends observed.

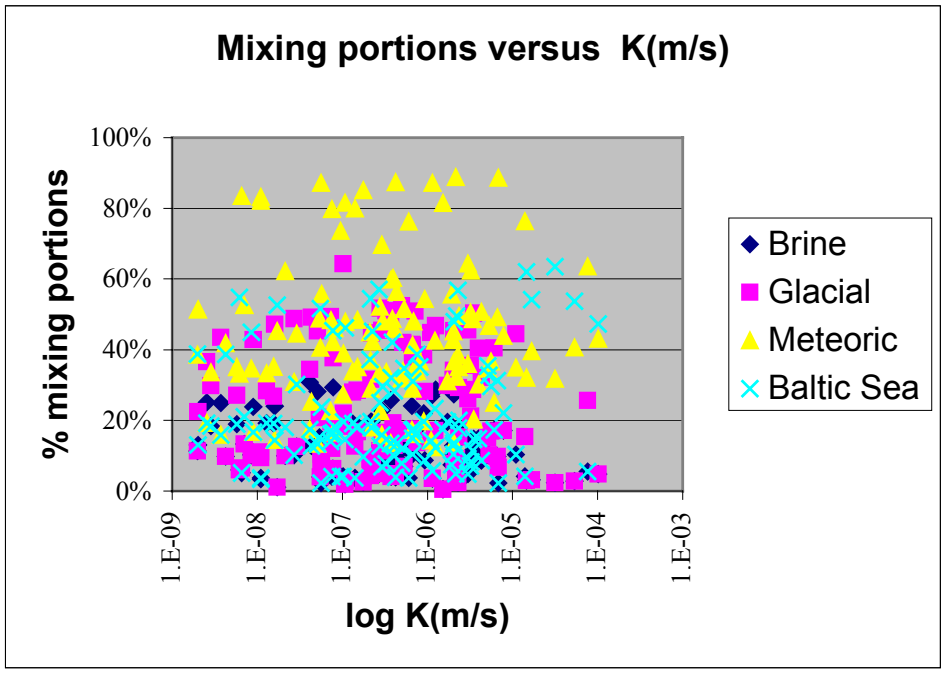

Figure 5-4: *Correlation between the meteoric, Baltic Sea, glacial and brine mixing proportions and hydraulic conductivity (log K(m/s)). No correlation between the mixing proportions and the hydraulic conductivity is observed.*

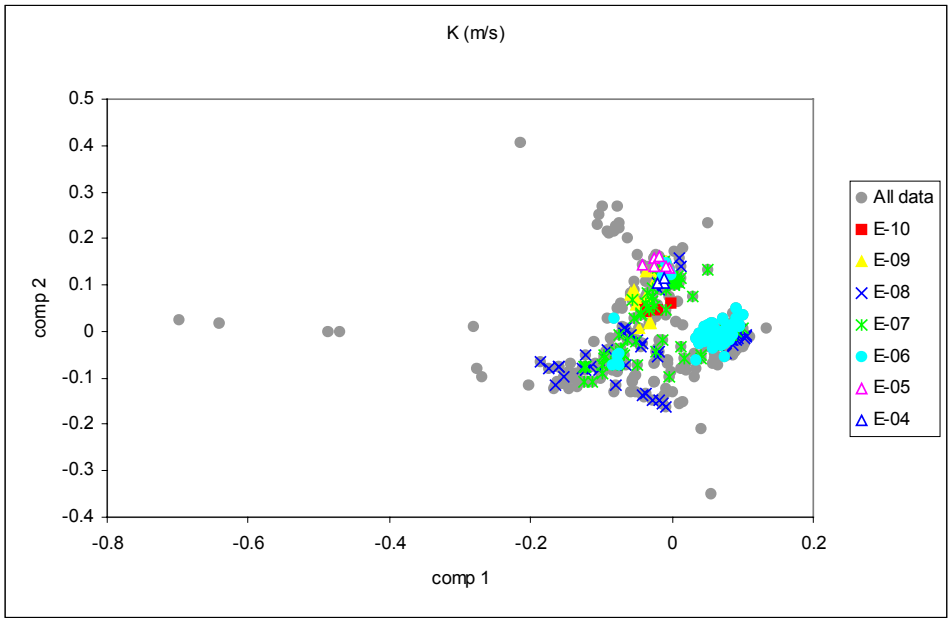

Figure 5-5: *PCA plot based on the chemical variables (i.e. the major elements and the environmental isotopes) included in the M3 analysis. The hydraulic conductivity values are superimposed as an independent variable. No correlation or specific trends were observed between the chemical parameters and the hydraulic conductivity.*

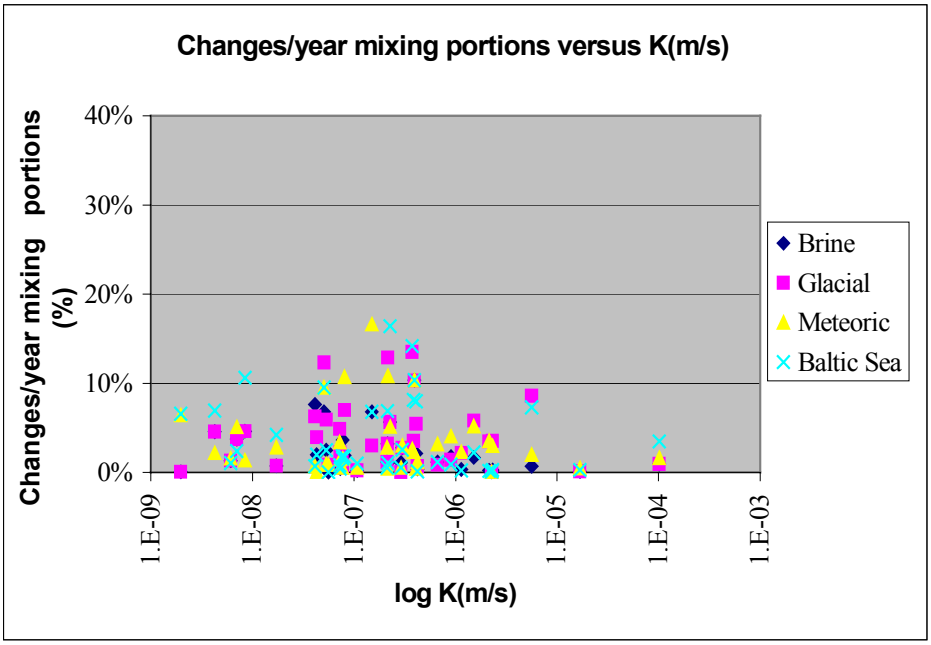

Figure 5-6: *Correlation between the changes in the mixing proportion per year and hydraulic conductivity (log K(m/s)). No correlation between the changes in the mixing proportions and the hydraulic conductivity is observed.*

5.3 GROUNDWATER CHANGES OVER TIME AT TUNNEL POSITION <2900m

Several tests were made to create a *Groundwater Calculation Model* or a "recipe" for the changes in the groundwater composition due to the tunnel construction. The model is empirical and predicts future changes on the basis of an extrapolation using the initial reference water proportions and the average observed rate of change in those proportions over time. This is just a test of whether changes over time are linear and if they can reasonably be averaged out and then used to predict future changes. It is important to note that these calculations represent a simplistic modelling of groundwater changes that are expected in the short term; models containing hydrodynamic and geological information are still necessary for long term predictions. The following strategies and models were selected:

- Divide the groundwaters into classes using PCA where the dominating reference water type in the first sample in the time series determines its class (Meteoric, Baltic, Glacial or Brine); this step was carried out to identify changes associated with the different water types.

- Calculate the changes in mixing proportions between the first and last sample in the time series collected from the boreholes at <2900m.

- Divide the changes in mixing proportions by the number of years to get an annula rate of change.

- Use the average change to add or remove mixing proportions from the first sample in the time series, to predict water compositions for the last sample at each control point.

- Compare the predicted water composition with the measured one (last sample).

To collect information for the groundwater prediction model the changes in the mixing proportions for the whole Äspö site (Table 5-1) and for a limited data set containing data from the Äspö island (Table 5-2) were examined. To make the comparison easier the mixing proportions were normalised to changes in mixing proportions (%) per year.

Table 5-1: Observations from the *Äspö site* (regional model) divided into three classes (Glacial, Meteoric and Baltic Sea) depending on the dominating mixing proportion in the first sample taken from the time series. The mean changes in mixing proportions (%) per year and the mean values for Cl and $\delta^{18}O$ were calculated.

	Brine	Glacial	Meteoric	Baltic Sea	Cl(mg/l)	dO18(o/ooSMOW)
	Diff/y	Diff/y	Diff/y	Diff/y	Diff/y	Diff/y
Mean Glacial	2.2%	-3.3%	1.0%	0.0%	876	0.3
Mean Meteoric	0.0%	-3.8%	-0.6%	4.4%	350	0.5
Mean Baltic Sea	0.6%	0.6%	1.4%	-2.7%	-548	-0.2
Avarage changes	0.9%	-2.6%	0.4%	1.4%	326	0.3

Table 5-2: Observations only from *Äspö island* (local model) divided into three classes (Glacial, Meteoric and Baltic Sea) depending on the dominating mixing proportion in the first sample from the time series. The mean changes in mixing proportions per year and the mean values for Cl and $\delta^{18}O$ were calculated.

	Brine	Glacial	Meteoric	Baltic Sea	Cl(mg/l)	dO18(o/ooSMOW)
	Diff/y	Diff/y	Diff/y	Diff/y	Diff/y	Diff/y
Mean Glacial	2.3%	-3.2%	0.8%	0.0%	952	0.2
Mean Meteoric	0.1%	-4.8%	-2.0%	6.7%	649	0.7
Mean Baltic Sea	-0.7%	-0.7%	1.2%	0.3%	-404	0.0
Avarage changes	0.9%	-3.3%	-0.2%	2.6%	584	0.3

The mean changes from the regional model above were used to extrapolate from the mixing proportions for the first sample to mixing proportions for the last sample at each control point. Some test results using the regional model are shown in Figure 5-7. Figure 5-7 shows that the predictions have similar errors and predict generally the magnitude, but not necessarily the direction of the groundwater change.

Table 5-3 shows that the average difference in mixing proportions between the predicted and the measured values is less than 2%. Table 5-4 shows that the major components vary in the way that some are over-predicted (positive values) and others are under-predicted (negative values). It is important to note that during sampling a variation of 2000mg/l Cl or more is normally obtained. The average difference for $\delta^{18}O$ is less than 1 unit which is regarded as highly accurate. For more details concerning the deviation between the predicted and measured values for the different groundwater samples, see Appendix 1.

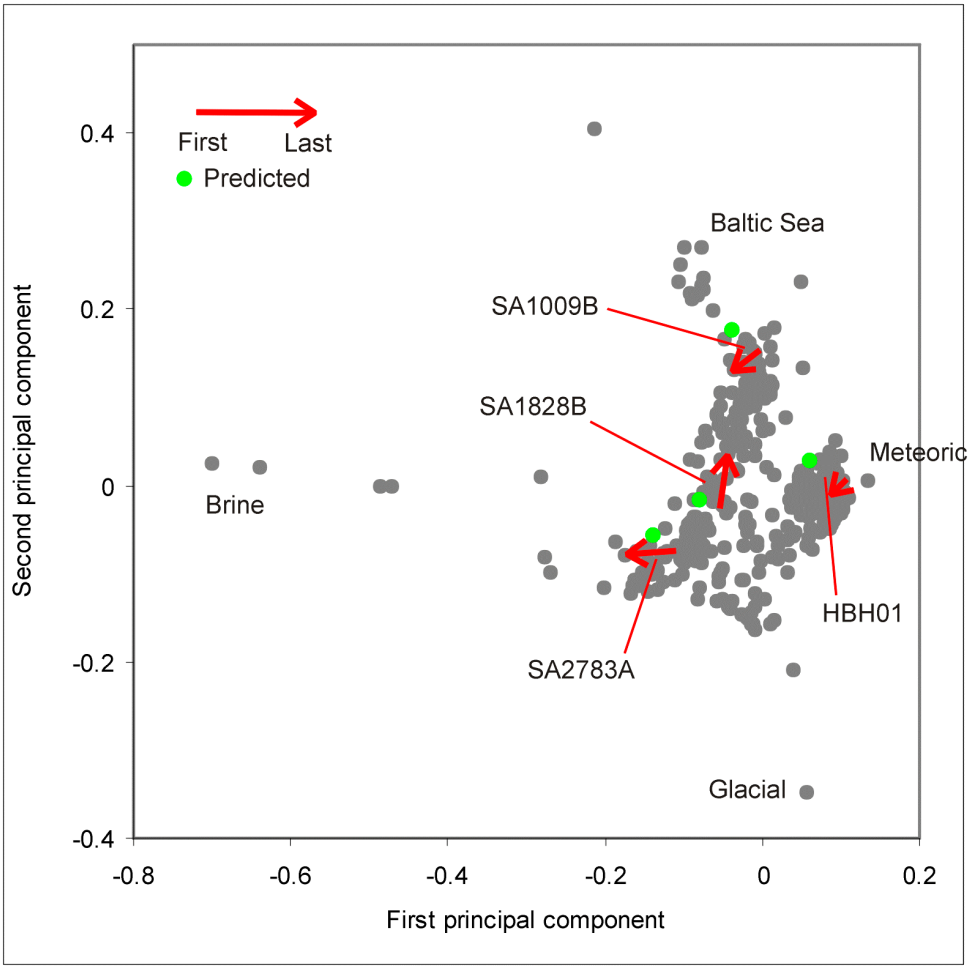

Figure 5-7: *Compositions of groundwaters at time of last sampling, estimated with the regional M3 model of changes over time (green dot) compared with actual first and last analyses (red arrow) of groundwater samples at some control points. The arrow represents the development in the measured groundwater composition between the first and last sample in the time series. The observed groundwater changes are generally gradual changes but dependent of the progress of the tunnel front during the Äspö-HRL construction.*

Table 5-3: Comparison between average differences for mixing proportion calculations between predicted and measured values. The comparison is based on all Task#5 data with the time series.

	Brine	Glacial	Meteoric	Baltic Sea
Average difference	**1.2%**	**-0.9%**	**-0.1%**	**-0.3%**

Table 5-4: Comparison between average differences for major elements, stable isotopes and tritium between predicted and measured values. The comparison is based on all Task#5 data with the time series.

	Na (mg/l)	K (mg/l)	Ca (mg/l)	Mg (mg/l)	CO3 (mg/l)	Cl (mg/l)
Average difference	**-91**	**18**	**1356**	**-31**	**-128**	**2199**

	SO4 (mg/l)	D (o/oo)	Tr (TU)	O18 (o/oo)
Average difference	**-99**	**-8**	**39**	**-1**

5.4 COMPARISION OF OBSERVED AND EXTRAPOLATED COMPOSITIONS AT TUNNEL POSITIONS <2900m

In order to compare the extrapolated values with the measured values the following properties were selected: Cl, $\delta^{18}O$ (water conservative), and the mixing proportion calculations for Meteoric water and the HCO_3 which were affected by reactions (Figures 5-8, 5-9, 5-10 and 5-11). The data used for this comparison were the distributed data from the HRL tunnel positions <2900m. Data were interpolated and visualised with the Voxel Analyst computer code.

Figures 5-8, 5-9 and 5-10 show a reasonable agreement between the measured and calculated groundwater compositions; Figure 5-11 less so. The deviations are generally smaller than the known uncertainties from natural variation, sampling uncertainties and modelling variations.

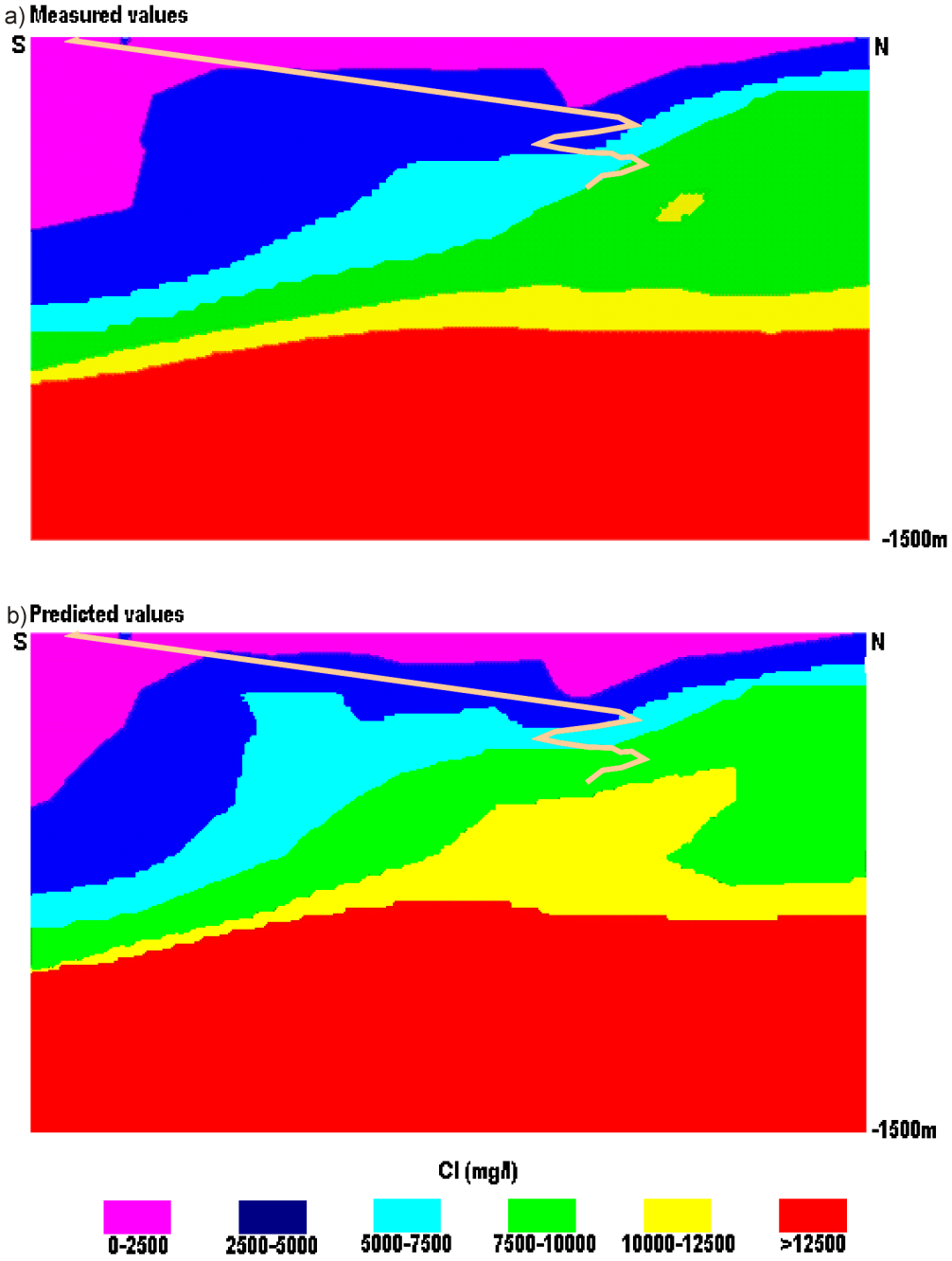

Figure 5-8: *Visualisation of the Cl concentration for the measured and calculated values. The cutting plane is N-S along the Äspö HRL tunnel.*

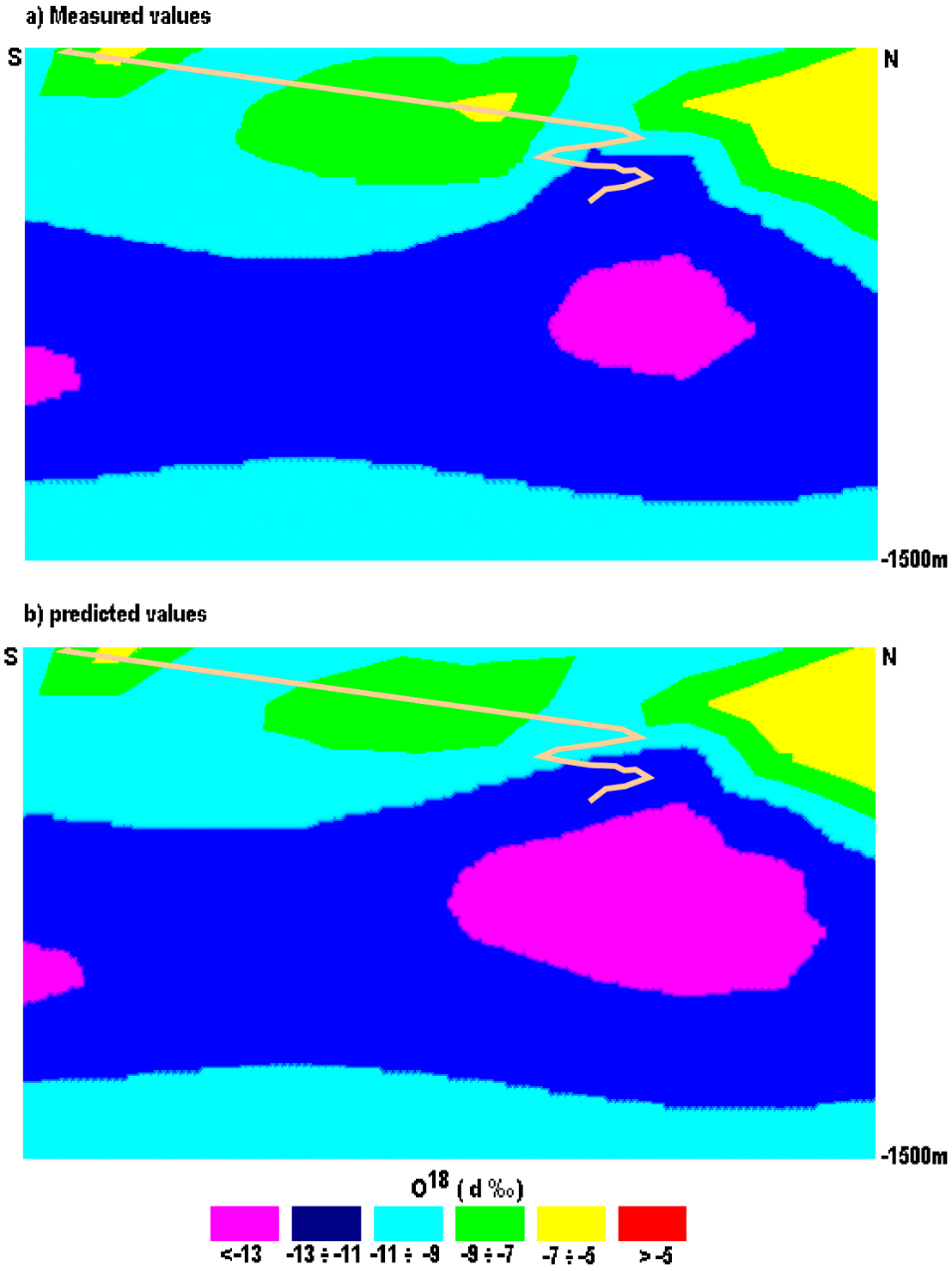

Figure 5-9: *Visualisation of $\delta^{18}O$ content for the measured and calculated values. The cutting plane is N-S along the Äspö HRL tunnel.*

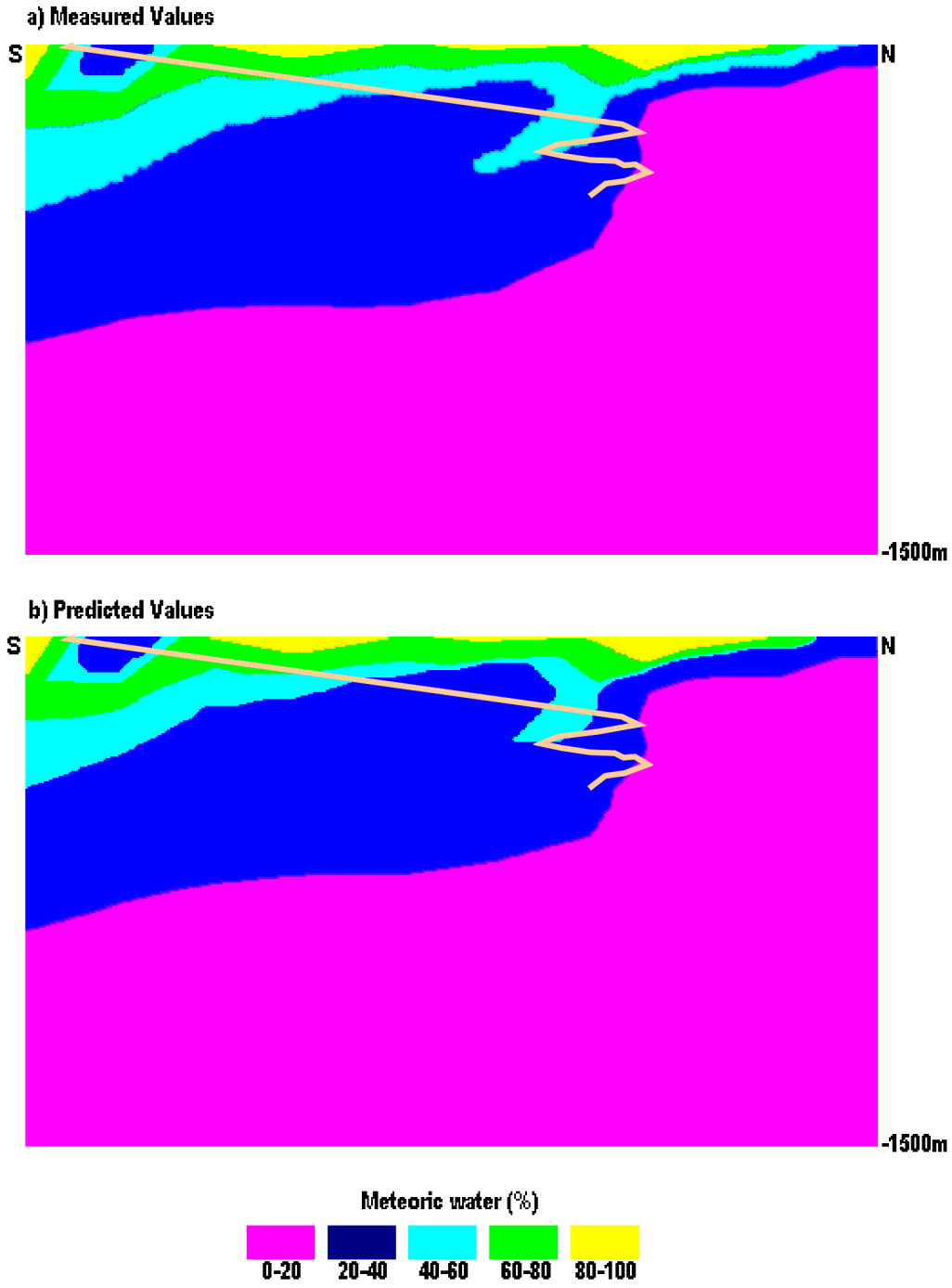

Figure 5-10: *Visualisation of the mixing proportion calculations for Meteoric water showing the mixing calculations based on measured and calculated groundwater compositions. The cutting plane is N-S along the Äspö HRL tunnel.*

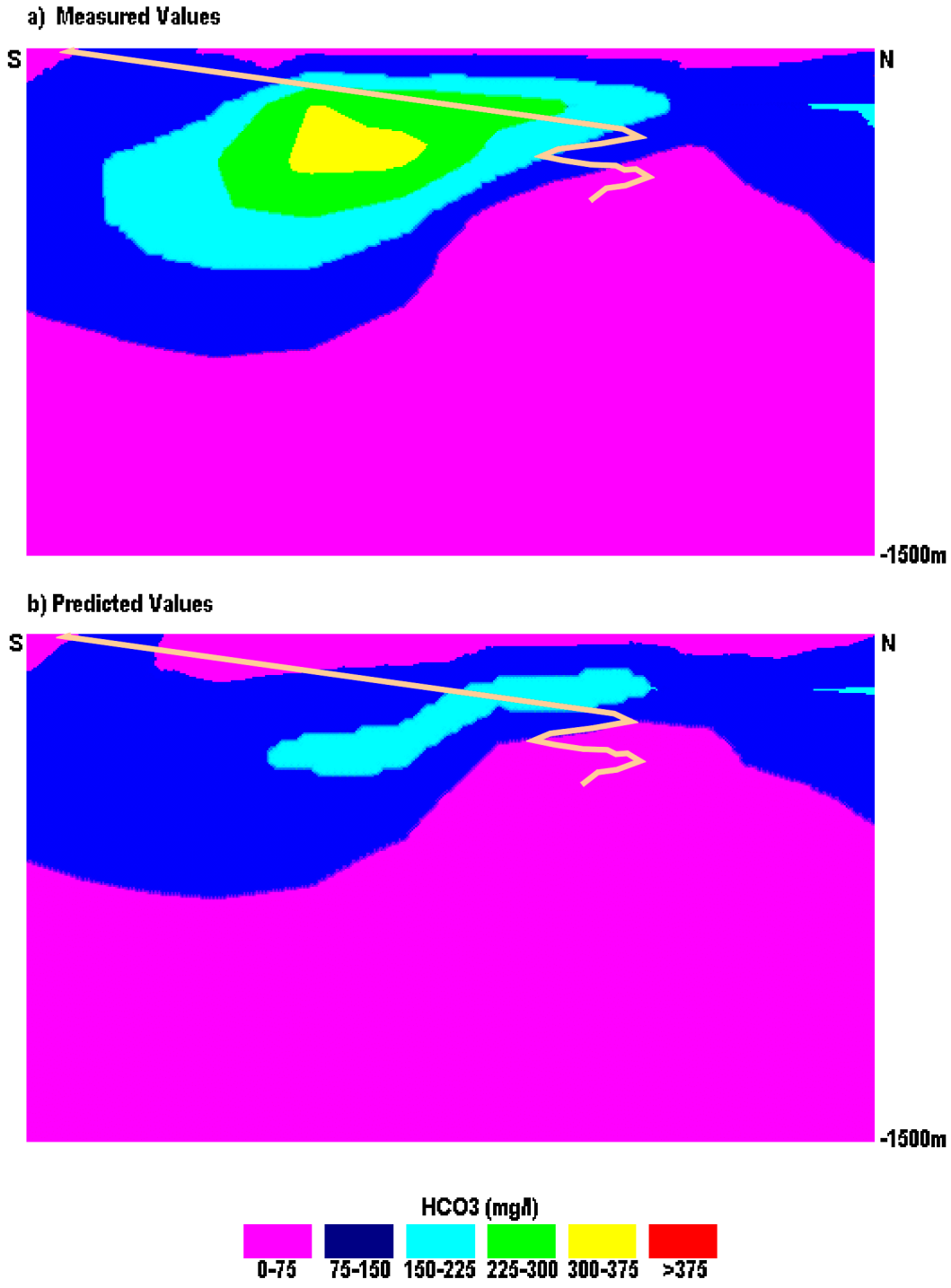

Figure 5-11: *Visualisation of HCO_3 concentration for the measured and calculated values. The cutting plane is N-S along the Äspö HRL tunnel.*

5.5 CALCULATIONS >2900m IN THE HRL TUNNEL

Five Control Points (CP) with positions >2900m in the HRL tunnel were suggested to be used for predictions and verifications of the models in Task #5. The name and the coordinates of the control points are listed in Table 5-5.

Table 5-5. Control points: name, date of sampling and coordinates.

ID code	Date	Secup	Seclow	Centr.	Northing	Easting	Elevation
KAS03	940412	533.0	626.0	579.5	7825.4	1781.8	-566.3
KAS07	940906	501.0	604.0	552.5	6995.8	2042.2	-465.0
KA3005A	941207	0.0	58.1	29.1	7422.2	2338.5	-402.2
KA3005A	950310	36.9	37.9	37.4	7426.3	2331.3	-402.8
KA3005A	960411	44.8	45.8	45.3	7430.2	2324.4	-403.4
KA3110A	950310	20.1	28.6	24.3	7299.2	2331.7	-416.0
KA3110A	980306	20.1	28.6	24.3	7299.2	2331.7	-416.0
KA3385A	950111	0.0	34.2	17.1	7234.8	2091.1	-447.5
KA3385A	980302	32.0	34.0	33.0	7219.9	2096.3	-448.8
KA3385A	950310	32.1	34.2	33.1	7219.8	2096.3	-448.8

The groundwater compositions at these control points were estimated in two ways:

1. **Interpolation** of the observed data (data set reflecting the tunnel construction) with Voxel Analyst; extracting the values corresponding to the control points coordinates from the 3D model.

2. **Extrapolation** of changes in M3 mixing proportions. The chemical changes in the data set <2900m were used in M3 as a "recipe" for extrapolating the changes in mixing proportions over time for each class of water (as described in Section 5.3). The results were interpolated using the Voxel Analyst and the values corresponding to the control points were extracted from the 3D model.

The values for the control point predictions were extracted from the 3D model of the site (Figures 4-5 and 4-6). As an example, the following figures (Figures 5-12 and 5-13) show the mixing proportions of Meteoric, Baltic Sea, Glacial and Brine waters obtained in 2 cases: Voxel interpolation of mixing proportions from the measured data and the interpolation of the compositions extrapolated using the average rates of change in M3 mixing proportions. In order to extract values from the Voxel model a tilted cutting plane was orientated through the control points. The red points represent the control points. The colour scale represents the values of the different mixing proportions, from light blue (0%) to light green (100%).

In Table 5-6, values from the interpolation and M3 predictions are listed for each control point. The outcome of the predictions is compared with measured values.

The values obtained from the interpolation show that the interpolation values for meteoric water are smaller than the measured values and the Baltic Sea proportions are higher than the measured values. The interpolation model shows more Baltic Sea water than the measured values, especially in the North side of the modelled area (KAS03, KAS07, KA3005A). Also, the Cl values from interpolation are generally higher than the measured values. These results are however in agreement with the hydrodynamic model of the system (see part III in this report). Therefore, we think that these results are biased by the boundary conditions or initial conditions and lack of data in this side of the model. The $\delta^{18}O$ values extracted from the interpolation are in general agreement with the measured values. The values at the control points obtained with the M3 prediction model show consistency with the measured data and interpolation. However, an increase of the Cl predicted values and the Brine predicted proportions at the control points can be observed. The $\delta^{18}O$ values and the Meteoric, Glacial and Baltic proportions predicted at the control points are in good agreement with the measured data and interpolation. M3 predictions show a general agreement with the measured values at the control points.

Measured data: cutting plane through the CP

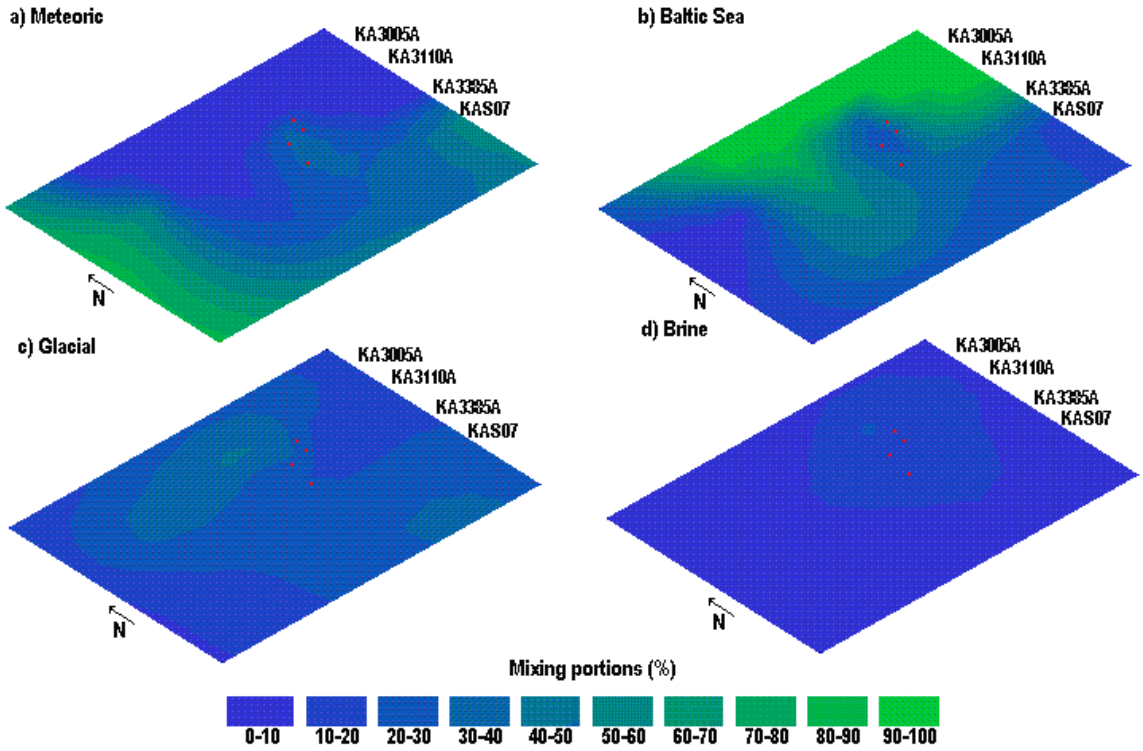

Figure 5-12: *Visualisation of the meteoric, Baltic Sea, glacial and brine mixing proportions based on measured values and Voxel interpolation. The cutting plane is placed at the repository depth, at the elevation of the control points KA3005A, KA3110A, KA3385A and KA3005A elevations. (The control point KAS03, which is situated more North, was modelled by using another cutting plane.)*

M3 predictions: cutting plane through the CP

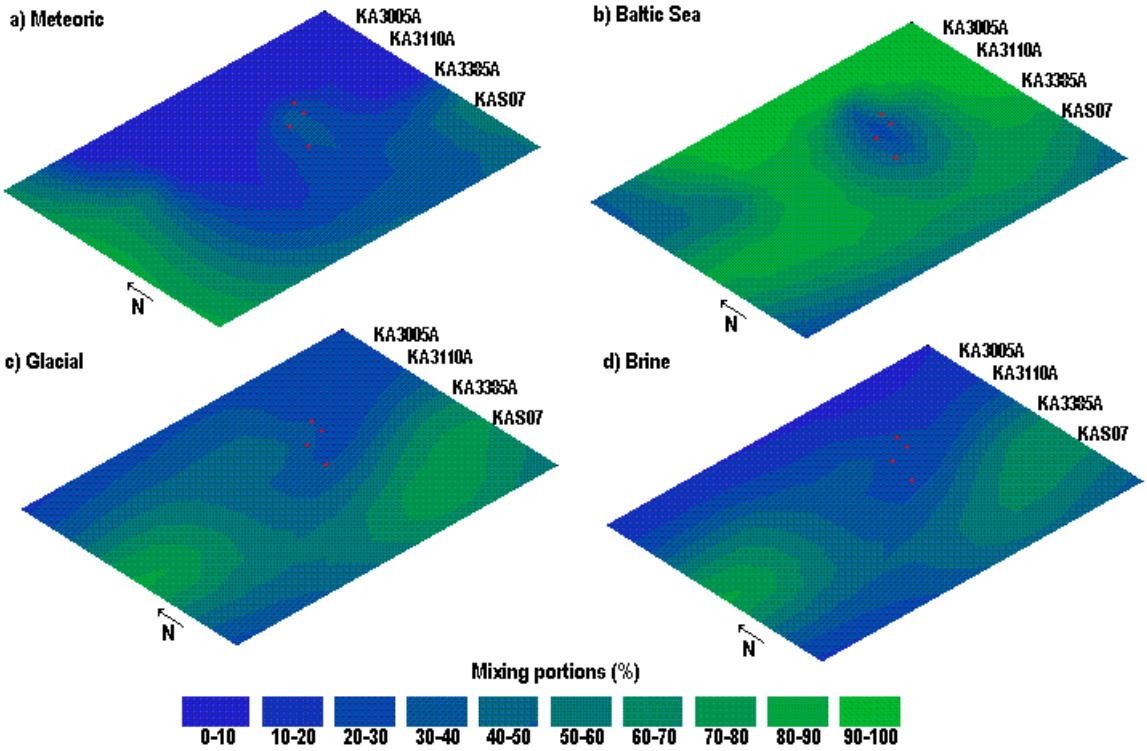

Figure 5-13: *Visualisation of the Meteoric, Baltic Sea, Glacial and Brine mixing proportions based on M3 modelling predictions and Voxel interpolation. The cutting plane is placed at the repository depth, at the elevation of the control points KA3005A, KA3110A, KA3385A and KA3005A elevations. (The control point KAS03, which is situated more North, is modelled by using another cutting plane.)*

Table 5-6. The results of the Voxel interpolation (Voxel) and M3 predictions (M3) are listed for each control point >2900m and are compared with the measured data (given data) for Cl, ^{18}O and mixing proportions for Meteoric water, Baltic Sea water, Brine water and Glacial water.

ID code	Elevation	Cl Measured	Cl Voxel	Cl M3	^{18}O Measured	^{18}O Voxel	^{18}O M3
KAS03	-566.3	4637	6000-7000	6000-7000	-13.6	<-13	<-13
KAS07	-465.0	5960	5000-6000	8000-9000	-11.2	<-11	-11
KA3005A	-402.2	4870			-9.7		
KA3005A	-402.8	5400	7000-8000	8000-9000	-10	-10	<-10
KA3005A	-403.4	4880			-10		
KA3110A	-416.0	3940	6000-7000	8000-9000	-9.2	-10	<-10
KA3110A	-416.0	3390			-7.7		
KA3385A	-447.5	6650			-10.4		
KA3385A	-448.8	6630	6000-7000	8000-9000	-10.1	-11	<-10
KA3385A	-448.8	6710			-10.5		

ID code	Elevation	Meteoric Measured	Meteoric Voxel	Meteoric M3	Baltic Sea Measured	Baltic Voxel	Baltic M3
KAS03	-566.3	28%	10-20%	10-20%	12%	20-30%	20-30%
KAS07	-465.0	39%	30-40%	30%	17%	20-30%	20-30%
KA3005A	-402.2	53%			19%		
KA3005A	-402.8	52%	20-30%	20-30%	16%	30-40%	30-40%
KA3005A	-403.4	54%			21%		
KA3110A	-416.0	48%	20-30%	30-40%	35%	30-40%	30-40%
KA3110A	-416.0	47%			43%		
KA3385A	-447.5	37%			19%		
KA3385A	-448.8	42%	30-40%	30-40%	18%	20-30%	20-30%
KA3385A	-448.8	36%			19%		

ID code	Elevation	Brine Measured	Brine Voxel	Brine M3	Glacial Measured	Glacial Voxel	Glacial M3
KAS03	-566.3	12%	10-20%	10-20%	47%	40-50%	40-50%
KAS07	-465.0	17%	10-20%	20-30%	27%	20-30%	30%
KA3005A	-402.2	14%			14%		
KA3005A	-402.8	16%	10-20%	20-30%	17%	20-30%	20-30%
KA3005A	-403.4	13%			13%		
KA3110A	-416.0	9%	10-20%	20-30%	9%	20-30%	20-30%
KA3110A	-416.0	5%			5%		
KA3385A	-447.5	19%			25%		
KA3385A	-448.8	18%	10-20%	20-30%	21%	20-30%	30%
KA3385A	-448.8	19%			27%		

6 COMPARISON OF SPATIAL INTERPOLATIONS VERSUS TEMPORAL EXTRAPOLATIONS

All the control points for Task #5 were used for comparison between predictions and measurements. The following modelling methods were compared:

- **Voxel Interpolation** of the measured data (data set reflecting the tunnel construction at <2900m) with Voxel Analyst; the values corresponding to the control point coordinates were extracted from the 3D model. This was performed on the data set from tunnel positions >2900m.

- **Extrapolations** of changes in mixing proportions calculated with M3. The chemical changes in the data set <2900m were used in M3 as a "recipe" for predictions. The results of these predictions were interpolated in Voxel Analyst and the values corresponding to the control points were extracted from the 3D model. This was performed for all CP with time series.

The results of the comparison are shown in Figures 6-1 to 6-6. Most of the control points are along the tunnel, for orientation see Figure 2-1. The tabulated values are listed in Appendix 2.

M3 predictions show a general agreement with the measured values at the control points especially when considering the uncertainty of the predictions which are in the order of ±0.1 units. The precision of the prediction appears to be similar to many models based on detailed hydrodynamic models used within Task #5. M3 can be used for predictive purposes if there is a time series of observations. If this is the case short term predictions (years) can be performed. If long term predictions (hundred of years) are to be performed then the M3 calculations should be guided by a hydrodynamic modelling.

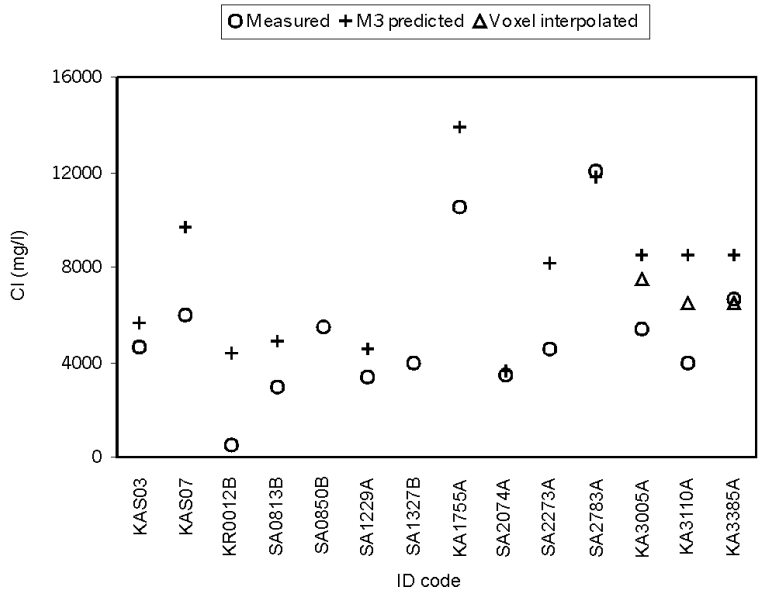

Figure 6-1: *Comparison of the predicted values using M3 and Voxel interpolation with measured data (given values) of Cl (mg/l) for the control points. No predictions are made for the control points SA0850B and SA1327B because of lack of time series.*

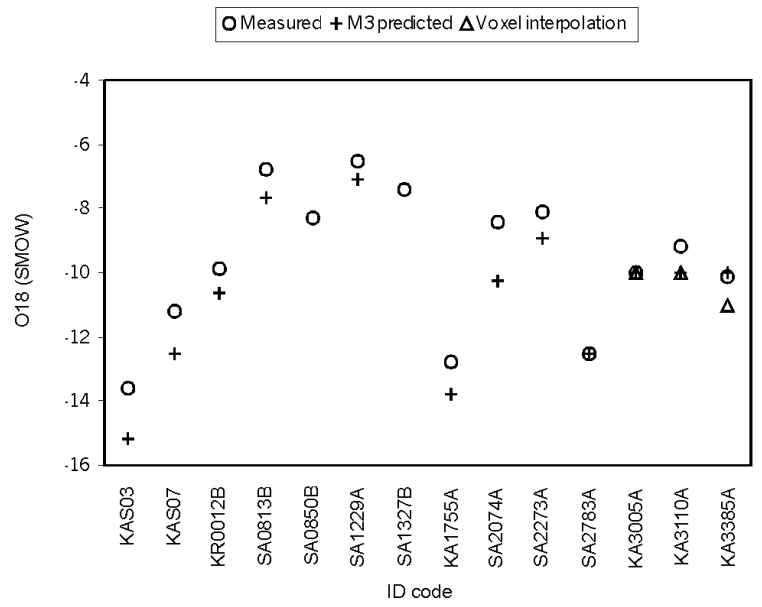

Figure 6-2: *Comparison of the predicted values using M3 and Voxel interpolation with measured data (given values) of oxygen-18 (SMOWl) for the control points. No predictions are made for the control points SA0850B and SA1327B because of lack of time series.*

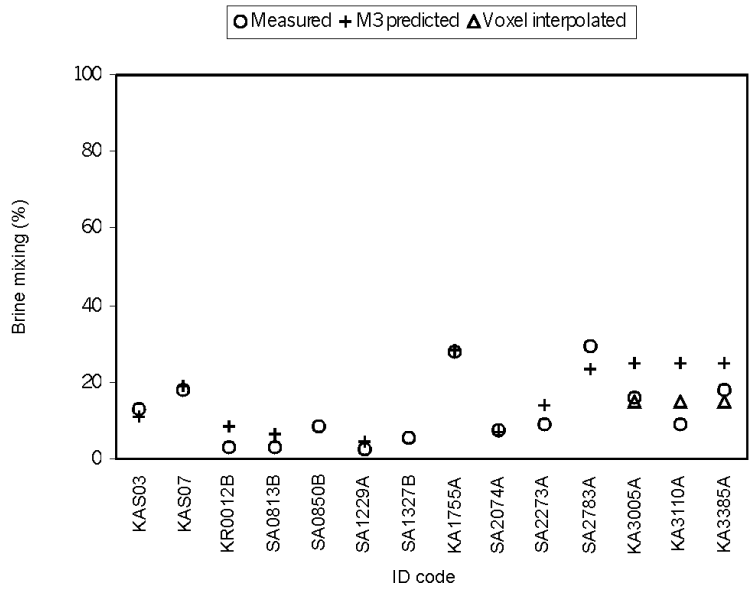

Figure 6-3: *Comparison of the predicted values using M3 and Voxel interpolation with measured data (given values) of Brine mixing proportion (%) for the control points. No predictions are made for the control points SA0850B and SA1327B because of lack of time series.*

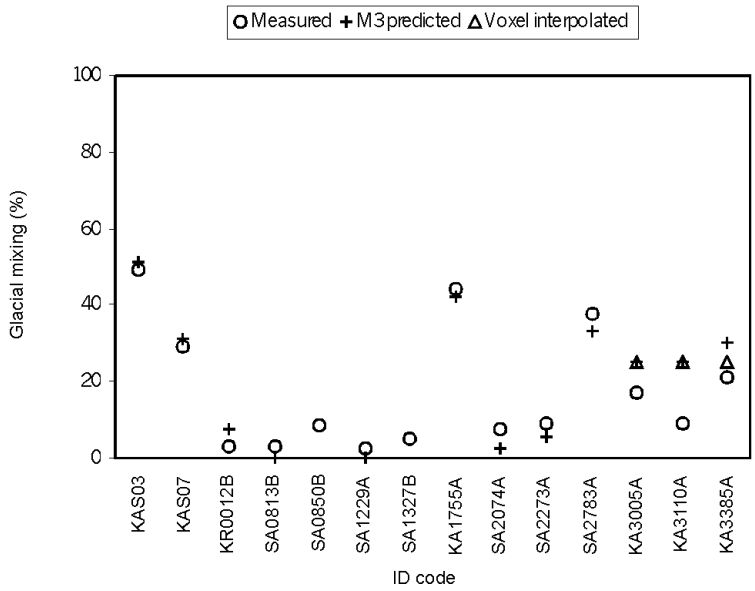

Figure 6-4: *Comparison of the predicted values using M3 and Voxel interpolation with measured data (given values) of Glacial mixing proportion (%) for the control points. No predictions are made for the control points SA0850B and SA1327B because of lack of time series.*

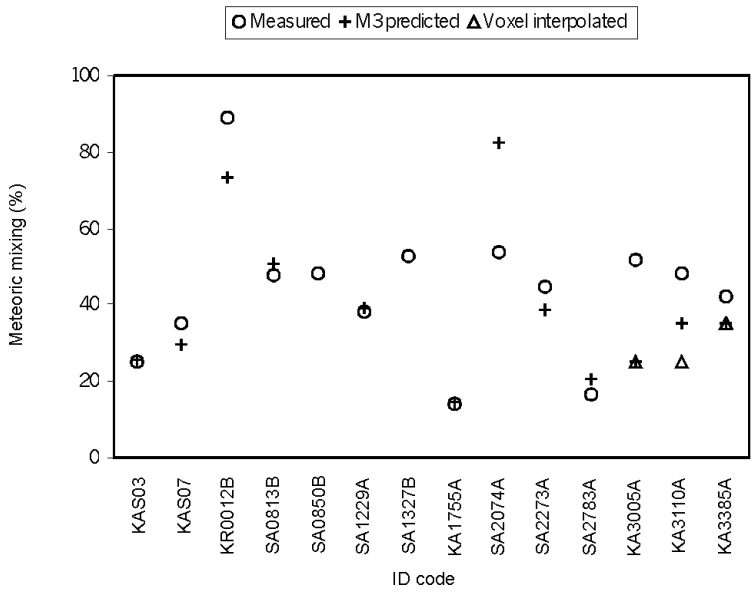

Figure 6-5: *Comparison of the predicted values using M3 and Voxel interpolation with measured data (given values) of Meteoric mixing proportion (%) for the control points. No predictions are made for the control points SA0850B and SA1327B because of lack of time series.*

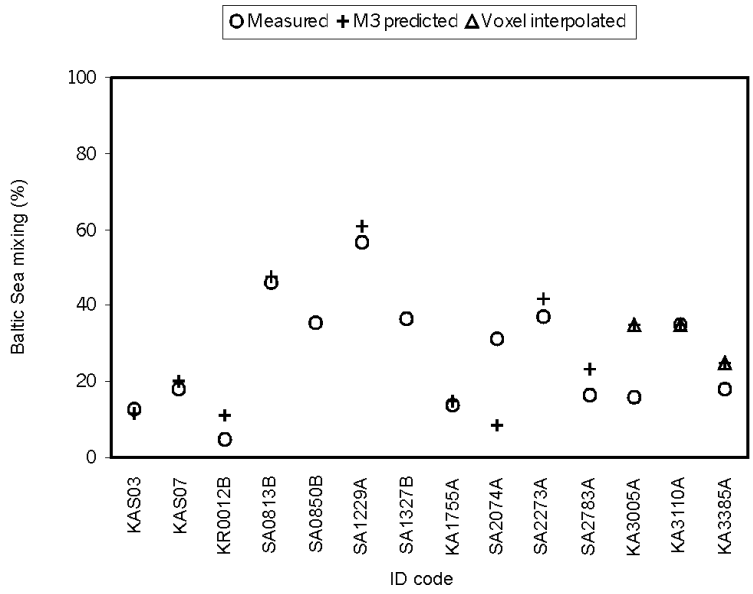

Figure 6-6: *Comparison of the predicted values using M3 and Voxel interpolation with measured data (given values) of Baltic mixing proportion (%) for the control points. No predictions are made for the control points SA0850B and SA1327B because of lack of time series.*

7 INTEGRATION OF M3-COMPOSITIONS WITH HYDRODYNAMIC MODELLING

An example of how M3 calculations have been used in Task #5 is the consistency check between compositional changes simulated by hydrodynamic modelling (see part III Report) and the above estimates of changes at Control Points at >2900m in the tunnel. The consistency check was done by comparing cutting planes corresponding to the main fracture zones produced by the two individual models. The salinity distribution obtained by the two approaches was compared for the following fracture zones: NE1, NE2, NE3, NNW1, NNW2, NNW3, NNW4, NNW5, NNW6, NNW7, NNW8, EW1N, EW1S, EW3, EW7, EN4N, EN4S, NW1 and SFZ11. Figures 4-8 to 4-12 show visualisations of initial conditions in some of these fracture zones. Figure 7-1 shows a schematic drawing of how the comparisons between the M3 model and the SKB hydrodynamic model were performed.

One way of integrating the chemical and hydrodynamic modelling is by means of particle tracking (see Figure 7-1). As an example, some flow paths to control points suggested by particle tracking modelling (Part III of this report) are compared with the spatial distribution of mixed reference water suggested by M3 in Figures 7-2 and 7-3. This indicates that mixing calculations support particle tracking since both are independent assessments of the possible groundwater sources and flow paths.

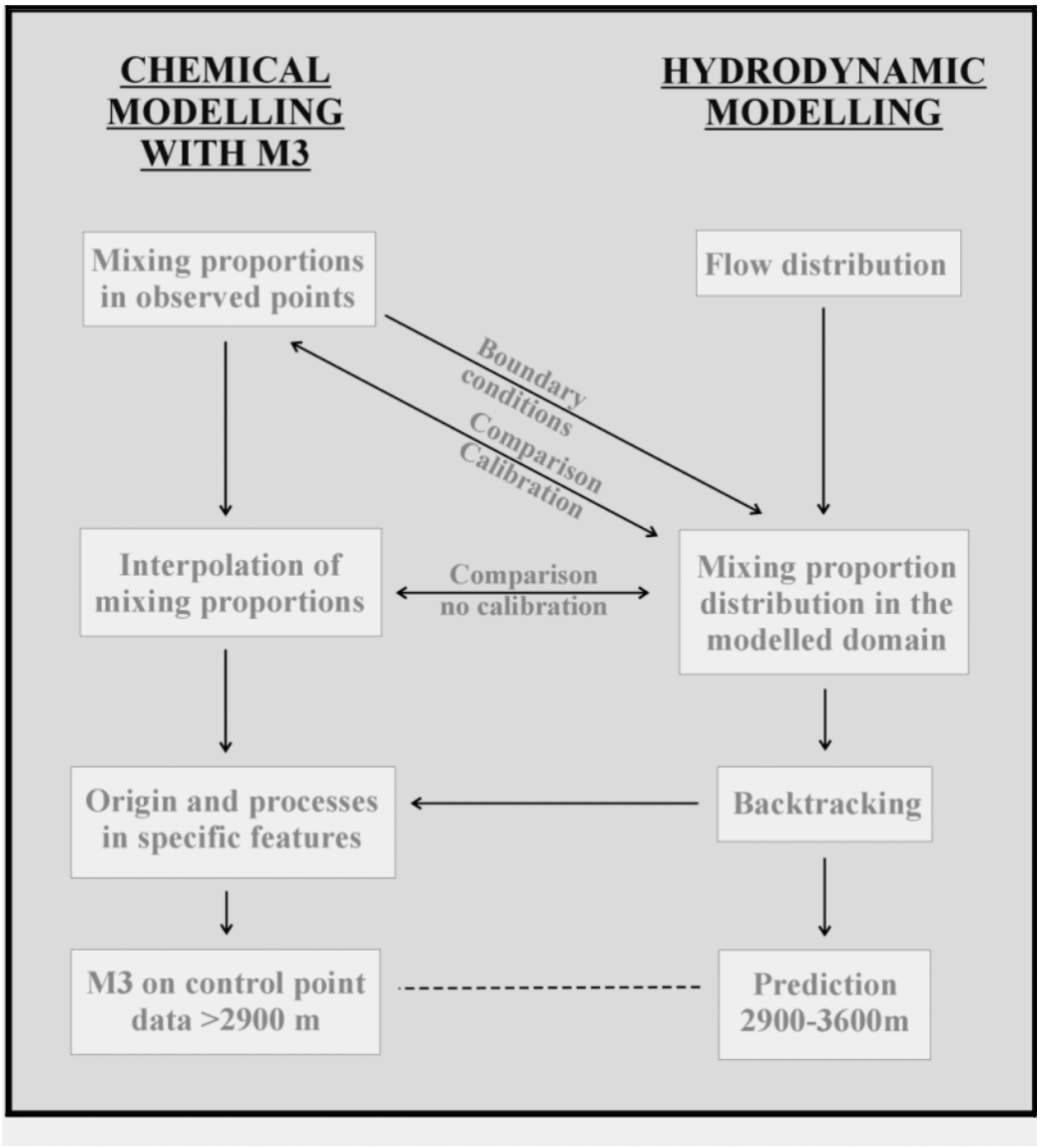

Figure 7-1: *A schematic drawing showing how the comparison between the M3 model and the SKB hydrodynamic model was performed.*

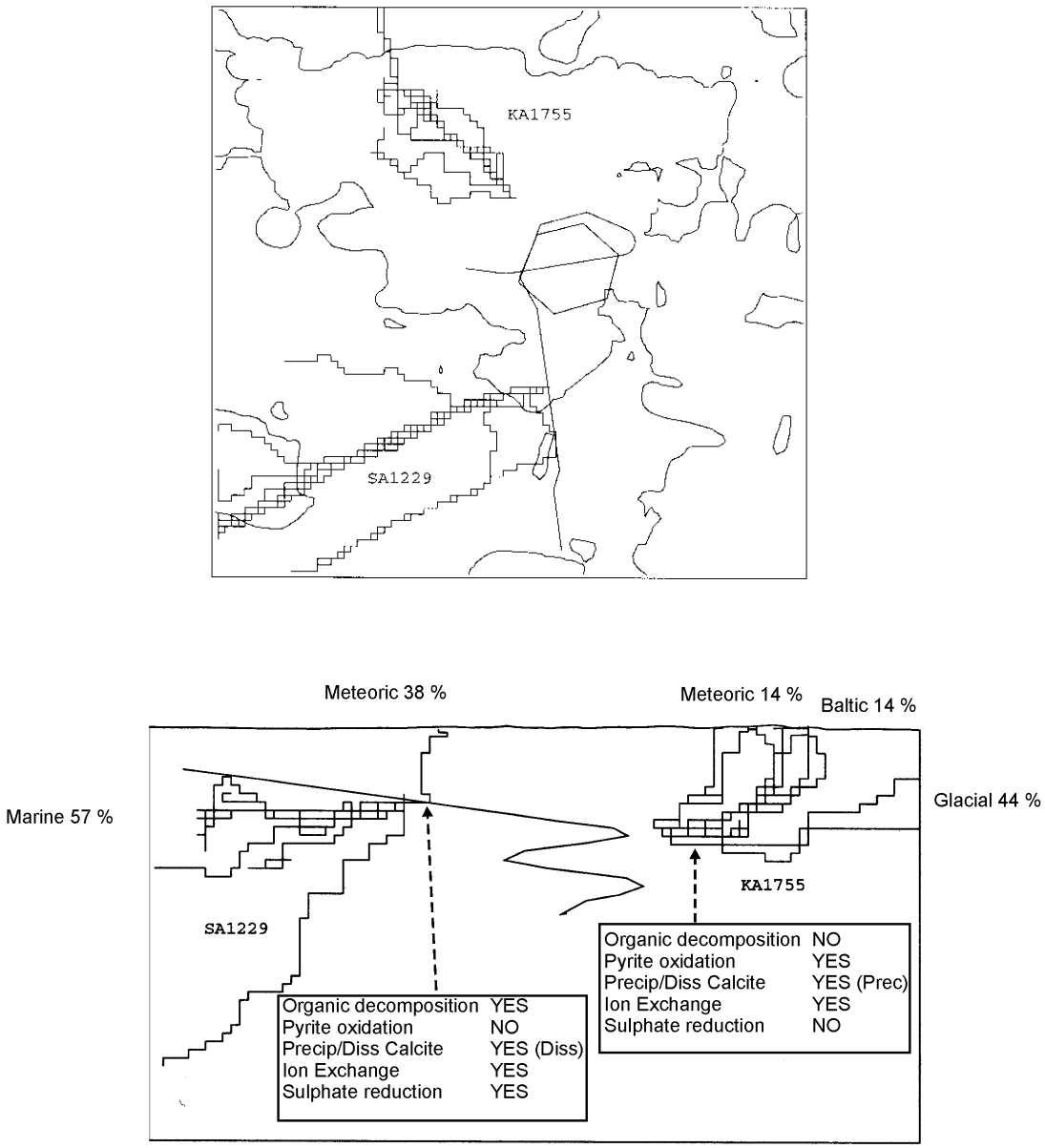

Figure 7-2: *The result from SKB Particle tracking (flow lines) is combined with the M3 mixing (see percentage values for each reference water) and mass balance calculations. The results from the mass balance calculations (boxed in) are used to indicate major reactions that may modify the groundwater composition at different site locations.*

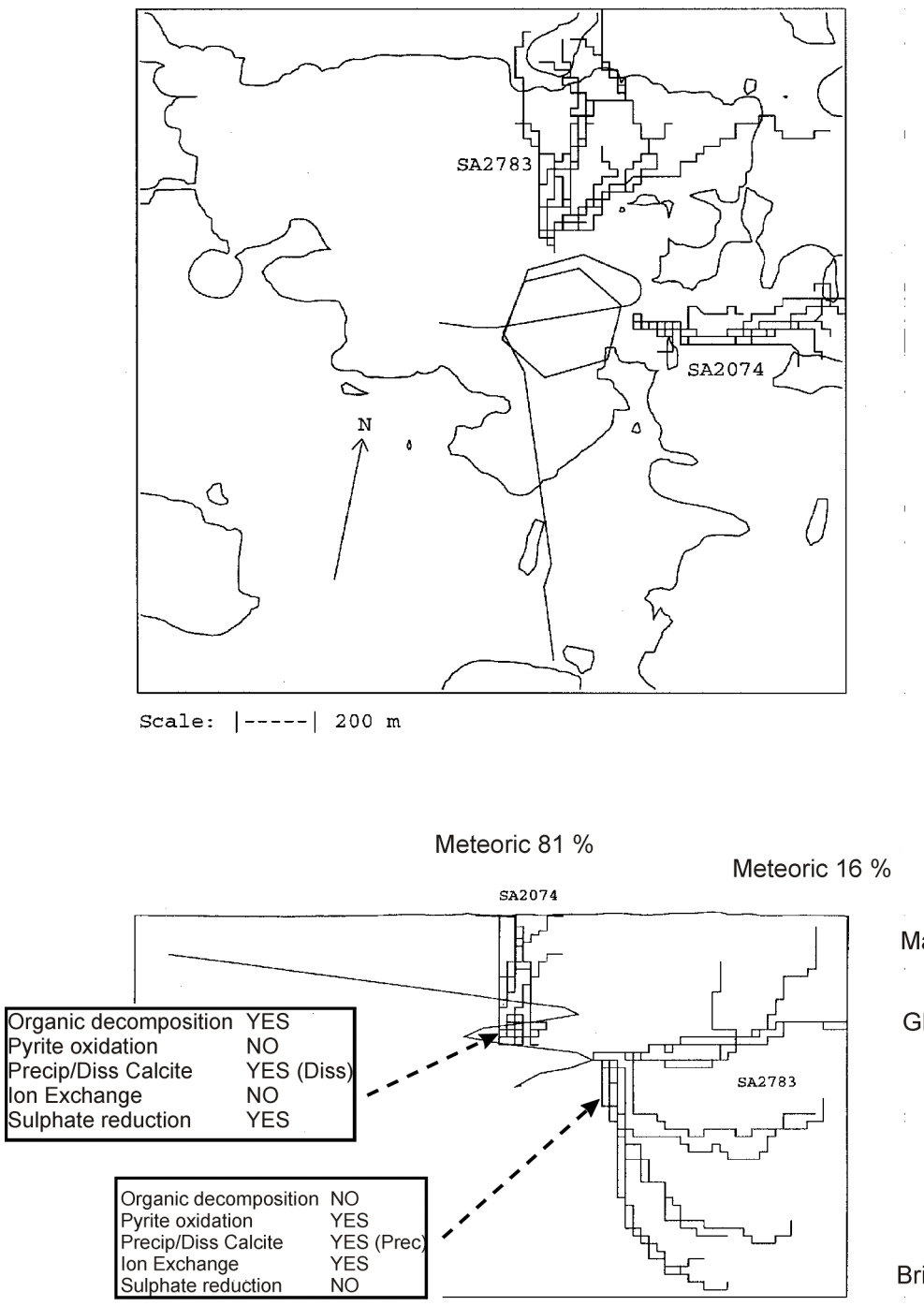

Figure 7-3: *The result from SKB Particle tracking (flow lines) is combined with the M3 mixing (see percentage values for each reference water) and mass balance calculations. The results from the mass balance calculations (boxed in) are used to indicate major reactions that may modify the groundwater composition at different site locations.*

8 CONCLUSIONS OF THE MODELLING

The aim of Task#5 has been to compare and ultimately integrate hydrochemistry and hydrogeology. The work presented here has shown that the task of integrating chemistry in the hydrodynamic models can be achieved by the concept of mixing proportions. Mixing proportions seem to be a convenient way to compare/integrate/support the results from hydrodynamic models. In this exercise we have used the M3 code to calculate groundwater mixing proportions for visualising the changes in groundwater compositions and to indicate the effects from reactions.

The conclusion based on the M3 modelling presented in this report is that the changes due to the Äspö HRL tunnel construction can be reasonably well predicted using a simple approach. The method used was to trace changes in samples taken in the time series from boreholes during the tunnel construction. The prevailing conditions such as a transient lowering of hydraulic head by 80m and samples taken from sections with a similar hydraulic conductivity of around 10^{-7} m^2/s were assumed to determine the changes in the groundwater chemistry. These changes can be transformed into mixing proportions by M3 and used as a "recipe" for short term predictions. In M3, proportions of Meteoric, Glacial, Baltic Sea and Brine water can be added or removed from a measured sample. A new water composition can be calculated where the effect from, e.g. addition of 5% meteoric water and removal of 8% sea water, can be modelled. The model calculates a new water composition for the major components and isotopes. For long term predictions models containing hydrodynamic and geological information should be used. However the M3 prediction is of interest since during site investigations simplistic calculations and predictions are needed (e.g. for planning, evaluation and scenario modelling).

One part of the consistency and integration between the hydrochemical and hydrodynamic modelling was the Particle Tracking. The result indicates that the mixing calculations can be integrated to support the results from the particle tracking since both are independent modelling tools describing the possible origin and flow paths of the groundwater.

The results of the Task#5 exercise showed that M3 can be used to decode the measured groundwater composition in terms of mixing proportions, indicate the effects from major reactions and can be used for short term groundwater chemical predictions. These results can be used to compare/integrate the results from hydrogeological models. The major achievement within Task#5 is that groundwater chemistry data can no longer be treated as unaffected by the flow and the flow calculations have to agree with the obtained chemical data. The following has been achieved:

1) Based on M3 calculations, groundwater data can be used to construct a mixing model of a site.

2) The concept of mixing proportions is an effective way of summarising the groundwater information at a site.

3) The results from the mixing model can be used in a flow model.

4) The results from the flow modelling can be used to test the validity of the chemical modelling and the results from the chemical modelling can be used to verify hydrodynamic flow modelling.

5) In addition to calculating mixing proportions, the M3 model can help to trace the effects from major reactions.

6) The Task#5 exercise has increased awareness of the effects from model uncertainties.

APPENDIX 1: Data set with time series

The difference between the predicted and measured values for the data set containing the time series. The difference for the mixing proportions, major components and isotopes are listed.

ID code	Secup	Seclow	Centr.	Date	Days from 1990-10-14 =(	Days from 1st obs.	Years from 1st obs.	Northing	Easting	Elevation	SNO
KAS02	309	345	327	920819	675	1422	3.9	7287.165	2114.836	-318.178	1990
KAS03	533	626	579.5	940412	1276	601	1.6	7825.385	1781.814	-566.304	2234
KAS05	440	549.6	494.8	940412	1276	588	1.6	7197.769	2074.653	-483.321	2235
KAS07	191	290	240.5	940406	1270	583	1.6	7131.309	2139.342	-201.271	2228
KAS07	501	604	552.5	940906	1423	736	2.0	6995.844	2042.233	-464.993	2273
KAS08	503	601	552	940406	1270	583	1.6	7172.453	2307.591	-441.306	2229
KAS09	116	150	133	951012	1824	1136	3.1	6857.829	2089.529	-110.585	2333
KAS12	234	277	255.5	930907	1059	371	1.0	7475.856	2182.879	-231.657	2161
KLX01	680	702.11	691.055	891101	-347	363	1.0	7307.837	595.69	-672.907	1633
HBH01	31	50.6	40.8	950324	1622	1182	3.2	6183.527	2166.468	-30.879	2307
HBH02	21	32.4	26.7	950324	1622	1181	3.2	6190.937	2161.031	-15.296	2308
HBH05	11	22	16.5	931112	1125	380	1.0	6185.414	2144.279	-8.697	2198
KR0012B	5	10.57	7.785	960521	2046	1798	4.9	6167.254	2165.756	-69.196	2361
KR0013B	7.05	16.94	11.995	951010	1822	1592	4.4	6166.277	2159.071	-69.269	2324
KR0015B	19.82	30.31	25.065	960521	2046	1504	4.1	6168.049	2144.354	-69.537	2363
HA1327B	3.5	29.5	16.5	931214	1157	377	1.0	6963.062	2118.058	-182.949	2208
KA1639A	13.4	14.4	13.9	930929	1081	90	0.2	7289.736	2021.422	-223.187	2177
KA1639A	15.4	25.9	20.65	930927	1079	48	0.1	7296.386	2020.416	-222.622	2171
KA1750A	4.4	5.4	4.9	930929	1081	90	0.2	7373.065	2068.565	-237.243	2179
KA1755A	88	160		960521	2046	222	0.6				2359
KBH02	240.25	372.85	306.55	931214	1157	111	0.3	6583.47	2128.279	-120.472	2210
SA0813B	5.6	19.5	12.55	960521	2046	1628	3.3	6479.609	2152.822	-112.929	2353
SA0923A	6	20	13	930207	847	434	1.2	6588.708	2125.893	-128.407	2075
SA0958B	5	19.7	12.35	940607	1332	349	1.0	6618.921	2151.272	-133.195	2254
SA1009B	6	19.5	12.75	960521	2046	1058	2.9	6672.091	2152.899	-139.744	2356
SA1062B	6	20	13	921202	780	223	0.6	6724.883	2145.887	-146.969	2050
SA1229A	6	20.5	13.25	960521	2046	1001	2.7	6885.159	2105.455	-171.291	2357
SA1420A	6	50	28	960521	2046	1376	3.6	7092.329	2080.819	-200.592	2358
SA1614B	5.8	19.3	12.55	940606	1331	564	1.5	7257.869	2039.086	-224.037	2249
SA1680B	6	20	13	930203	843	106	0.3	7317.959	2060.113	-230.324	2066
SA1696B	5.9	19.2	12.55	940606	1331	594	1.6	7332.421	2065.722	-232.645	2250
SA1730A	5.6	20	12.8	951011	1823	980	2.7	7369.317	2065.943	-237.012	2331
SA1828B	5.8	20	12.9	940606	1331	564	1.5	7401.58	2157.075	-249.511	2252
SA2074A	6	38.7	22.35	950518	1677	832	2.3	7290.03	2348.258	-281.676	2317
SA2175B	5.8	20	12.9	940530	1324	168	0.5	7200.014	2294.498	-293.825	2244
SA2240B	5.7	19.8	12.75	931207	1150	70	0.2	7172.049	2249.831	-301.544	2204
SA2273A	5.8	20	12.9	960521	2046	903	2.5	7149.762	2221.715	-305.968	2355
SA2273B	5.8	20	12.9	940530	1324	181	0.5	7162.946	2217.931	301.932	2245

				Measured	Measured	Measured	Measured	Measured	Measured	Measured	Measured	Measured	Measured
ID code	Secup	Seclow	Centr.	Na	K	Ca	Mg	HCO3	Cl	SO4	D	Tr	O18
				(mg/l)	(mg/l)	(mg/l)	(mg/l)	(mg/l)	(mg/l)	(mg/l)	(o/oo)	(TU)	(o/oo)
KAS02	309	345	327	1150	7.5	671	48.5	138	3250	249	-94.9	8	-13.3
KAS03	533	626	579.5	1564	6.7	1162	48.4	38	4637	270	-106.3	6.8	-13.6
KAS05	440	549.6	494.8	2450	10	2560	42.1	5	8402	534	-96.8	8.4	-13
KAS07	191	290	240.5	1479	10.2	559	125	335	3743.8	74.4	-65.4	22	-8
KAS07	501	604	552.5	1890	9.5	1610	59.6	13	5960	446	-80.4	12.7	-11.2
KAS08	503	601	552	2180	13.3	1522	144.8	63	6452	391	-73.8	13	-9.2
KAS09	116	150	133	1465.1	33.89	198.9	139.7	175	2804.3	298.34	-56.7	33.8	-7
KAS12	234	277	255.5	1650	12.5	1070	107	61	4860	233	-82	4.2	-10.5
KLX01	680	702.11	691.055	1610	7.3	1330	24	24	4680	390	-98.8	0.6	-11.8
HBH01	31	50.6	40.8	286	3.8	94.4	16.2	290	550	103	-72.7	31	-9.8
HBH02	21	32.4	26.7	45.9	1.4	38	3.8	170	100	13.8	-73.9	35	-9.9
HBH05	11	22	16.5	25.4	2.6	42.6	8.8	172	27.6	36.6	-64.7	24	-9.4
KR0012B	5	10.57	7.785	326.9	3.73	83.6	14.4	302	495.6	102	-70.4	38	-9.9
KR0013B	7.05	16.94	11.995	620	4	270	47.1	267	1458.9	125.53	-70.6	71	-9.5
KR0015B	19.82	30.31	25.065	442	3.45	143	23	340	726	110	-72.9	34	-9.7
HA1327B	3.5	29.5	16.5	1760	13.7	684	157	259	4310	255	-54.5	13	-7.4
KA1639A	13.4	14.4	13.9	2218	8.2	1967	68.3	23	6960	480	-90.2	4.2	-12.4
KA1639A	15.4	25.9	20.65	1620	6	774	45.9	19	4230	130	-107.6	12	-14.6
KA1750A	4.4	5.4	4.9	2062	7.8	1684	71.2	33	6230	462	-80	8.4	-11.6
KA1755A	88	160		2836	9.47	3540.5	37.6	8	10565	611	-96.1	10	-12.8
KBH02	240.25	372.85	306.55	1800	21	638	160	340	4210	228	-59.2	6.8	-7.7
SA0813B	5.6	19.5	12.55	1522.7	19.39	275.5	111.6	319	2963.9	251.98	-53.2	19.4	-6.8
SA0923A	6	20	13	1800	30	678	162	655	4310	128	-59.7	8.4	-7.7
SA0958B	5	19.7	12.35	1634.1	21.4	477.8	125.1	274	3641	303	-55.6	22.8	-7.2
SA1009B	6	19.5	12.75	1598.1	35.94	239.4	150	110	3169.5	371.03	-57.4	24.5	-7
SA1062B	6	20	13	1930	34	545	177	403	4350	187	-58	8	-7.7
SA1229A	6	20.5	13.25	1639.8	28.04	413.1	137.2	303	3392.9	248	-46.3	15.2	-6.5
SA1420A	6	50	28	1315.8	21.1	245.4	119.1	214	2676.7	280.88	-60.3	23.7	-7.1
SA1614B	5.8	19.3	12.55	1831.3	7.37	1207	98.3	109	5176.1	333	-77.6	8.4	-10.4
SA1680B	6	20	13	1100	10	583	63.3	137	2790	194	-85.5	17	-10.7
SA1696B	5.9	19.2	12.55	1932.5	9.14	1740.4	71.4	89	6275.2	459	-81	7	-11.1
SA1730A	5.6	20	12.8	2384.2	8.23	2616.5	56.4	36	8650.5	530.46	-87.1	8.45	-11.9
SA1828B	5.8	20	12.9	1861.5	11.67	1063.9	138.8	111	5123	251	-67.8	8.4	-8.9
SA2074A	6	38.7	22.35	1454	9.3	560.4	119.3	128	3414.1	262	-65.1	33	-8.4
SA2175B	5.8	20	12.9	1959.5	15.29	1037.1	161.6	127	5442	267	-62	8.4	-8.2
SA2240B	5.7	19.8	12.75	2110	17.5	1010	180	171	5460	254	-57.3	5.9	-8.1
SA2273A	5.8	20	12.9	1804.9	14	823.8	134.6	175	4530.9	273.72	-62.8	20.3	-8.1
SA2273B	5.8	20	12.9	1761.7	7.82	1135.1	127.5	117	5105.2	196	-71.3	10.1	-9.5

				Mixing	Mixing	Mixing	Mixing	Predicted	Predicted	Predicted	Predicted
ID code	Secup	Seclow	Centr.	Brine	Glacial	Meteoric	Baltic Sea	Brine	Glacial	Meteoric	Baltic Sea
KAS02	309	345	327	10%	38%	41%	10%	18%	31%	30%	20%
KAS03	533	626	579.5	13%	49%	25%	13%	11%	51%	26%	12%
KAS05	440	549.6	494.8	23%	46%	16%	16%	22%	41%	17%	19%
KAS07	191	290	240.5	4%	4%	60%	32%	11%	22%	56%	12%
KAS07	501	604	552.5	18%	29%	35%	18%	19%	31%	30%	20%
KAS08	503	601	552	17%	17%	37%	30%	19%	26%	34%	20%
KAS09	116	150	133	3%	3%	39%	54%	6%	-5%	42%	58%
KAS12	234	277	255.5	15%	21%	49%	15%	14%	24%	48%	14%
KLX01	680	702.11	691.055	15%	45%	26%	15%	15%	47%	23%	15%
HBH01	31	50.6	40.8	4%	5%	87%	4%	6%	-6%	92%	8%
HBH02	21	32.4	26.7	2%	8%	87%	2%	5%	-3%	91%	7%
HBH05	11	22	16.5	3%	5%	88%	3%	4%	8%	83%	4%
KR0012B	5	10.57	7.785	3%	3%	89%	5%	8%	7%	73%	11%
KR0013B	7.05	16.94	11.995	1%	1%	81%	18%	11%	14%	60%	14%
KR0015B	19.82	30.31	25.065	4%	4%	87%	6%	8%	2%	79%	11%
HA1327B	3.5	29.5	16.5	6%	6%	42%	45%	6%	2%	43%	49%
KA1639A	13.4	14.4	13.9	19%	41%	20%	19%	18%	39%	24%	18%
KA1639A	15.4	25.9	20.65	10%	51%	28%	10%	10%	54%	26%	10%
KA1750A	4.4	5.4	4.9	19%	31%	31%	19%	18%	32%	32%	18%
KA1755A	88	160		28%	44%	14%	14%	28%	42%	14%	15%
KBH02	240.25	372.85	306.55	6%	6%	42%	45%	5%	4%	41%	51%
SA0813B	5.6	19.5	12.55	3%	3%	48%	46%	7%	-5%	51%	48%
SA0923A	6	20	13	1%	1%	45%	53%	1%	-3%	42%	59%
SA0958B	5	19.7	12.35	5%	5%	43%	47%	7%	3%	45%	45%
SA1009B	6	19.5	12.75	6%	6%	33%	55%	5%	-5%	39%	62%
SA1062B	6	20	13	4%	4%	37%	54%	3%	1%	37%	59%
SA1229A	6	20.5	13.25	2%	2%	38%	57%	5%	-5%	39%	61%
SA1420A	6	50	28	5%	5%	49%	42%	16%	8%	58%	18%
SA1614B	5.8	19.3	12.55	16%	20%	48%	16%	17%	19%	47%	18%
SA1680B	6	20	13	10%	19%	60%	10%	7%	22%	63%	8%
SA1696B	5.9	19.2	12.55	18%	29%	35%	18%	9%	19%	63%	9%
SA1730A	5.6	20	12.8	22%	39%	20%	20%	20%	28%	32%	21%
SA1828B	5.8	20	12.9	13%	13%	46%	28%	17%	17%	47%	18%
SA2074A	6	38.7	22.35	8%	8%	54%	31%	7%	2%	82%	8%
SA2175B	5.8	20	12.9	11%	11%	38%	39%	12%	10%	36%	42%
SA2240B	5.7	19.8	12.75	10%	10%	35%	45%	11%	11%	35%	43%
SA2273A	5.8	20	12.9	9%	9%	45%	37%	14%	5%	39%	42%
SA2273B	5.8	20	12.9	13%	13%	53%	21%	16%	14%	50%	20%

				Predicted	Predicted	Predicted	Predicted	Predicted	Predicted	Predicted	Predicted	Predicted	Predicted
ID code	Secup	Seclow	Centr.	Na	K	Ca	Mg	HCO3	Cl	SO4	D	Tr	O18
				(mg/l)	(mg/l)	(mg/l)	(mg/l)	(mg/l)	(mg/l)	(mg/l)	(o/oo)	(TU)	(o/oo)
KAS02	309	345	327	1949	28	3542	48	25	9378	232	-92	40	-13
KAS03	533	626	579.5	1169	17	2138	28	15	5647	139	-113	31	-15
KAS05	440	549.6	494.8	2282	28	4357	45	22	11324	266	-99	26	-14
KAS07	191	290	240.5	1139	16	2082	27	19	5499	136	-90	62	-12
KAS07	501	604	552.5	2009	28	3687	47	24	9725	238	-92	39	-13
KAS08	503	601	552	2037	28	3747	48	25	9874	241	-88	43	-12
KAS09	116	150	133	1600	57	1118	135	58	4773	238	-59	67	-7
KAS12	234	277	255.5	1429	20	2630	33	21	6930	169	-90	55	-12
KLX01	680	702.11	691.055	1566	22	2886	36	19	7601	185	-107	30	-14
HBH01	31	50.6	40.8	627	10	1076	19	19	2912	77	-71	96	-9
HBH02	21	32.4	26.7	563	9	983	16	18	2643	69	-74	94	-10
HBH05	11	22	16.5	412	6	744	10	15	1974	50	-84	85	-11
KR0012B	5	10.57	7.785	932	15	1635	26	20	4388	113	-80	78	-11
KR0013B	7.05	16.94	11.995	1247	19	2231	33	21	5943	150	-83	67	-11
KR0015B	19.82	30.31	25.065	925	14	1638	25	20	4379	112	-76	84	-10
HA1327B	3.5	29.5	16.5	1464	49	1204	114	50	4662	213	-67	64	-8
KA1639A	13.4	14.4	13.9	1897	26	3512	43	22	9234	224	-99	33	-13
KA1639A	15.4	25.9	20.65	1079	15	1997	25	14	5250	128	-116	30	-16
KA1750A	4.4	5.4	4.9	1905	26	3526	43	23	9271	225	-94	40	-13
KA1755A	88	160		2697	27	5472	36	19	13912	305	-99	22	-14
KBH02	240.25	372.85	306.55	1403	50	981	119	51	4185	209	-68	62	-8
SA0813B	5.6	19.5	12.55	1490	48	1308	112	50	4880	215	-61	71	-8
SA0923A	6	20	13	1269	57	300	139	59	2826	205	-62	67	-7
SA0958B	5	19.7	12.35	1447	46	1311	106	47	4806	207	-68	64	-9
SA1009B	6	19.5	12.75	1619	61	985	145	61	4590	245	-58	65	-7
SA1062B	6	20	13	1413	58	617	139	58	3609	220	-64	62	-8
SA1229A	6	20.5	13.25	1595	60	968	143	60	4519	241	-58	65	-7
SA1420A	6	50	28	1710	24	3103	42	25	8220	204	-76	66	-10
SA1614B	5.8	19.3	12.55	1771	25	3255	42	24	8581	210	-84	55	-11
SA1680B	6	20	13	787	11	1454	18	16	3826	94	-92	67	-12
SA1696B	5.9	19.2	12.55	919	13	1674	22	17	4428	110	-90	67	-12
SA1730A	5.6	20	12.8	2083	29	3811	50	26	10064	247	-89	41	-12
SA1828B	5.8	20	12.9	1845	26	3392	43	25	8942	219	-82	55	-11
SA2074A	6	38.7	22.35	764	11	1374	20	18	3652	92	-77	86	-10
SA2175B	5.8	20	12.9	1828	46	2300	100	44	7125	245	-72	54	-9
SA2240B	5.7	19.8	12.75	1805	46	2219	101	45	6950	243	-73	54	-9
SA2273A	5.8	20	12.9	2006	46	2727	98	44	8150	263	-68	57	-9
SA2273B	5.8	20	12.9	1721	27	3016	48	27	8099	208	-80	59	-11

				Difference	Difference	Difference	Difference	Total diff.	Total diff.
ID code	Secup	Seclow	Centr.	Brine	Glacial	Meteoric	Baltic Sea	+	-
KAS02	309	345	327	8%	-7%	-11%	10%	18%	-18%
KAS03	533	626	579.5	-2%	2%	1%	-1%	3%	-3%
KAS05	440	549.6	494.8	0%	-4%	1%	3%	5%	-5%
KAS07	191	290	240.5	7%	17%	-4%	-20%	24%	-24%
KAS07	501	604	552.5	1%	2%	-5%	2%	5%	-5%
KAS08	503	601	552	2%	10%	-3%	-9%	12%	-12%
KAS09	116	150	133	2%	-8%	3%	3%	8%	-8%
KAS12	234	277	255.5	-2%	3%	-1%	-1%	3%	-3%
KLX01	680	702.11	691.055	0%	2%	-3%	1%	3%	-3%
HBH01	31	50.6	40.8	2%	-11%	5%	4%	11%	-11%
HBH02	21	32.4	26.7	3%	-11%	4%	5%	11%	-11%
HBH05	11	22	16.5	0%	4%	-5%	1%	5%	-5%
KR0012B	5	10.57	7.785	5%	4%	-16%	6%	16%	-16%
KR0013B	7.05	16.94	11.995	11%	14%	-21%	-4%	25%	-25%
KR0015B	19.82	30.31	25.065	5%	-2%	-8%	5%	10%	-10%
HA1327B	3.5	29.5	16.5	0%	-4%	1%	3%	4%	-4%
KA1639A	13.4	14.4	13.9	-1%	-2%	5%	-1%	5%	-5%
KA1639A	15.4	25.9	20.65	0%	3%	-3%	0%	3%	-3%
KA1750A	4.4	5.4	4.9	0%	0%	0%	0%	1%	-1%
KA1755A	88	160		0%	-2%	0%	1%	2%	-2%
KBH02	240.25	372.85	306.55	-1%	-3%	-1%	5%	5%	-5%
SA0813B	5.6	19.5	12.55	4%	-8%	3%	1%	8%	-8%
SA0923A	6	20	13	0%	-4%	-3%	7%	7%	-7%
SA0958B	5	19.7	12.35	2%	-2%	2%	-2%	4%	-4%
SA1009B	6	19.5	12.75	-1%	-11%	6%	7%	12%	-12%
SA1062B	6	20	13	-1%	-4%	0%	5%	5%	-5%
SA1229A	6	20.5	13.25	2%	-7%	1%	4%	7%	-7%
SA1420A	6	50	28	11%	3%	9%	-24%	24%	-24%
SA1614B	5.8	19.3	12.55	1%	-1%	-2%	2%	2%	-2%
SA1680B	6	20	13	-3%	2%	3%	-3%	5%	-5%
SA1696B	5.9	19.2	12.55	-10%	-9%	28%	-9%	28%	-28%
SA1730A	5.6	20	12.8	-2%	-11%	12%	1%	13%	-13%
SA1828B	5.8	20	12.9	5%	4%	1%	-10%	10%	-10%
SA2074A	6	38.7	22.35	0%	-5%	28%	-23%	28%	-28%
SA2175B	5.8	20	12.9	0%	-1%	-3%	4%	4%	-4%
SA2240B	5.7	19.8	12.75	1%	0%	0%	-2%	2%	-2%
SA2273A	5.8	20	12.9	5%	-4%	-6%	5%	10%	-10%
SA2273B	5.8	20	12.9	2%	1%	-2%	0%	3%	-3%

				Difference	Difference	Difference	Difference	Difference	Difference	Difference	Difference	Difference	Difference
ID code	Secup	Seclow	Centr.	Na	K	Ca	Mg	HCO3	Cl	SO4	D	Tr	O18
				(mg/l)	(mg/l)	(mg/l)	(mg/l)	(mg/l)	(mg/l)	(mg/l)	(o/oo)	(TU)	(o/oo)
KAS02	309	345	327	799	20	2871	-1	-113	6128	-17	2	32	1
KAS03	533	626	579.5	-395	10	976	-20	-23	1010	-131	-7	24	-2
KAS05	440	549.6	494.8	-168	18	1797	3	17	2922	-268	-2	18	-1
KAS07	191	290	240.5	-340	6	1523	-98	-316	1756	61	-25	40	-4
KAS07	501	604	552.5	119	18	2077	-12	11	3765	-208	-12	26	-1
KAS08	503	601	552	-143	15	2225	-97	-38	3422	-150	-15	30	-3
KAS09	116	150	133	135	24	920	-5	-117	1968	-60	-2	33	0
KAS12	234	277	255.5	-221	7	1560	-74	-40	2070	-64	-8	51	-2
KLX01	680	702.11	691.055	-44	14	1556	12	-5	2921	-205	-8	29	-3
HBH01	31	50.6	40.8	341	7	982	3	-271	2362	-26	1	65	0
HBH02	21	32.4	26.7	517	8	945	12	-152	2543	55	0	59	0
HBH05	11	22	16.5	387	4	701	2	-157	1947	14	-19	61	-2
KR0012B	5	10.57	7.785	605	11	1552	12	-282	3892	11	-9	40	-1
KR0013B	7.05	16.94	11.995	627	15	1961	-15	-246	4484	24	-13	-4	-2
KR0015B	19.82	30.31	25.065	483	11	1495	2	-320	3653	2	-3	50	0
HA1327B	3.5	29.5	16.5	-296	35	520	-43	-209	352	-42	-12	51	-1
KA1639A	13.4	14.4	13.9	-321	18	1545	-25	-1	2274	-256	-9	29	-1
KA1639A	15.4	25.9	20.65	-541	9	1223	-21	-5	1020	-2	-8	18	-1
KA1750A	4.4	5.4	4.9	-157	18	1842	-28	-10	3041	-237	-14	32	-1
KA1755A	88	160		-139	18	1932	-2	11	3347	-306	-3	12	-1
KBH02	240.25	372.85	306.55	-397	29	343	-41	-289	-25	-19	-9	55	-1
SA0813B	5.6	19.5	12.55	-33	29	1032	0	-269	1916	-37	-8	52	-1
SA0923A	6	20	13	-531	27	-378	-23	-596	-1484	77	-2	59	0
SA0958B	5	19.7	12.35	-187	25	833	-19	-227	1165	-96	-13	41	-1
SA1009B	6	19.5	12.75	21	25	746	-5	-49	1421	-126	0	40	0
SA1062B	6	20	13	-517	24	72	-38	-345	-741	33	-6	54	0
SA1229A	6	20.5	13.25	-44	32	555	5	-243	1126	-7	-12	50	-1
SA1420A	6	50	28	394	3	2858	-77	-189	5543	-77	-15	43	-3
SA1614B	5.8	19.3	12.55	-60	17	2048	-57	-85	3405	-123	-7	46	-1
SA1680B	6	20	13	-313	1	871	-45	-121	1036	-100	-7	50	-2
SA1696B	5.9	19.2	12.55	-1013	4	-67	-49	-72	-1847	-349	-9	60	-1
SA1730A	5.6	20	12.8	-302	21	1195	-7	-10	1413	-283	-2	33	0
SA1828B	5.8	20	12.9	-16	14	2328	-96	-86	3819	-32	-15	47	-2
SA2074A	6	38.7	22.35	-690	2	814	-100	-110	238	-170	-12	53	-2
SA2175B	5.8	20	12.9	-131	31	1263	-62	-83	1683	-22	-10	46	-1
SA2240B	5.7	19.8	12.75	-305	29	1209	-79	-126	1490	-11	-16	48	-1
SA2273A	5.8	20	12.9	201	32	1903	-36	-131	3619	-11	-5	37	-1
SA2273B	5.8	20	12.9	-40	19	1881	-79	-90	2994	12	-9	49	-1

					Days from	Days from	Years from				
ID code	Secup	Seclow	Centr.	Date	1990-10-14 =(	1st obs.	1st obs.	Northing	Easting	Elevation	SNO
SA2289B	6	19.4	12.7	940530	1324	181	0.5	7158.515	2202.689	-307.718	2246
SA2322A	6	20.1	13.05	940527	1321	241	0.7	7136.119	2174.475	-312.606	2243
SA2583A	5.7	20	12.85	940518	1312	72	0.2	7301.166	2035.311	-343.513	2240
SA2600A	5.8	19.4	12.6	960521	2046	806	2.2	7315.455	2044.414	-345.048	2351
SA2703A	5.7	19.6	12.65	940517	1311	83	0.2	7411.496	2082.084	-358.592	2237
SA2783A	5.8	19.9	12.85	960520	2045	826	2.3	7442.809	2160.694	-371.361	2352
SA2880A	11.92	13.92	12.92	960412	2007	170	0.5	7455.116	2259.267	-384.736	2349
Average difference											

				Measured	Measured	Measured	Measured	Measured	Measured	Measured	Measured	Measured	Measured
ID code	**Secup**	**Seclow**	**Centr.**	**Na**	**K**	**Ca**	**Mg**	**HCO3**	**Cl**	**SO4**	**D**	**Tr**	**O18**
SA2289B	6	19.4	12.7	1952.7	12.16	968.6	162.1	178	5167.3	219	-60.8	8.4	-8
SA2322A	6	20.1	13.05	1908.3	9.44	977.4	142.5	184	5034.3	213	-68	8.4	-8.6
SA2583A	5.7	20	12.85	2170	8.51	1859.6	73.9	44	6895.6	492	-85.9	5.9	-10.7
SA2600A	5.8	19.4	12.6	2125.4	9.1	1485.7	85	114	5920.7	403.81	-75.5	11	-9.8
SA2703A	5.7	19.6	12.65	2824	7.79	3581.3	40.3	12	10591.6	600	-93.7	4.2	-13.1
SA2783A	5.8	19.9	12.85	3053.2	10.89	4061.5	48.6	15	12054	616	-90	22	-12.5
SA2880A	11.92	13.92	12.92	3156.4	13.64	4378.1	41.1	22	12956.3	626	-84.5	21	-12.1
Average difference													

				Mixing	Mixing	Mixing	Mixing	Predicted	Predicted	Predicted	Predicted
ID code	Secup	Seclow	Centr.	Brine	Glacial	Meteoric	Baltic Sea	Brine	Glacial	Meteoric	Baltic Sea
SA2289B	6	19.4	12.7	10%	10%	42%	39%	12%	11%	41%	36%
SA2322A	6	20.1	13.05	11%	11%	48%	29%	14%	11%	46%	29%
SA2583A	5.7	20	12.85	20%	32%	29%	20%	20%	34%	27%	20%
SA2600A	5.8	19.4	12.6	18%	18%	46%	18%	24%	28%	23%	25%
SA2703A	5.7	19.6	12.65	28%	45%	13%	13%	27%	42%	16%	16%
SA2783A	5.8	19.9	12.85	29%	38%	16%	16%	23%	33%	21%	23%
SA2880A	11.92	13.92	12.92	31%	34%	17%	17%	28%	36%	18%	18%
Average difference											

				Predicted	Predicted	Predicted	Predicted	Predicted	Predicted	Predicted	Predicted	Predicted	Predicted
ID code	**Secup**	**Seclow**	**Centr.**	**Na**	**K**	**Ca**	**Mg**	**HCO3**	**Cl**	**SO4**	**D**	**Tr**	**O18**
SA2289B	6	19.4	12.7	1765	40	2442	84	39	7241	230	-74	56	-10
SA2322A	6	20.1	13.05	1727	34	2671	68	33	7545	218	-76	59	-10
SA2583A	5.7	20	12.85	2061	28	3818	47	24	10037	243	-94	36	-13
SA2600A	5.8	19.4	12.6	2536	35	4661	60	29	12289	300	-86	35	-12
SA2703A	5.7	19.6	12.65	2590	27	5195	37	20	13260	295	-99	23	-14
SA2783A	5.8	19.9	12.85	2419	33	4488	55	27	11790	285	-91	31	-13
SA2880A	11.92	13.92	12.92	2714	30	5364	44	23	13766	311	-94	27	-13
Average difference													

				Difference	Difference	Difference	Difference	Total diff.	Total diff.
ID code	**Secup**	**Seclow**	**Centr.**	**Brine**	**Glacial**	**Meteoric**	**Baltic Sea**	**+**	**-**
SA2289B	6	19.4	12.7	3%	1%	-1%	-3%	4%	-4%
SA2322A	6	20.1	13.05	2%	0%	-2%	-1%	2%	-2%
SA2583A	5.7	20	12.85	0%	2%	-2%	0%	2%	-2%
SA2600A	5.8	19.4	12.6	6%	10%	-23%	7%	23%	-23%
SA2703A	5.7	19.6	12.65	-1%	-3%	2%	2%	5%	-5%
SA2783A	5.8	19.9	12.85	-6%	-5%	4%	7%	11%	-11%
SA2880A	11.92	13.92	12.92	-3%	2%	0%	1%	3%	-3%
Average difference				**1%**	**-1%**	**0%**	**0%**	**9%**	**-9%**

				Difference	Difference	Difference	Difference	Difference	Difference	Difference	Difference	Difference	Difference
ID code	**Secup**	**Seclow**	**Centr.**	**Na**	**K**	**Ca**	**Mg**	**HCO3**	**Cl**	**SO4**	**D**	**Tr**	**O18**
SA2289B	6	19.4	12.7	-187	28	1473	-78	-139	2074	11	-14	48	-2
SA2322A	6	20.1	13.05	-181	24	1693	-75	-151	2510	5	-8	50	-2
SA2583A	5.7	20	12.85	-109	19	1959	-27	-20	3141	-249	-8	30	-2
SA2600A	5.8	19.4	12.6	411	26	3176	-25	-85	6369	-104	-11	24	-2
SA2703A	5.7	19.6	12.65	-234	20	1613	-3	8	2669	-305	-5	19	-1
SA2783A	5.8	19.9	12.85	-634	22	426	6	12	-264	-331	-1	9	0
SA2880A	11.92	13.92	12.92	-442	17	986	2	1	810	-315	-9	6	-1
Average difference				**-91**	**18**	**1356**	**-31**	**-128**	**2199**	**-99**	**-8**	**39**	**-1**

APPENDIX 2: Data set comparing predictions/measurements at Control Points

The difference between the predicted and measured values for the Control Points (CP) along the HRL tunnel. The difference for the mixing proportions, major components and isotopes are listed.

ID code	Secup	Seclow	Centr	Date	Northing	Easting	Elevation
KAS03	533	626	579.5	940412	7825.385	1781.814	-566.304
KAS07	501	604	552.5	940906	6995.844	2042.233	-464.993
KR0012B	5	10.57	7.785	960521	6167.254	2165.756	-69.196
SA0813B	5.6	19.5	12.55	960521	6479.609	2152.822	-112.929
SA0850B	1	19.8	10.4	910820	6514.633	2146.364	-117.736
SA1229A	6	20.5	13.25	960521	6885.159	2105.455	-171.291
SA1327B	6	20.3	13.15	921015	6987.423	2111.44	-184.085
KA1755A	88	160	124	960521	7492.4893	2022.4483	-277.58133
SA2074A	6	38.7	22.35	950518	7290.03	2348.258	-281.676
SA2273A	5.8	20	12.9	960521	7149.762	2221.715	-305.968
SA2783A	5.8	19.9	12.85	960520	7442.809	2160.694	-371.361
KA3005A	36.9	37.9	37.4	950310	7426.3	2331.3	-402.8
KA3110A	20.1	28.6	24.3	950310	7299.2	2331.7	-416
KA3385A	32	34	33	980302	7219.9	2096.3	-448.8

ID code	Cl (mg/l) Measured	Cl (mg/l) M3 predicted	Cl (mg/l) Voxel interpolated	O18 (SMOW) Measured	O18 (SMOW) M3 predicted	O18 (SMOW) Voxel interpolated
KAS03	4637	5647	-	-13.6	-15	-
KAS07	5960	9725	-	-11.2	-13	-
KR0012B	495.6	4388	-	-9.9	-11	-
SA0813B	2963.9	4880	-	-6.8	-8	-
SA0850B	5440	-	-	-8.3	-	-
SA1229A	3392.9	4519	-	-6.5	-7	-
SA1327B	3920	-	-	-7.4	-	-
KA1755A	10565	13912	-	-12.8	-14	-
SA2074A	3414.1	3652	-	-8.4	-10	-
SA2273A	4530.9	8150	-	-8.1	-9	-
SA2783A	12054	11790	-	-12.5	-13	-
KA3005A	5400	8500	7500	-10	-10	-10
KA3110A	3940	8500	6500	-9.2	-10	-10
KA3385A	6630	8500	6500	-10.1	-10	-11

ID code	Brine (%) Measured	Brine (%) M3 predicted	Brine (%) Voxel interpolated	Glacial (%) Measured	Glacial (%) M3 predicted	Glacial (%) Voxel interpolated
KAS03	13%	11%	-	49%	51%	-
KAS07	18%	19%	-	29%	31%	-
KR0012B	3%	8%	-	3%	7%	-
SA0813B	3%	7%	-	3%	0%	-
SA0850B	8%	-	-	8%	-	-
SA1229A	2%	5%	-	2%	0%	-
SA1327B	5%	-	-	5%	-	-
KA1755A	28%	28%	-	44%	42%	-
SA2074A	8%	7%	-	8%	2%	-
SA2273A	9%	14%	-	9%	5%	-
SA2783A	29%	23%	-	38%	33%	-
KA3005A	16%	25%	15%	17%	25%	25%
KA3110A	9%	25%	15%	9%	25%	25%
KA3385A	18%	25%	15%	21%	30%	25%

ID code	Meteoric (%) Measured	Meteoric (%) M3 predicted	Meteoric (%) Voxel interpolated	Baltic Sea (%) Measured	Baltic Sea (%) M3 predicted	Baltic Sea (%) Voxel interpolated
KAS03	25%	26%	-	13%	12%	-
KAS07	35%	30%	-	18%	20%	-
KR0012B	89%	73%	-	5%	11%	-
SA0813B	48%	51%	-	46%	48%	-
SA0850B	48%	-	-	35%	-	-
SA1229A	38%	39%	-	57%	61%	-
SA1327B	53%	-	-	37%	-	-
KA1755A	14%	14%	-	14%	15%	-
SA2074A	54%	82%	-	31%	8%	-
SA2273A	45%	39%	-	37%	42%	-
SA2783A	16%	21%	-	16%	23%	-
KA3005A	52%	25%	25%	16%	35%	35%
KA3110A	48%	35%	25%	35%	35%	35%
KA3385A	42%	35%	35%	18%	25%	25%

APPENDIX 3: M3 issues

This Appendix addresses some specific M3 issues related to uncertainties pointed out by the Task #5 reviewers together with some frequently asked questions.

Over exaggeration of the spread of water types: Since all water samples are described by four end-members, all samples are shown to include a percentage of each end-member. In reality this may not be the case and it may mean that, for example, the extent of e.g. glacial water at depth may not be as widespread as indicated. In order to investigate this, a correlation test between the measured $\delta^{18}O$ values and calculated mixing proportions of glacial water was conducted (see, Figure A-1). The test shows good correlation between measured low $\delta^{18}O$ values ("cold water") and the calculated mixing proportions of glacial water. This can also be seen by comparing for example Figure 4-4 (in the main report) illustrating the measured $\delta^{18}O$ ("cold/warm water") distribution with Figure 4-6 showing the calculated proportion of glacial water at the Äspö site.

A correlation test between measured Cl values and calculated mixing proportions of meteoric water is shown in Figure A-1b. The figure shows a correlation between decreasing salinity and increasing mixing proportions of meteoric water. The simplification made in Task #5 where one reference water was omitted (Modified Sea water, i.e. sea water affected by microbial sulphate reduction) leads to an overestimation of Meteoric water (on average 10%) and an underestimation of Baltic Sea water (on average 7%). To demonstrate the effect, a test was performed where Modified Sea water was included in the calculations and the mixing proportions for all water types were plotted versus sampling depth. In Figure A-2 the results based on Task #5 data are shown and in Figure A-3 the results based on the new model including Modified Sea water are shown. The results show that by including the Modified Sea water the proportions between Meteoric water and Baltic Sea water changed. The Baltic Sea water (Baltic + Modified Sea) is occurring at larger proportions at shallow depth and the Meteoric water in lower proportions at greater depth (many observations are under the detection limit of the method). The proportioning between Glacial water and Brine are generally not affected. The model including the Modified Baltic Sea water is the standard model used for Äspö modelling (e.g. Laaksoharju and Wallin, 1997; Laaksoharju et al., 1999a, b) and describes better the observed groundwater than the simplified model used for Task#5.

a)

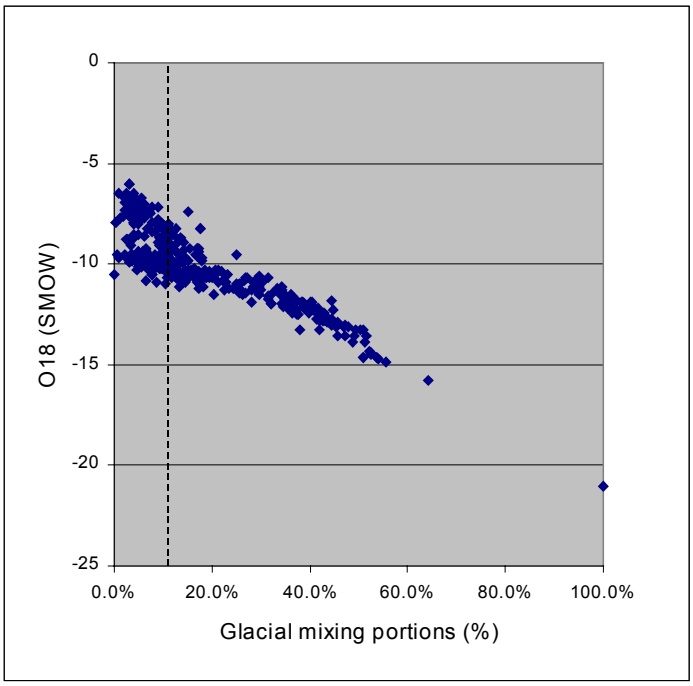

b)

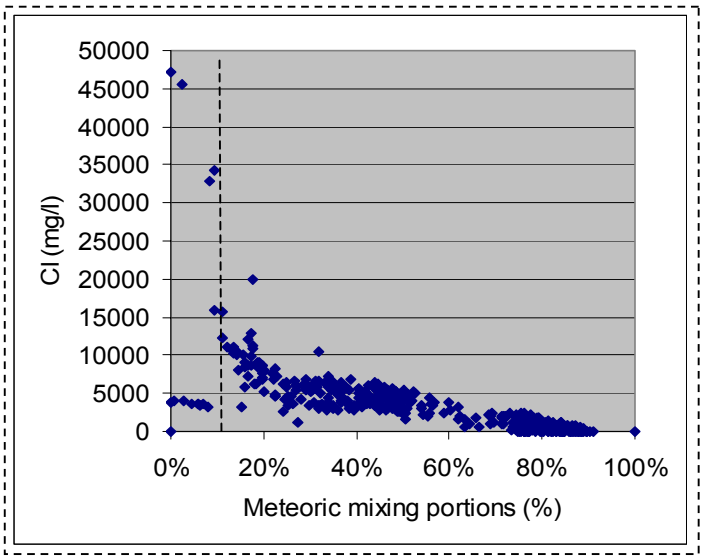

Figure A-1: a) *The correlation between measured $\delta^{18}O$ values and calculated mixing proportions of Glacial water. The figure shows good correlation between "cold water" (low oxygen-18 content) and calculated mixing proportions of Glacial water. b) The correlation between measured Cl values and calculated mixing proportions of meteoric water. The figure shows good correlation between decreasing salinity and increasing mixing proportions of Meteoric water. A mixing portion less than 10% of a water type is regarded as under the detection limit of the method. This limit is indicated by the broken line in the figures.*

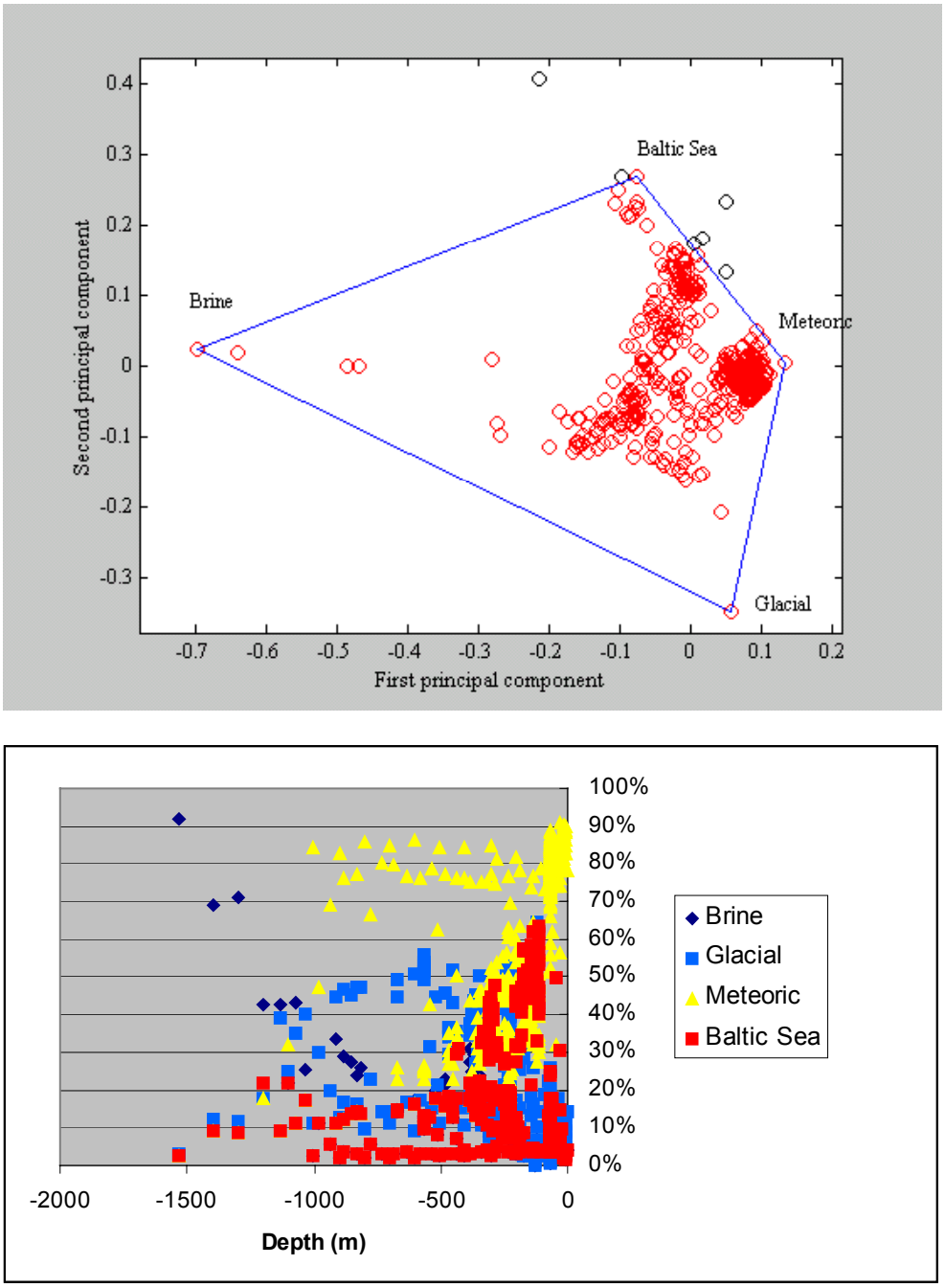

Figure A-2: *The upper figure shows the PCA used for Task#5 data. For simplification only four reference waters where used. The lower figure shows a plot where the calculated mixing proportions (%) for the four reference waters (Brine, Glacial, Meteoric and Baltic Sea) are plotted versus sampling depth. A mixing proportion less than 10% of a water type is regarded as under the detection limit. The method uncertainty of the calculated mixing proportions is ±10%.*

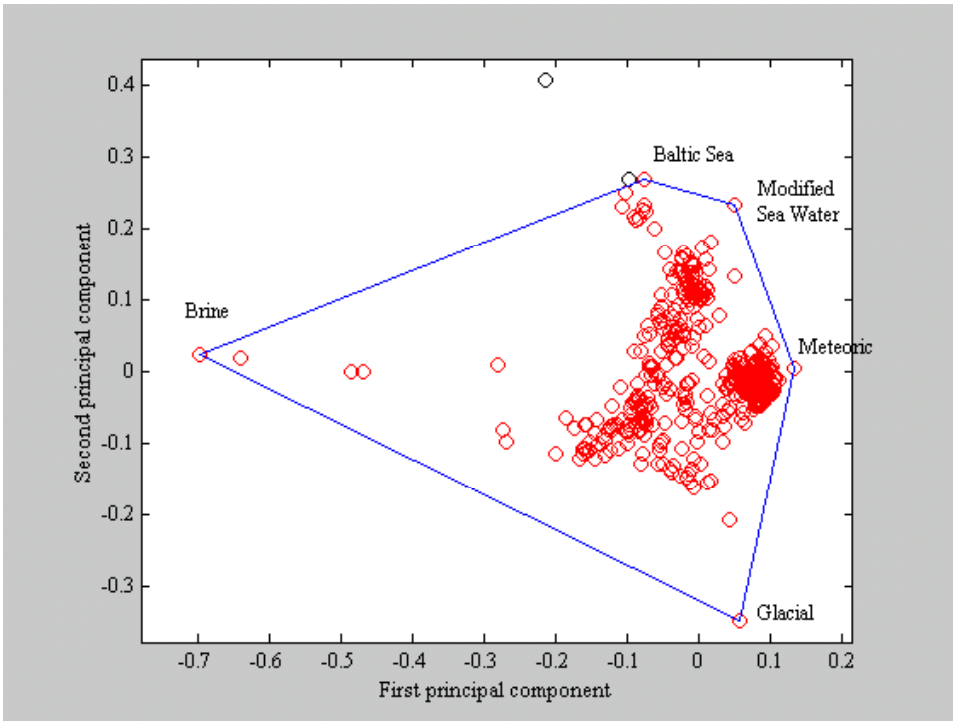

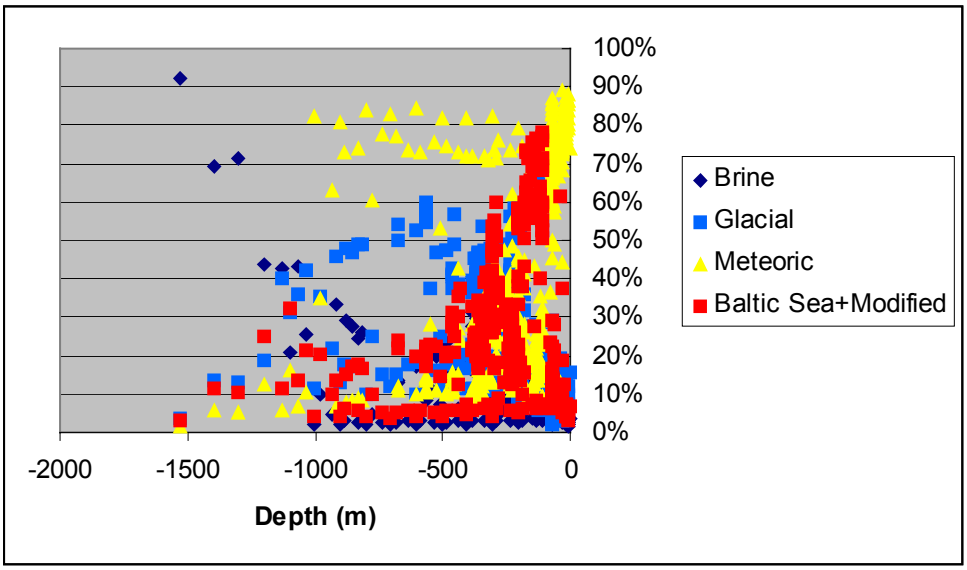

Figure A-3: *The upper figure shows the PCA including the reference water Modified Sea water. This PCA is the standard model for the Äspö site. The lower figure shows a plot where the calculated mixing portions (%) for the reference waters (Brine, Glacial, Meteoric and Baltic Sea (Baltic Sea + Modified Sea water) are plotted versus sampling depth. The proportions of Modified Sea water were added to the proportions of Baltic Sea water to facilitate comparison with the results in Figure A-2. . A mixing proportion less than 10% of a water type is regarded as under the detection limit. The method uncertainty of the calculated mixing proportions is ±10%. The model shows that proportions between Sea water and Meteoric water were affected by including the new reference water.*

Analytical uncertainties: Figure A-4 shows the effect from the analytical uncertainties on the modelling. One test was conducted by altering the major components and isotopes (^{3}H $\delta^{2}H$ and $\delta^{18}O$) with ±5% (which is the measured analytical uncertainty based on independent laboratories) from the reported values in the sample SA1420A from the HRL-tunnel. Another test was changing the tritium from the reported value of 17 TU to 0 TU simulating erroneous tritium measurements in the sample. Due to analytical problems the tritium analyses for some Äspö samples showed this error range. For the Task #5 exercise those observations known to have tritium errors were not included in the database. The conclusion from Figure A-4 is that analytical uncertainty shifts the position of the point in the plot to a minor degree and hence has little effect on the modelling or change the overall interpretation. The analytical uncertainties should be taken into account when selecting two reference waters with a similar composition (not the case in Äspö). The effects of the analytical uncertainties should be plotted in the PC-plot as shown in Figure A-4.

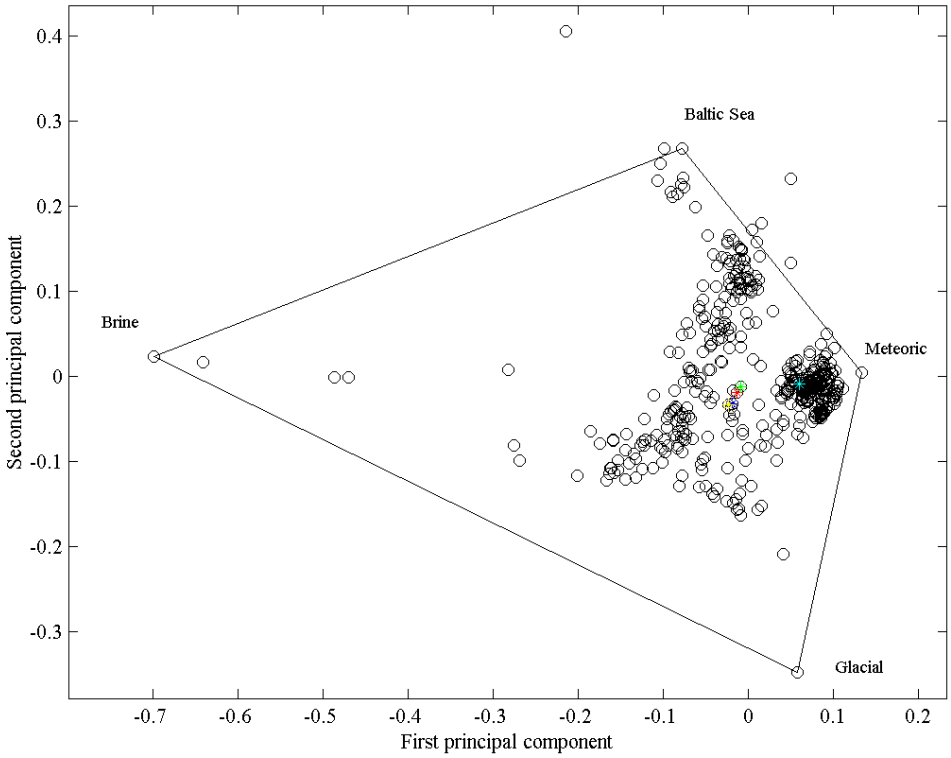

Figure A-4: *The Principal Component plot based on the water conservative tracers Na, K, Ca, Mg, Cl, SO_4, HCO_3, ^{3}H, $\delta^{2}H$ and $\delta 1^{8}O$ applied on Task#5 data. The figure shows the effect from the analytical uncertainties on the position of a sample in the plot and hence the effect on the modelling. Initially the measured components were altered by +5% (blue dot) and by -5% (green dot) from the reported value (red dot) for sample SA1420A. The observed changes are minor. Tritium was then changed from the measured 17TU to 0TU (yellow dot) but keeping the other elements as reported. This mostly changed the position in the PC-plot and changed also the mixing calculations in the following way (the mixing calculations based on the sample where TU was 0 and where TU was 17 are in brackets): Brine +0.02% (13.24%, 13.22%), Glacial +6.10% (22.96%, 16.86%), Meteoric –6.12% (50.57%, 56.69%) and Baltic Sea +0.02% (13,24%, 13.22%). The tests show that the changes in the plot are minor and less than the reported model uncertainty of ±10% and do, therefore, not affect the overall interpretation.*

Uniqueness in the calculations: From a two-dimensional surface, mixing proportions containing a maximum of three reference waters can be calculated so that a mathematically unique solution is obtained. To avoid this shortcoming and to be able to use more than three reference waters in the model a control point P is calculated in the centre point of the polygon. The control point P is located in the weight point of the polygon and is therefore dependent of the shape of the polygon. The function of the point is to fix the mixing calculations which otherwise may have non-unique mixing proportions in the centre of the plot. Although the point is only a control point in the mixing calculations, it does have values of the principal components and of the mixing proportions associated with it. The control point functions as a 'pseudo-reference water' in the calculations, so that an implied component of the mixing model has equal proportions of each reference water. A polygon containing, say, four reference waters, has in the centre point a mixing proportion of 25% of each reference water in the calculations. If there is a sample at that location the sample will have those mixing proportions. By using this addition, a mathematically (but not hydrochemically) unique solution can be achieved from a two-dimensional plane with more than three reference waters.

Conceptually there is a risk of non-uniqueness in the calculation of mixing proportions since they are based on the assumption that all waters contain a proportion of every reference water and the closer to one reference water a sample lies in the plot, the larger the proportion of that reference water in the sample. There may be physical constraints that prevent waters from mixing (depth, geological features etc.) and similar water compositions may have a different mixing history. In theory a sample in the PC-plot may be described as a mixture of all reference waters or as a mixture between two reference waters e.g. such as the Baltic Sea and Glacial reference waters (see Figure A-5). Samples that plot straight on a mixing line between Baltic Sea and Glacial reference waters (even a small deviation requires an additional reference water) may well be a result of a two end-member mixing and for those relatively few samples (<8% of the samples in Task #5 may have this problem) a model including all reference waters is inaccurate. How such samples are modelled in M3 is shown in Figure A-5. The above uncertainties have been handled in M3 by calculating an uncertainty of 0.1 mixing units (with a confidence interval of 90%) and stating that a mixing portion <10% is under the detection limit of the method. The advantage of using all the reference waters in the modelling is that the same model is employed for all the samples which makes the comparison and visualisation of different fracture systems easy and the integration with hydrodynamic modelling possible. If individual models are constructed for different parts of the fracture system the integration and comparison becomes difficult.

If there are enough observations the M3 site scale modelling should be succeeded by a local scale modelling in order to obtain a higher resolution and hence lower the uncertainties. The general rule is that the number of observations should exceed the number of variables. In the Äspö-HRL case this is a subgroup of >10 samples reflecting a certain flow path or a subsystem e.g. samples from the Redox Zone. Such modelling can give additional information but generally the site scale modelling is necessary when visualising and integrating the results with other models. The general uncertainties concerning the origin, mixing and reactions in the groundwaters is generally reduced if the sampling programme satisfactorily reflects the spatial and temporal distribution of the groundwater types at a site.

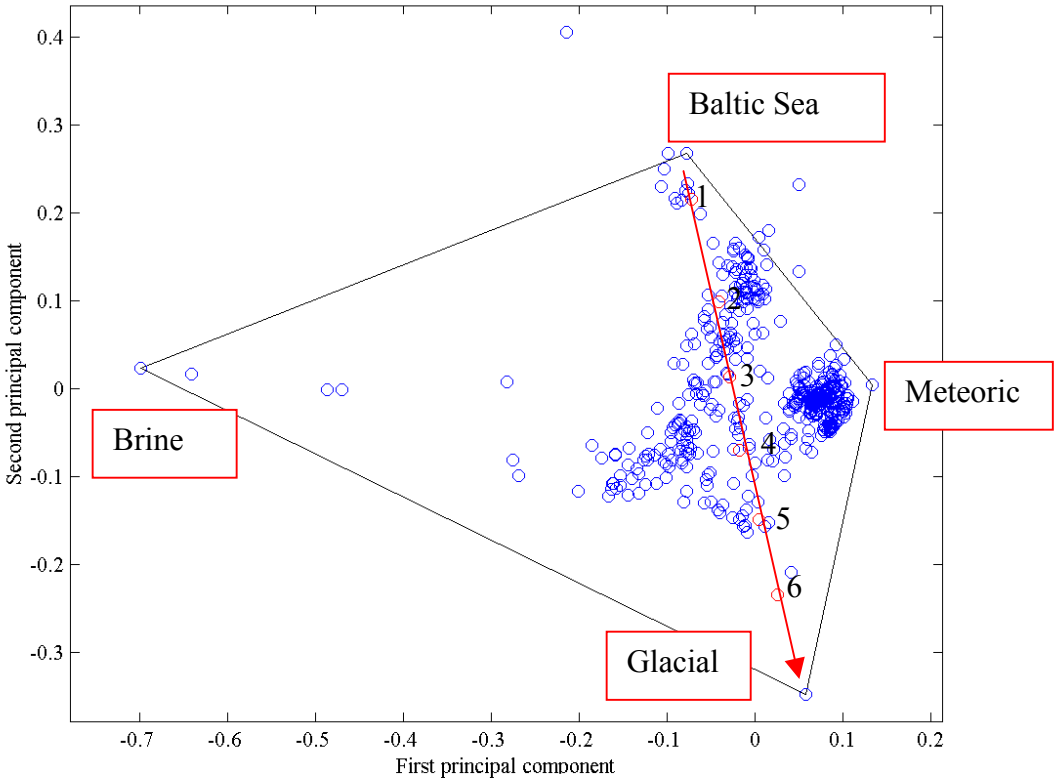

Figure A-5: *In theory samples plotting straight along a mixing line (red arrow) between Baltic Sea and Glacial reference waters may be described as a mixture of all reference waters or as a mixture between the Baltic Sea water and Glacial water. In M3 all the samples are described as mixtures of all reference waters and the modelled samples 1-6 are described by the following mixing proportions: Sample#1 = Brine (3.07%), Glacial (3.07%), Meteoric (9.83%) and Baltic Sea (84.02%); Sample#2 = Brine (8.40%), Glacial (8.40%), Meteoric (36.69%) and Baltic Sea (46.51%); Sample#3 = Brine (13.23%), Glacial (13.23%), Meteoric (53.42%) and Baltic Sea (20.12%); Sample#4 = Brine (12.20%), Glacial (30.92%), Meteoric (44.67%) and Baltic Sea (12.20%); Sample#5 = Brine (8.73%), Glacial (50.46%), Meteoric (32.09%) and Baltic Sea (8.73%); Sample#6 = Brine (5.11%), Glacial (71.91%), Meteoric (17.86%) and Baltic Sea (5.11%). The conceptual uncertainties have been handled in M3 by calculating an uncertainty of ±10% mixing units (with a confidence interval of 90%) and stating that a mixing portion <10% is under the detection limit of the method. The above example shows that in this particular case generally only two reference waters are dominating and lie above the uncertainty range of the method. The advantage by employing the same model on all the samples is that the results become comparable and the integration with hydrogeological models possible.*

Trace elements: By including trace elements, radioactive elements or special isotopes (i.e. U, Ra, Rn, ^{36}Cl) where they contribute with new information not accounted for by the other 10 elements, the shape and resolution of the PCA may change and hence the outcome of the mixing calculations. Lack of data generally hinder a site scale test being performed. In the present modelling, the selected reference waters can describe the observed groundwater composition for the major components and isotopes fairly well which together account for more than 95% of what is dissolved in the groundwater.

Different scale and concentration of the elements in PCA: This is not a problem in PCA since it was originally constructed to be able to compare elements with different scales and concentrations.

What is moving the location of a sample in the PC-plot? The major process is mixing since this generally affects all the components, meanwhile reactions and analytical errors generally affect only some groundwater components and hence do not move significantly the location of a sample in the PC-plot. In Figure A-6 the sample SA1420A is mixed with 50% meteoric water to simulate a dilution process. The new calculated water composition is inserted in the PCA and plots as expected half way between the measured sample and the reference Meteoric water.

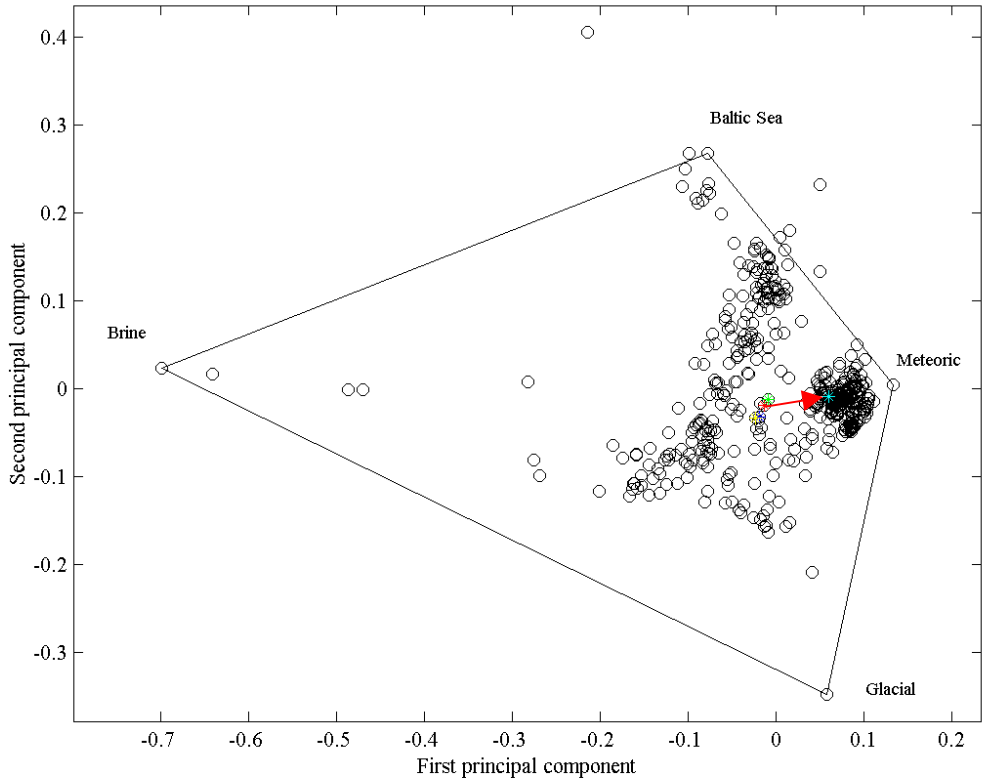

Figure A-6: *The selected sample (SA1420) is used to demonstrate the effect from mixing of 50% meteoric water to the original water composition (red dot) and to demonstrate how the new calculated water composition (cyan dot) is located in the PC-plot. The total change is shown by the red arrow. The mixing affects more the position of a sample in the plot since all the elements are affected. Reactions or analytical errors generally affect only some elements in the water sample; the effects are therefore minor on the location of a sample (see the green, blue and yellow dots in the plot). For more detailed discussion of analytical errors see Figure A-4.*

Normal distribution of the data assumed in the PCA data: The PCA assumes a normal distribution of the data. If the data had another distribution (e.g. log-normal) the PCA would probably be able to summarise more of the information in the first and second principal component resulting in a higher variability than the reported 72%, and at a lower uncertainty. The given uncertainty range of ±0.1 in calculating the mixing proportions should cover for this uncertainty.

Removing/adding observations in the PCA. The PCA is affected by data removed/added from the data set. When doing so the complete analysis has to be repeated since the analysis is always relative to the analytical data and the selected reference waters. The data distribution in the PCA is used to select the number and type of reference waters needed in the analysis. If only samples prior to the tunnel construction are included in the PCA (i.e. 37% of the original samples used in Figure A-2 and in Task#5) it affects the appearance of the PC-plot (see Figure A-7).

From experience the more extreme the added sample is the more it changes the appearance of the PC-plot. In Figure A-7 the selected sample (SA1420A) is used to demonstrate the effect from removing all the other observations from the Äspö HRL-tunnel construction phase but keeping the samples prior to the tunnel construction. The test shows that removing 63% of the observations did not considerably change the mixing proportions, and the uncertainties are less than the reported method uncertainty of ±10% mixing units.

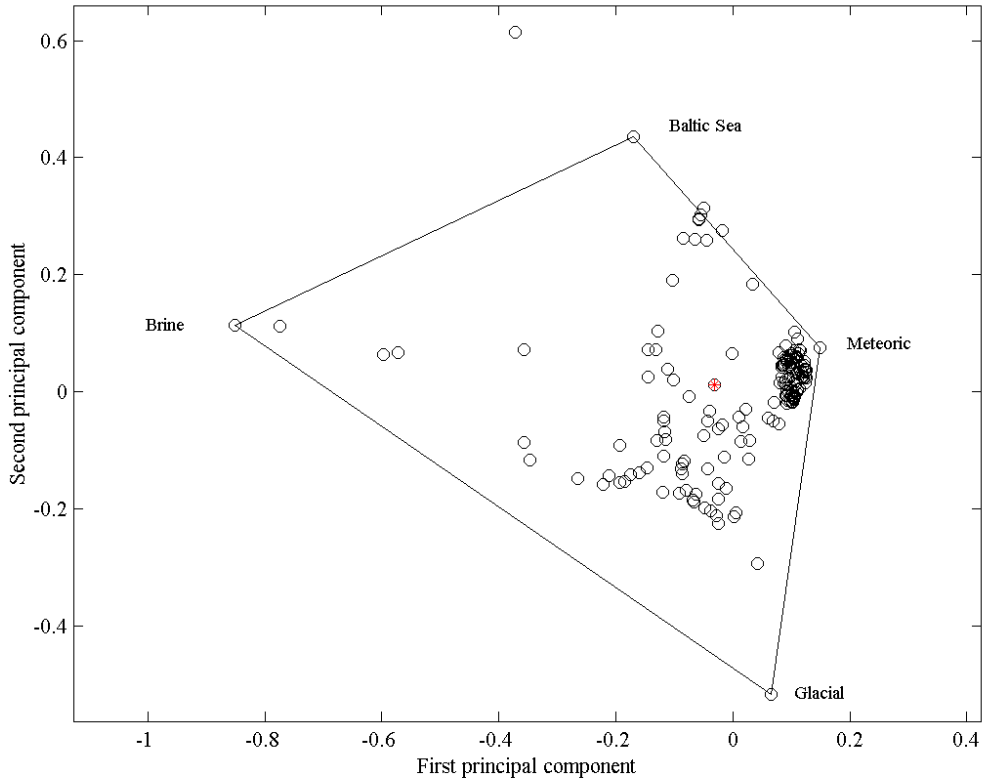

Figure A-7: *The selected sample (SA1420A) is used to demonstrate the effect from removing all the other observations but retaining the samples prior to the Äspö HRL-tunnel construction (37% of the original data set). Sample SA1420 (red dot) has the following mixing proportions (the original mixing proportions in brackets when using the whole data set): Brine 12.43% (13.22%), Glacial 19.29% (16.86%), Meteoric 55.85% (56.69%) and Baltic Sea 12.43% (13.22%). The test shows that removing 63% of the observations did not considerably change the mixing proportions.*

Margin of error in M3 calculations: M3 calculations using the Äspö-HRL data have a ±10% margin of error. However, many of the water compositions reported for use have

end-member proportions of <10%. When a mixing portion is less than <10% it is regarded as being under the detection limit of the M3 method and can therefore be omitted. If the mixing proportions are later to be compared with other models and perhaps to be used to calculate a chemical composition such as Cl content, it is more convenient if the mixing proportions from the reference waters add up to 100%. The margin of error may be such that reference waters with similar composition (not the case at Äspö) may be difficult to separate in the calculations. The effect on the modelling from such a margin of error should always be tested.

Use of the third principal component in the M3 calculation: M3 calculations are based on the first and second principal components. A version of M3 does handle the third principal component. However, in the modelling presented in this study, the first and second principal components summarise 72% of the information, while the first, second and third principal components summarise 82% of the information. The third principal component adds 10% more information. Therefore, in the present modelling exercise the selected reference waters probably describe the observed groundwater composition for the major components and isotopes fairly well. Although the third principal component usually accounts for only a small portion of the variance of the data, it provides a check on the assumptions about mixing end-members. If all the reference waters contribute to all samples then in three dimensions the variance for the third principal component should be low as is the case for Äspö. Figure A-8 shows the effect from modelling the Äspö data by using two principal components versus three principal components. The results show that mostly tritium is better described when using the third principal component in the modelling; the other constituents are not significantly affected.

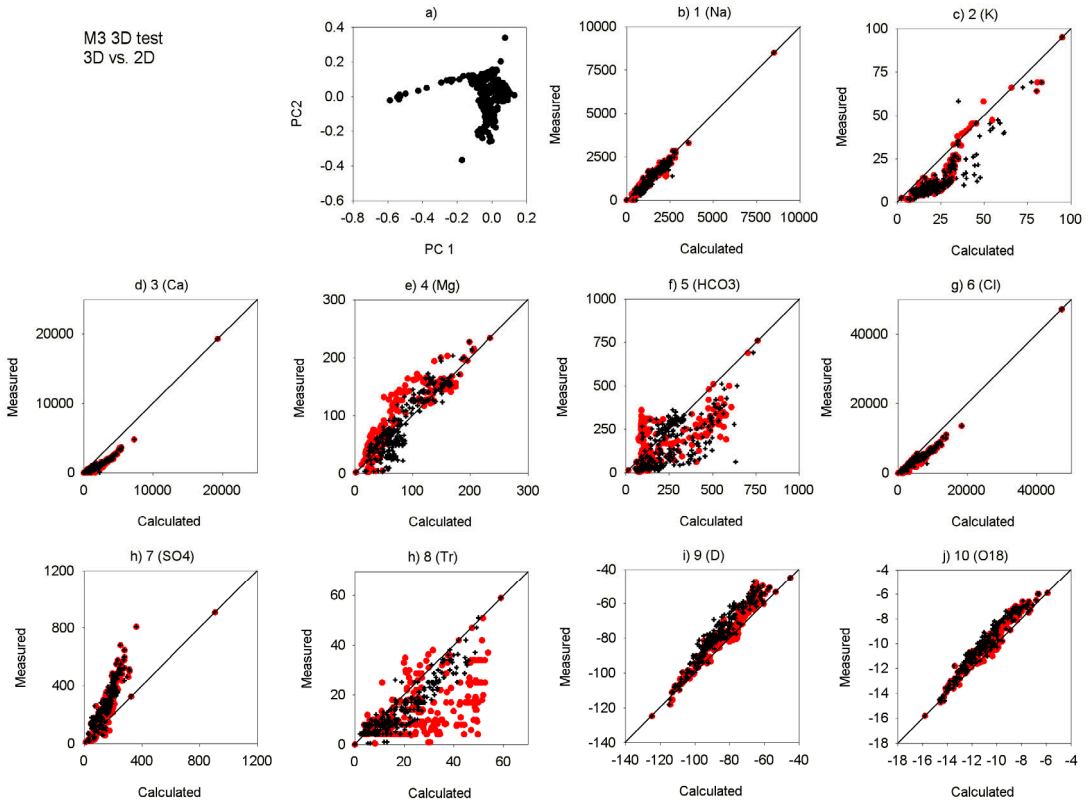

Figure A-8: *The Äspö groundwater data (based on a more extensive data set than used in Task#5) is modelled to be a mixture of Brine, Glacial, Meteoric and Baltic Sea reference waters. The measured/calculated values are compared when two principal components are used (red dots) and when three principal components are used (black dots). If the value plots on the line the predicted and measured value coincide, if the value plots above/under the line there is a deviation between the measured and predicted values. A deviation for the water conservative elements such as Cl, oxygen-18 (^{18}O) and deuterium (^{2}H) indicates scatter in the model. A deviation for a reactive element such as carbonate (HCO_3) can indicate gain (values over the line) or losses (values under the line) associated with reactions. The results show that tritium is better described when using the third principal component; the other constituents are not considerably affected. When calculating in 3D the complexity of the calculations increases; in addition the procedure of selecting reference waters becomes more complex when working in 3D than in 2D.*

Use of both conservative and reactive elements in the M3 modelling: Both reactive and conservative elements are used in the M3 modelling in order to separate the samples, construct a mixing model and to trace the effects from reactions. This is an advantage since more information is summarised but also a disadvantage since the complexity increases and hence the uncertainty.

An advantage is that the chemical signature of the samples is used rather than using a few water conservative elements when identifying and naming the reference waters or the end-members. The PCA containing all the variables is useful, for example when: a) tritium and carbonate separate modern meteoric input from water that may be 3000 years old, b) the sulphate content can be used for separating glacial water from modern snow melt water, and c) identifying unchanged sea water from water that may have undergone microbial sulphate reduction in sea bed sediments and may therefore have a different residence time.

Another advantage is that reactive end-members such as modified sea water (affected by sulphate reduction) can be distinguished in the modelling. In addition when all the elements are included in the model it is convenient to make the mass-balance calculations and test the validity of the model. A test was conducted where the Task #5 data was used to calculate a PC-plot where only the conservative element Cl and the stable isotopes ^{18}O and ^{2}H (^{2}H is conservative except for brine-type water in contact with the rock for millions of years) were included (Figure A-9).

However, by using all the variables, the conceptual uncertainty may decrease but the method uncertainties are increasing. The uncertainty problem is handled in M3 with an uncertainty range of ±10% (within a confidence interval of 90%) from the reported values.

The test shows that Figure A-9 has a different orientation and resolution compared with Figure A-2. The reason is that the information content is different. Figure A-9 lacks the information from elements such as bicarbonate which contains information of, for example, organic decomposition, tritium concerning surface water contribution, magnesium and sulphate concerning the sea water contribution, all of which can be useful in separation of the waters. The resolution for, for example meteoric water, is low, showing that these observations form tight clusters in the plot. The risk of non-uniqueness in the calculations is higher when using few groundwater elements (little information) than when using many groundwater elements (more information). The drawback by including many groundwater elements in the modelling is that the complexity increases and hence the uncertainty range has to be increased in the modelling.

A test was performed to illustrate the form a PCA could take if the Äspö groundwater data were a result of pure mixing and all the elements were behaving conservatively, see Figure A-10. The calculations were conducted by applying the mixing proportions of the Task #5 dataset on the reference water compositions to predict new compositions for all samples. The variance for the first two principal components increased from 72% for the original data in Task #5 to 82%, which indicates that the information is better summarised by the two first principal components (the information is less complex). The PC-plot is always orientated to display the largest possible resolution and the appearance is therefore almost a mirror image compared with the PCA used in Task #5 (see PCA in Figure A-2) and with a higher resolution (better separation of the samples) compared with the results in Figure A-9. The test indicates that if all the elements were conservative tracers this would not affect the calculations dramatically from those used in Task #5.

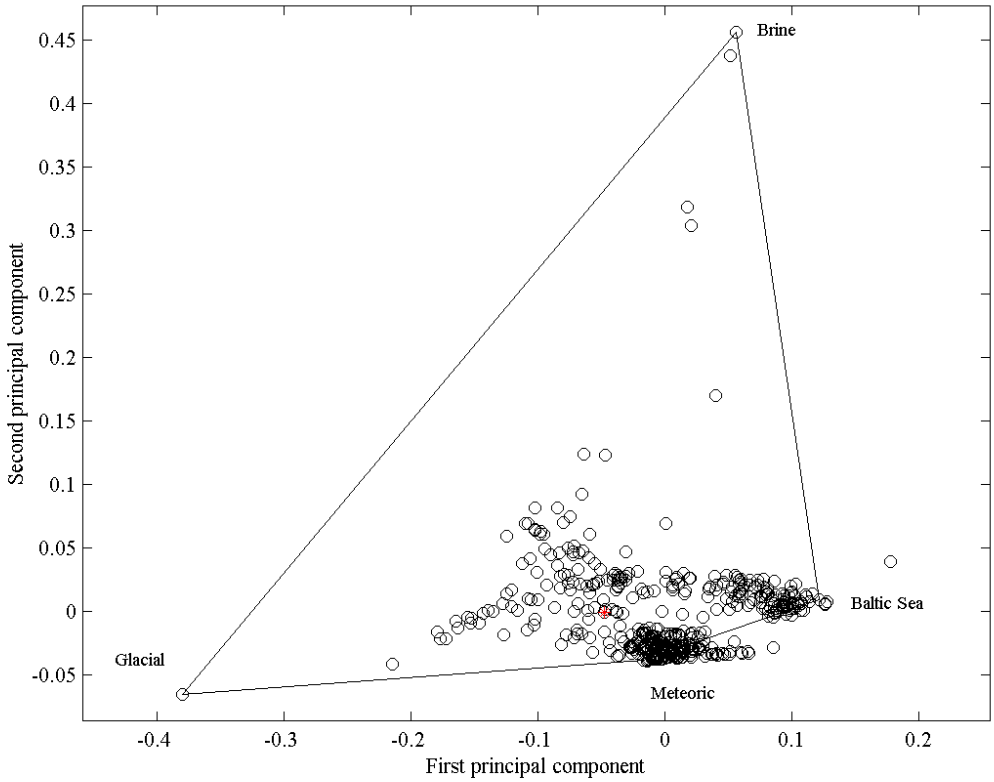

Figure A-9: *A test was conducted based on Task#5 data where only the conservative elements Cl, $\delta^{18}O$ and ^{2}H were used in the PCA. The PC-plot is always orientated to display the largest possible resolution and the appearance may therefore change when using a different set of variables in the calculations. Sample SA1420 (red dot) has the following mixing proportions (the original mixing proportions in brackets when using all the elements in the PCA): Brine 7.21% (13.22%), Glacial 13.94% (16.86%), Meteoric 71.64% (56.69%) and Baltic Sea 7.21% (13.22%). The test shows that using the water conservative tracers changed the mixing proportions within the uncertainty range ±10% mixing units except for Meteoric water that changed 15% but the relative importance of the reference waters remained unchanged.*

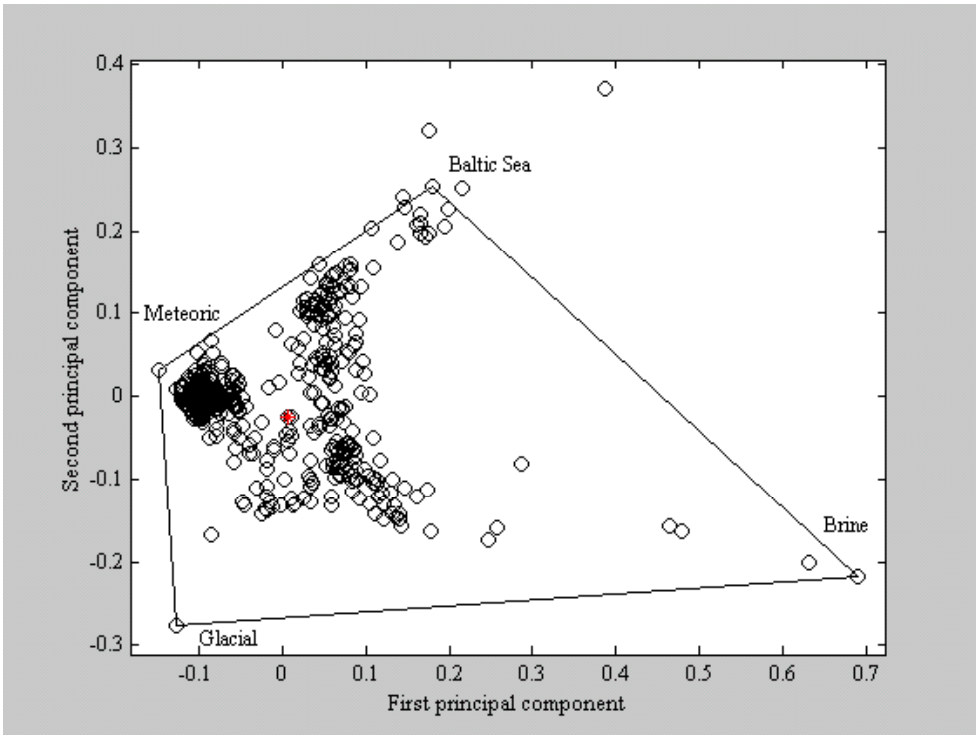

Figure A-10: *A test was conducted based on Task#5 data where new water compositions were calculated for all the samples using the reference water compositions and the mixing proportions from Task#5. This was done to illustrate the form a PCA could take if the Äspö groundwater data were a result of pure mixing (no reactions allowed) and all the elements were behaving conservatively. The PC-plot is always orientated to display the largest possible resolution and the appearance is therefore changed when using different values in the calculations. Sample SA1420 (red dot) has the following mixing proportions (the original mixing proportions in brackets when using measured data in the PCA): Brine 13.12% (13.22%), Glacial 17.22% (16.86%), Meteoric 56.55% (56.69%) and Baltic Sea 13.12% (13.22%). The test shows that if all the elements were conservative tracers this would not affect the calculations dramatically. The first and second principal components summarise 82% of the total information content in the variables.*

Part III

THE ORIGIN AND COMPOSITION OF GROUNDWATER LEAKING INTO THE ÄSPÖ TUNNEL

Urban Svensson

Computer-aided Fluid Engineering AB

1 INTRODUCTION

1.1 BACKGROUND

The Äspö Hard Rock Laboratory (HRL) is a laboratory for the development and testing of methods for detailed characterisation of the rock volume from excavated tunnels. Further, Äspö is a full scale laboratory for testing construction and handling techniques and for the demonstration of important parts of a repository system. Finally, it provides a multitude of data for development of our knowledge of important processes in deep crystalline bedrock and for testing of models for groundwater composition, groundwater flow and radionuclide migration.

A major milestone was reached 1996 with the completion of the pre-investigation and construction phases. The comprehensive research conducted has enabled valuable development and verification of site characterisation methods applied from the ground surface, boreholes and underground excavations. The hydrogeological characterisation of the area has in this context been revised and updated, see Rhén et al. (1997).

As part of the continued research at Äspö HRL, different modelling tasks have been carried out. This report deals with one such modelling task (Task number 5) concerned with the integration of hydrological and hydrochemical models and data. As a general background we may quote the following sentences from Wikberg (1998):

> The aim of Task #5 is to compare and ultimately integrate hydrochemistry and hydrology. The proposed modelling task will also be useful for a future assessment of the stability of the hydrodynamic and hydrochemical conditions at Äspö. This modelling approach could then be used for any future repository site investigations and evolution, especially in a crystalline bedrock environment.
>
> The specific objectives are:
>
> - To assess the consistency of groundwater flow models and hydrochemical mixing-reaction models through integration and comparison of hydraulic and chemical data obtained before and during tunnel construction.
> - To develop a procedure for integration of hydrological and hydrochemical information which could be used for disposal site assessments.
>
> The basic concept of the modelling task is to utilise the data sets on groundwater chemistry and hydrogeology obtained before and during construction of the Äspö facility.

1.2 OBJECTIVES

The objectives of this study are derived from the general ones stated above. In order to meet these the following objectives have been formulated:

- Develop a numerical model that can simulate the origin and composition of the water leaking into the Äspö tunnel.
- Calibrate the model with respect to measured composition of the groundwater in the Äspö area.
- Evaluate the performance of the model. This should be done by additional simulations and by a critical review of concepts and data used.

1.3 STRUCTURE OF REPORT

As explained in Part I, the Task #5 project has been performed in steps; a work report was delivered in January 1999, giving predictions of the first step. The present report focuses on the final results, but will also cover the results from the first step. In the following, we will refer to the first step as Model99, when assumptions, results, etc are discussed. In most of the chapters in this report there will hence be a section giving the corresponding characteristics/results of the Model99. In Chapter 8 (discussion), the two model steps will be evaluated and the lessons learned stated.

2 SITE DESCRIPTION

The Äspö Hard Rock Laboratory is located near the Oskarshamn nuclear power plant on the east cost of Sweden, see Figure 2-1. The access tunnel starts on the mainland, goes under the Baltic Sea and reaches the spiral part of the tunnel beneath the island of Äspö. The total length of the tunnel is 3600 metres and it reaches a depth of 450 metres below ground level. A vertical elevator shaft connects the laboratory to the Äspö Research Complex. During the construction phase, 1990-1995, extensive field investigations were carried out and data collected. Some of these data will be used in the present study. In Figure 2-1 a black rectangle shows the boundaries of the site scale model presented in Svensson (1997b); the same model domain will be used in the present study.

Mean precipitation minus evapotranspiration, P-E, has been estimated to be about 200 mm/year for the region, Rhén et al. (1997). For the island of Äspö one can expect that the groundwater recharge (i.e. P-E) is smaller as the distance to the sea is smaller (no storage of water in lakes and ponds during periods of heavy precipitation). A value of 50 mm/year will be used in this study.

Around the island of Äspö, the Baltic Sea has a salinity of about 0.6%. It is known from boreholes on Äspö that the fresh water lens below Äspö has a thickness of 100-200 metres under natural conditions; below this level the salinity increases to reach a value of about 2% at a depth of 800 metres below ground level. As the water density increases with salinity we have a density stratified water below the Island of Äspö. This is an important feature of the groundwater flow system.

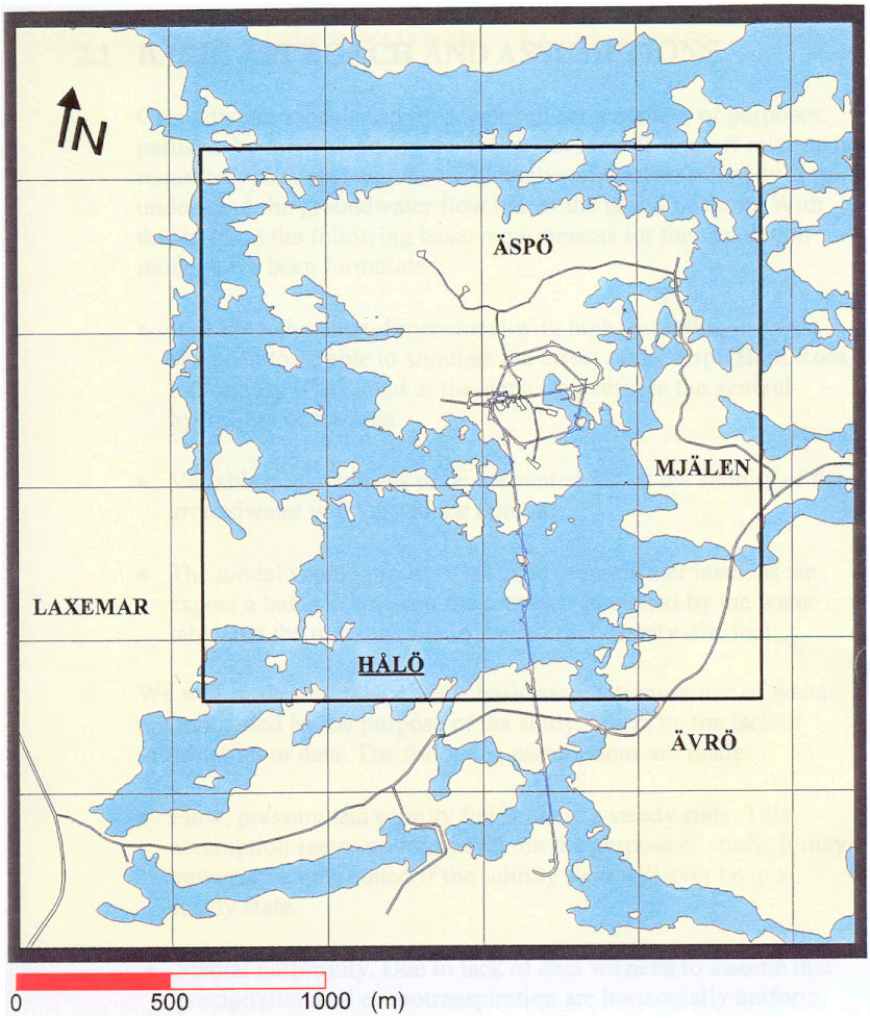

Figure 2-1. *The island of Äspö and the Äspö Hard Rock Laboratory. The black rectangle shows the model area. N is magnetic north.*

3 BASIC CONCEPTUAL ASSUMPTIONS

3.1 BACKGROUND

The hydrochemical field data has been presented as distributions of four basic water types: Meteoric, Baltic, Glacial and Äspö Brine. The Meteoric water has recently been in contact with the atmosphere and originates from precipitation, while Baltic water has its origin from the Baltic Sea. The Glacial water is believed to come from the meltwater of the last inland ice about 12 000 (or more) years ago. The Äspö Brine water is characterised by its high salinity and its age; it is estimated that it has not been in contact with the atmosphere for at least 1 million years. The Äspö Brine fraction increases with depth and may be the dominating fraction below a depth of, say, 800 metres in the Äspö area.

The numerical model should be able to determine the composition, expressed as the four water types mentioned, of the water leaking into the tunnel. Two problems, which call for basic conceptual assumptions, can be identified when formulating such a model:

- Order of magnitude calculations show that water from outside the computational domain (to be specified) will contribute to the inflow to the tunnel already after a few years after the start of the construction of the tunnel. We thus need an assumption about the water composition outside the domain.
- The hydrochemical data show that large fractions of Glacial water are present already at a depth of a few hundred meters. As there is no source of Glacial water one would expect that this water should have been replaced by younger water during the last 12 000 years. As mentioned, the inflow to the tunnel will replace the water in the computational domain with water from outside the domain in a few years time. So, even if we specify a large fraction of Glacial water as an initial condition we would soon "run out" of this water type.

3.2 KEY ASSUMPTIONS

To deal with these problems we need to introduce some assumptions about the water composition at the boundaries of the computational domain. The following concepts and assumptions are introduced, see Figure 3-1:

- Top of domain: On land we use a boundary condition of 100% Meteoric water and for the bottom of the Baltic Sea we assume 100% Baltic water.
- Bottom of domain: We call this water "Mixed Water Bottom" (MWB).
- Vertical boundaries:
  - If s (Salinity) $\leq 0.1\%$ we assume that the water is of Meteoric origin.
  - If $0.1 < s \leq 1.2\%$ we call this water type "Mixed Water High" (MWH).
  - If $s > 1.2\%$ we call this water type "Mixed Water Low" (MWL).

The reason for introducing MWB, MWH and MWL is that we can base an assumption about the composition of these waters on field data. There is also a reason for choosing the salinity value 1.2% as the division between MWH and MWL. When the inland ice had its frontline above Äspö one can expect that Glacial water penetrated very deep into the rock. At about 800 to 1 000 metres, the Äspö Brine provided a lower limit for the circulation. Presumably a mixture of Glacial and Äspö Brine waters resulted in the transition region between the two water types. At about 8 000 years ago the Litorina Sea, with a maximum salinity of about 1.2%, replaced most of the water due to its high density. The maximum penetration depth is however given by the salinity 1.2% and we can therefore assume that MWL is composed mainly of Glacial and Äspö Brine water. Based on these arguments, we assume the following for MWH and MWL:

- MWH. Composition based on field data from borehole KLX01 (see Figure 3-2): 10% Baltic, 35% Meteoric, 45% Glacial and 10% Äspö Brine.
- MWL. 10% Baltic, 10% Meteoric, 40% Glacial and 40% Äspö Brine. This is to some degree supported by measurements in KLX02, at a depth with a salinity of 1.5%.

For the water entering through the bottom of the domain, MWB, it will be assumed that the composition is the same as for MWL.

3.3 CONDUCTIVITY AND POROSITY FIELDS

It is not the purpose of this project to develop new concepts concerning the conductivity and porosity fields. However, these fields will have a very strong influence on the simulations; the time for water from outside the domain to reach the tunnel is for example linearly related to the adopted value of the kinematic porosity. Another reason for bringing these topics up is that novel and recently developed methods will be used for the specification of these fields. The methods have been described elsewhere; in Svensson(1999a, b) the method for generating conductivity fields is given and in Svensson (2001a) the concepts regarding the porosity are described. A brief account of the basic concept of these methods will however be provided.

The basic idea of the methods is to generate a fracture network and then represent this network in a continuum model. Each fracture in the network has a rectangular shape, a certain thickness and material properties like transmissivity and porosity. Further details will be given in Chapter 4. Provided the network is properly represented in the computational grid, conductivity and porosity fields with a certain correlation structure and connectivity are obtained. For further details, see the above mentioned reports.

3.4 MODEL99

The first step simulations were based on the same arguments concerning the salinity distributions at the vertical boundaries. However, it was assumed that all water with a salinity larger than 2.0% could be classified as Äspö Brine. For the vertical boundaries we thus have the additional conditions "if $s \geq 2.0\%$, 100% Äspö Brine is assumed". As the bottom boundary is normally in a region with $s > 2.0\%$, it was assumed that the bottom boundary condition was "100% Äspö Brine". There was hence no need to introduce MWB, as in the final model.

A major difference, as compared to the final model, is that conductivity and porosity fields were not based on a fracture network. Instead the conductivity field was based on "major deterministic fracture zones and rock block domains in between these zones". This was the method used in Svensson (1997b), based on data given in Rhèn et al. (1997). Some details of this method will be given in Chapter 4. In the Model99, the kinematic porosity was related to the conductivity, according to Rhén et al. (1997).

3.5 CONCLUDING REMARKS

The assumptions introduced will make it possible to set up a simulation model that can be used to calculate the composition of the water leaking into the tunnel. However, the assumptions made are based on speculations, that are only partly supported by field data. The compositions of MWB, MWH and MWL are therefore regarded as tentative and will be considered again in the calibration of the model.

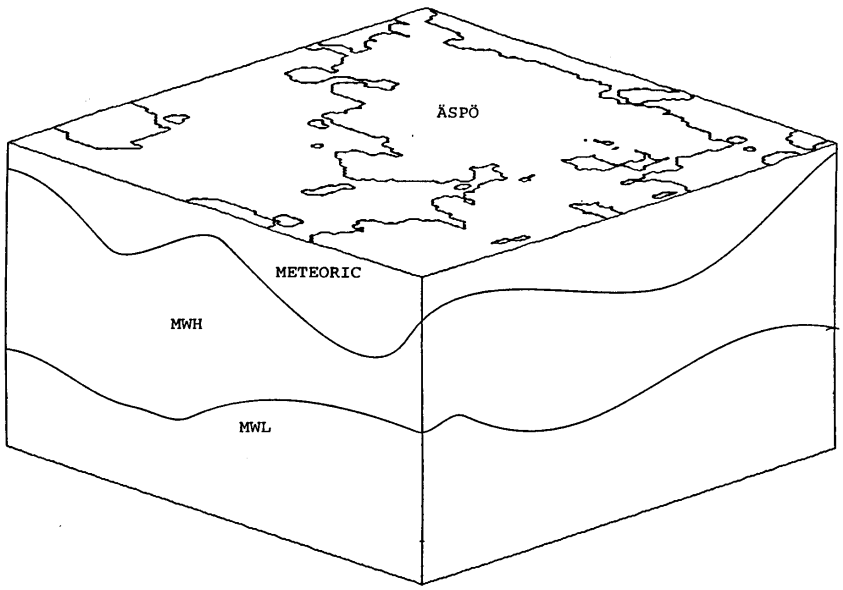

Figure 3-1. *Illustration of basic conceptual assumptions.*

Figure 3-2. *Boreholes on Laxemar, Ävrö and Äspö.*

4 MATHEMATICAL MODEL

4.1 BASIC APPROACH AND ASSUMPTIONS

Groundwater models can be developed for a number of purposes; perhaps the most common one is that the rainfall - runoff relation is requested. As stated above, the objective of the present study is to understand the groundwater composition below the island of Äspö. With this in mind the following basic requirements for the simulation model have been formulated:

- It needs to be three-dimensional with high resolution in space. We need to be able to simulate the effect of the Äspö Hard Rock Laboratory (HRL) and at the same time resolve the general hydrology of the area.
- Variable density needs to be accounted for, as the salinity of the groundwater will vary in the domain.
- The model should predict a realistic groundwater level, as we expect a balance between the pressure generated by the water table and the pressure due to the internal density distribution.

We will further introduce some basic assumptions; some of which are motivated by the purpose of the study, others by the lack of information or data. The following assumptions are made:

- Spatial uniformity. Due to lack of data we need to assume that precipitation and evapotranspiration are horizontally uniform. Variations in vegetation and soil types are also neglected.
- The simple algorithm introduced in Svensson (2001b) can handle the unsaturated zone.

The computational domain was introduced in Figure 2-1. The motives for the size and orientation of the domain can be summarised as follows:

- The orientation should follow the Äspö coordinate system, for simple and secure integration with the Äspö data base.
- The size should be comparable to the expected "radius of influence" of the Äspö HRL. From the drawdowns, due to the Äspö HRL, one can estimate this radius to be about 1 km.
- The computational grid should not have more than 500 000 cells, in order to avoid extreme execution times on a low-end workstation.

These considerations led to a domain of 1.8 x 1.8 x 1.0 km^3, centred around the Äspö HRL, represented in a computational grid of 90 x 90 x 58 cells.

These are the basic requirements and assumptions of the model.

4.2 GOVERNING EQUATIONS

For the momentum balance it will be assumed that the Darcy law applies, i.e. the time derivative is neglected. Further, the storativity term in the mass balance equation is also neglected as this is believed to be a second order term in the present context.

Within these assumptions, and the ones in the previous section, the following set of equations can be formulated.

Momentum:

$$0 = -\frac{\partial p}{\partial x} - \frac{\rho g}{K_x} u \tag{1}$$

$$0 = -\frac{\partial p}{\partial y} - \frac{\rho g}{K_y} v \tag{2}$$

$$0 = -\frac{\partial p}{\partial z} - \frac{\rho g}{K_z} w - \rho g \tag{3}$$

Salinity balance:

$$\frac{\partial sn}{\partial t} + \frac{\partial}{\partial x} us + \frac{\partial}{\partial y} vs + \frac{\partial}{\partial z} ws = \frac{\partial}{\partial x}\left(Dn \frac{\partial s}{\partial x} \right) + \frac{\partial}{\partial y}\left(Dn \frac{\partial s}{\partial y} \right) + \frac{\partial}{\partial z}\left(Dn \frac{\partial s}{\partial z} \right) \tag{4}$$

Mass balance:

$$\frac{\partial}{\partial x} \rho u + \frac{\partial}{\partial y} \rho v + \frac{\partial}{\partial z} \rho w = 0 \tag{5}$$

Equation of state:

$$\rho = \rho_0 (1 + \alpha s) \tag{6}$$

Where *u, v, w* are Darcy velocities, *p* pressure, *s* salinity (in %, by weight), K_x, K_y, K_z conductivities, *D* hydraulic dispersion coefficient, *n* kinematic porosity, α a coefficient $\left(= 7.8 \times 10^{-3}\right)$, ρ_0 a reference density of water (= 1 000 kg/m^3), ρ density of water and g gravitational acceleration. The coordinate system is denoted *x, y, z* with *x* in the east direction, *y* north and *z* vertical upwards.

It is still unclear (at least to the author) how the hydraulic dispersion coefficient ought to be interpreted and determined in a fractured rock. For a porous media, where a representative elementary volume can be defined, general tensor expressions are available, see Bear et al. (1987). A further complicating factor is that we are going to apply the salinity equation in a discretized form, i.e. on our computational grid.

A suggestion is that the dispersion coefficient should account for sub-grid mixing processes. Due to the uncertainty about the interpretation of the process we will assume that the dispersion coefficient is isotropic, proportional to the local velocity and the grid-size, hence:

$$D = \beta \Delta |U| \tag{7}$$

where β is an unknown coefficient, Δ the grid-spacing and $|U|$ the magnitude of the pore-velocity. As seen, the effect of molecular diffusion is also neglected in (7). As D is multiplied with n in equation (4) we will further assume that $n\,|U|$ is equal to the magnitude of the Darcy velocity. A constant value of 2 metres was set for the product $\beta\Delta$.

In order to track the various components of the groundwater an advection/diffusion equation is solved for each component:

$$\frac{\partial c_i n}{\partial t} + \frac{\partial u_j c_i}{\partial x_j} = \frac{\partial}{\partial x_j}\left(n D_c \frac{\partial c_i}{\partial x_j} \right), \quad \mathrm{i} = \mathrm{l}, \mathrm{k} \tag{8}$$

where c_i is the marker for water type i. We will not consider dispersion effects in the present context and D_c is hence zero. To track the component that originates, say, from the Baltic Sea we put the relevant c-value to 1.0 in all cells that represent the bottom of the Baltic Sea and to 0.0 at all other boundaries.

4.3 GEOMETRIC FRAMEWORK AND MATERIAL PROPERTIES

Major fracture zones on Äspö are shown in Figure 4-1. The thick lines in the figure indicate regional fracture zones; these were used in the regional groundwater model, see Svensson (1997a), and are in the site model essential for the connection of boundary conditions to the local fracture zone system. The fracture zones are assumed to be two-dimensional and planar. Data about the fracture zones are given by Rhén et al. (1997), from where the thicknesses, b, and transmissivities, T, given in Table 4-1, are taken. In this table also the fracture transport aperture, e_T, and the kinematic porosity $(= e_T / b)$ are given. The fracture aperture is calculated from the semi-empirical formula by Rhén et al. (1997):

$$e_T = 1.428 T^{0.523} \tag{9}$$

In the following these major fracture zones will be called the deterministic fracture zones in contrast to the background, or stochastic, fracture network to be discussed next.

The background fracture network needs to be specified with respect to orientation, size distribution, fracture intensity, thickness and transmissivity distributions. The same specification as in Svensson (1999b) will be used and the reader is referred to this report for details. Here, only the main features of the fracture network will be listed:

- Orientation. Two vertical fracture sets; one NE and one NW trending. The spread around these main directions is given by a Fisher distribution. As the NW-direction should be more conductive, 70% of the fractures will have this trend (with Fisher's $\kappa = 12$) and 30% will have a NE trend (with $\kappa = 7$). The spatial distribution is assumed to be uniform.

- Intensity. The fracture intensity is specified from a power law distribution. For a length interval, *dl*, we then get:

$$n = \mathrm{I} * \left[\left(\frac{l + dl}{l_{ref}} \right)^{\alpha} - \left(\frac{l}{l_{ref}} \right)^{\alpha} \right] / \alpha \qquad (10)$$

  where *n* is the number of fractures per unit volume, I the intensity, l_{ref} a reference length (=500 m) and α , the power law exponent, put to -2.6 (see LaPointe et al., 1999). The intensity was determined to 10^{-8} by generating fractures in the interval 320 to 1 000 metres and compare the number with the number of deterministic fracture zones in the domain.

- Shape. All fractures are assumed to be square with length, *L*, and thickness, *b*. The thickness is assumed to be 0.02L.

- Transmissivity. The tentative formula found in the calibration of the laboratory model (Svensson, 1999b) is used. This formula relates the transmissivity to the fracture size:

$$T = \begin{cases} 10^{-5} \left(L / 100 \right)^2 \left[\mathrm{m}^2 / s \right] & \text{for } L \le 100 \text{ m} \\ 10^{-5} \left[\mathrm{m}^2 / s \right] & \text{for } L > 100 \text{ m} \end{cases} \qquad (11)$$

The properties of the background fracture network are summarised in Table 4-2. Equation (9) was used to calculate the transport aperture also for the background fractures.

The computational domain is $1.8 \times 1.8 \times 1.0\ \mathrm{km}^3$, which is represented in a grid with a total of 469 800 cells $(90 \times 90 \times 58)$. Part of the grid is shown in Figure 4-2. As can be seen the grid follows the topography (boundary-fitted grid), but has a uniform cell size (= 20 metres) in the horizontal plane. The vertically non-uniform grid is restricted to the

top 100 metres of the domain. For this part of the grid we start with a cell size distribution (from ground level downwards) as follows: 0.5, 1.0, 1.5, 2.0, 5.0, 7×10.0 and 20.0 metres. This sequence of cells is then stretched/compressed to follow the topography, which means that the cell-sizes in the sequence are somewhat smaller below the Baltic and somewhat larger below land. Below 100 metres the cell size is 20 metres in all three directions. It should be noted that the grid follows the sea-bed and not the free surface of the Baltic.

Conductivities for the top five cell layers, i.e. down to 10 metres, are given a special interpretation. One reason for this is that the soil cover can be expected to have a conductivity which is high, but rapidly decreasing with depth. Another is that small ephemeral rills and channels need to be accounted for by the conductivity of the near ground surface cells. The conductivity of the top five cell layers are considered as calibration parameters and will be determined in the following chapter.

A further modification of the conductivity field is needed to account for unsaturated conditions. A method to predict the depth of the unsaturated zone was introduced in Svensson (2001b). Here a brief account of the basic idea of the method will be given.

- Determine the position of the groundwater level from the pressure field, i.e. the zero pressure surface.
- Above the groundwater level the horizontal conductivity is decreased to a level that practically eliminates all horizontal flow. A vertical flow (precipitation) can however be present.
- The region with negative pressure represents the unsaturated zone. Comparisons with analytical solutions for idealised cases show that this interpretation is correct.

It should be emphasised that this method can handle both natural conditions and the drawdown due to the tunnel, without changing the prescribed flux at the top boundary (set to 50 mm/year). For natural conditions most of this flux will find its way to the sea, while most of the prescribed flux will reach large depths, when the tunnel is present.

Below the Baltic a clay layer of a few metres thickness is normally found. This was considered in the model by prescribing a conductivity of 10^{-10} m/s to a 3 metres thick layer, centred 5 metres below the sea bed.

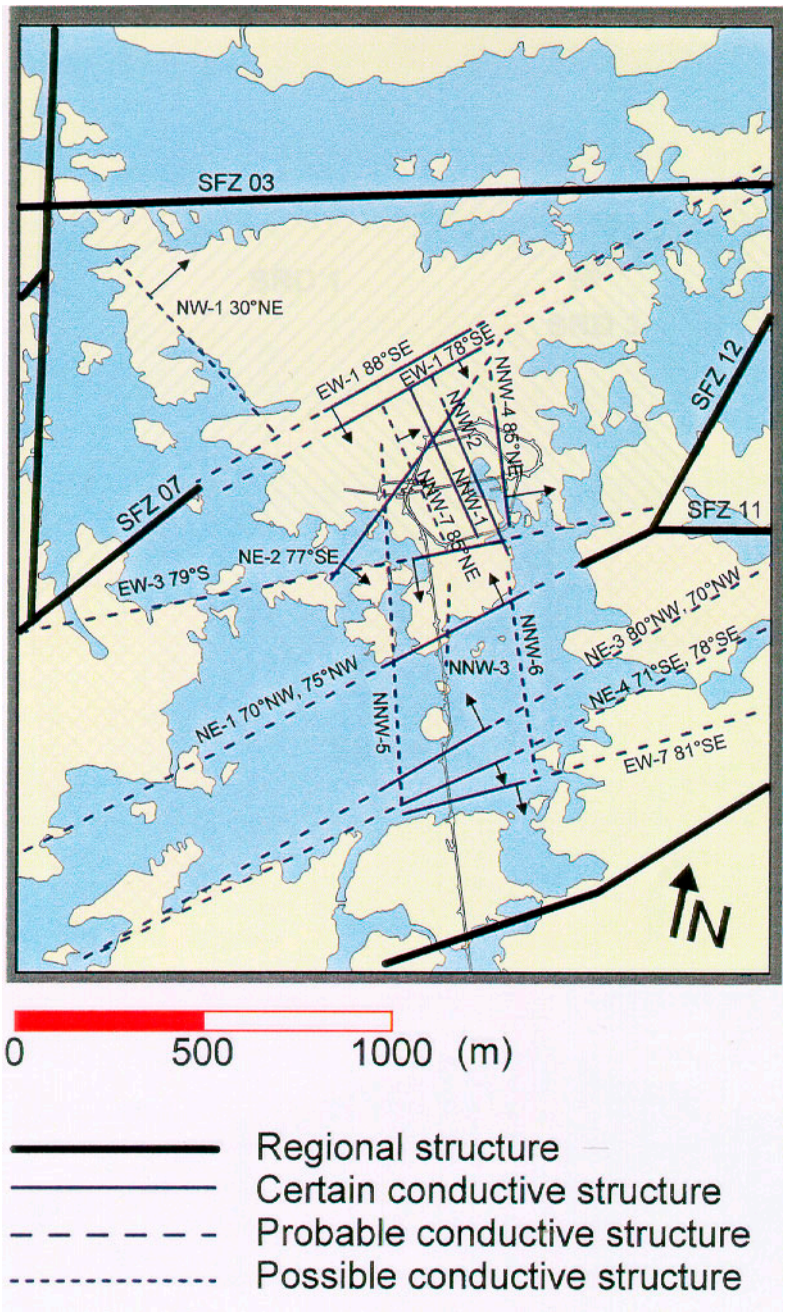

Figure 4-1. *Major fracture zones in the area, after Rhén et al. (1997).*

Table 4-1. Properties of the deterministic fracture zones.

Fracture zone	Thickness (m)	Transmissivity x 10^{-5}[m^2/s]	Modified Transmissities during calibration x10^{-5}[m^2/s]	Transport aperture (m) x 10^{-3}	Kinematic porosity x 10^{-3}
NW1	10	0.041		0.6	0.06
EW1, 88°	20	0.052		0.7	0.037
EW1, 78°	20	1.2		3.8	0.19
EW3	10	1.7		3.8	0.38
NE2	10	0.012	0.1	1.04	0.10
NE4	10	3.1		6.26	0.63
EW7	10	1.5		4.28	0.43
NE3	10	32.0		20.5	2.05
NE1	10	22.0	24	12.7	1.27
NNW1	10	0.86	0.4	2.1	0.21
NNW2	10	2.4	1.2	3.8	0.38
NNW3	10	2.0		5.0	0.50
NNW4	10	6.5		9.2	0.92
NNW5	10	0.4		2.1	0.21
NNW6	10	1.4		4.1	0.41
NNW7	10	0.75	2.0	5.0	0.50
NNW8	10	0.84		3.2	0.32
SFZ03	10	0.3		1.85	0.18
SFZ07	10	0.3		1.85	0.18
SFZ11	10	0.3		1.85	0.18
SFZ12	10	10.0		11.6	1.16

Table 4-2. Properties of the fractures forming the background fracture network. Note: The transmissivities given are only used to calculate the transport aperture for the fracture set. When conductivity fields are generated, the transmissivities are calculated from Equation (11).

Fracture set	Length interval (m)	Thickness (m)	Number of fractures generated	Number of fractures isolated	Trans-missivity (m^2/s) x 10^{-6}	Transport aperture (m) x 10^{-3}	Kinematic porosity x 10^{-3}
1	160-320	4.2	314	0	10.0	3.47	0.83
2	80-160	2.1	1558	35	10.0	3.47	1.65
3	40-80	1.0	7389	1242	2.7	1.75	1.75
4	20-40	0.5	30744	18632	0.68	0.85	1.70

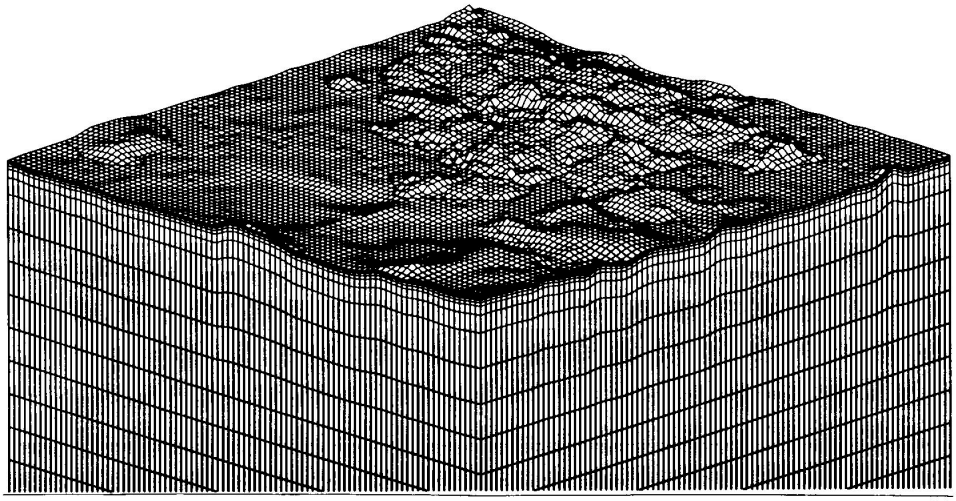

Figure 4-2. *Computational grid close to ground. 100 metres below sea level a uniform grid is used. The vertical scale has been stretched in the figure. View from south-east.*

4.4 SPATIAL ASSIGNMENT METHOD

All fractures (deterministic and background) will be represented in the computational grid by the same method, described in detail in Svensson (1999a) and Svensson (2001a). There is hence no need to repeat that here. However, the key features of the method will be briefly described as a general background.

A staggered grid is to be used, which means that scalar quantities, like pressure and salinity, are stored at cell centres while velocity vectors are stored at cell wall centres. Each variable is assumed to be representative for a certain control volume, which is the volume the discretized equations are formulated for. For a velocity cell it is clear that the driving pressure force can be easily formulated. As we are going to apply the Darcy law to the velocity cell, we also need a relevant cell conductivity to obtain the cell wall velocity. The kinematic porosity is a scalar quantity and we thus need a representative value for the scalar control volume. The key idea of the method can now be stated as follows:

- A conductive element contributes to the grid value of a variable by an amount that is equal to the intersecting volume times the value of the variable in question. Contributions from all elements that intersect the control volume are added and the sum is divided by the volume of the cell.

Before the fractures are represented as grid conductivities one needs to consider how isolated fractures are to be treated. Depending on the situation studied we may choose to remove or keep isolated fractures, or groups of fractures, in the conductivity field. If we choose to remove the isolated fractures, as is done in this study, the following steps are performed:

- The deterministic fractures are considered to be water-conducting and can thus form a "starting" network in the sorting procedure.
- Fractures that cross the boundaries of the domain are not removed as we can not for certain say that these are isolated.
- A sorting procedure determines if a fracture, or a group of fractures, is isolated and, if so, removes these fractures.

The method outlined for the unsaturated zone may result in a vertical column of cells that has very low conductivities on all vertical cell walls. As we have a recharge at ground level an isolated column of water may result if, at some level, a low vertical conductivity is generated. The remedy to this problem was to prescribe a minimum conductivity, equal to 10^{-8} m/s, below Äspö, down to a depth of 60 metres.

4.5 BOUNDARY CONDITIONS

At the top boundary a net recharge of 50 mm/year is specified above sea level. Below the Baltic Sea a hydrostatic pressure is prescribed, with respect to the local water depth. The salinity is fixed to the salinity of the Baltic (= 0.6%).

At the vertical and bottom boundaries pressure and salinity fields from the regional groundwater model are used. Two sets of boundary conditions are generated; one for natural conditions and one for completed tunnel. Boundary conditions during the propagation of the tunnel are found from a linear interpolation based on the total inflow to the tunnel, i.e. the ratio present inflow/inflow to completed tunnel is used. Note also that the water compositions at the vertical boundaries are related to the salinity distribution. This means that also the compositions will change with time. Further details of how the boundary conditions are generated can be found in Svensson (1997b).

When the Äspö HRL is included in a simulation we need to consider the inflows to the tunnel. These inflows are not boundary conditions in the usual meaning; a more relevant name is perhaps “distributed mass sinks”. The measured inflows to tunnel sections need to be assigned to computational cells with a fracture zone crossing. Based on the measured data given by Rhén et al. (1997), the distributions given by Table 4-3 have been estimated. Distributions are given for all tunnel front positions to be considered in this report.

4.6 NUMERICAL TOOL AND OUTPUT PARAMETERS

The system of equations is solved by the general equation solver PHOENICS, Spalding (1981). PHOENICS is based on a finite-volume formulation of the basic equations and embodies a wide range of coordinate systems (cartesian, body-fitted, cylindrical, etc) and numerical techniques (higher order schemes, solvers, etc).

4.7 MODEL99

The first step model differs from the final one in three respects:

- Flow, pressure and salinity fields were assumed to be in a quasi-steady state. A series of steady state fields, each representing a certain tunnel front position, was first calculated and stored. These fields were then used for transient transport calculations, i.e. the tracer equations (Equation 8).

- A method to represent the unsaturated zone, described in Svensson (1995), was used. This method was later found to have less satisfactory convergence properties and replaced by a new algorithm in the final model.

- As mentioned, the conductivity field was based on a number of deterministic fracture zones (same as in the final model) and rock block domains, giving the properties in between the zones. The rock block domains are illustrated in Figure 4-3 and the properties of the zones and the blocks are given in Tables 4-4 to 4-6. These tables also give the calibrated transmissivities and conductivities. For the top five cell layers, Table 4-6, only data from the calibration are available.

Table 4-3. Inflows to Äspö HRL. Measured inflows at various tunnel front positions and assigned fracture zones for withdrawal. Basic data from Rhén et al. (1997).

Tunnel section[m]	Measured inflow [l/s]										Selected zone(s) for with-drawal
	Tunnel front position [m]										
	0 ↓ 960	960 ↓ 1190	1190 ↓ 1380	1380 ↓ 1750	1750 ↓ 2160	2160 ↓ 2590	2590 ↓ 2900	2900 ↓ 3170	3170 ↓ 3600	3600	
0-850	0.87	1.42	2.00	2.00	2.00	2.00	2.00	2.00	2.00	1.90	NE4
850-1030		4.00	5.00	5.88	5.88	5.88	5.88	5.88	5.50	5.52	NE3
1030-1160		0.67	3.07	3.08	3.08	3.15	3.37	3.16	2.93	1.40	NNW3
1160-1310			4.32	7.50	7.50	7.50	7.50	7.00	7.00	7.00	NE1
1310-1460				0.90	1.08	1.08	1.21	1.22	1.20	2.03	EW3
1460-1584				0.07	0.30	0.30	0.30	0.30	0.30	0.61	NE2
1584-1745				0.07	0.20	0.18	0.14	0.14	0.13	0.27	NNW7
1745-1883					0.42	0.50	0.61	0.63	0.53	0.36	NNW1, NNW2
1883-2028					0.29	0.58	0.62	0.53	0.47	0.47	NNW4
2028-2178						0.99	1.06	0.95	0.80	0.70	NNW4
2178-2357						0.69	1.04	1.18	1.23	1.42	NNW1, NNW2
2357-2496						0.03	0.09	0.07	0.07	0.17	NE2
2496-2699							0.44	0.93	0.93	0.93	NNW7
2699-2875							0.08	0.50	0.50	0.38	NNW1, NNW2
2875-2994							0.01	1.20	1.28	1.12	NNW4
2994-3179								1.80	3.31	2.33	NNW4
3179-3426									0.48	0.96	NNW1, NNW2
3426-3600									0.05	0.46	NNW5
Shaft					3.3	4.0	3.2	2.9	2.06	1.54	NNW7

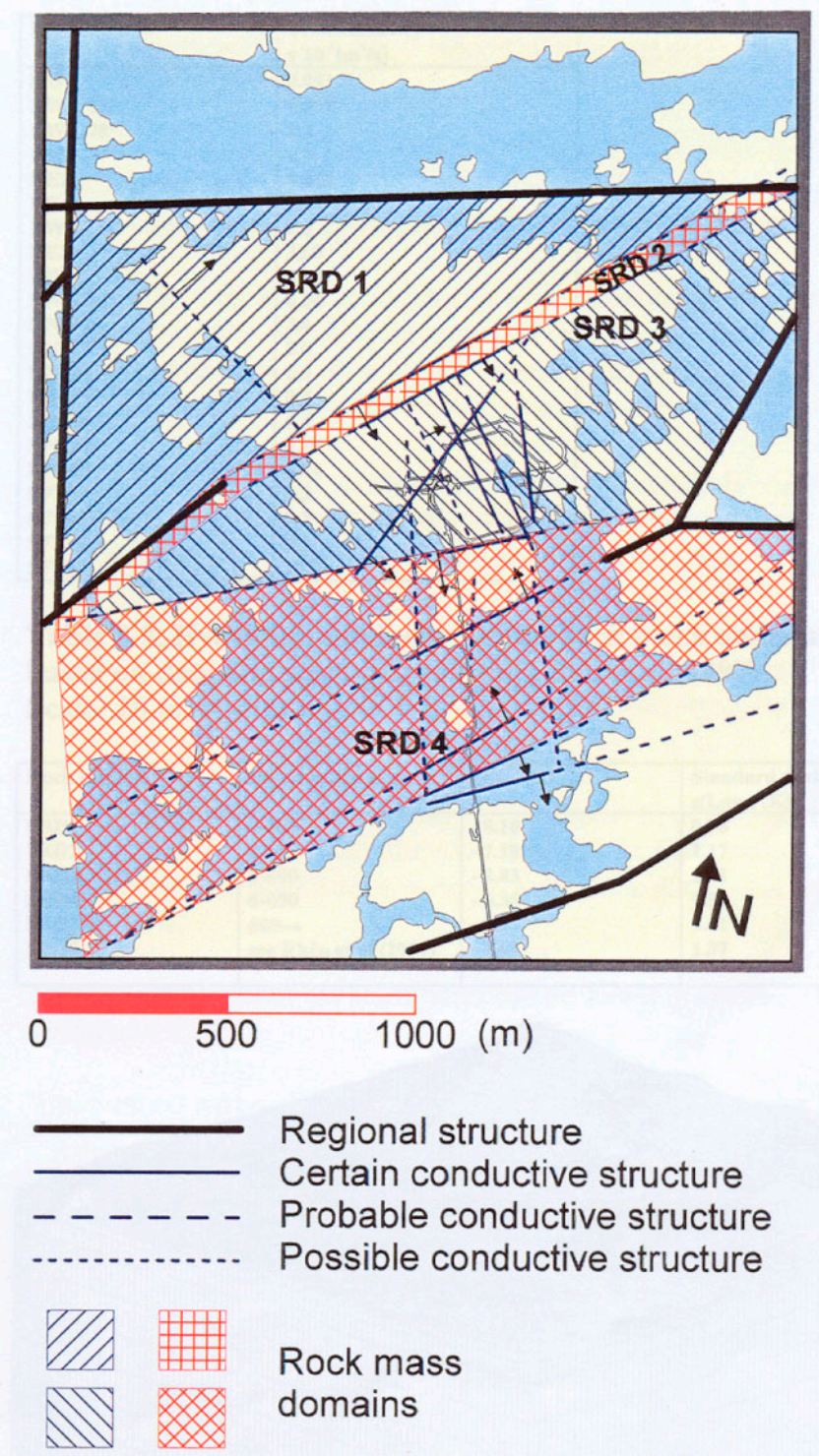

Figure 4-3. *Rock block domains, for further details see Rhén et al. (1997).*

Table 4-4. Model99. Transmissivities of conductive structures on Äspö, after Rhén et al. (1997).

Fracture zone	Transmissivity x 10^{-5} [m^2/s]	Modified transmissities after calibration x 10^{-5} [m^2/s]
NW1	0.041	
EW1, 88°	0.052	
EW1, 78°	1.2	
EW3	1.7	1.2
NE2	0.012	0.8
NE4	3.1	
EW7	1.5	
NE3	32.0	
NE1	22.0	30
NNW1	0.86	3.0
NNW2	2.4	1.0
NNW3	2.0	
NNW4	6.5	
NNW5	0.4	
NNW6	1.4	
NNW7	0.75	8.0
NNW8	0.84	0.1
SFZ03	0.3	
SFZ07	0.3	
SFZ11	0.3	
SFZ12	10.0	

Table 4-5. Modell99. Hydraulic conductivities for rock block domains, based on data and scaling laws from Rhén et al. (1997).

Scale: 20 m.

Rock block domain	Depth range (metres)	Log_{10} (K)	Log_{10} (K) after calibration	Standard deviations (Log_{10} (K))
SRD1	0-600	-8.10	-7.8	0.70
SRD2	0-600	-7.18	-7.8	1.17
SRD3	0-600	-8.83	-8.7	1.01
SRD4	0-600	-6.36	-7.6	1.51
SRD1-4	600→	-8.25		1.61
SRD5	see Rhén et al. (1997)	-7.68		1.37

Table 4-6. Model99. Conductivities for the top five cell layers as given by the calibration process.

Layer (m)	Conductivity m/s
0-0.5	10^{-3}
0.5-1.5	10^{-3}
1.5-3.0	$5. \times 10^{-4}$
3.0-5.0	10^{-3}
5.0-10.0	$3. \times 10^{-7}$

5 CALIBRATION

5.1 INTRODUCTION

The present simulations are partly based on two hydrological models; a site-model, Svensson (1997b), and a regional model, Svensson (1997a), that provides boundary conditions for the site-model. The boundary conditions will be taken from the regional model also in this model formulation. However, the present version of the site-model is quite different from the original one, with respect to the conductivity and porosity fields. A new calibration of the hydrological model is hence required.

When basic conceptual assumptions were discussed, see Chapter 2, it was stated that the water composition at the bottom and vertical boundaries of the domain were tentative and should be considered again in the calibration process. Three water types, MWH, MWL and MWB, were introduced, with tentative compositions from borehole measurements.

The focus of the calibration process for water composition is thus on the composition of MWH, MWL and MWB.

In the Task #5 description it was suggested that the calibration should be based on measured water composition in boreholes, with the tunnel front at position 2 900 metres. A review of the field data on water composition shows that more data are available for position 3 170 metres (April -94) and the calibration will therefore be based on conditions prevailing at that time.

5.2 CALIBRATION CRITERIA

In the calibration we will try to fulfil the following criteria:

- **Groundwater table for natural conditions.** The distribution can be found in Rhén et al. (1997). One can expect that a certain variation of the groundwater table is found, between seasons and years, and a fair agreement is hence sought.

- **Pressure response in boreholes.** During the construction of the Äspö HRL, the pressure was monitored in a number of borehole sections. The drawdowns at tunnel front position 2875 metres can be found in Rhén et al. (1997); these data will be compared with simulated drawdowns.

- **Kinematic porosity.** The kinematic porosity field is based on the estimated flow aperture of each fracture or zone in the network. In the calibration process this basic distribution will be kept, but each value will be multiplied by a constant, that is to be determined. The time history of the upconing, i.e. the salinity variation in time, will be utilized for this purpose.

- **Water composition for natural conditions.** The water composition in the Äspö area was measured prior to the construction of the Äspö HRL. We will run the model for this situation, assuming steady state conditions, and compare the result with field data. In the steady state the water composition in the domain is completely determined by the boundary conditions and should thus be sensitive to the assumed compositions of MWH, MWL and MWB. A general agreement between measured and simulated distributions is the criteria set.

- **Water composition for tunnel front at 3 170 metres.** The water composition in 19 boreholes was measured at this tunnel front position. We want to ensure as close agreement as possible with these data.

- **Water composition at time 1996-05.** The measured composition in eight borehole sections, after the completion of the tunnel, will be compared to simulated values. As close agreement as possible is the objective of this part of the calibration.

5.3 CALIBRATION PROCESS

It was decided to perform the calibration in three steps. First the hydrological model was calibrated (the first two criteria above). This involved determining the conductivity for the top five layers of the model and adjusting the transmissivity of some deterministic fracture zones. It was the ambition to keep these adjustments as small as possible. Next the kinematic porosity factor was determined from the measured upcoing dynamics and finally the water composition was considered. Adjustments of the compositions of MWH, MWL and MWB were evaluated, with the ambition to get as close agreement with field data as possible.

5.4 RESULTS

The groundwater table for natural conditions is compared to measurements in Figure 5.1 and the drawdowns in borehole sections, for a tunnel front position of 2875 metres, are given in Table 5.1. Starting with the groundwater table, it is seen that the predicted maximum ground water level is about 4 metres. A general agreement with the measured levels (given in Rhén et al. (1997)) is also found. The calculated drawdowns in borehole sections in the domain were compared with measured ones, all for tunnelfront position 2875 metres. It was anticipated that the drawdowns should be sensitive to various realisations of the background fracture network. In order to study this five realisations of the network were generated and the drawdown for each borehole section and each realisation was calculated. The result can be studied in Table 5-1, the location of boreholes can be found in Figure 3-2. It is seen that different realisations are best for different boreholes. Realisation two has only two borehole sections with an error larger than 10 metres and is for this reason considered to be the best one. In the following, it is this realisation of the conductivity field that will be used, if not otherwise stated.

It was found that an increase of the kinematic porosity, based on the flow aperture, with a factor of five gives a realistic description of the upconing process, see Figure 5.2. We do not know the exact position of the upconing front and therefore both the maximum predicted salinity at a depth of 370 metres and the predicted salinity at the tunnel position 2 800 metres are given in Figure 5.2. The measurements are from boreholes SA2783 and SA2880. This calibration result is considered to be important, as it focuses on the transport velocity of a fluid property.

These results were obtained by prescribing certain conductivities to the top five layers, see Table 5.2, and by making small adjustments to the transmissivities of the major fracture zones (given in Table 4-1). A small background conductivity, with a lognormal distribution, was also added to all cells. This conductivity had a value of 10^{-10} m/s north of the line y = 7050 metres (in the Äspö coordinate system) and a value of 10^{-9} m/s south of this line. The standard deviation of $Log_{10}(K)$ was 0.8 for the whole domain.

The compositions of MWH and MWL given in Chapter 2 were found to give results in fair agreement with field data, both for initial conditions and for the tunnel front at position 3 170 metres. The composition of MWB has no significant influence on these comparisons, but is important when water from the bottom boundary reach the tunnel level. The salinity at the bottom boundary, generated by the regional model, will reach 5-6% when the tunnel is completed. Borehole KLX02, at 1 500 metres, has a salinity of 7-8% and Äspö Brine fraction of 90%. Based on these data and the comparison of measured and simulated water composition at time 1996-05, the following composition for MWB was considered to be more accurate: 5% Meteoric, 5% Baltic, 10% Glacial and 80% Äspö Brine. This is the composition of MWB to be adopted. A small adjustment of the composition of MWL (giving 12% Meteoric, 12% Baltic, 45% Glacial and 31% Äspö Brine) was found to give a minor improvement of the results. With these modifications good agreement was also obtained for the comparison at time 1996-05. Some results that confirm these statements will now be given.

The calculated initial distributions are given in Figure 5.3. The sections are through the centre of the spiral part of the tunnel. The distributions are in general agreement with field data, see Gurban et al. (1998). Of particular significance is the band of glacial water occupying about 50% of the pore volume at a depth of about 600 metres. Point by point comparisons with field data can be found in Table 5-3. It should be mentioned that measurements are available also for depths above 300 metres. These were however not included in the table as the model predicts 100% Meteoric water for depths smaller than 200 to 300 metres. In order to be able to compare the average values for the composition, it was decided to exclude these data.

Next we consider the simulated water composition for tunnel front position 3170 metres. Point comparisons with field data can be found in Table 5-4; the comparison in Table 5-4 is also shown as a graph in Figure 5-4. A certain agreement in proportions of different water types, as well as trends along the tunnel, can be found. It is not easy to anticipate the degree of agreement one can expect in a simulation like this. This question will be addressed in the discussion section.

Distributions for tunnel front position 3 170 metres are shown in Figure 5-5. This figure is included as an illustration of how the tunnel affects the distributions and is not directly used in the calibration process.

Finally, the comparison for 1996-05 is shown in Table 5-5. Also in this comparison both the trends and the average compositions are in fair agreement with field data.

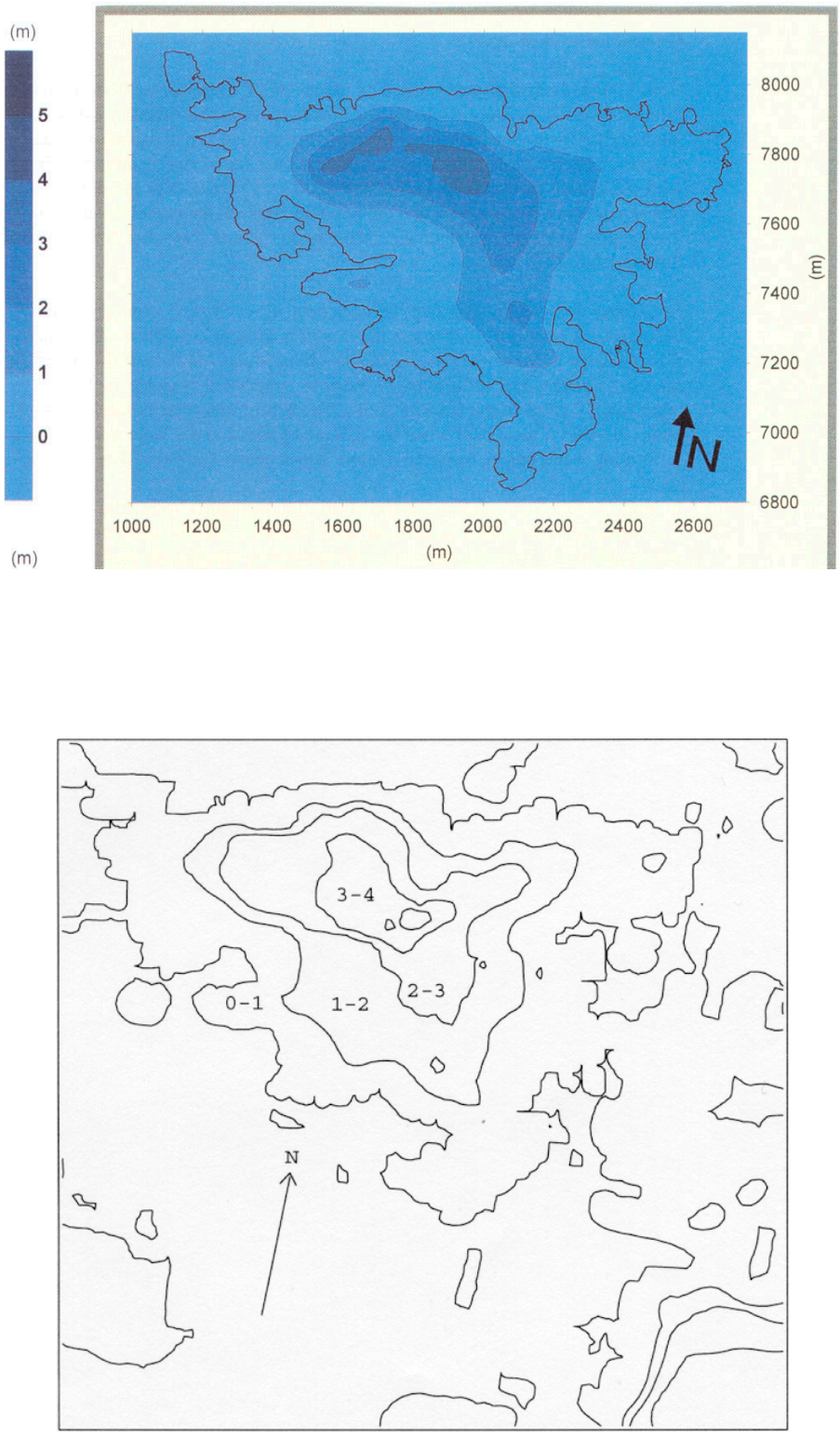

Figure 5-1. *Measured (top) and calculated water table for natural conditions.*

Table 5-1. Errors in calculated drawdown (calculated- measured) for tunnel front at 2875 metres, using five realisations of the conductivity field.

Borehole section	Depth m b s l	Realisation 1	2	3	4	5
K02-B5	-190.00	5.37	7.84	8.53	15.56	0.72
K02-B4	-310.00	- 9.58	-9.81	-11.36	-10.02	-10.31
K02-B3	-530.00	3.63	5.75	4.09	5.60	4.83
K02-B2	-830.00	- 5.84	-5.50	- 5.69	- 5.43	- 5.54
K02-B1	-870.00	- 5.43	-5.21	- 5.34	- 5.16	- 5.24
K03-C5	-210.00	6.64	5.85	8.11	7.02	5.46
K03-C4	-350.00	0.80	0.62	1.74	0.13	0.33
K03-C3	-510.00	1.78	1.20	2.28	2.51	1.57
K03-C2	-610.00	1.47	0.98	1.64	1.78	1.67
K03-C1	-670.00	0.54	0.22	0.38	0.28	0.78
K05-E4	-270.00	2.65	5.59	1.19	5.81	0.26
K05-E3	-310.00	- 8.85	- 4.45	- 1.91	0.47	-0.15
K05-E2	-430.00	- 9.44	- 7.11	- 5.93	- 5.35	-5.54
K05-E1	-450.00	- 7.46	- 4.83	- 4.51	- 4.23	-3.68
K06-F6	-90.07	9.30	9.55	6.95	9.27	8.94
K06-F4	-250.00	- 2.15	- 2.92	- 4.17	- 5.22	- 1.47
K06-F3	-290.00	11.45	16.49	15.17	14.71	13.24
K06-F2	-330.00	- 2.94	0.55	- 3.38	- 1.26	- 2.63
KO6-F1	-370.00	- 4.48	- 0.01	- 6.55	- 2.89	- 5.32
K07-J5	-110.00	-34.67	-27.76	-31.98	-28.15	-29.55
K07-J4	-210.00	-10.42	- 6.42	- 4.28	- 5.17	- 8.83
K07-J3	-290.00	- 4.48	- 1.00	- 2.94	- 6.21	- 1.21
K07-J2	-370.00	2.50	3.47	2.52	3.05	2.88
K07-J1	-470.00	- 5.41	- 4.65	- 5.26	- 4.75	- 5.07
K08-M3	-150.00	2.37	7.08	- 4.10	2.76	1.04
K08-M2	-310.00	7.42	9.63	3.98	9.38	7.67
K08-M1	-450.00	- 6.20	- 5.50	- 5.74	- 5.38	-5.69
K09-AE	-90.07	0.49	1.64	0.80	1.55	0.97
K09-AD	-110.00	0.37	4.73	1.39	8.17	1.90
K09-AC	-150.00	- 1.20	6.17	- 0.08	5.39	7.31
K09-AB	-210.00	1.89	4.88	6.47	6.34	11.75
K09-AA	-350.00	- 2.32	- 2.25	- 2.23	- 2.64	- 2.61
K10-BA	-50.35	- 2.41	- 2.38	- 2.76	- 2.41	-2.19
K11-CF	- 30.48	- 5.99	- 6.09	- 6.45	- 5.58	-5.90
K11-CE	- 50.35	- 6.02	- 6.20	- 6.49	- 5.50	-6.01
K11-CD	- 90.07	- 1.41	- 1.05	- 1.51	- 1.39	-1.33
K11-CC	-130.00	- 2.42	- 2.11	- 2.49	- 2.11	-2.25
K11-CB	-170.00	2.79	3.03	2.81	3.21	3.04
K11-CA	-210.00	- 2.07	- 1.61	- 1.95	- 1.57	-1.72
K12-DE	- 90.07	- 3.02	- 4.97	- 6.58	- 1.89	0.44
K12-DD	-110.00	- 1.45	- 4.02	- 4.50	- 3.52	1.44
K12-DC	-230.00	2.17	4.68	- 1.97	3.25	1.83
K12-DB	-270.00	4.67	9.84	- 0.26	4.56	6.94
K12-DA	-350.00	2.91	6.49	- 1.03	3.47	3.22
K14-FE	-7 0.21	- 1.03	- 0.43	- 0.69	- 0.48	-0.43
K14-FD	-110.00	2.08	2.61	0.55	1.59	1.35
K14-FC	-130.00	2.88	3.56	3.04	4.65	3.02
K14-FB	-130.00	1.66	1.94	1.23	3.83	1.79
K14-FA	-170.00	2.74	0.86	2.20	5.28	2.95
K16-?D	-110.00	0.36	0.52	- 3.14	0.52	1.54
K16-?C	-230.00	- 8.69	- 6.93	-10.48	- 8.82	-8.90
K16-?B	-410.00	- 5.67	- 5.12	- 5.32	- 5.00	-5.25
K16-?A	-490.00	- 4.16	- 3.76	- 4.35	- 3.64	-4.88
KB2-B6	-50.35	1.97	- 1.22	1.48	0.71	2.45
KB2-B5	-70.21	12.71	6.36	6.47	9.41	10.62
KB2-B4	-90.07	10.72	7.10	8.08	9.74	9.88
KB2-B3	-130.00	6.22	5.94	6.19	5.74	5.78
Mean error (m)		- 0.99	0.21	- 1.20	0.39	- 0.07

Table 5-2. Conductivities for the top five cell layers, as given by the calibration process.

Layer (m)	Conductivity m/s
0-0.5	10^{-4}
0.5-1.5	10^{-4}
1.5-3.0	4×10^{-5}
3.0-5.0	10^{-6}
5.0-10.0	10^{-7}

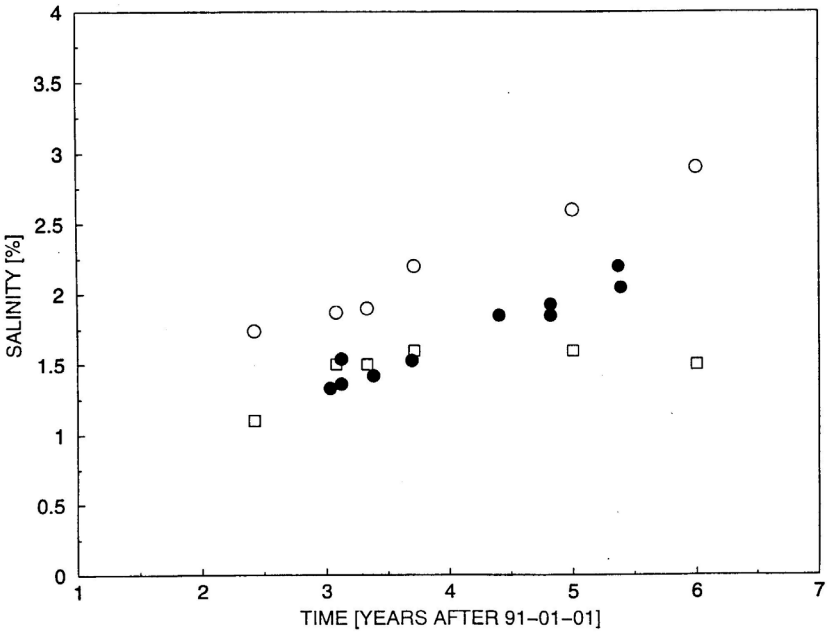

Figure 5.2. *The upconing process. Salinity as a function of time at a depth of 370 metres.*

- *Field data (SA2783 and SA2880)*

○ *Simulated maximum salinity.*

□ *Simulated salinity at tunnel coordinate 2 800 metres.*

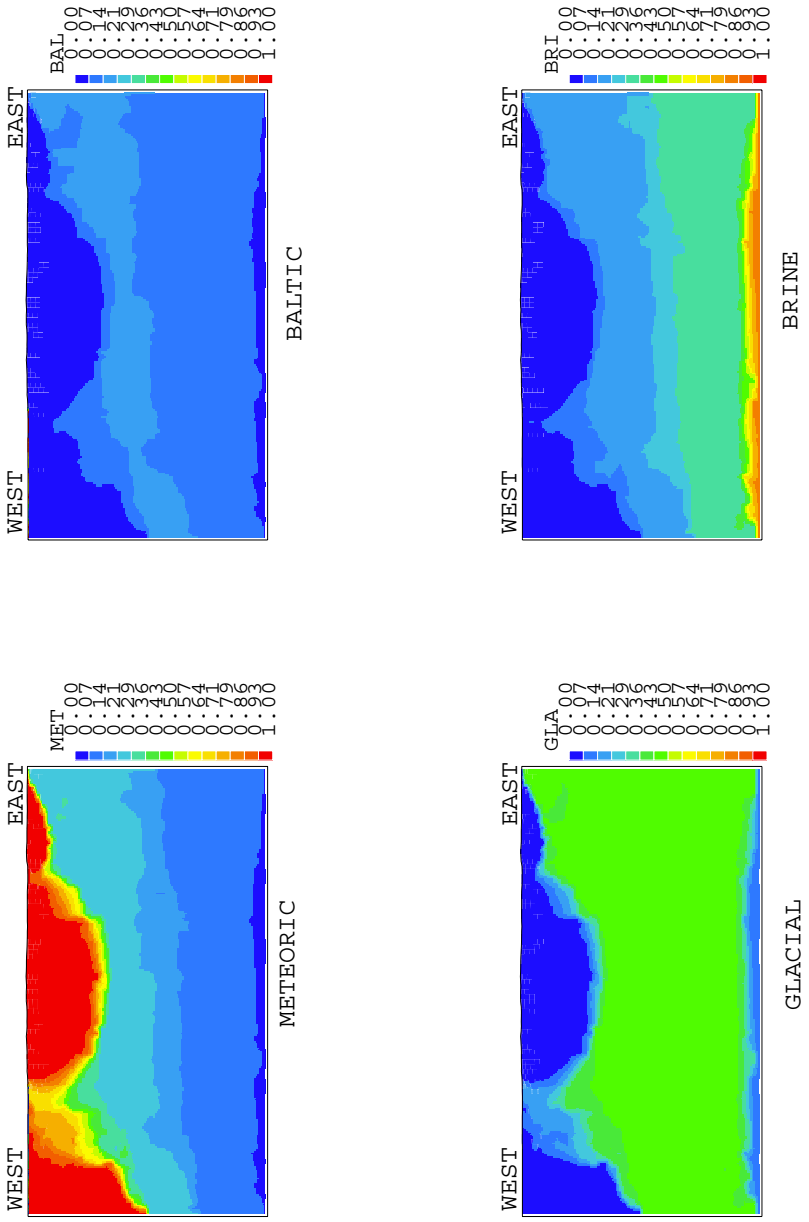

Figure 5-3. *Vertical sections through the centre of the spiral part of the tunnel, showing the simulated initial distributions of various water types.*

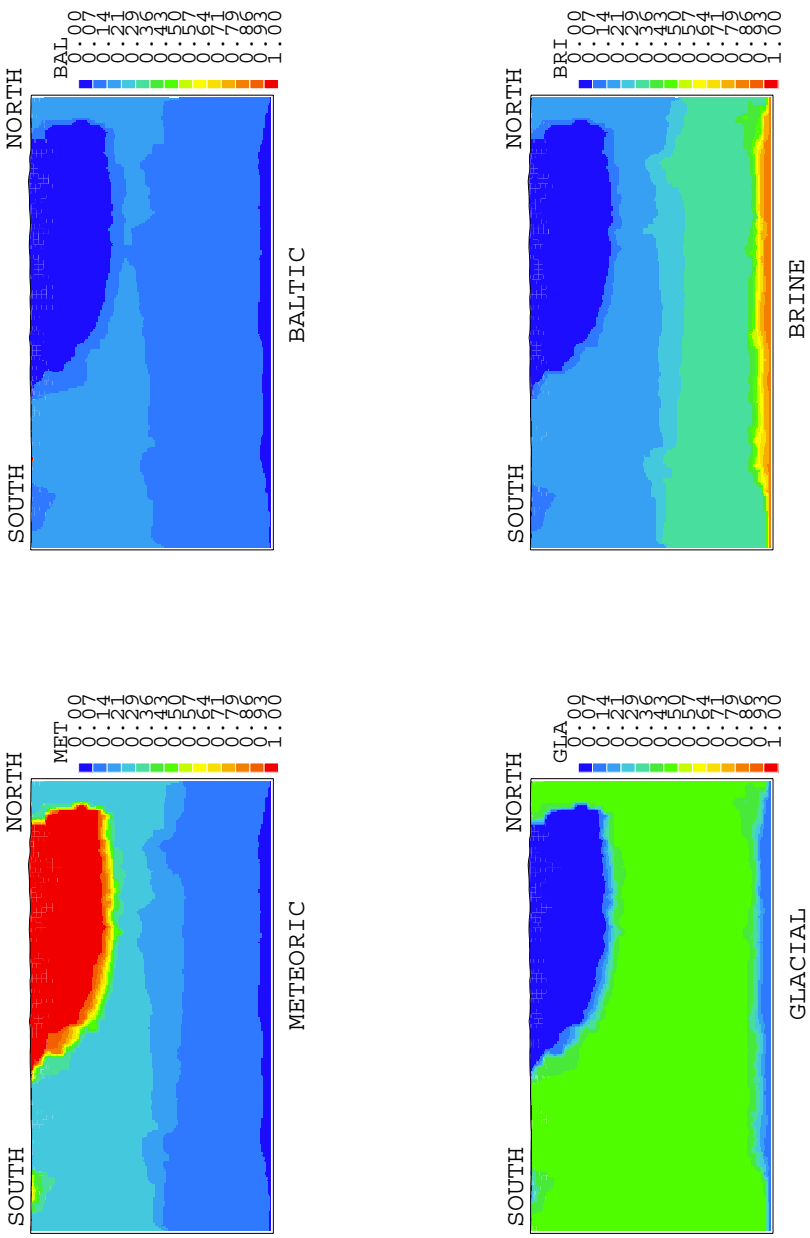

Figure 5-3. *Cont.*

Table 5-3. Comparison between measured and simulated water compositions in borehole sections prior to tunnel construction.

Borehole depth [m]	Measured (top) and simulated water composition			
	Meteoric	Baltic	Glacial	Äspö Brine
KAS02C	30.1	14.8	40.4	14.8
300 m	66.3	6.5	19.9	7.3
KAS02D	26.9	15.0	43.0	15.0
440 m	21.7	14.2	45.0	19.1
KAS02E	17.9	17.9	44.7	19.6
520 m	20.4	13.9	45.0	20.6
KAS02F	13.6	13.6	45.4	27.4
840 m	12.0	12.0	45.0	31.0
KAS02G	12.3	12.3	46.8	28.7
880 m	11.9	11.9	44.8	31.3
KAS03D	20.2	14.7	50.3	14.7
340 m	26.7	14.6	43.9	14.8
KAS03E	22.6	12.8	51.7	12.8
440 m	24.5	14.9	45.0	15.7
KAS03F	16.0	16.0	50.9	17.1
600 m	15.5	12.8	45.0	26.7
KAS03G	14.4	14.4	47.2	24.0
820 m	12.0	12.0	45.0	31.0
KAS03H	11.1	11.1	44.5	33.4
900 m	11.9	11.8	44.5	31.8
KAS04C	24.9	17.3	40.5	17.3
360 m	28.8	13.8	42.1	15.4
KAS06C	34.5	35.4	15.1	15.1
320 m	33.8	12.6	38.9	14.7
KAS06D	33.7	31.3	17.6	17.6
420m	22.3	14.4	45.0	18.3
Average	21.4	17.4	41.4	19.8
	23.7	12.7	42.2	21.4

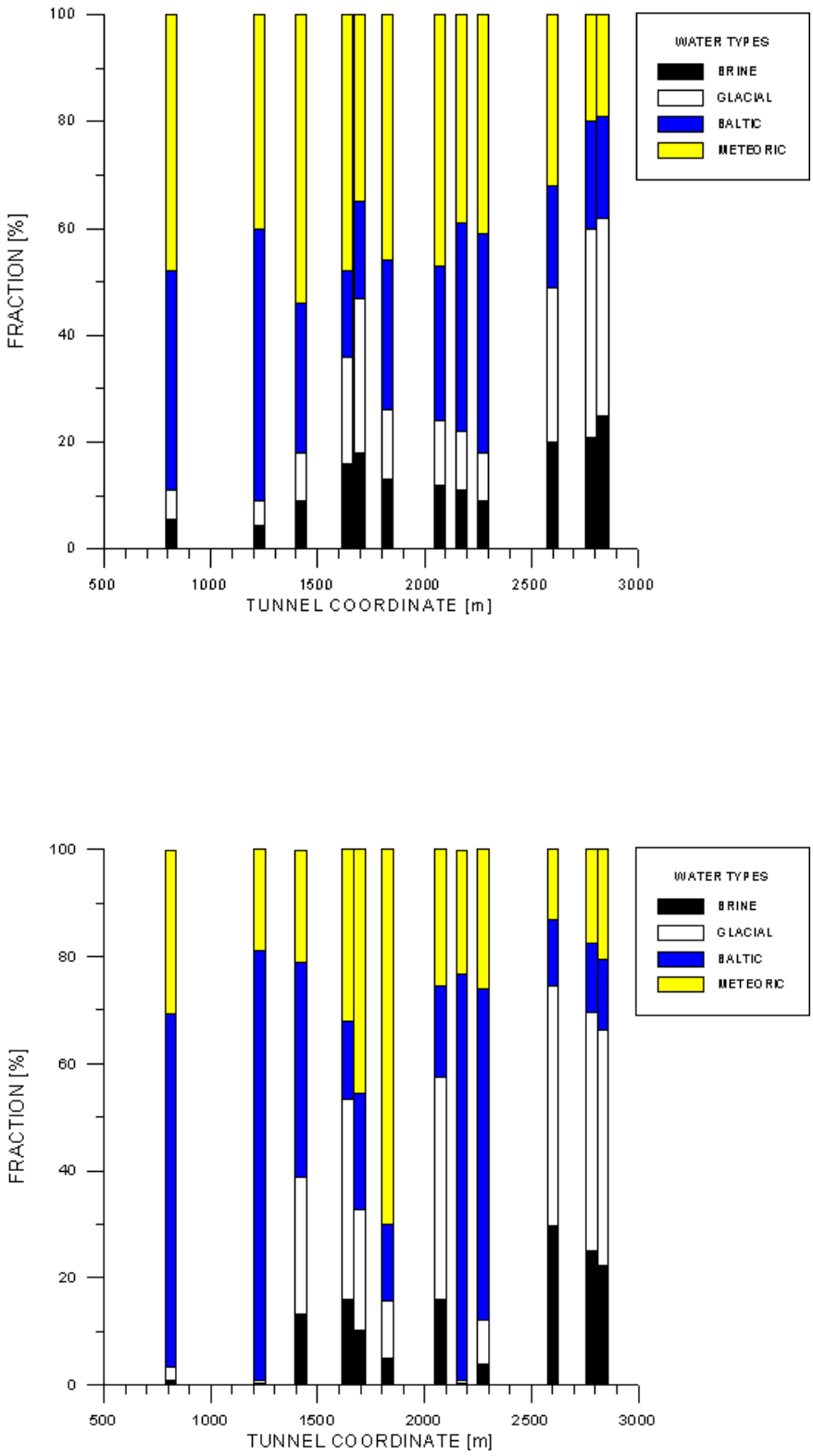

Figure 5-4. *Comparison between measured (top) and simulated water composition distribution for tunnel front at 3 170 metres.*

Table 5-4. Comparison between measured and simulated water composition in boreholes. Tunnelfront: 3 170 m.

Borehole depth [m]	Measured (top) and simulated water composition			
	Meteoric	Baltic	Glacial	Äspö Brine
KAS09	35.0	57.0	4.0	4.0
100 m	17.9	82.0	0.1	0.0
KAS14	32.0	64.0	2.0	2.0
100 m	21.7	77.3	0.8	0.3
SA0813	48.0	41.0	5.5	5.5
100 m	30.6	66.0	2.5	0.8
SA1229	40.0	51.0	4.5	4.5
160 m	18.9	80.2	0.7	0.2
SA1420	54.0	28.0	9.0	9.0
200 m	21.2	40.1	25.6	13.2
KAS07	60.0	32.0	4.0	4.0
200 m	18.2	81.2	0.4	0.2
SA1641	48.0	16.0	20.0	16.0
220 m	32.1	14.6	37.3	16.0
SA1696	35.0	18.0	29.0	18.0
220m	45.5	21.8	22.6	10.0
SA1828	46.0	28.0	13.0	13.0
240 m	70.1	14.4	10.7	4.9
SA2074	47.0	29.0	12.0	12.0
280 m	25.4	17.0	41.6	16.0
SA2175	39.0	39.0	11.0	11.0
280 m	23.3	75.8	0.6	0.2
SA2273	41.0	41.0	9.0	9.0
300 m	26.2	61.9	8.2	3.8
SA2600	32.0	19.0	29.0	30.0
340 m	13.1	12.3	45.0	29.7
SA2783	20.0	20.0	39.0	21.0
360 m	17.7	12.9	44.4	25.1
SA2834	19.0	19.0	37.0	25.0
360 m	20.5	13.2	44.0	22.4
KAS08	37.0	29.0	17.0	17.0
440 m	25.6	20.4	36.8	17.2
KAS07	27.0	18.0	37.0	18.0
460 m	15.8	12.9	45.0	26.3
KAS05	16.0	16.0	45.0	23.0
480 m	13.0	12.2	45.0	29.7
KAS03	25.0	23.0	49.0	13.0
560 m	23.5	14.6	44.9	16.9
Average	36.9	30.9	19.8	12.9
	25.3	38.5	24.0	12.3

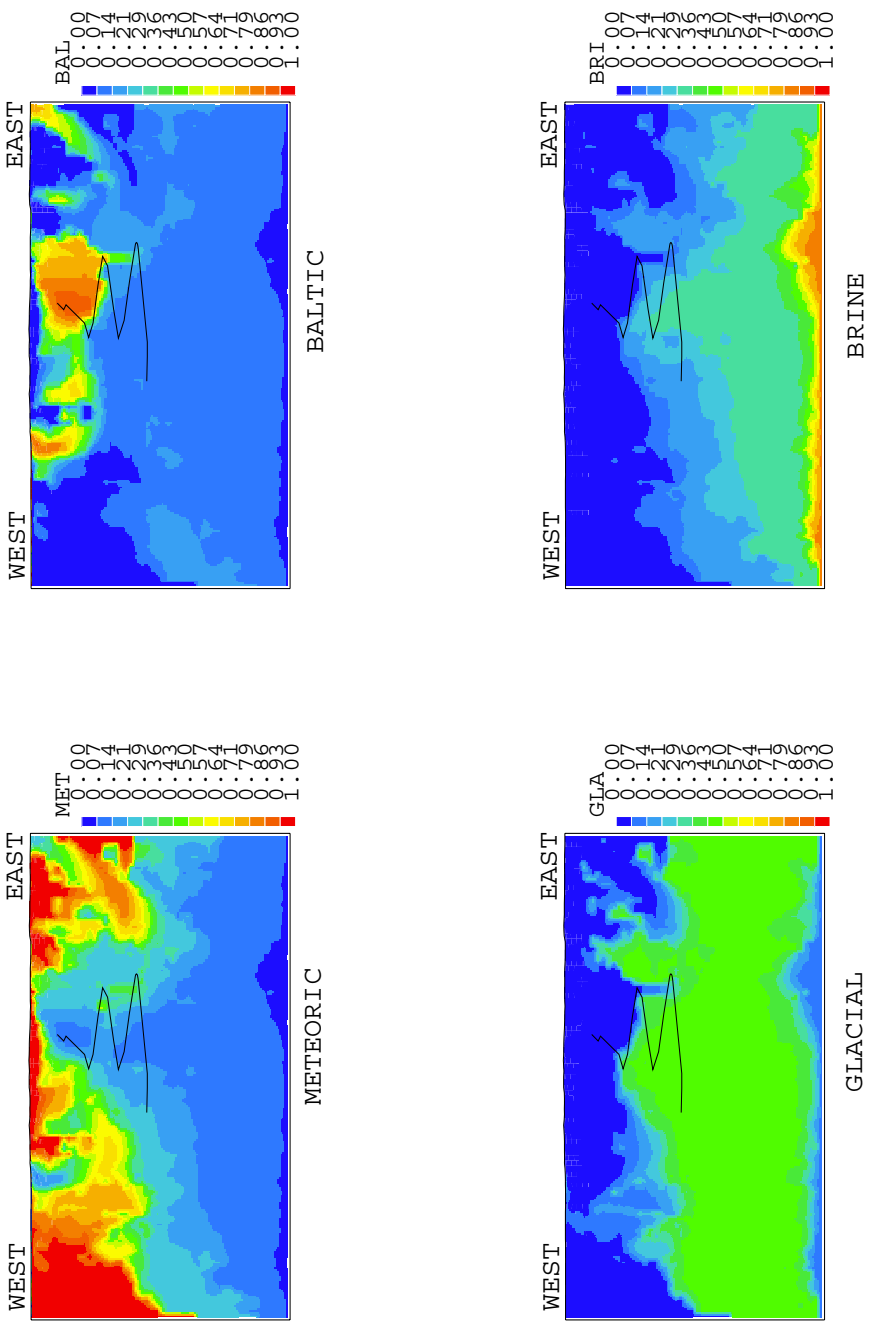

Figure 5-5. *Vertical sections through the centre of the spiral part of the tunnel, showing the simulated distributions of various water types. Tunnel front position: 3 170 metres.*

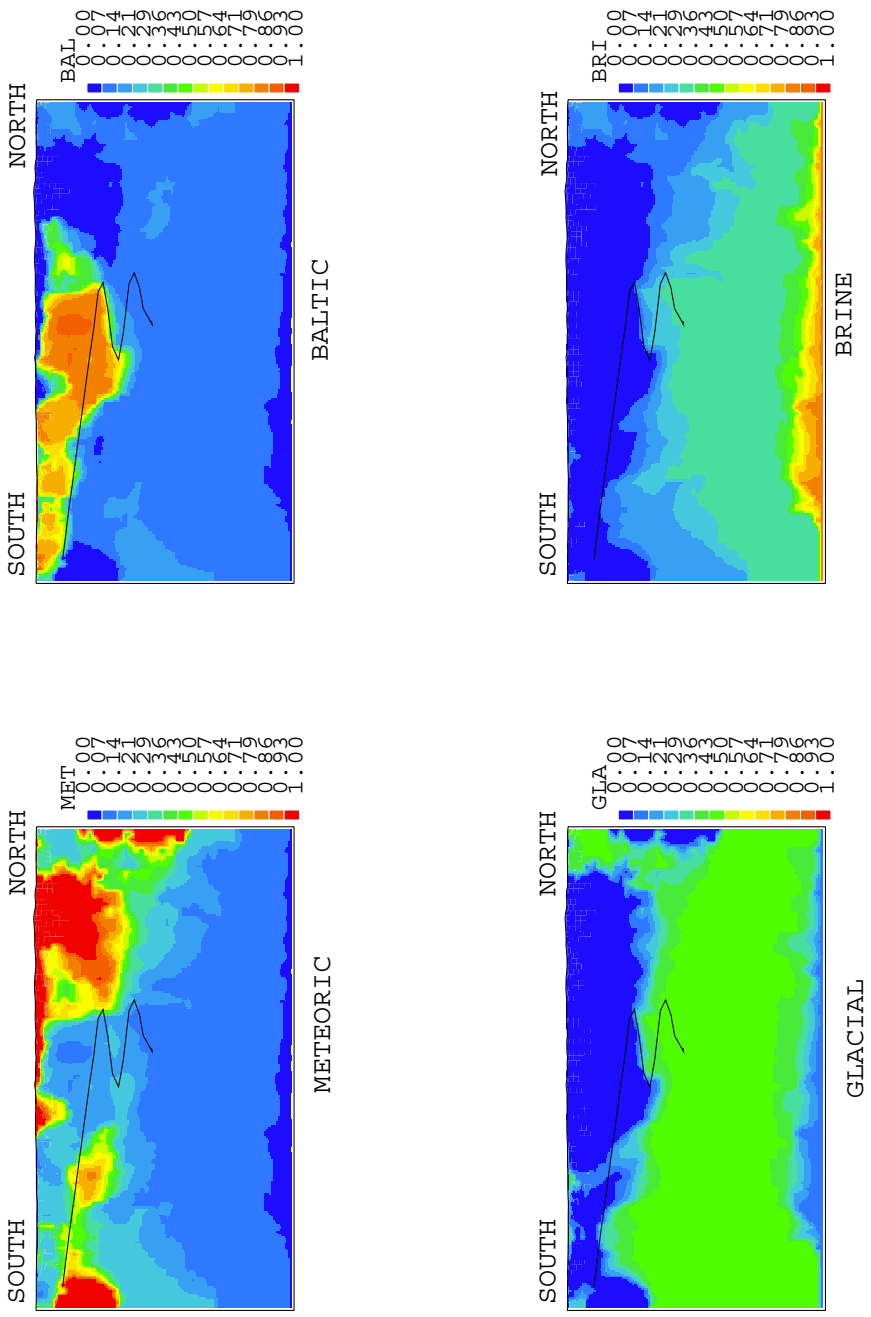

Figure 5-5. *Cont.*

Table 5-5. Comparison between measured and simulated water composition in boreholes at time 1996-05.

Borehole depth [m]	Measured (top) and simulated water composition			
	Meteoric	Baltic	Glacial	Äspö Brine
SA2273	46.0	38.0	8.0	8.0
300m	30.6	64.7	3.1	1.6
Sa2600	48.0	20.0	16.0	16.0
340m	16.5	12.4	38.2	32.8
SA2783	17.0	17.0	37.0	29.0
360m	35.2	13.2	32.2	19.4
SA2880	18.0	18.0	34.0	31.0
380m	35.5	18.4	31.1	14.9
KA3005	54.0	21.0	13.0	13.0
400m	34.9	13.0	30.8	21.2
SA3067	18.0	18.0	43.0	21.0
400m	60.2	25.3	10.8	3.7
KA3110	47.0	37.0	8.0	8.0
400m	46.7	35.7	12.4	5.2
KA3385	38.0	18.0	25.0	18.0
440m	18.4	13.0	42.2	26.5
Average	35.8	23.4	23.0	18.0
	34.8	24.5	25.1	15.7

5.5 MODEL99

A less ambitious calibration was performed in the first step of the project. As the hydrological model was the same as the site-model presented in Svensson (1997b), it was concluded that the model was calibrated from the hydrological point of view. The focus of the calibration process was therefore on the compositions of MWH and MWL. The calibration criteria were based on the initial conditions and the conditions for tunnel front position 3 170 metres. Comparisons with field data were carried out and it was found that the initial guess of the compositions of MWH and MWL, see Chapter 2, were adequate, i.e. the comparisons did not motivate any changes.

The calculated initial distributions are given in Figure 5-6. The sections are through the centre of the spiral part of the tunnel. The distributions are in general agreement with field data, Gurban et al. (1998). Of particular significance is the band of Glacial water occupying about 50% of the pore volume at a depth of about 600 metres. Point by point comparisons with field data can be found in Table 5-6. This comparison shows that the numerical model gives 100% Meteoric water down to a depth of about 300 metres below Äspö; the field data indicate more mixed water also close to the ground. This difference is probably due to too little dispersion in the model, as was discussed in Svensson (1997b) in relation to the salinity distribution. This is thus a deficiency of the hydrological model that we have to accept at this stage. A general agreement for the depth interval 300 to 800 metres can however be found from the comparison.

Next we consider the simulated water composition for tunnel front position 3 170 metres. Point comparisons with field data can be found in Tables 5-7 and 5-8; the comparison in Table 5-7 is also shown as a graph in Figure 5-7. A certain agreement in proportions of different water types, as well as trends along the tunnel, can be found.

Distributions of the four water types for tunnel front position 3 170 metres are shown in Figure 5-8. This figure is included as an illustration of how to the tunnel affects the distributions and is not directly used in the calibration process.

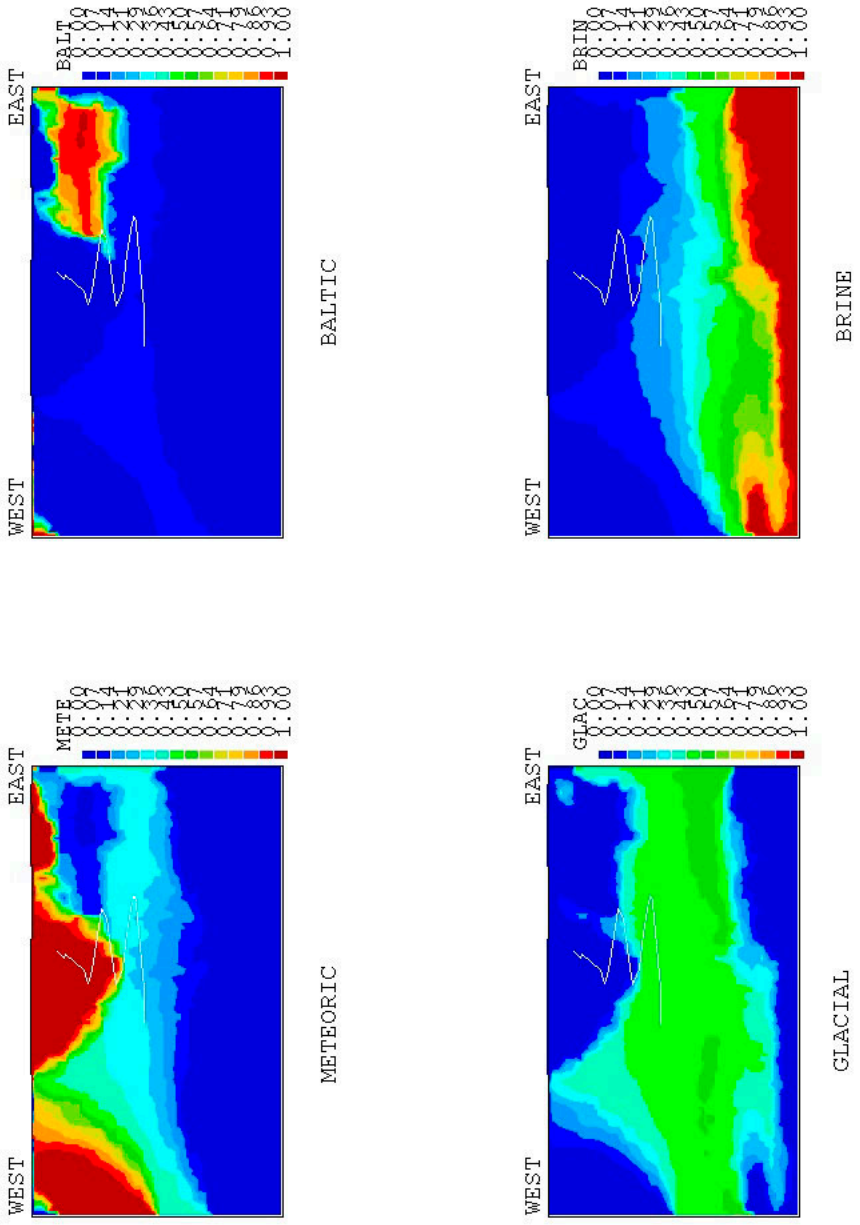

Figure 5-6. *Model99. Vertical sections through the centre of the spiral part of the tunnel, showing the simulated initial distributions of various water types.*

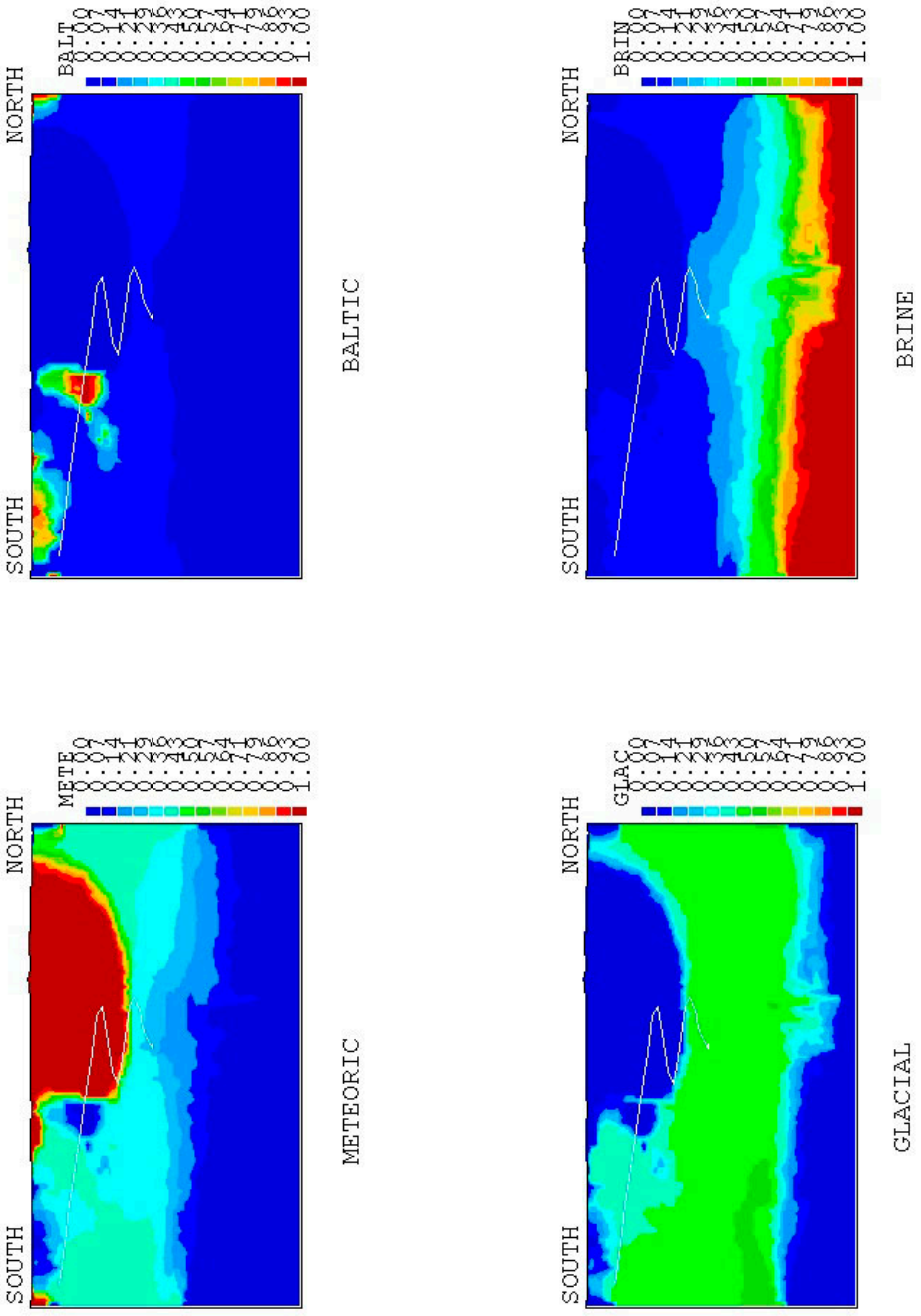

Figure 5-6. *Cont.*

Table 5-6. Model99. Comparison between measured and simulation water compositions in borehole sections prior to tunnel construction.

Borehole Depth [m]	Measured (top) and simulated water composition			
	Meteoric	Baltic	Glacial	Äspö Brine
KAS02A	30.8	10.2	48.8	10.2
200 m	100.0	0.0	0.0	0.0
KAS02B	28.9	14.9	41.2	14.9
300 m	99.3	0.1	0.4	0.2
KAS02C	30.1	14.8	40.4	14.8
300 m	99.3	0.1	0.4	0.2
KAS02D	26.9	15.0	43.0	15.0
440 m	26.2	7.1	44.0	22.7
KAS02E	17.9	17.9	44.7	19.6
520 m	18.6	5.0	45.0	31.3
KAS02F	13.6	13.6	45.4	27.4
840 m	0.6	0.2	30.0	69.3
KAS02G	12.3	12.3	46.8	28.7
880 m	0.3	0.1	13.5	86.1
KAS03A	27.3	4.2	64.3	4.2
120 m	100.0	0.0	0.0	0.0
KAS03B	33.6	7.7	51.0	7.7
180 m	100.0	0.0	0.0	0.0
KAS03C	31.8	7.9	52.4	7.9
220 m	100.0	0.0	0.0	0.0
KAS03D	20.2	14.7	50.3	14.7
340 m	36.7	9.9	43.0	10.4
KAS03E	22.6	12.8	51.7	12.8
440 m	35.7	9.6	43.2	11.4
KAS03F	16.0	16.0	50.9	17.1
600 m	18.7	5.1	45.5	30.7
KAS03G	14.4	14.4	47.2	24.0
820 m	1.7	0.5	34.4	63.3
KAS03H	11.1	11.1	44.5	33.4
900 m	2.9	0.8	25.7	70.6
KAS04A	63.5	5.5	25.6	5.5
180 m	100	0.0	0.0	0.0
KAS04B	34.9	10.3	44.5	10.3
260 m	100.0	0.0	0.0	0.0
KAS04C	24.9	17.3	40.5	17.3
360 m	34.5	8.5	42.1	15.0
KAS06A	48.6	11.4	28.7	11.4
200 m	85.9	1.7	8.8	3.6
KAS06B	47.9	17.5	17.3	17.3
280 m	73.5	3.9	16.4	6.2
KAS06C	34.5	35.4	15.1	15.1
320 m	32.7	14.9	40.4	12.0
KAS06D	33.7	31.3	17.6	17.6
420 m	26.9	7.3	44.3	21.5
Average	26.4	20.0	39.2	16.1
800<Z<300m	28.7	8.4	43.5	19.4

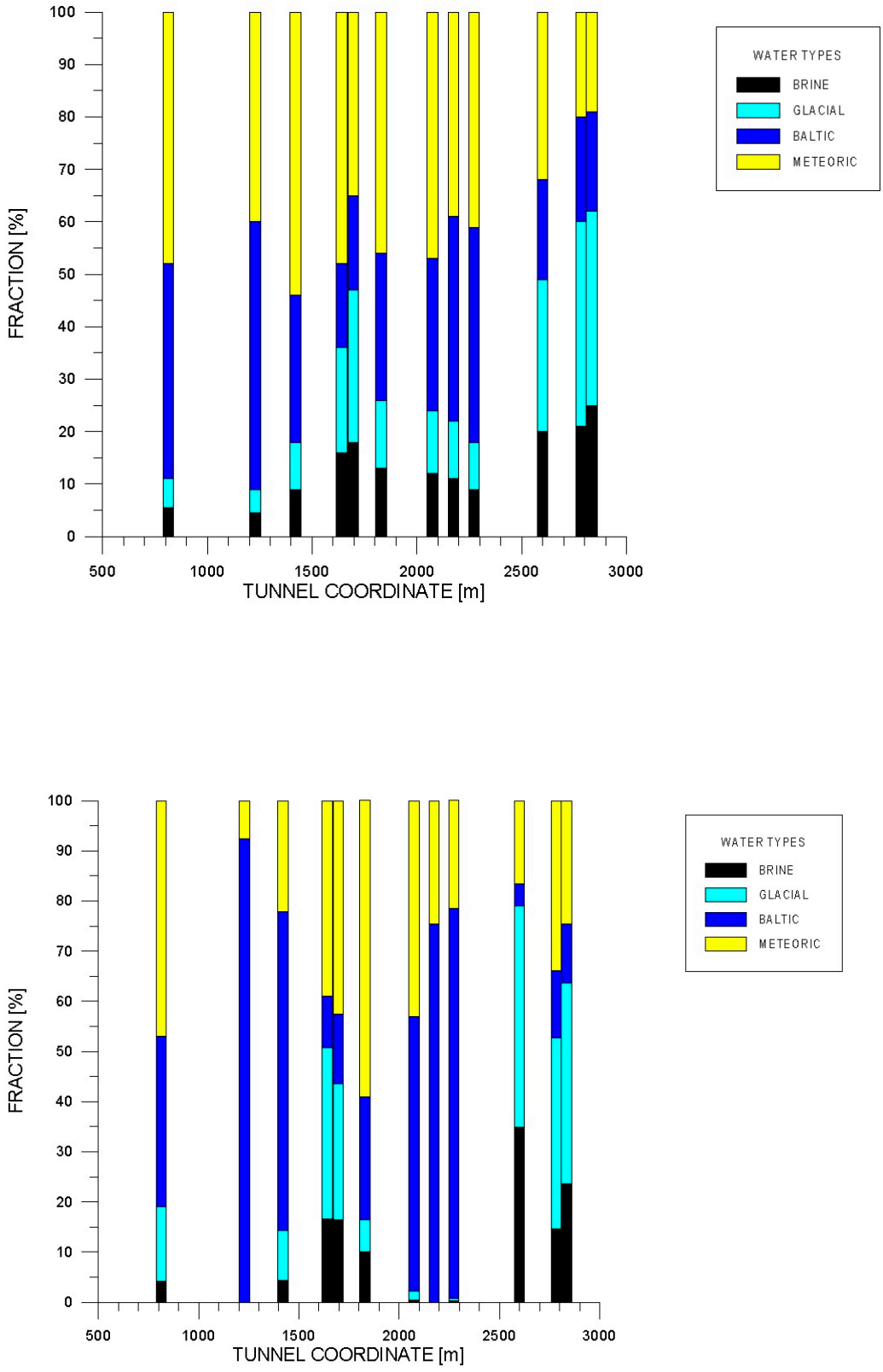

Figure 5-7. *Model99. Comparison between measured (top) and simulated water distribution for tunnel front at 3 170 metres.*

Table 5-7. Model99. Comparison between measured and simulated water composition in boreholes close to the tunnel.
Tunnelfront: 3 170 m.

Borehole depth [m]	Measured (top) and simulated water composition			
	Meteoric	Baltic	Glacial	Äspö Brine
SA0813	48.0	41.0	5.5	5.5
100 m	34.0	34.0	14.8	4.2
SA1229	40.0	51.0	4.5	4.5
160 m	7.5	92.5	0.0	0.0
SA1420	54.0	28.0	9.0	9.0
200 m	22.1	63.5	10.0	4.4
SA1641	48.0	16.0	20.0	16.0
220 m	38.9	10.3	34.2	16.6
SA16.96	35.0	18.0	29.0	18.0
220 m	42.5	13.9	27.1	16.5
SA1828	46.0	28.0	13.0	13.0
240 m	59.1	24.6	6.3	10.1
SA2074	47.0	29.0	12.0	12.0
280 m	43.0	54.7	1.8	0.5
SA2175	39.0	39.0	11.0	11.0
280 m	24.5	75.5	0.0	0.0
SA2273	41.0	41.0	9.0	9.0
300 m	21.5	77.9	0.5	0.2
SA2600	32.0	19.0	29.0	30.0
340 m	16.6	4.4	44.1	34.9
SA2783	20.0	20.0	39.0	21.0
360 m	33.9	13.4	38.0	14.7
SA2834	19.0	19.0	37.0	25.0
360 m	24.4	11.8	40.0	23.7
Average	39.1	29.1	18.2	13.7
Depth>200 m	31.7	39.7	18.1	10.5

Table 5-8. Model99. Comparison between measured and simulated water composition in some additional boreholes.
Tunnelfront: 3 170 m.

Borehole depth [m]	Measured (top) and simulated water composition			
	Meteoric	Baltic	Glacial	Äspö Brine
KAS09	35.0	57.0	4.0	4.0
100 m	6.6	93.4	0.0	0.0
KAS14	32.0	64.0	2.0	2.0
100 m	7.4	92.3	0.2	0.1
KAS07	60.0	32.0	4.0	4.0
200 m	17.5	82.5	0.0	0.0
KAS08	37.0	29.0	17.0	17.0
440 m	31.0	67.0	1.4	0.6
KAS07	27.0	18.0	37.0	18.0
460 m	18.8	5.1	45.6	30.5
KAS05	16.0	16.0	45.0	23.0
480 m	8.5	2.3	44.8	44.5
KAS03	25.0	23.0	49.0	13.0
560 m	23.8	6.4	44.9	24.8

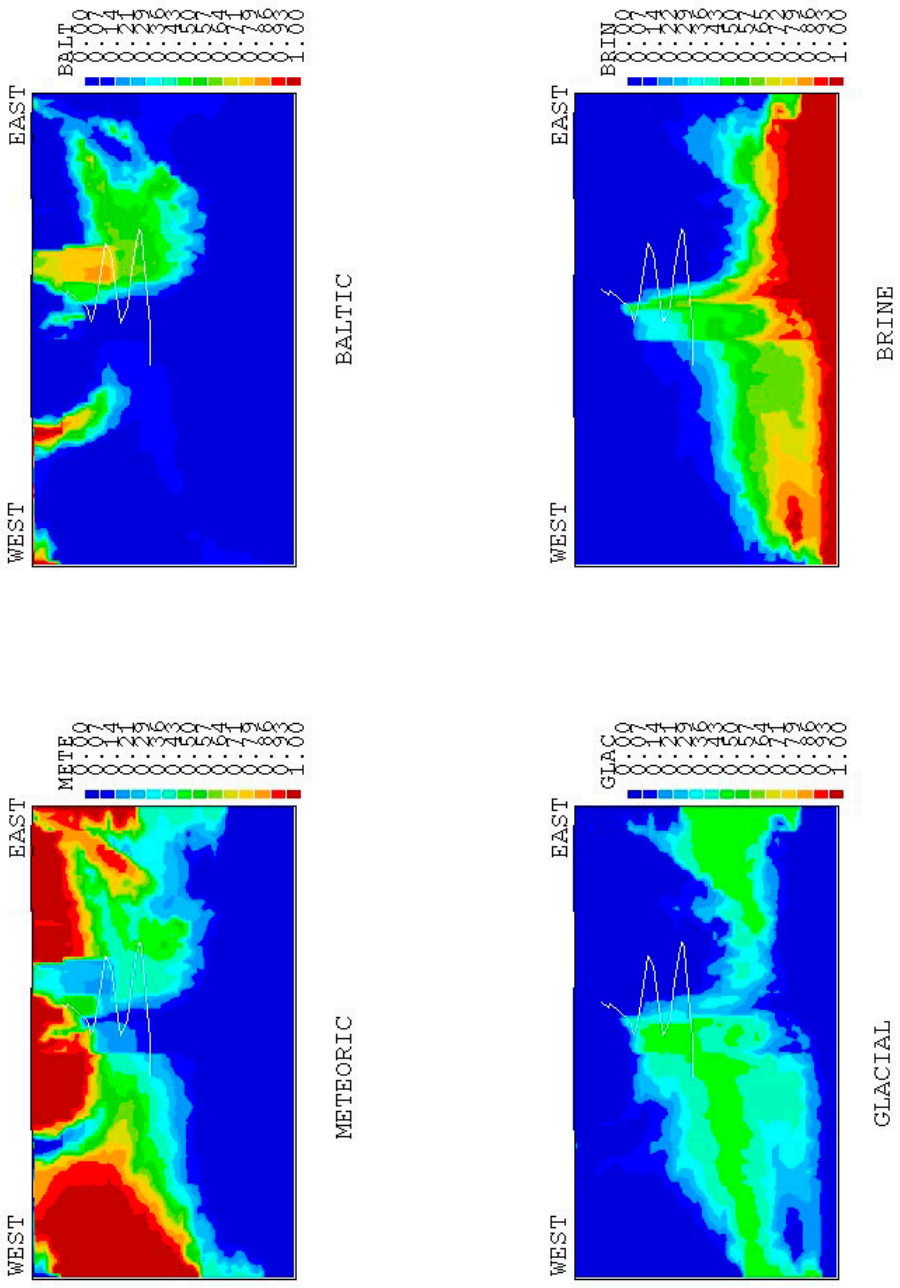

Figure 5-8. *Model99. Vertical sections through the centre of the spiral part of the tunnel, showing the simulated distributions of various water types.*
Tunnel front position: 3 170 metres.

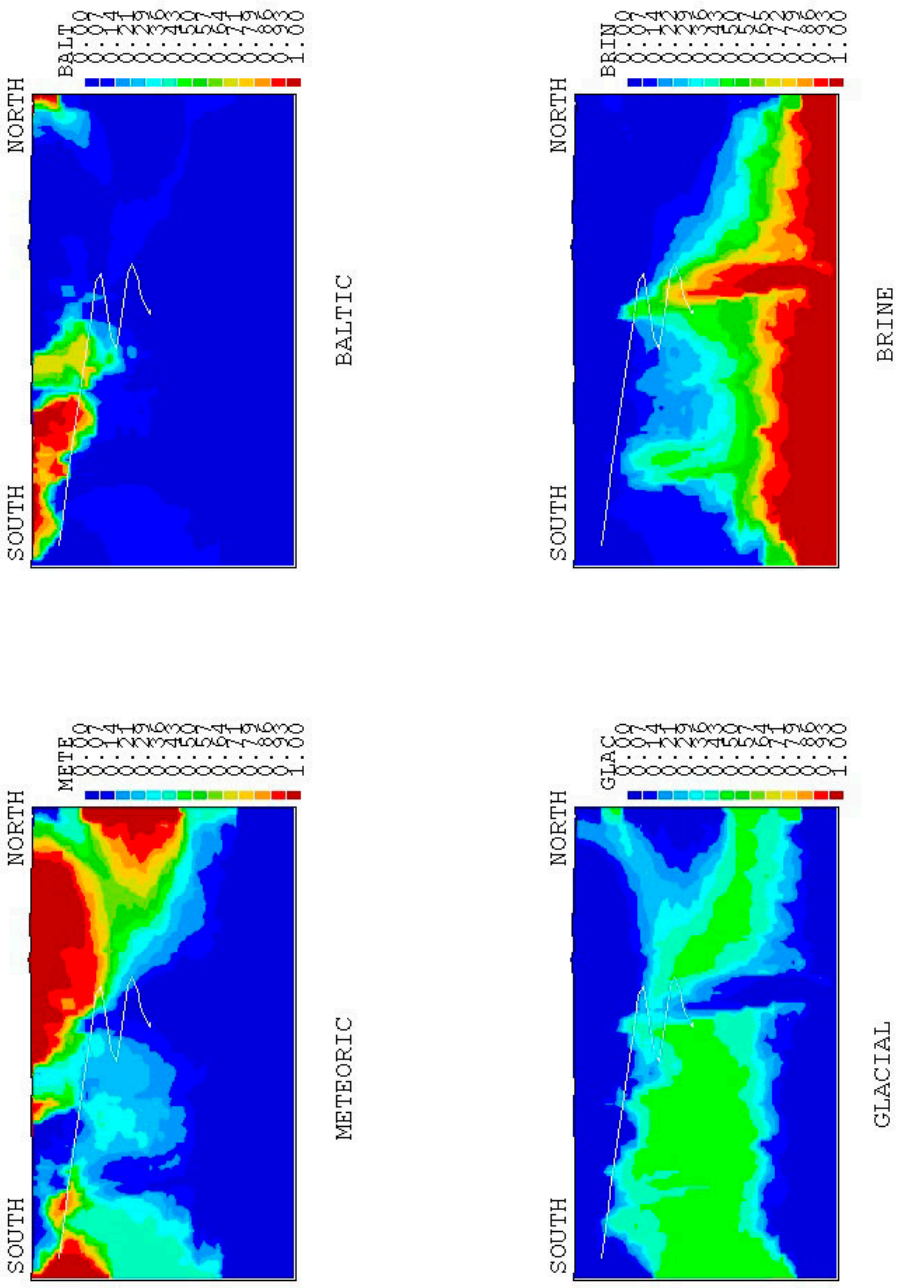

Figure 5-8. Cont.

6 MAIN RESULTS

6.1 INTRODUCTION

Additional simulation results will now be presented with the objective to create a more complete view of how the simulation model works and what accuracy that can be expected.

The pressure response and the change in water composition due to the excavation of the tunnel will be studied as a transient process. The construction of the tunnel started 1990-10-01, but it was then outside our computational domain. The starting time of the simulation is 1991-01-01; this is thus our "time zero". The tunnel was completed in September 1994. Some of the simulations will however be continued till 1997-01-01.

The pressure response will be studied in borehole sections, in boreholes drilled from ground; the positions of these boreholes can be found in Figure 3-2. The changes in water composition along the tunnel are measured and simulated in boreholes drilled from the tunnel. These borehole sections have names that indicate the position along the tunnel coordinate, for example SA1229, which is close to tunnel coordinate 1 229 metres.

6.2 PRESSURE RESPONSE

The pressure in the borehole sections will be presented as fresh water hydraulic head, which is calculated from the pressure, p, as: $p / \rho_0 g - h$, where ρ_0 is freshwater density, g acceleration due to gravity and h depth below mean sea level. The freshwater head for various borehole sections and tunnel front positions can be studied in Table 6-1. The pressure drop in borehole sections for tunnel front position 2 875 metres was studied in the calibration section and a close agreement with field data was found. We will therefore not deal with pressure drops in borehole sections further in this report.

Groundwater tables for four tunnel front positions are given in Figure 6-1. The maximum lowering of the groundwater table is found in the western part of the spiral, which is in agreement with field data (Rhén et al., 1997).

Table 6-1. Calculated freshwater hydraulic head in borehole sections for various tunnel front positions.

Borehole section	Freshwater hydraulic head [m]										
	Tunnel front position [m]										
	0	0 ↓ 960	960 ↓ 1190	1190 ↓ 1380	1380 ↓ 1750	1750 ↓ 2160	2160 ↓ 2590	2590 ↓ 2900	2900 ↓ 3170	3170 ↓ 3600	3600 Time: 97-01-01
K02-B5	1.3	1.2	0.6	-1.1	-4.3	-39.3	-49.5	-45.6	-48.6	-42.7	-42.3
K02-B4	1.4	1.3	0.5	-1.5	-4.4	-24.7	-31.9	-32.8	-39.0	-37.5	-38.6
K02-B3	2.7	2.6	1.5	-1.1	-3.4	-10.8	-14.4	-15.6	-20.0	-21.5	-22.9
K02-B2	6.7	6.4	4.8	1.8	-0.3	-3.0	-4.7	-5.1	-6.5	-7.3	-7.4
K02-B1	7.5	7.2	5.5	2.4	0.3	-2.1	-3.7	-4.0	-5.2	-5.9	-5.7
K03-C5	2.1	2.1	1.8	1.4	0.9	-2.5	-4.1	-4.1	-5.6	-5.3	-5.5
K03-C4	1.9	1.8	1.3	0.2	-0.6	-3.8	-5.3	-5.5	-7.0	-7.1	-7.1
K03-C3	2.8	2.7	2.0	0.7	-0.2	-2.7	-4.0	-4.3	-5.5	-5.7	-5.9
K03-C2	3.6	3.4	2.7	1.3	0.4	-1.8	-2.9	-3.2	-4.2	-4.4	-4.7
K03-C1	4.2	4.1	3.2	1.8	0.8	-1.2	-2.3	-2.6	-3.4	-3.7	-4.0
K04-D6	2.1	2.0	1.7	0.8	-0.2	-9.3	-13.1	-13.4	-17.0	-16.6	-16.5
K04-D5	1.7	1.7	1.2	0.1	-1.7	-17.1	-22.9	-22.8	-27.6	-26.4	-26.3
K04-D4	1.6	1.5	1.0	-0.3	-2.1	-16.8	-22.6	-23.0	-28.5	-27.7	-27.4
K04-D3	1.6	1.5	0.9	-0.5	-2.3	-17.4	-23.1	-23.6	-29.2	-28.4	-28.3
K04-D2	1.5	1.5	0.8	-0.6	-2.6	-17.2	-22.9	-23.6	-29.6	-29.0	-28.9
K04-D1	1.5	1.4	0.7	-0.9	-3.0	-17.2	-22.7	-24.1	-31.3	-31.1	-31.1
K05-E4	1.3	1.2	0.5	-1.4	-5.2	-29.9	-37.5	-36.7	-40.4	-37.5	-41.4
K05-E3	1.3	1.2	0.4	-2.2	-6.1	-20.6	-27.0	-28.9	-31.6	-30.7	-36.6
K05-E2	2.0	1.9	0.9	-2.0	-5.2	-13.8	-17.9	-19.3	-22.5	-23.2	-26.5
K05-E1	2.1	2.0	1.0	-1.9	-4.9	-13.0	-17.0	-18.2	-21.6	-22.5	-25.3
K06-F6	0.6	0.5	0.1	-1.4	-5.0	-11.9	-15.2	-15.6	-17.7	-17.4	-19.3
K06-F4	1.1	1.0	0.3	-1.6	-4.2	-17.5	-24.9	-25.8	-30.5	-30.3	-30.7
K06-F3	1.2	1.1	0.4	-1.7	-4.2	-16.1	-23.5	-25.0	-30.5	-31.5	-32.2
K06-F2	1.4	1.3	0.5	-1.7	-4.2	-15.4	-22.2	-23.7	-29.7	-31.9	-32.9
K06-F1	1.6	1.5	0.6	-1.6	-4.0	-15.4	-21.3	-22.8	-29.5	-33.4	-35.3
K07-J5	0.9	0.8	0.3	-1.3	-4.5	-16.6	-22.1	-22.2	-25.3	-24.4	-25.6
K07-J4	0.9	0.8	0.1	-2.7	-9.9	-19.2	-23.1	-24.0	-26.1	-25.5	-30.1
K07-J3	1.2	1.1	0.2	-3.6	-9.3	-15.4	-18.4	-19.3	-21.0	-21.0	-23.9
K07-J2	1.7	1.5	0.4	-4.0	-7.6	-10.2	-12.1	-12.6	-13.8	-14.3	-14.7
K07-J1	2.3	2.2	0.9	-2.9	-5.9	-8.1	-9.8	-10.2	-11.3	-11.9	-12.3
K08-M3	1.2	1.2	0.7	-0.7	-2.8	-19.7	-26.6	-27.2	-32.8	-32.0	-31.2
K08-M2	1.3	1.2	0.3	-1.9	-4.1	-12.0	-20.6	-22.2	-28.9	-31.4	-30.9
K08-M1	2.1	2.0	0.9	-2.1	-4.6	-7.5	-10.2	-10.8	-13.9	-15.6	-15.3
K09-AE	0.4	0.4	-0.5	-6.5	-11.0	-12.2	-13.2	-13.5	-13.5	-13.6	-12.9
K09-AD	0.4	0.4	-2.1	-13.0	-17.6	-18.9	-20.0	-20.7	-20.3	-19.9	-16.3
K09-AC	0.6	0.5	-3.8	-20.2	-24.8	-26.1	-27.5	-28.6	-27.8	-26.9	-19.8
K09-AB	0.9	0.7	-3.8	-18.2	-22.1	-23.4	-24.7	-25.7	-25.0	-24.1	-17.7
K09-AA	1.5	1.3	-2.1	-5.7	-7.4	-8.2	-8.9	-9.0	-9.1	-8.9	-7.9
K10-BA	0.3	0.3	-0.2	-4.6	-8.6	-9.9	-10.9	-11.1	-11.1	-11.4	-11.2
K11-CF	0.0	0.0	-0.4	-3.9	-7.2	-8.4	-9.3	-9.5	-9.7	-9.8	-9.7
K11-CE	0.0	0.0	-0.4	-4.1	-7.5	-8.8	-9.7	-9.9	-10.1	-10.1	-10.1
K11-CD	0.3	0.3	-0.4	-6.2	-11.0	-12.3	-13.4	-13.6	-13.7	-13.8	-13.5
K11-CC	0.5	0.5	-0.4	-0.7	-13.8	-15.1	-16.3	-16.5	-16.5	-16.6	-16.3
K11-CB	0.7	0.6	-0.3	-9.6	-16.9	-18.3	-19.5	-19.7	-19.6	-19.7	-19.5
K11-CA	0.9	0.8	-0.2	-8.3	-14.6	-16.3	-17.6	-17.9	-18.0	-18.2	-18.0
K12-DE	1.4	1.3	1.0	0.1	-1.1	-10.2	-15.7	-16.4	-22.9	-23.9	-22.7
K12-DD	1.3	1.2	0.9	0.0	-1.3	-10.6	-16.1	-16.8	-23.3	-24.3	-23.1
K12-DC	1.3	1.3	0.7	-0.8	-2.6	-16.6	-22.5	-23.9	-31.3	-31.8	-30.4
K12-DB	1.4	1.3	0.6	-1.0	-3.1	-19.5	-25.7	-27.7	-35.6	-35.8	-34.3
K12-DA	1.5	1.4	0.6	-1.3	-3.3	-15.8	-21.6	-23.3	-32.8	-34.9	-33.9
K14-FE	0.2	0.1	-0.4	-4.9	-8.8	-10.0	-11.0	-11.2	-11.4	-11.6	-11.3
K14-FD	0.4	0.4	-0.6	-7.1	-11.9	-13.2	-14.3	-14.6	-14.7	-14.8	-14.0
K14-FC	0.5	0.4	-0.7	-8.0	-13.1	-14.4	-15.5	-15.9	-15.9	-16.0	-15.0
K14-FB	0.5	0.4	-1.5	-8.6	-12.7	-13.8	-14.8	-15.2	-15.1	-15.0	-13.2
K14-FA	0.7	0.5	-3.0	-10.1	-13.1	-14.1	-14.9	-15.1	-15.0	-14.6	-12.2

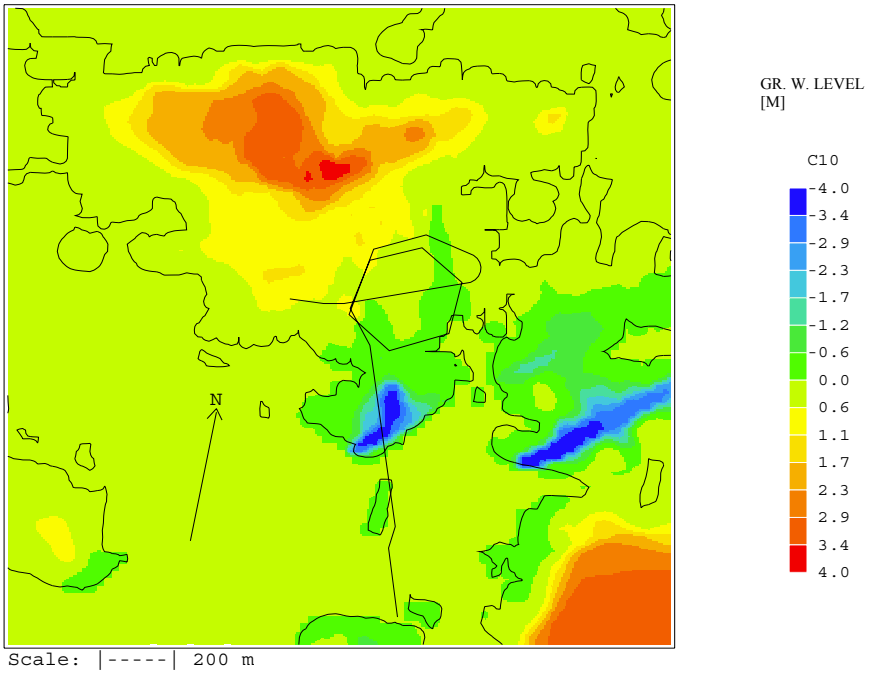

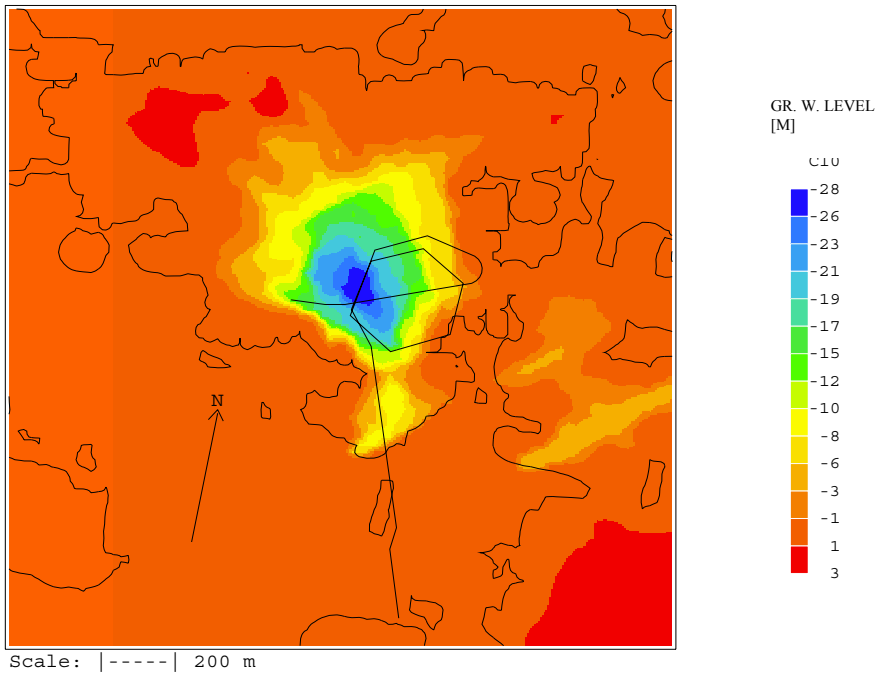

Figure 6-1. *Groundwater table for various tunnel front positions. Top: Tunnel front at about 1 400 metres. Bottom: Tunnel front at about 2 100 metres.*

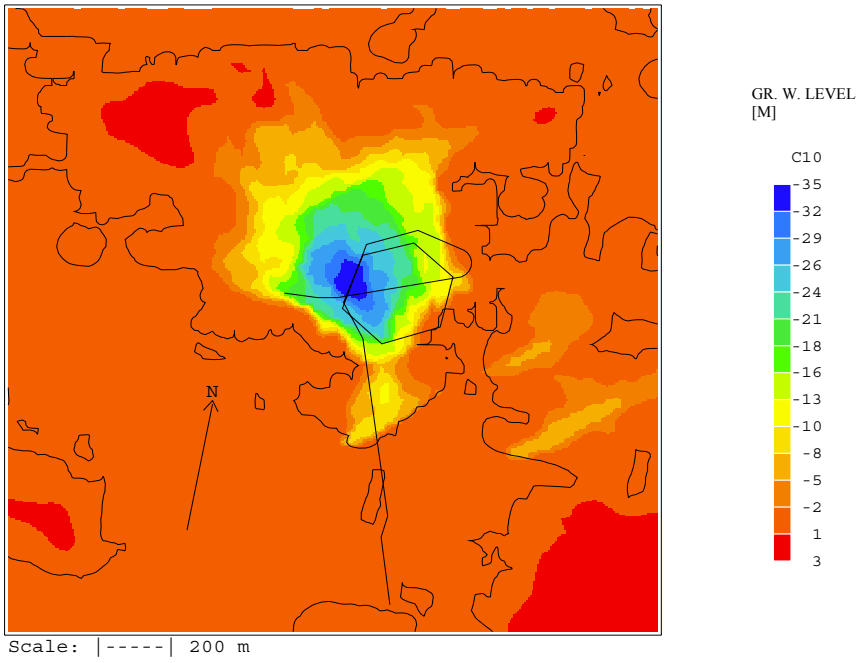

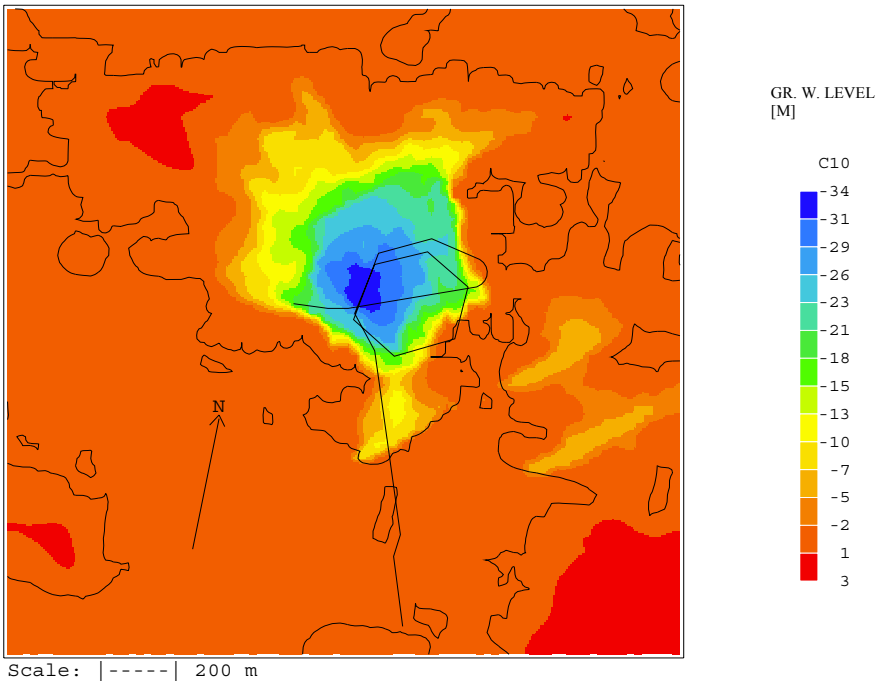

Figure 6-1. *Cont. Top: Tunnel front at about 3 000 metres. Bottom: Tunnel front at about 3 600 metres.*

6.3 WATER COMPOSITION AND FLOWPATHS

The response in water composition, due to the excavation of the tunnel, is studied in ten control points along the tunnel. Results are given in Figures 6-2 to 6-11. In each figure the part that originates from the boundaries of the computational domain is given and the time when the tunnel front passed the point is given in the figure legend. The following conclusions can be drawn from the figures:

- Water that has crossed the domain boundaries will leak into the tunnel soon, i.e. 0.5 to 2.0 years, after the tunnel front passed the control point.
- The fraction of glacial water decreases during the excavation of the tunnel.
- Changes are small after the tunnel construction was completed, which is at time 3.7 years in the figures.

A deeper understanding of the development of the water composition in the control points can be gained by an analysis of the flow paths to the control point. This will be done by a method that is sometimes called "back-tracking". Marked fluid elements or imaginary particles are thus tracked in a reversed flow field. By this method we can calculate the positions a particle, which is entering the tunnel, had at all earlier times. The flow field is however not changed continuously; the tunnel propagation is divided into ten steps and the flow field is updated each time the tunnel passes one of these steps. This is thus an inherent approximation in the method.

The origin of the water in seven control points along the tunnel was tracked for four tunnel front positions (1 400, 2 100, 3 000 and 3 600 metres). The result can be studied in Figures 6-12 to 6-16. When the tunnel front is at position 1 400 metres it has passed five of the control points. The flow paths from the positions before the construction to the control points are given in Figures 6-12 and 6-13. From the figures one can conclude that water from ground level is already found in SA1229 and KA1061, while more complex patterns are found for other points. This means that we do not need to consider SA1229 and KA1061 at later times as the flow path would be the same. Backtracking of water entering at tunnel front position 2 100 metres is studied next, see Figure 6-14. The origin is now further away but the patterns are the same. Next we study the water found in SA2074 and SA2783 when the tunnel front is at 3 000 metres (Figure 6-15) and at 3 600 metres (Figure 6-16). At the later stage it is seen that most of the water entering the tunnel originates from the domain boundaries.

6.4 CONDITIONS 1997-01-01

It was stated above that the water composition does not change much after the tunnel construction is completed. Results for 1997-01-01 thus represents a quasi-steady state and is, for this reason, of special interest. The water composition of inflows to the tunnel, are given in Figure 6-17 and the horizontal distributions at a depth of 450 metres are found in Figure 6-18. These two figures show that the simulated water composition around the tunnel is very complex with all four water types present at most positions.

6.5 CONCLUDING REMARKS

In the presentation of results the overall consistency has not been mentioned. It is however useful to study the results also from this point of view. As an example we can mention the direct flow paths to ground level for control points KA1061 and SA1229 (Figures 6-12 and 6-13) and the fast contribution from domain boundaries found for these points (Figures 6-5 and 6-6).

6.6 MODEL99

The same set of simulations was carried out also with the first model version. It is therefore expected that the results can be understood with less explanations:

- The pressure response in borehole sections is given in Table 6-2, and the groundwater table for various tunnelfront positions is presented in Figure 6-19.
- The calculated water composition in the ten control points can be found in Figures 6-20 to 6-29. The measured distributions were not all available at this time and hence not included in the figures.
- Flow paths to control points are illustrated in Figures 6-30 to 6-34.
- And, finally, the water composition of inflows to the tunnel 1997-01-01 is shown in Figure 6-35, and the horizontal distributions at a depth of 450 metres are found in Figure 6-36.

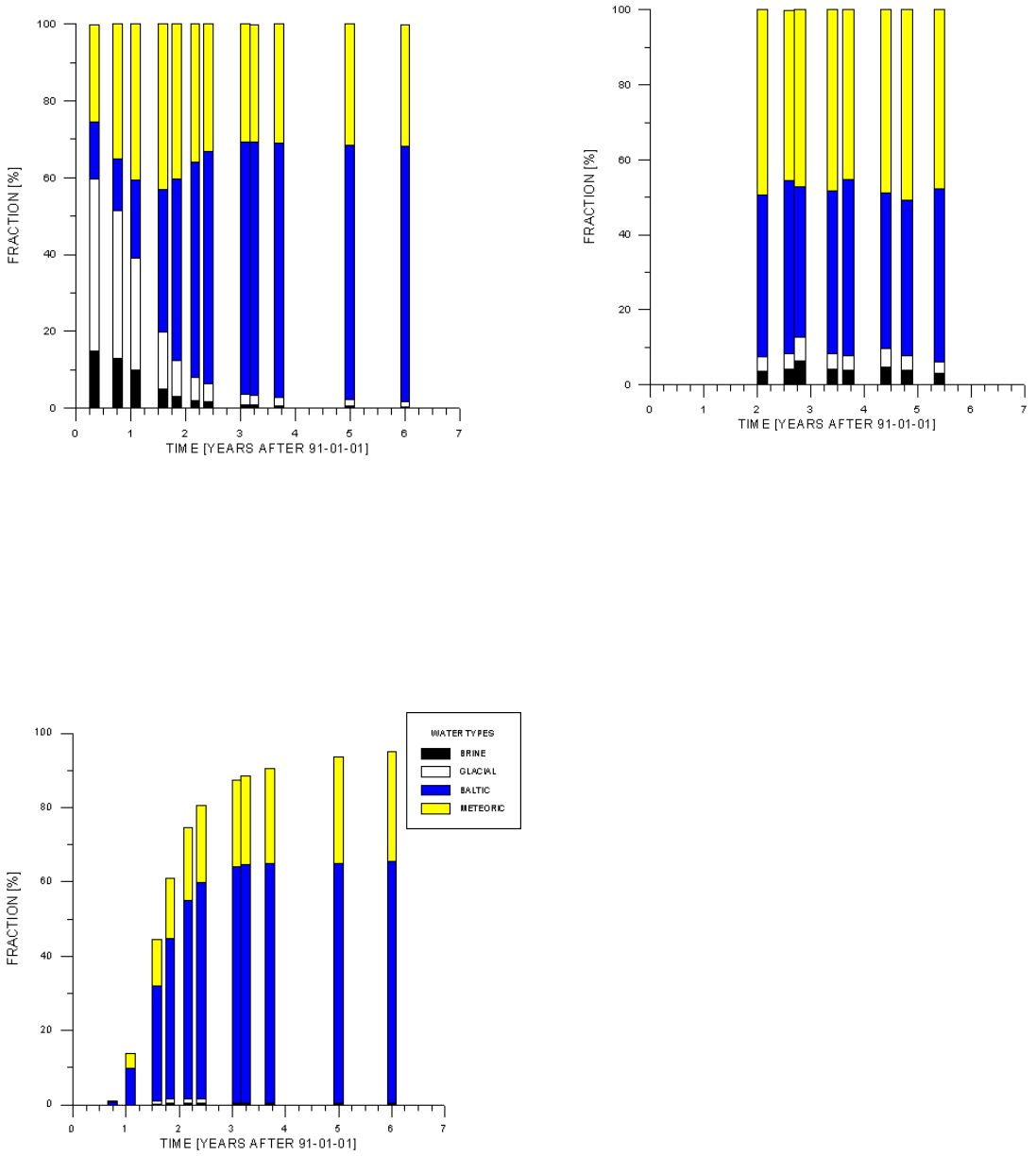

Figure 6-2. *Water composition in control point SA0813 as a function of time. Measured (top right) and simulated (top left) composition and fraction coming from the domain boundaries. Time for tunnel passing the point: 0.58.*

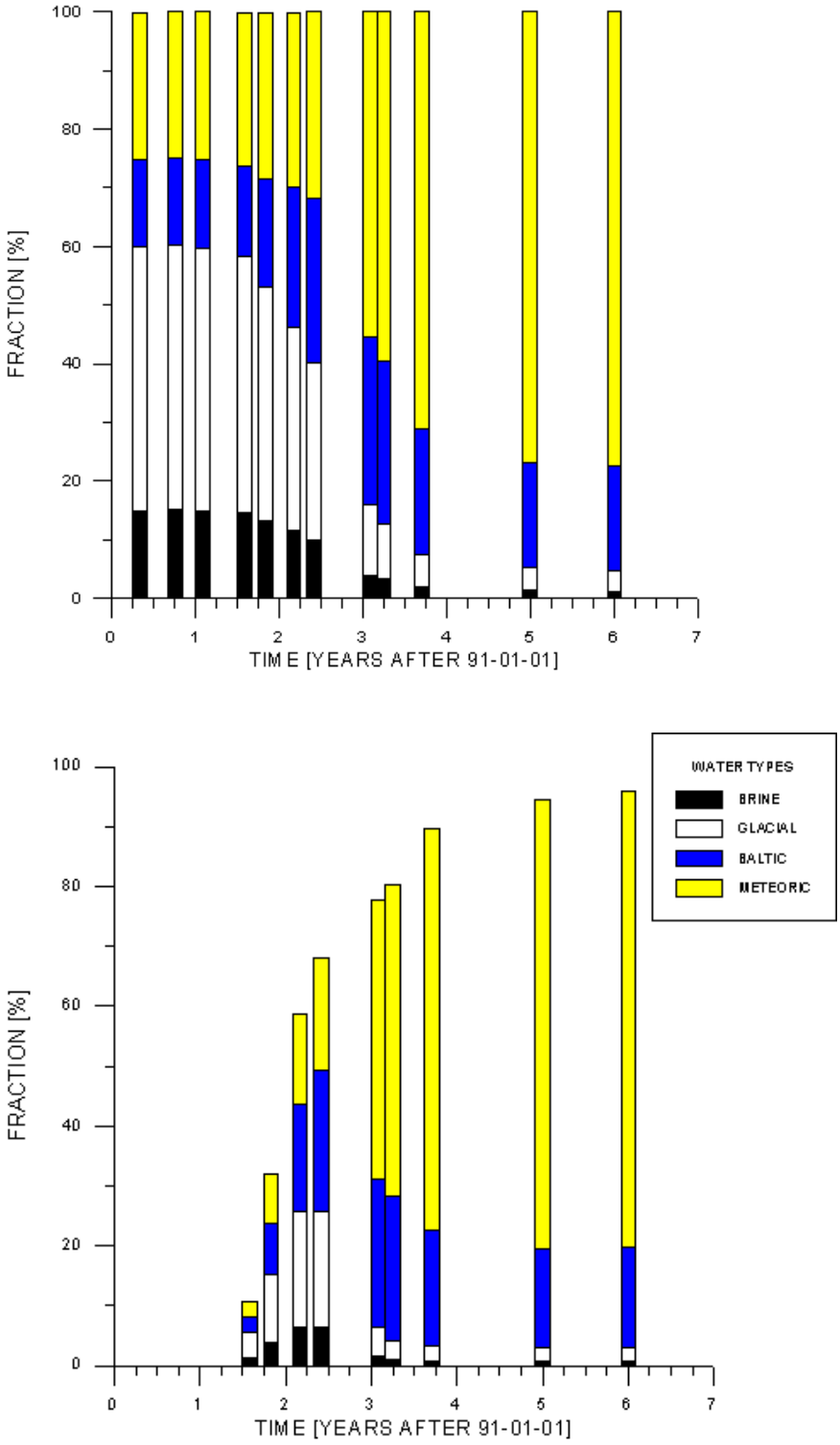

Figure 6-3. *Water composition in control point SA0850 as a function of time (top) and fraction coming from the domain boundaries. Time for tunnel passing the point: 0.63.*

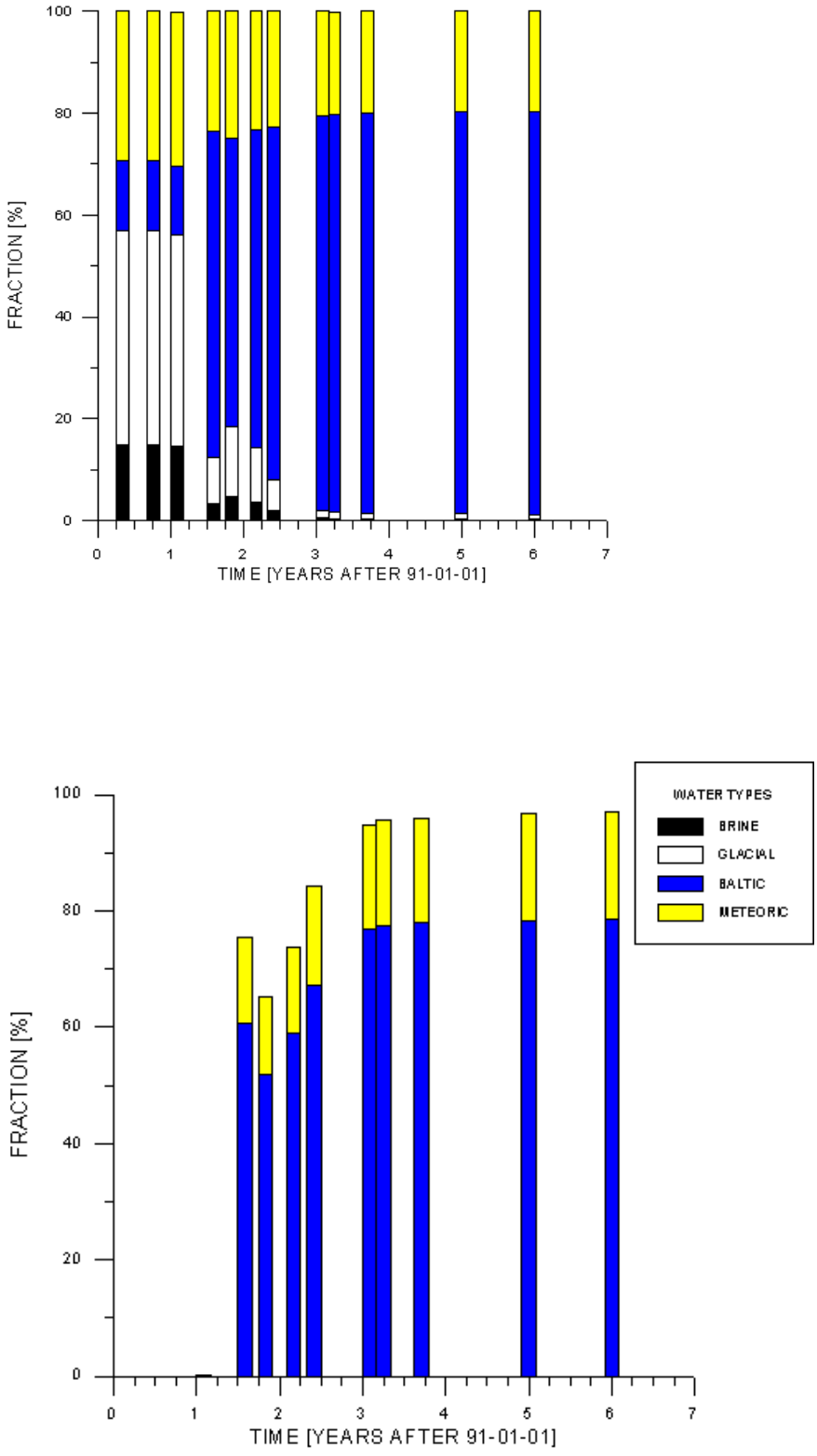

Figure 6-4. *Water composition in control point KA1061 as a function of time (top) and fraction coming from the domain boundaries. Time for tunnel passing the point: 0.92.*

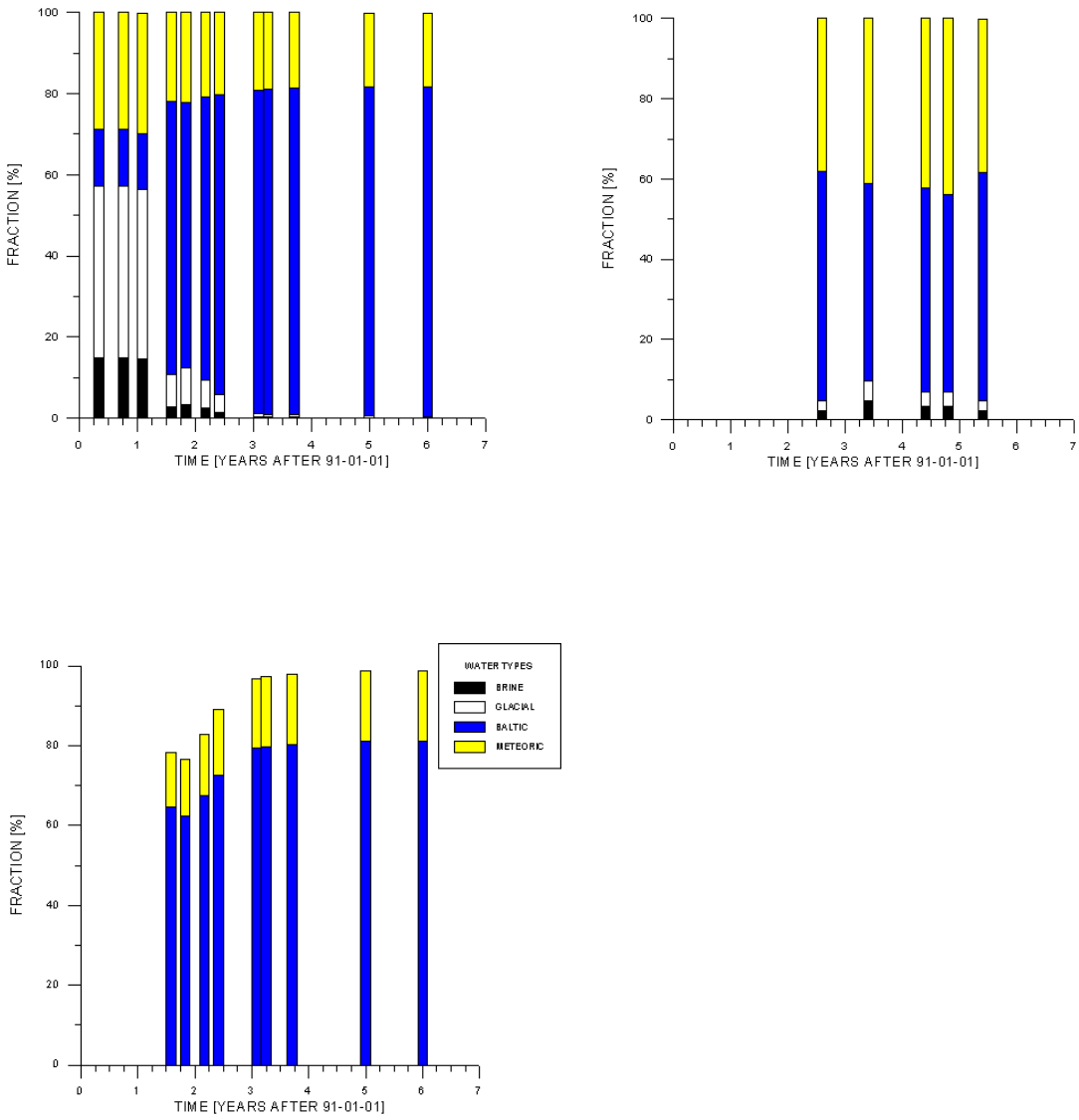

Figure 6-5. *Water composition in control point SA1229 as a function of time. Measured (top right) and simulated (top left) composition and fraction coming from the domain boundaries. Time for tunnel passing the point: 1.12.*

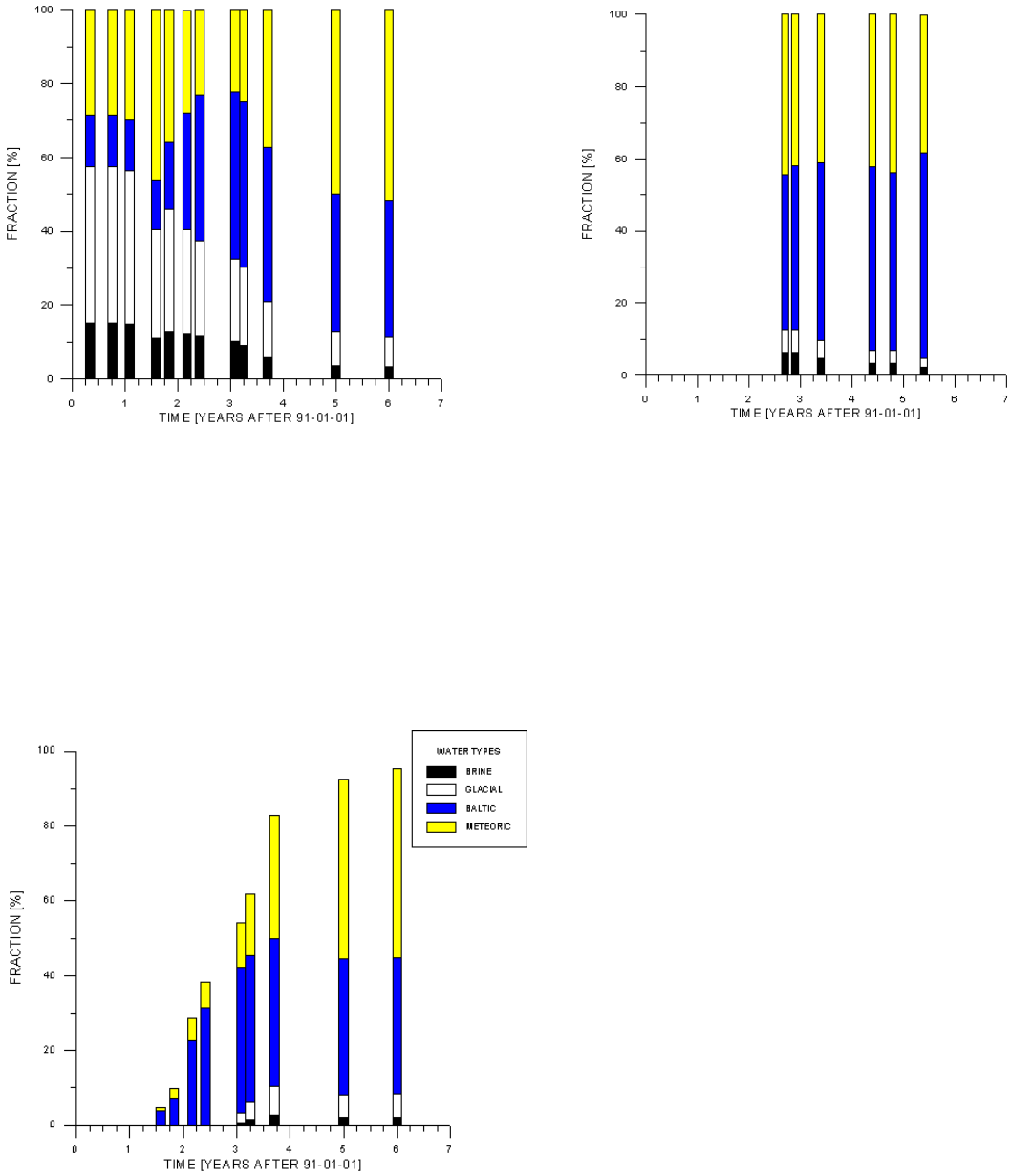

Figure 6-6. *Water composition in control point SA1327 as a function of time. Measured (top right) and simulated (top left) composition) and fraction coming from the domain boundaries. Time for tunnel passing the point: 1.41.*

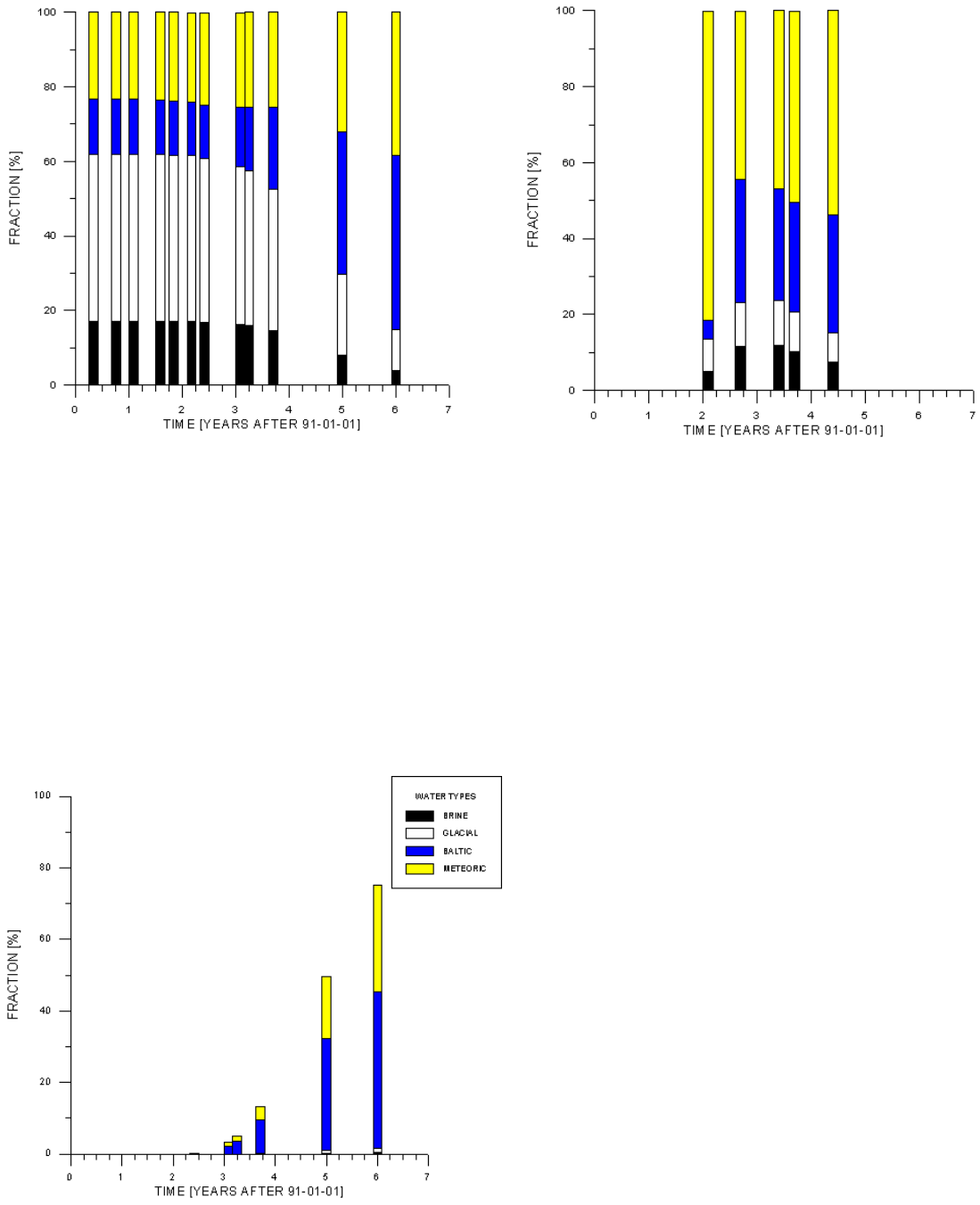

Figure 6-7. *Water composition in control point SA2074 as a function of time. Measured (top right) and simulated (top left) composition) and fraction coming from the domain boundaries. Time for tunnel passing the point: 2.09.*

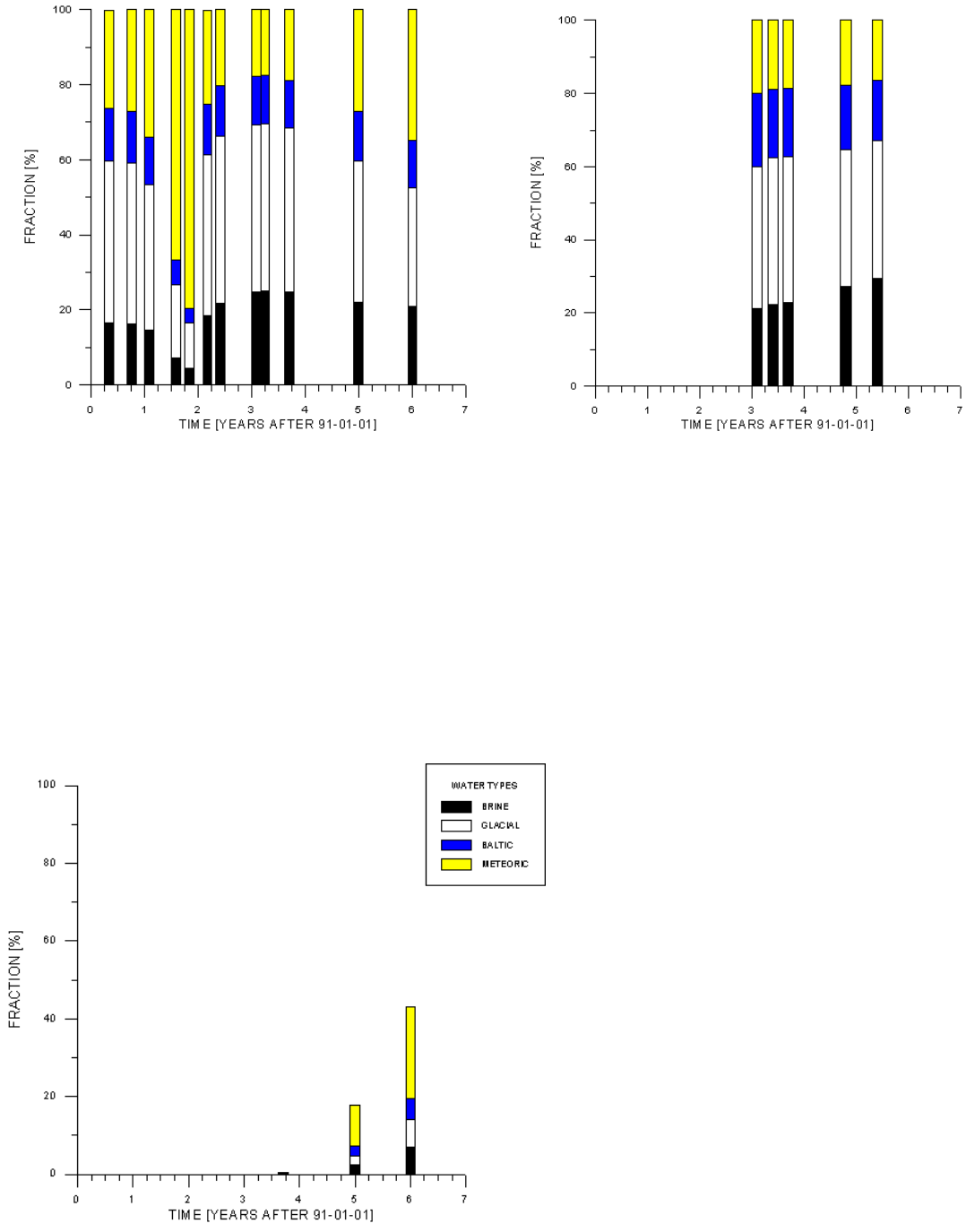

Figure 6-8. *Water composition in control point SA2783 as a function of time. Measured (top right) and simulated (top left) composition) and fraction coming from the domain boundaries. Time for tunnel passing the point: 3.03.*

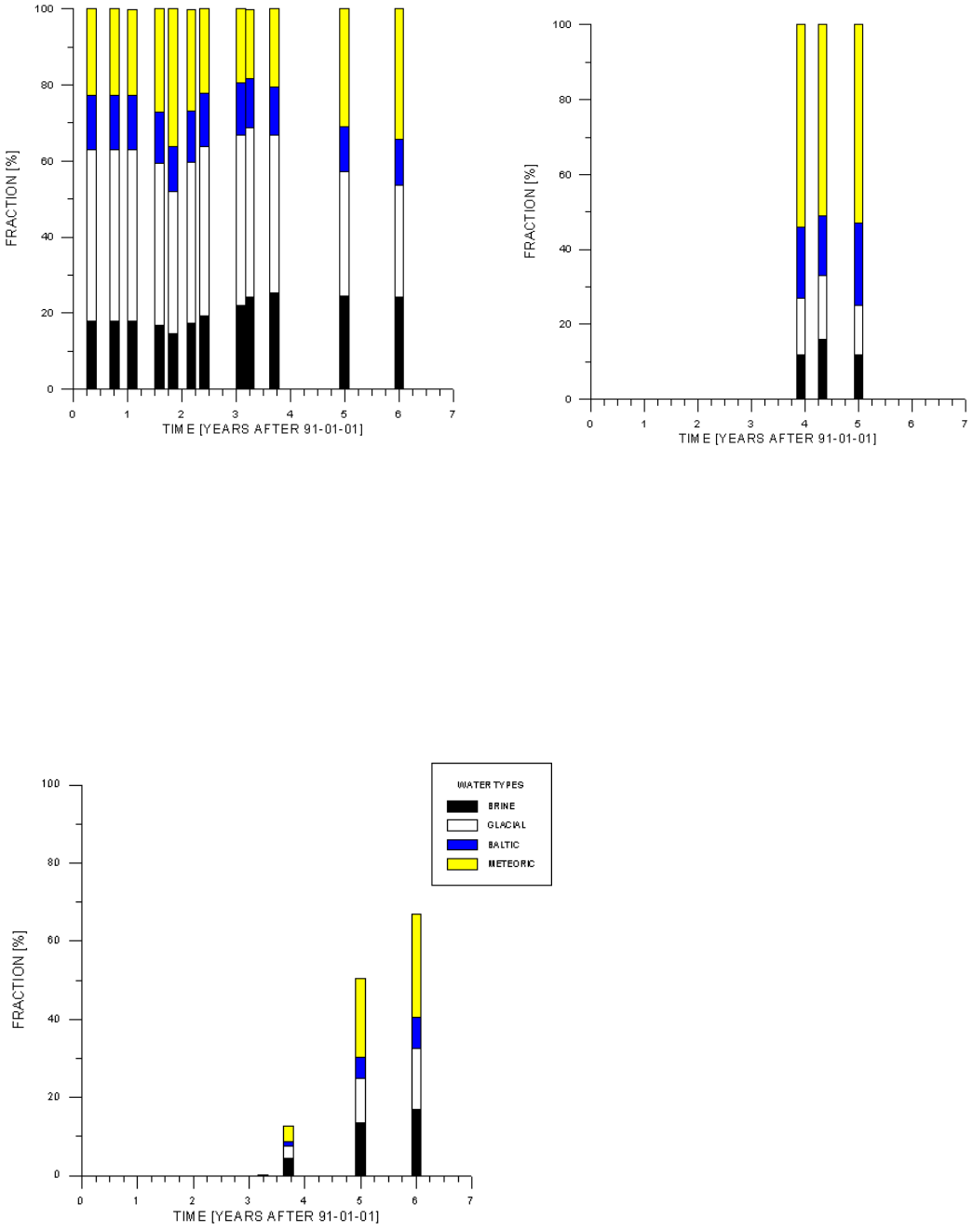

Figure 6-9. *Water composition in control point KA3005 as a function of time. Measured (top right) and simulated (top left) composition and fraction coming from the domain boundaries. Time for tunnel passing the point: 3.13.*

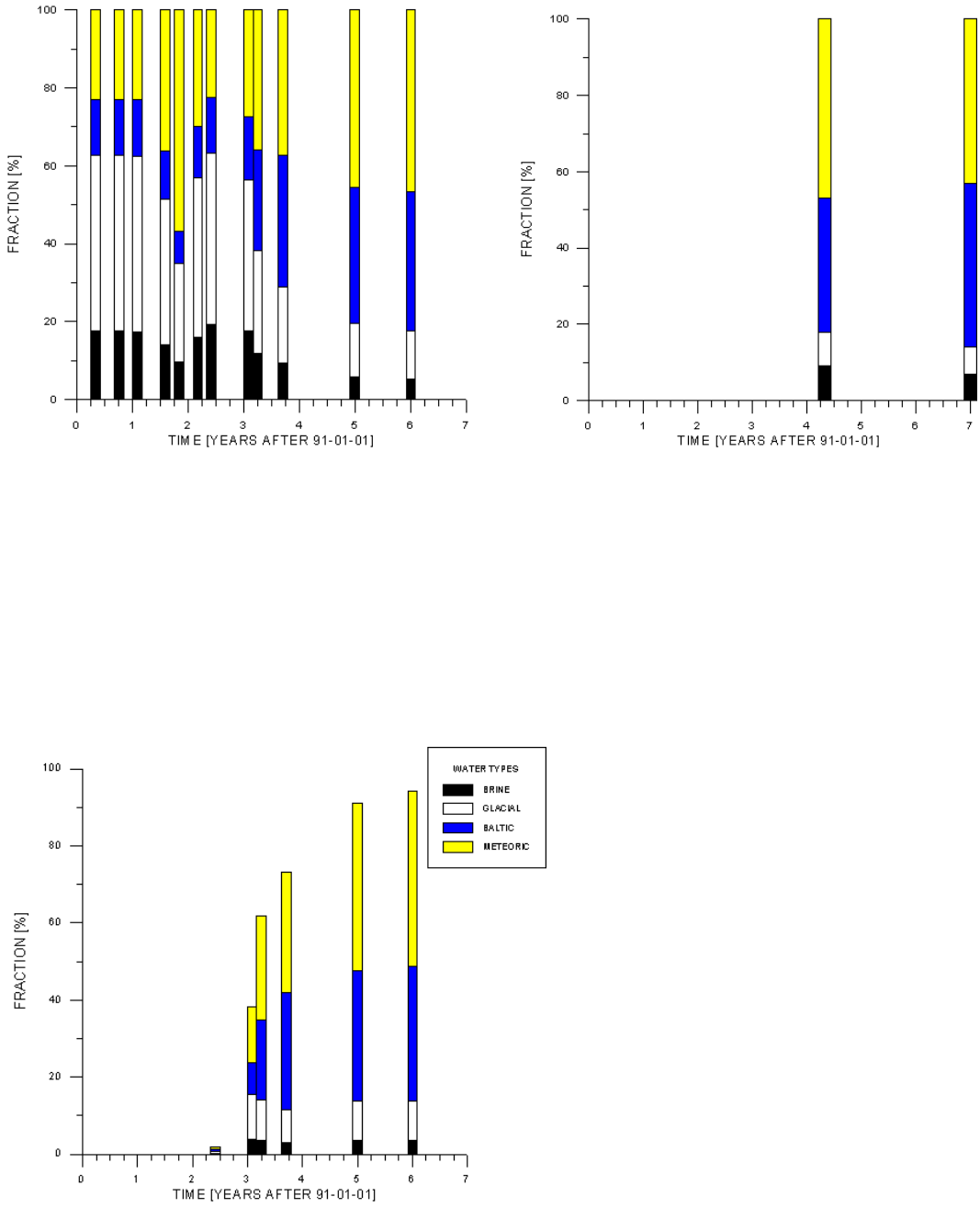

Figure 6-10. *Water composition in control point KA3110 as a function of time. Measured (top right) and simulated (top left) composition) and fraction coming from the domain boundaries. Time for tunnel passing the point: 3.20.*

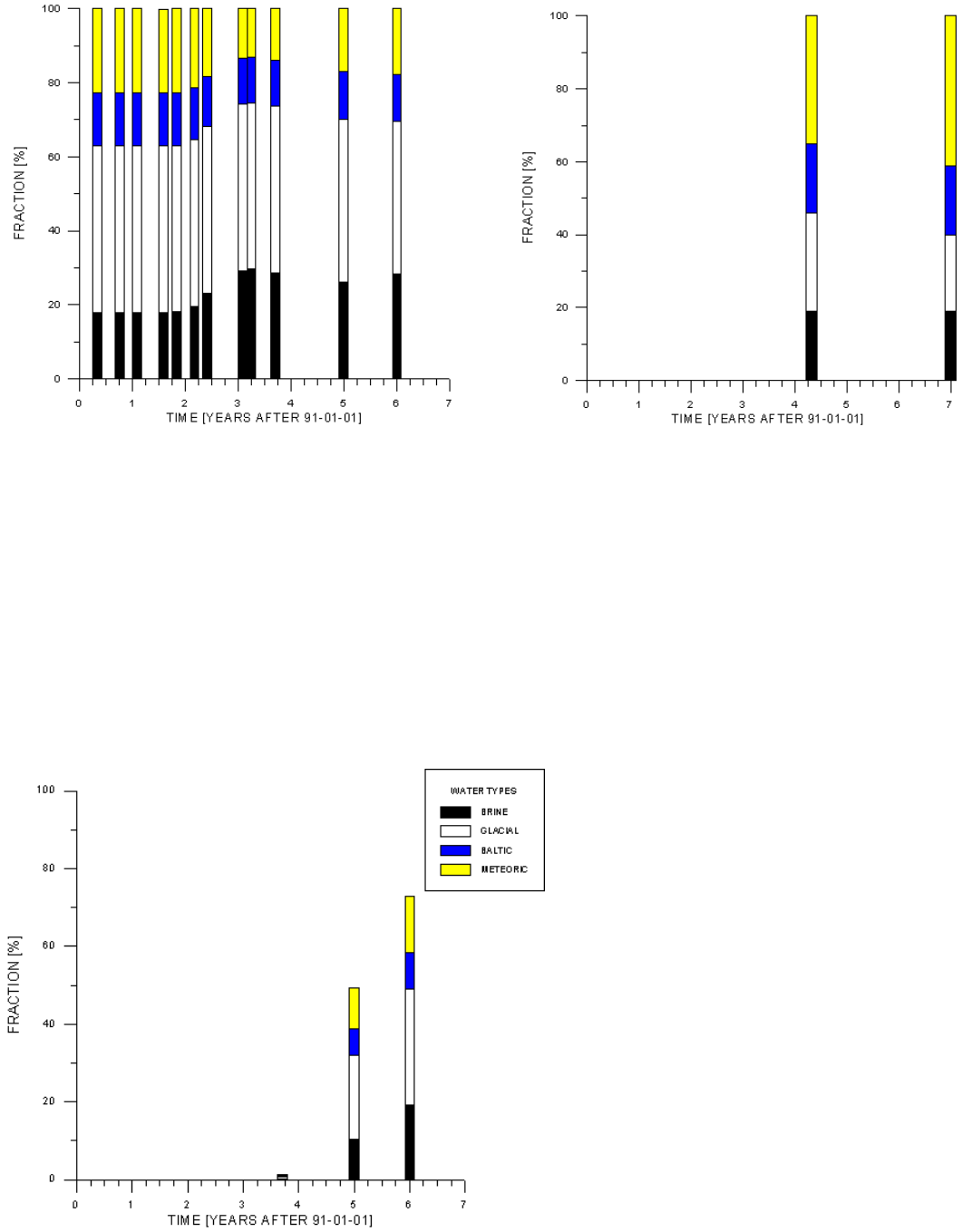

Figure 6-11. *Water composition in control point KA3385 as a function of time. Measured (top right) and simulated (top left) composition) and fraction coming from the domain boundaries. Time for tunnel passing the point: 3.60.*

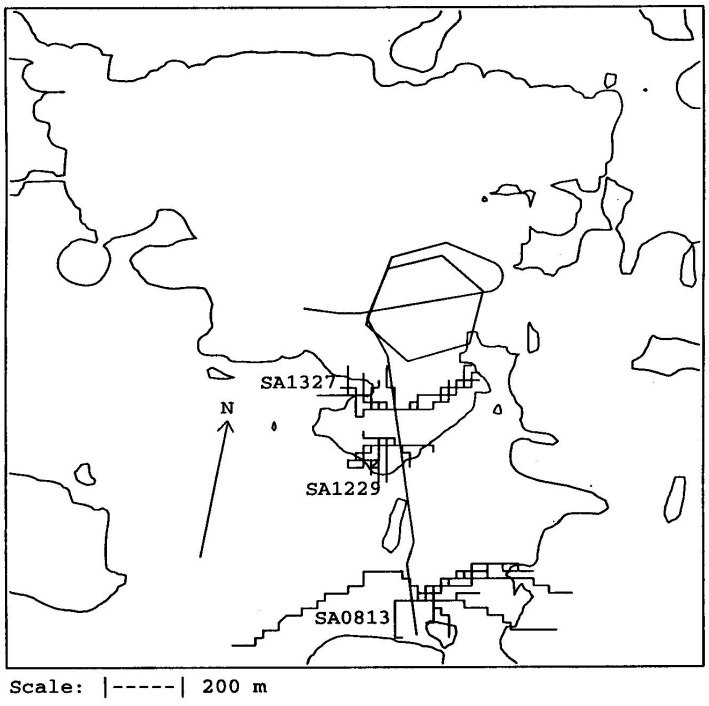

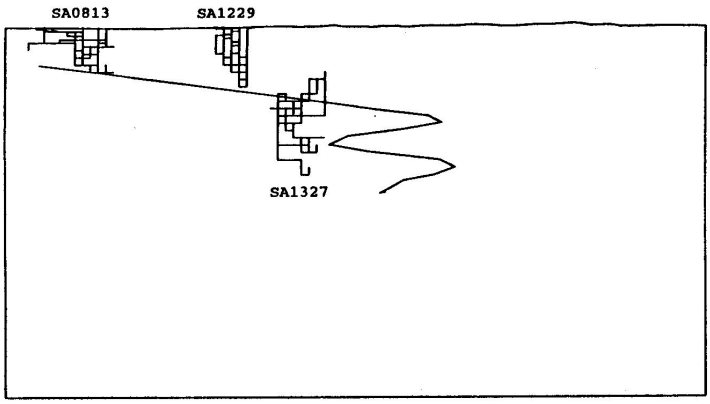

Figure 6-12. *Flow paths for water in control points SA0813, SA1229 and SA1327. Horizontal view (top) and view from east. Tunnel front at: 1 400 metres.*

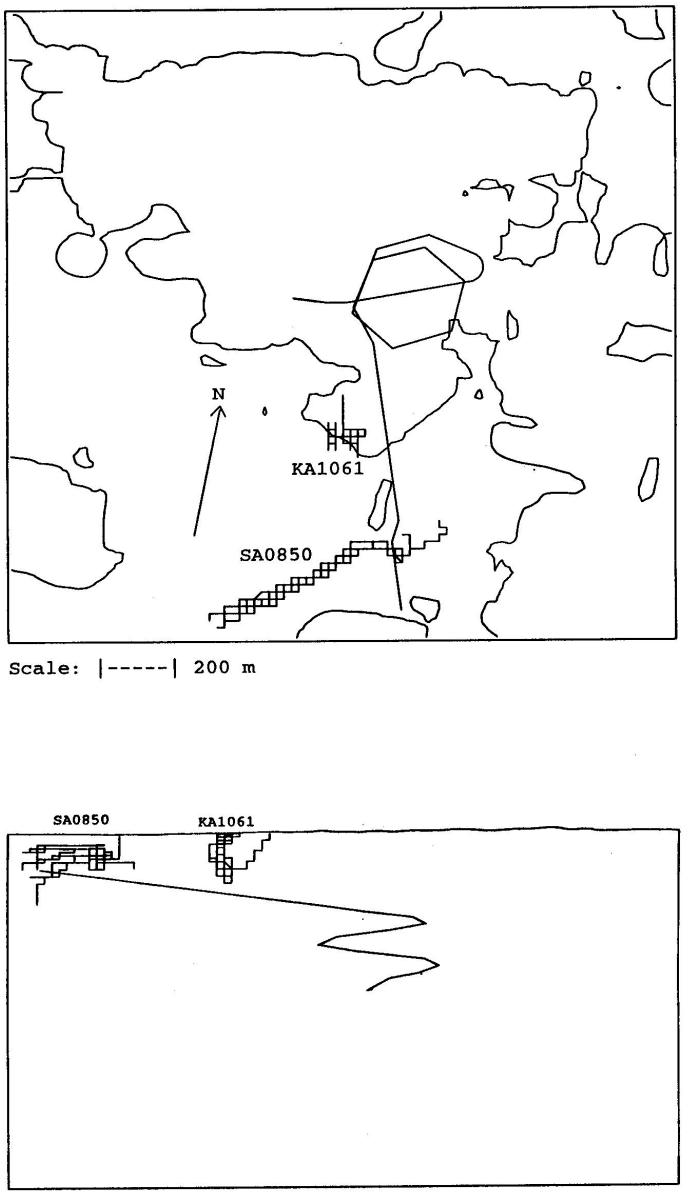

Figure 6-13. *Flow paths for water in control points SA0850 and KA1061. Horizontal view (top) and view from east. Tunnel front at: 1 400 metres.*

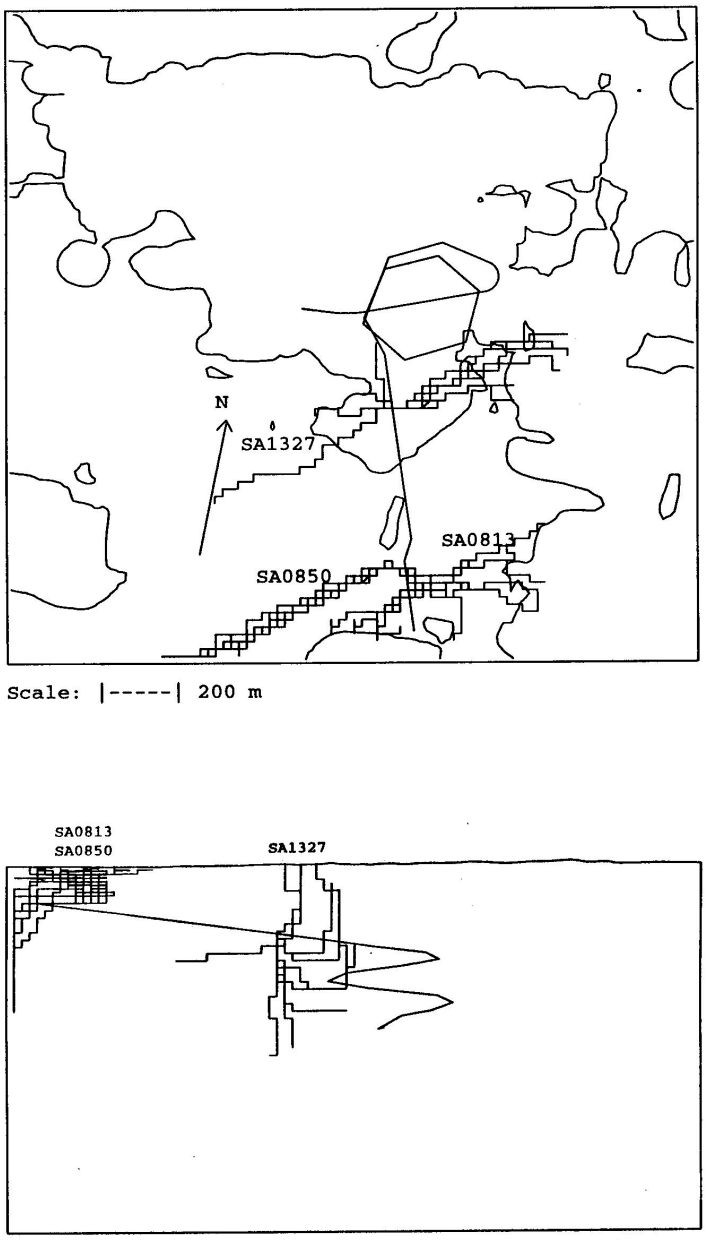

Figure 6-14. *Flow paths for water in control points SA0813, SA0850 and SA1327. Horizontal view (top) and view from east. Tunnel front at: 2 100 metres.*

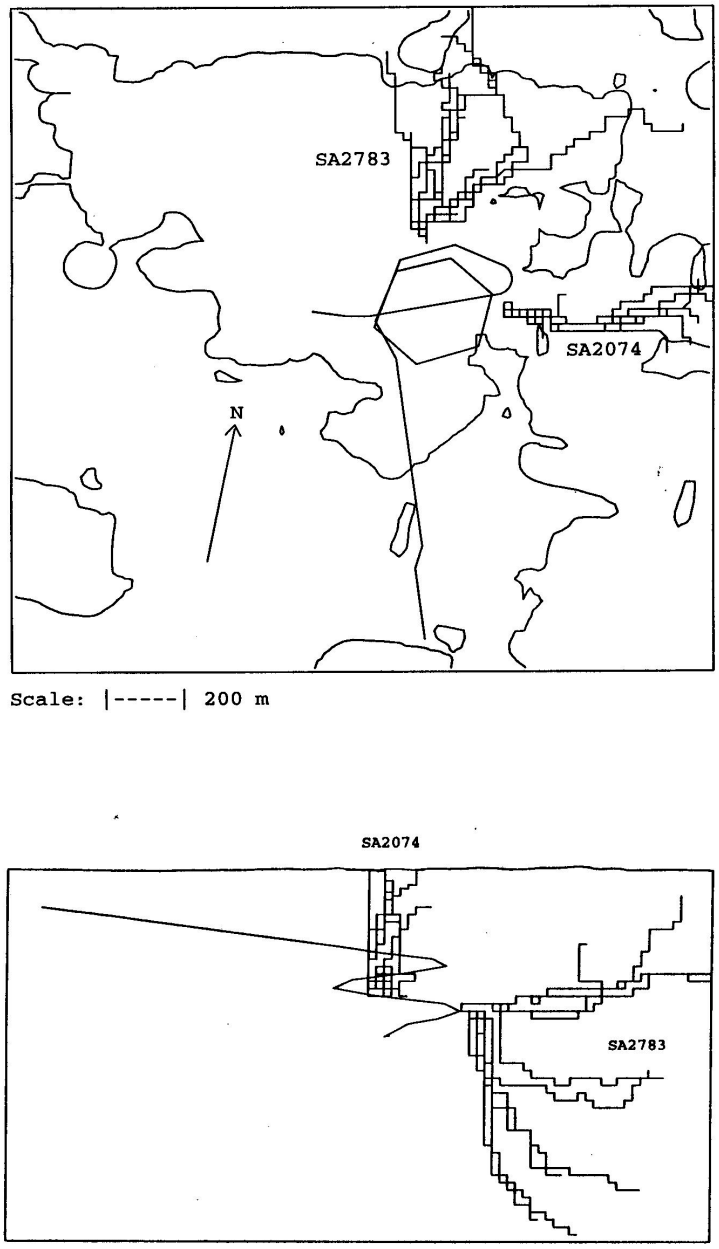

Figure 6-15. *Flow paths for water in control points SA2074 and SA2783. Horizontal view (top) and view from east. Tunnel front at: 3 000 metres.*

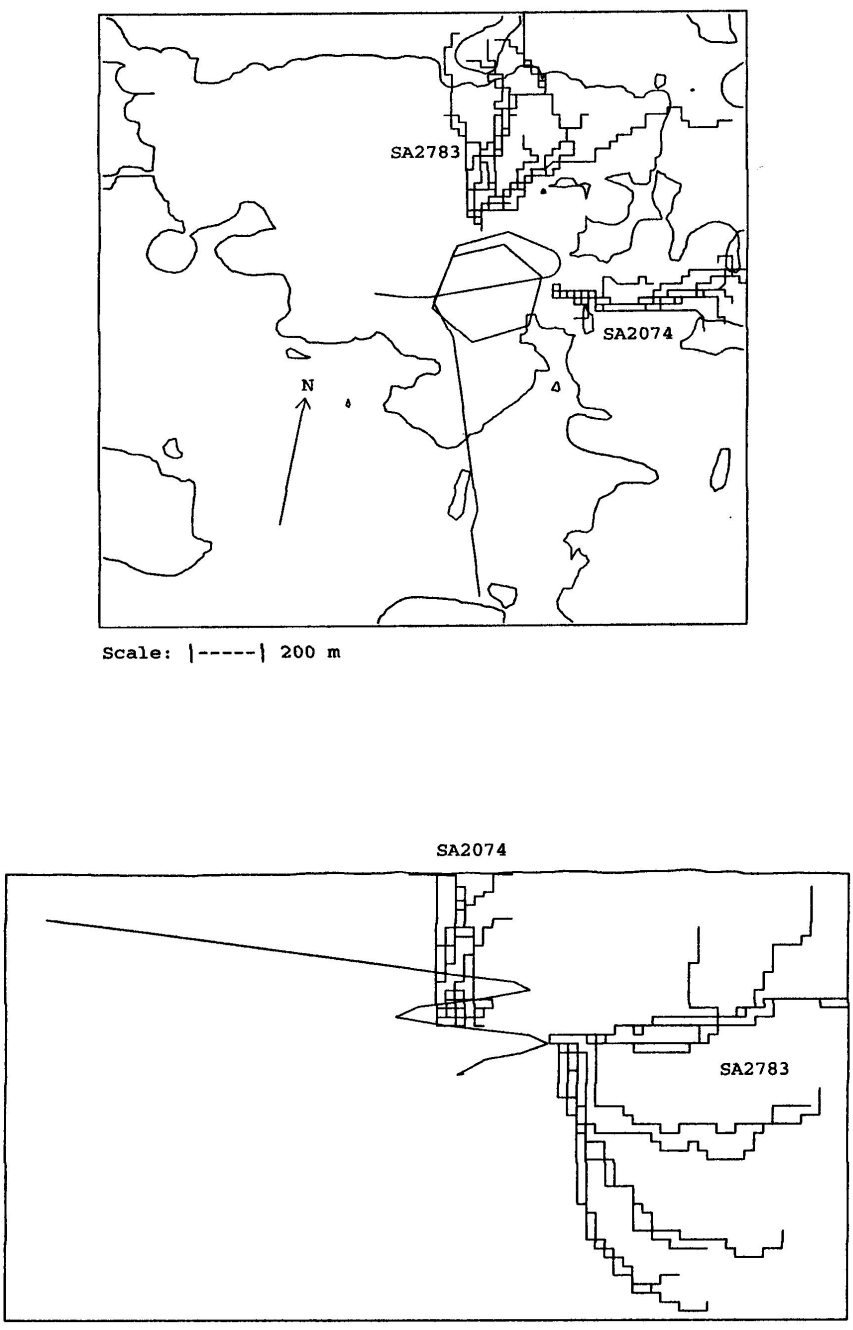

Figure 6-16. *Flow paths for water in control points SA2074 and SA2783. Horizontal view (top) and view from east. Tunnel front at: 3 600 metres.*

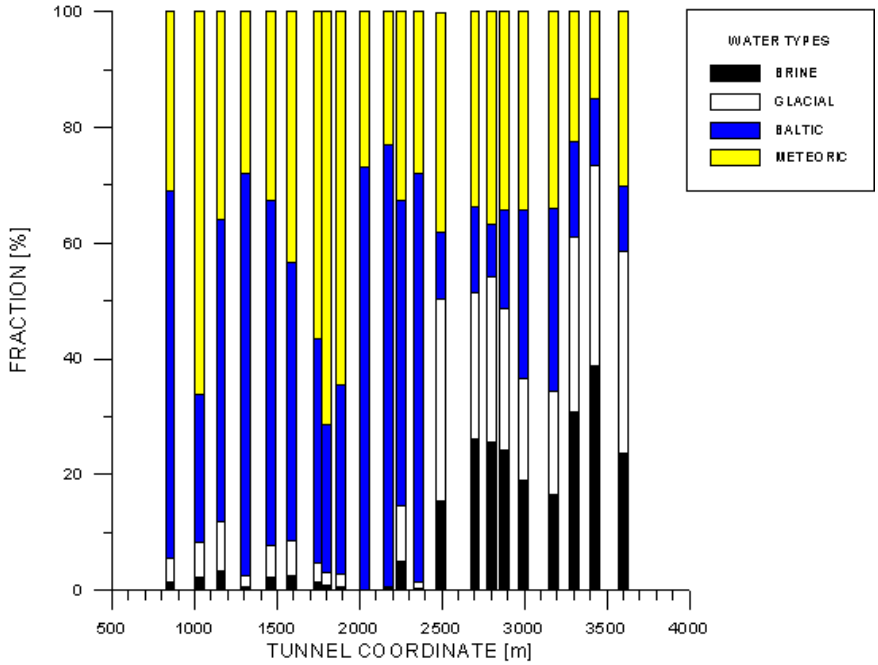

Figure 6-17. *Water composition of inflows to tunnel 1997-01-01.*

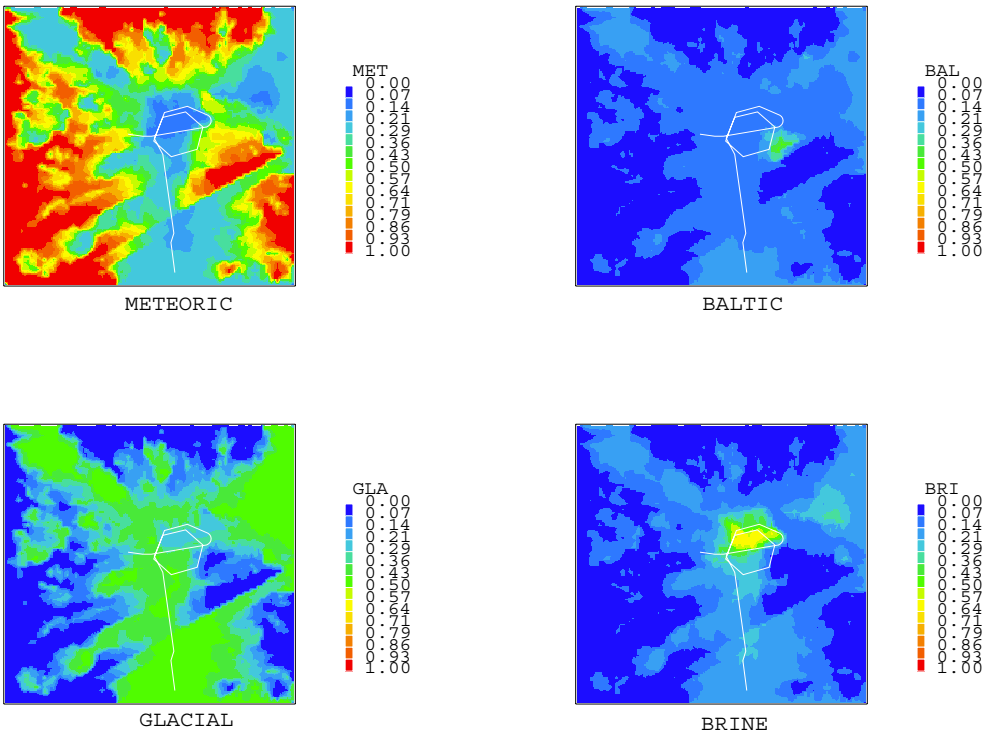

Figure 6-18. *Water composition 1997-01-01 at a depth of 450 metres.*

Table 6-2. Model99. Calculated freshwater hydraulic head in borehole sections for various tunnel front positions.

Borehole section	Freshwater hydraulic head [m]										
	Tunnel front position [m]										
	0	0 ↓ 960	960 ↓ 1190	1190 ↓ 1380	1380 ↓ 1750	1750 ↓ 2160	2160 ↓ 2590	2590 ↓ 2900	2900 ↓ 3170	3170 ↓ 3600	3600
K02-B5	1.5	1.4	1.3	0.6	-0.6	-28.2	-36.4	-35.1	-41.3	-38.0	-37.1
K02-B4	1.6	1.5	1.4	0.5	-1.0	-23.8	-30.7	-30.6	-37.5	-35.4	-35.4
K02-B3	2.8	2.7	1.7	-0.2	-1.2	-13.2	-17.3	-18.0	-23.1	-22.9	-23.0
K02-B2	6.7	6.5	5.1	1.9	-0.1	-3.9	-5.9	-6.3	-8.0	-8.2	-8.1
K02-B1	7.5	7.3	5.7	2.4	0.4	-2.8	-4.7	-5.1	-6.3	-6.5	-6.4
K03-C5	1.7	1.7	1.6	1.3	1.0	-1.8	-2.8	-3.0	-4.4	-4.3	-4.2
K03-C4	1.9	1.8	1.5	1.0	0.6	-3.2	-4.7	-4.9	-6.8	-6.8	-6.7
K03-C3	2.7	2.7	2.1	1.2	0.6	-2.9	-4.3	-4.5	-6.2	-6.3	-6.2
K03-C2	3.6	3.6	2.9	1.7	1.0	-1.8	-2.9	-3.1	-4.3	-4.4	-4.3
K03-C1	4.3	4.2	3.4	2.1	1.3	-1.0	-2.0	-2.2	-3.1	-3.1	-3.1
K04-D6	1.8	1.7	1.6	1.1	-0.4	-14.6	-19.5	-19.7	-26.0	-25.0	-24.2
K04-D5	1.7	1.7	1.6	1.0	0.2	-15.5	-20.6	-20.7	-27.0	-25.8	-25.0
K04-D4	1.6	1.6	1.5	0.9	-0.0	-15.5	-20.7	-21.1	-27.9	-27.0	-26.2
K04-D3	1.6	1.6	1.5	0.8	-0.1	-16.0	-21.4	-21.7	-28.6	-27.7	-26.8
K04-D2	1.6	1.6	1.4	0.7	-0.3	-16.2	-21.6	-22.1	-29.3	-28.4	-27.6
K04-D1	1.6	1.5	1.4	0.6	-2.3	-23.2	-29.5	-30.7	-34.9	-32.8	-39.1
K05-E4	1.5	1.5	1.2	0.2	-2.4	-27.6	-34.2	-33.9	-38.5	-37.7	-41.3
K05-E3	1.5	1.5	1.2	0.0	-6.1	-20.6	-27.0	-28.9	-31.6	-30.7	-36.6
K05-E2	2.0	2.0	1.2	-0.2	-2.0	-15.8	-20.3	-21.1	-25.4	-24.7	-27.0
K05-E1	2.1	2.1	1.2	-0.3	-2.0	-14.9	-19.1	-19.8	-24.1	-23.5	-25.4
K06-F6	0.4	0.3	0.1	-1.1	-4.1	-6.1	-7.0	-7.5	-8.2	-8.2	-10.7
K06-F4	1.1	1.1	0.9	0.0	-0.9	-13.3	-21.7	-24.8	-32.1	-34.0	-34.4
K06-F3	1.2	1.2	0.9	-0.2	-1.2	-11.8	-20.1	-23.2	-30.6	-33.4	-34.6
K06-F2	1.4	1.3	0.9	-0.3	-1.3	-10.8	-18.4	-21.2	-28.9	-33.7	-35.9
K06-F1	1.6	1.6	1.0	-0.1	-1.2	-11.9	-18.4	-20.8	-29.0	-34.9	-37.2
K07-J5	0.9	0.9	0.8	0.3	-0.8	-19.1	-25.8	-26.3	-32.3	-31.2	-30.9
K07-J4	1.2	1.1	0.7	-1.0	-6.7	-21.6	-25.9	-25.9	-29.2	-27.5	-31.4
K07-J3	1.3	1.2	0.3	-2.7	-7.6	-11.6	-13.1	-13.8	-15.1	-15.1	-18.2
K07-J2	1.7	1.6	0.4	-3.0	-5.4	-7.0	-7.9	-8.3	-9.2	-9.5	-10.1
K07-J1	2.3	2.2	0.8	-2.3	-4.2	-5.6	-6.6	-6.8	-7.7	-8.0	-8.0
K08-M3	1.0	1.0	0.9	0.4	-0.2	-10.0	-15.0	-17.4	-25.5	-27.1	-25.4
K08-M2	1.3	1.2	0.7	-0.4	-1.4	-8.2	-17.7	-20.7	-30.5	-35.6	-35.8
K08-M1	2.1	2.1	0.8	0.3	-2.4	-4.9	-7.5	-8.1	-12.0	-13.6	-12.9
K09-AE	0.4	0.4	-0.0	-2.6	-3.9	-4.1	-4.3	-4.4	-4.4	-4.4	-4.4
K09-AD	0.5	0.4	-1.5	-8.1	-9.7	-9.9	-10.2	-10.6	-10.3	-10.0	-7.6
K09-AC	0.6	0.5	-1.9	-9.4	-11.3	-11.6	-12.0	-12.5	-12.2	-11.8	-9.1
K09-AB	0.9	0.8	-3.1	-12.7	-14.3	-14.6	-15.1	-15.8	-15.3	-14.6	-10.3
K09-AA	1.5	1.3	-2.1	-5.1	-6.2	-6.5	-6.8	-6.9	-7.0	-6.6	-5.8
K12-DE	1.4	1.3	1.3	1.0	0.6	-7.5	-11.5	-13.1	-23.9	-25.2	-23.0
K12-DD	1.3	1.3	1.2	0.8	0.4	-9.1	-13.6	-15.2	-25.4	-26.6	-24.4
K12-DC	1.2	1.2	1.0	0.4	-0.2	-12.6	-17.9	-20.4	-31.8	-33.6	-30.3
K12-DB	1.3	1.2	1.1	0.4	-0.4	-14.1	-19.6	-22.5	-34.1	-36.0	-32.5
K12-DA	1.5	1.4	1.0	0.2	-0.7	-11.7	-17.2	-19.6	-32.3	-35.5	-32.9
K14-FE	0.2	0.1	-0.2	-2.6	-3.9	-4.1	-4.2	-4.3	-4.3	-4.4	-4.4
K14-FD	0.5	0.4	-0.8	-5.0	-6.7	-7.0	-7.2	-7.4	-7.4	-7.2	-6.5
K14-FC	0.5	0.5	-0.9	-5.2	-7.1	-7.4	-7.7	-7.9	-7.9	-7.8	-7.1
K14-FB	0.5	0.5	-0.9	-5.1	-7.0	-7.3	-7.6	-7.8	-7.8	-7.7	-7.0
K14-FA	0.7	0.6	-0.7	-5.5	-7.8	-8.3	-8.7	-8.9	-8.9	-8.9	-8.4

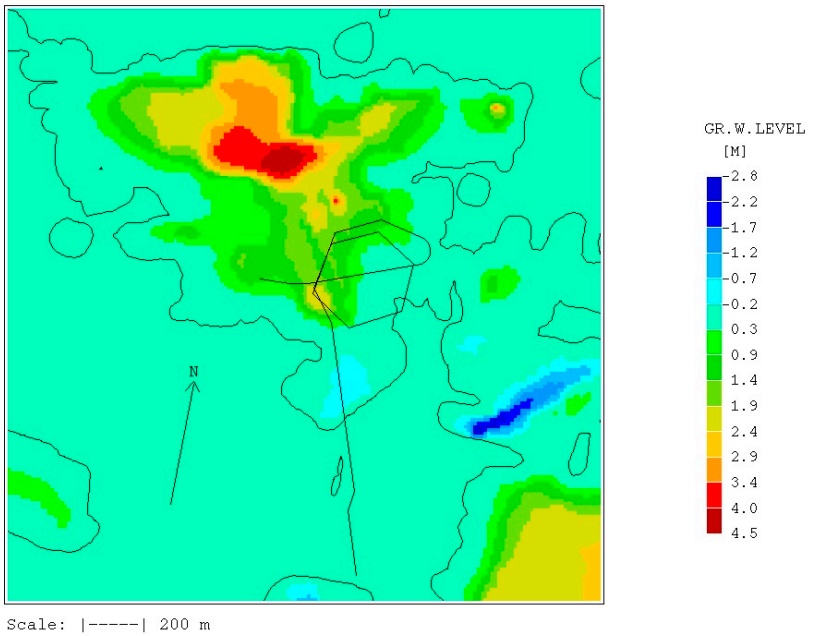

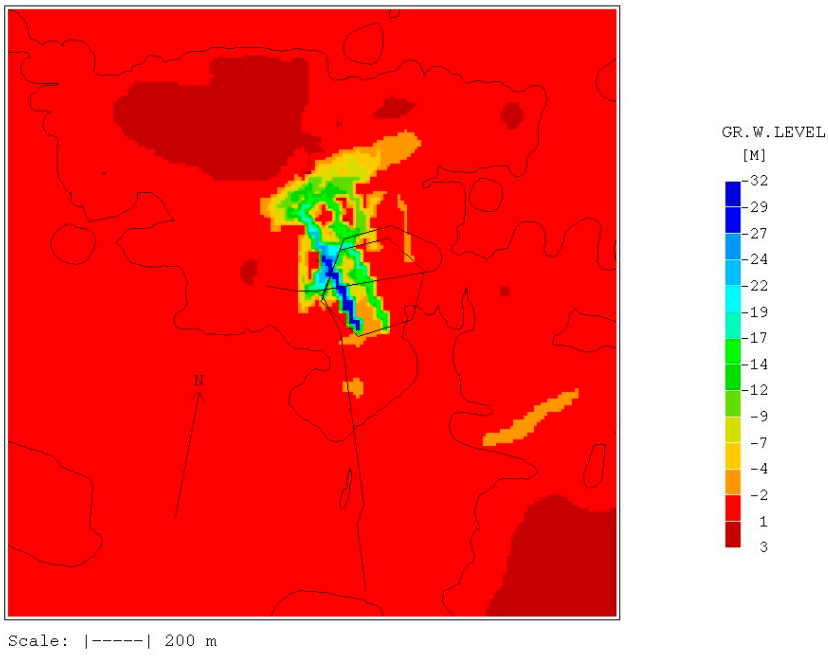

***Figure 6-19**. Model99. Groundwater table for various tunnel front positions.*
Top: Tunnel front at about 1 400 metres.
Bottom: Tunnel front at about 2 100 metres.

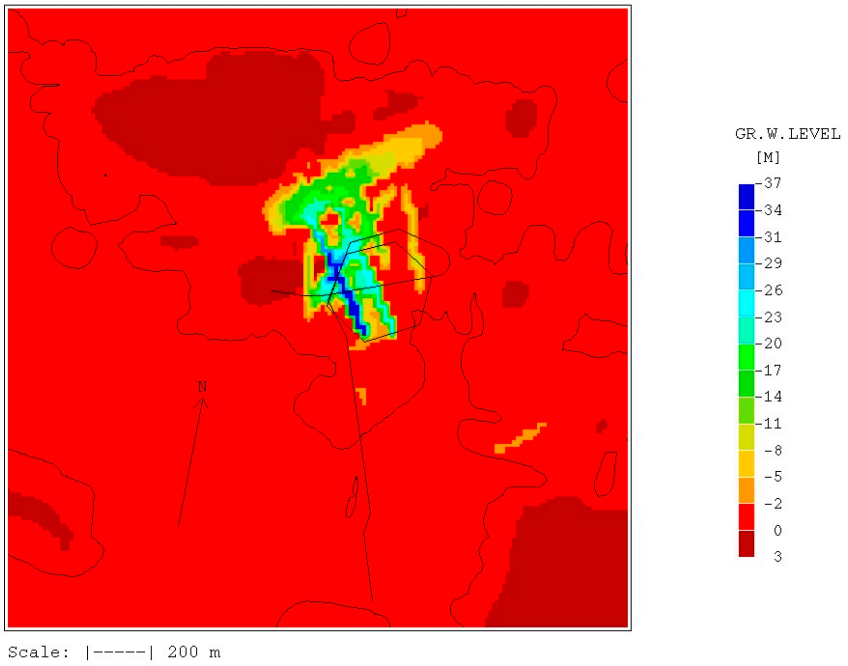

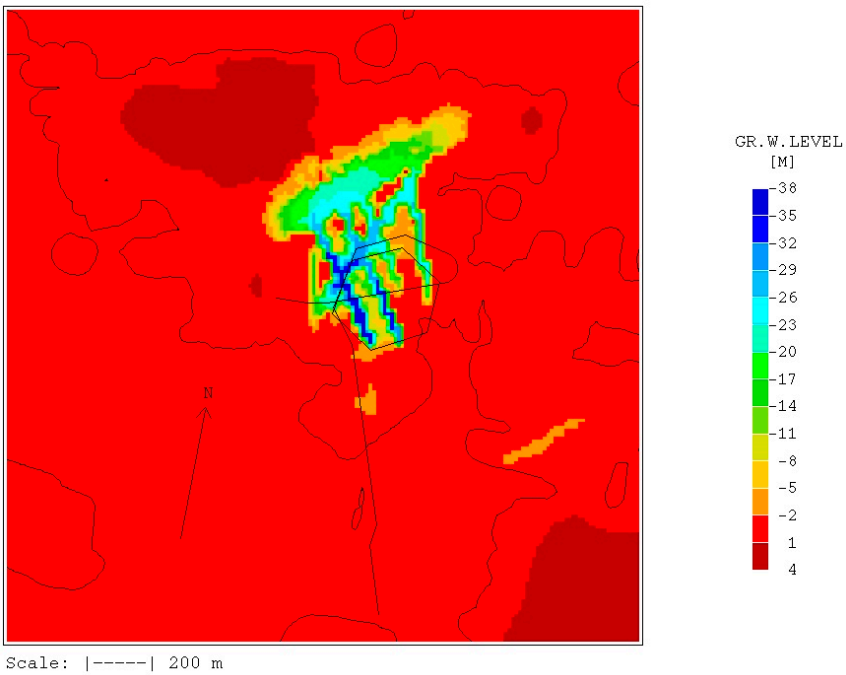

Figure 6-19. *Cont.*
Top: Tunnel front at about 3 000 metres.
Bottom: Tunnel front at about 3 600 metres.

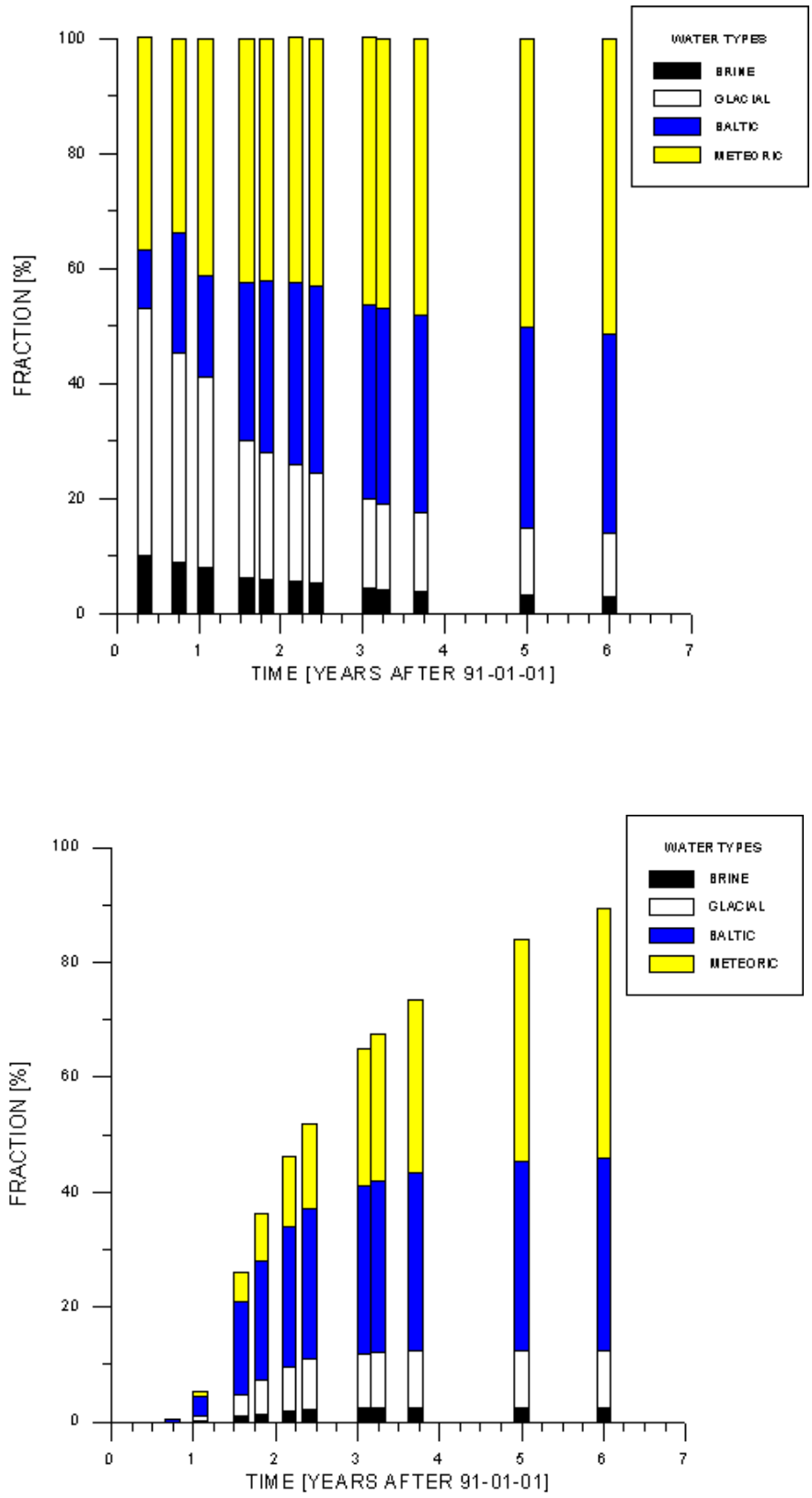

Figure 6-20. *Model99. Water composition in control point SA0813 as a function of time (top) and fraction coming from the domain boundaries. Time for tunnel passing the point: 0.58.*

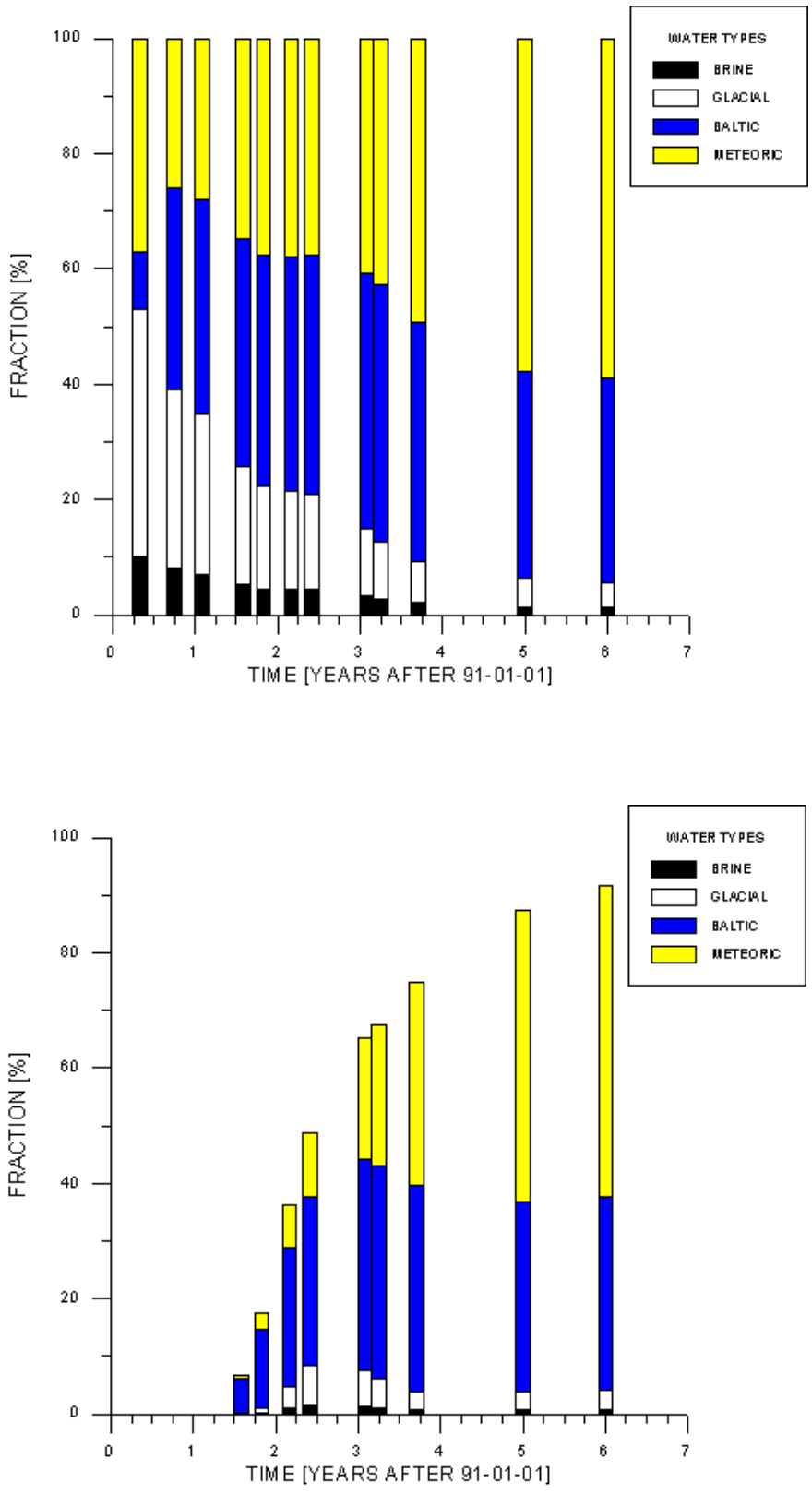

Figure 6-21. *Model99. Water composition in control point SA0850 as a function of time (top) and fraction coming from the domain boundaries. Time for tunnel passing the point: 0.63.*

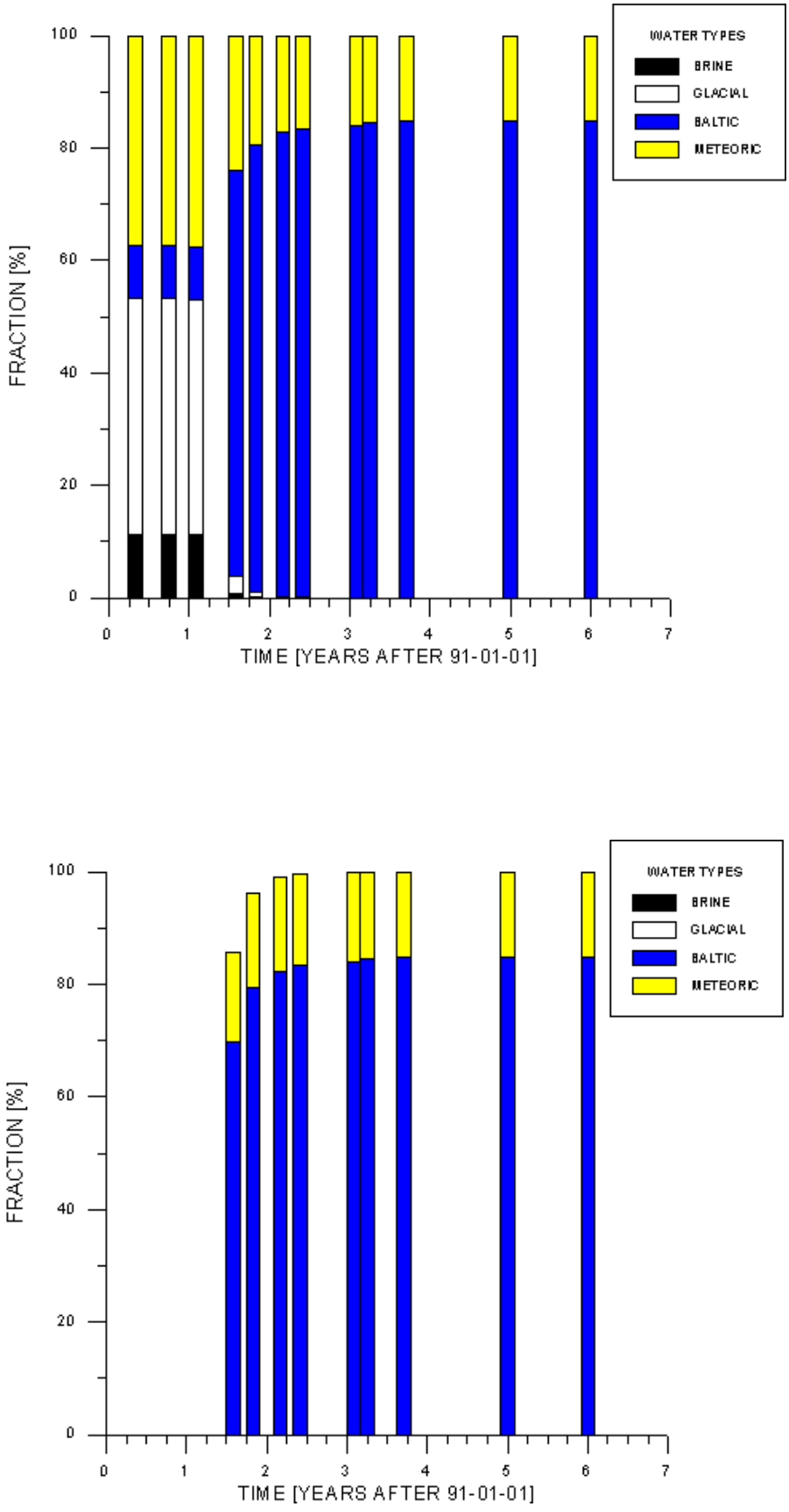

Figure 6-22. *Model99. Water composition in control point KA1061 as a function of time (top) and fraction coming from the domain boundaries. Time for tunnel passing the point: 0.92.*

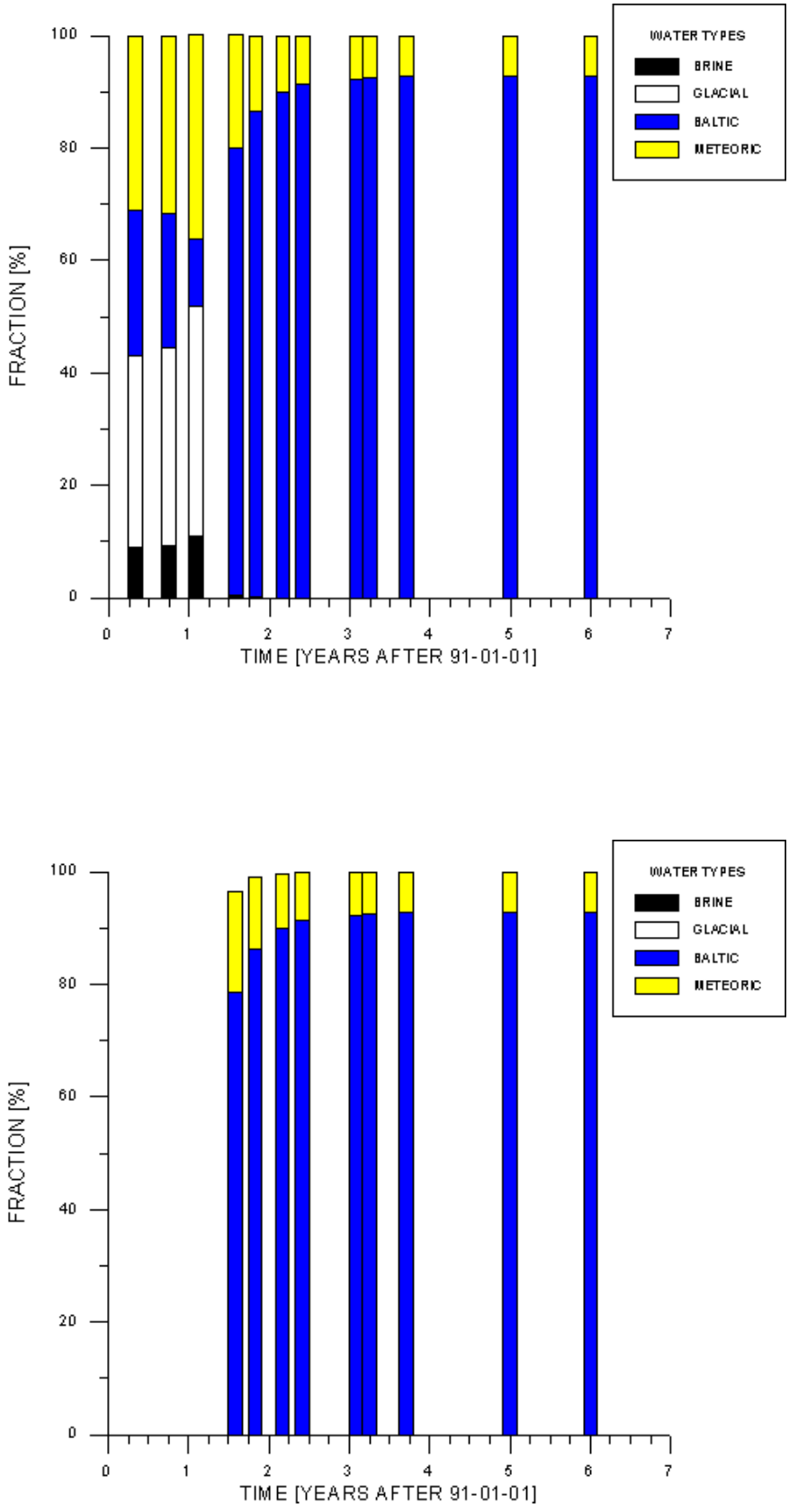

Figure 6-23. *Model99. Water composition in control point SA1229 as a function of time (top) and fraction coming from the domain boundaries. Time for tunnel passing the point: 1.12.*

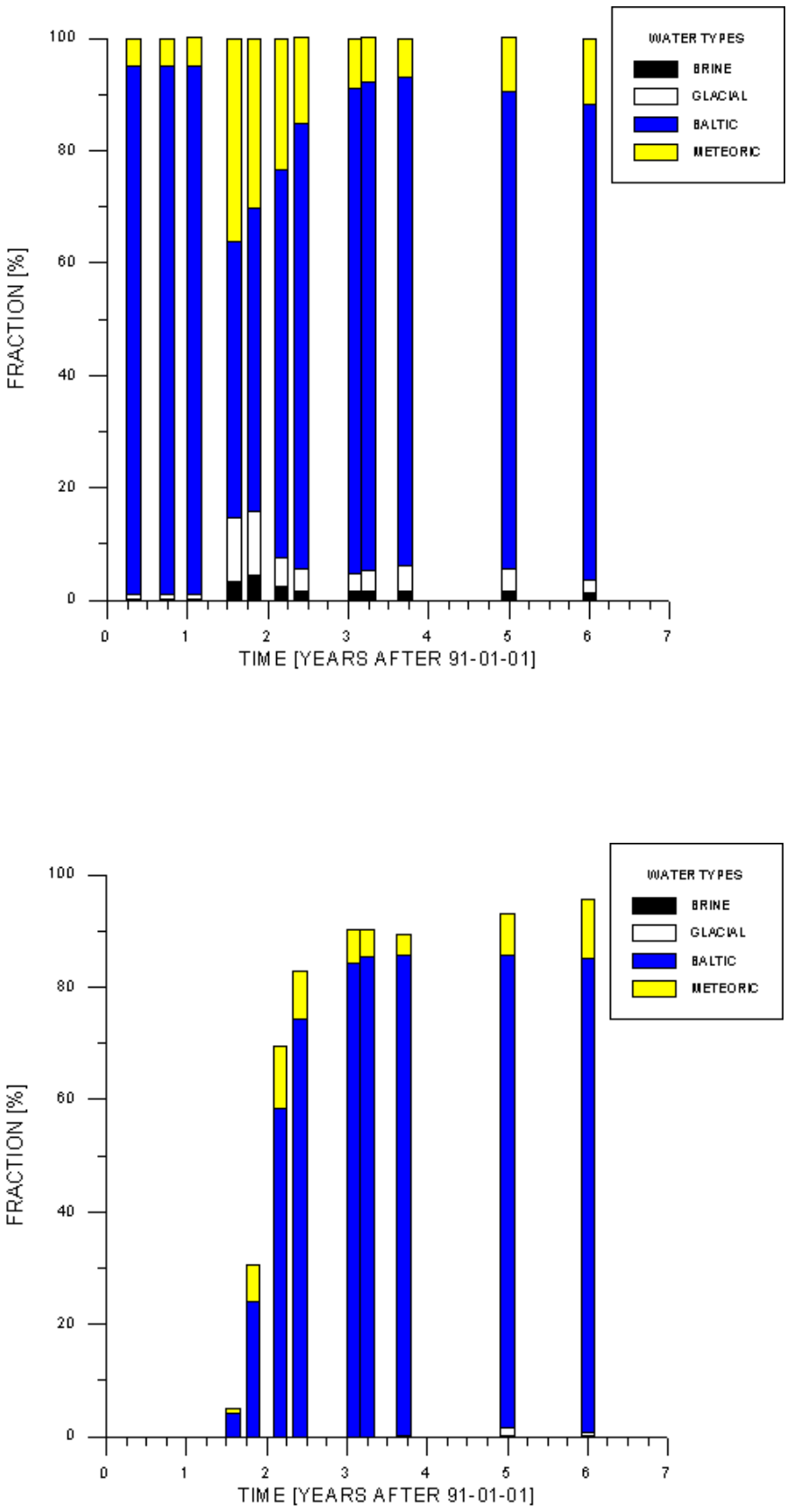

Figure 6-24. *Model99. Water composition in control point SA1327 as a function of time (top) and fraction coming from the domain boundaries. Time for tunnel passing the point: 1.41.*

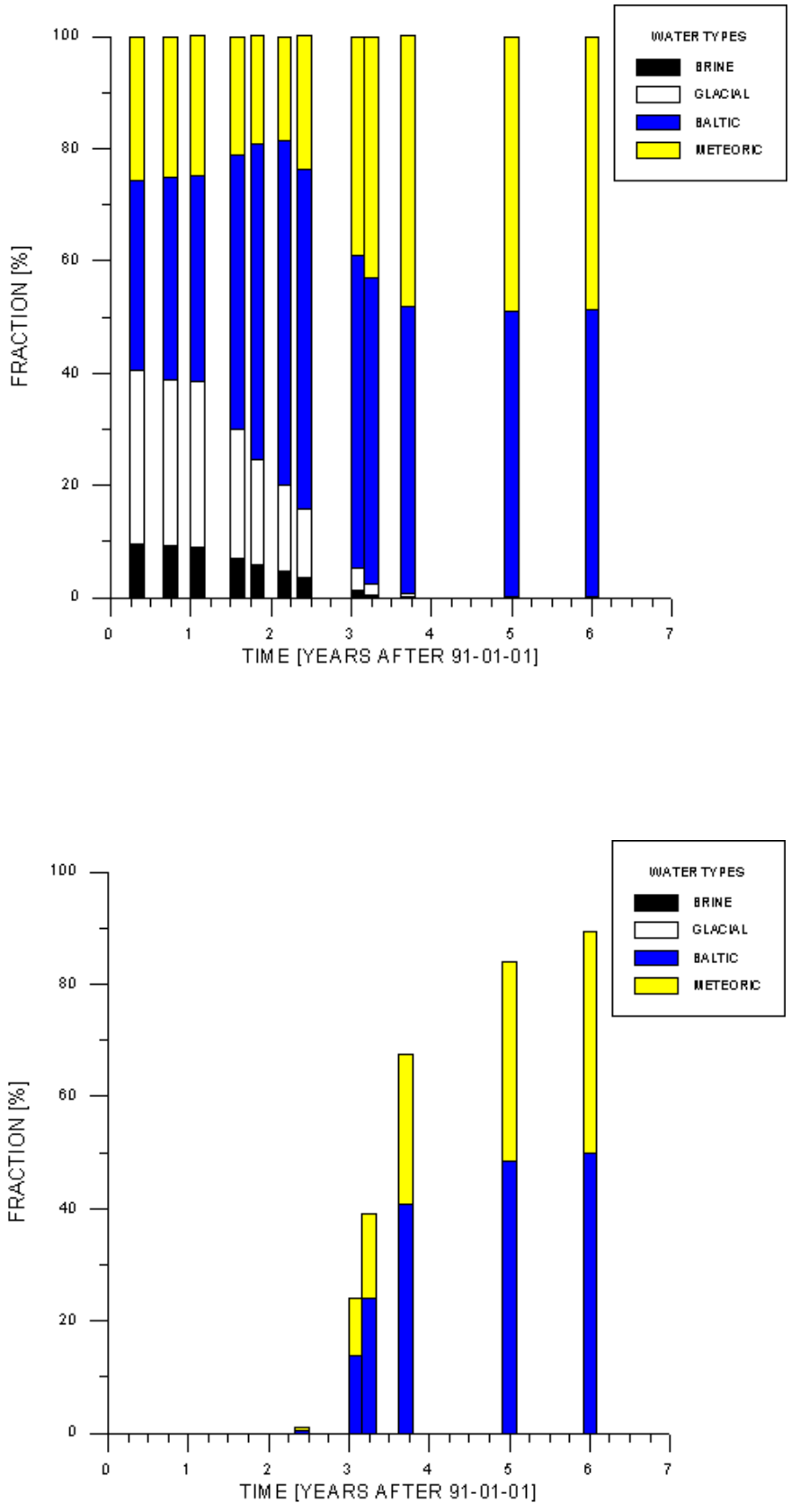

Figure 6-25. *Model99. Water composition in control point SA2074 as a function of time (top) and fraction coming from the domain boundaries. Time for tunnel passing the point: 2.09.*

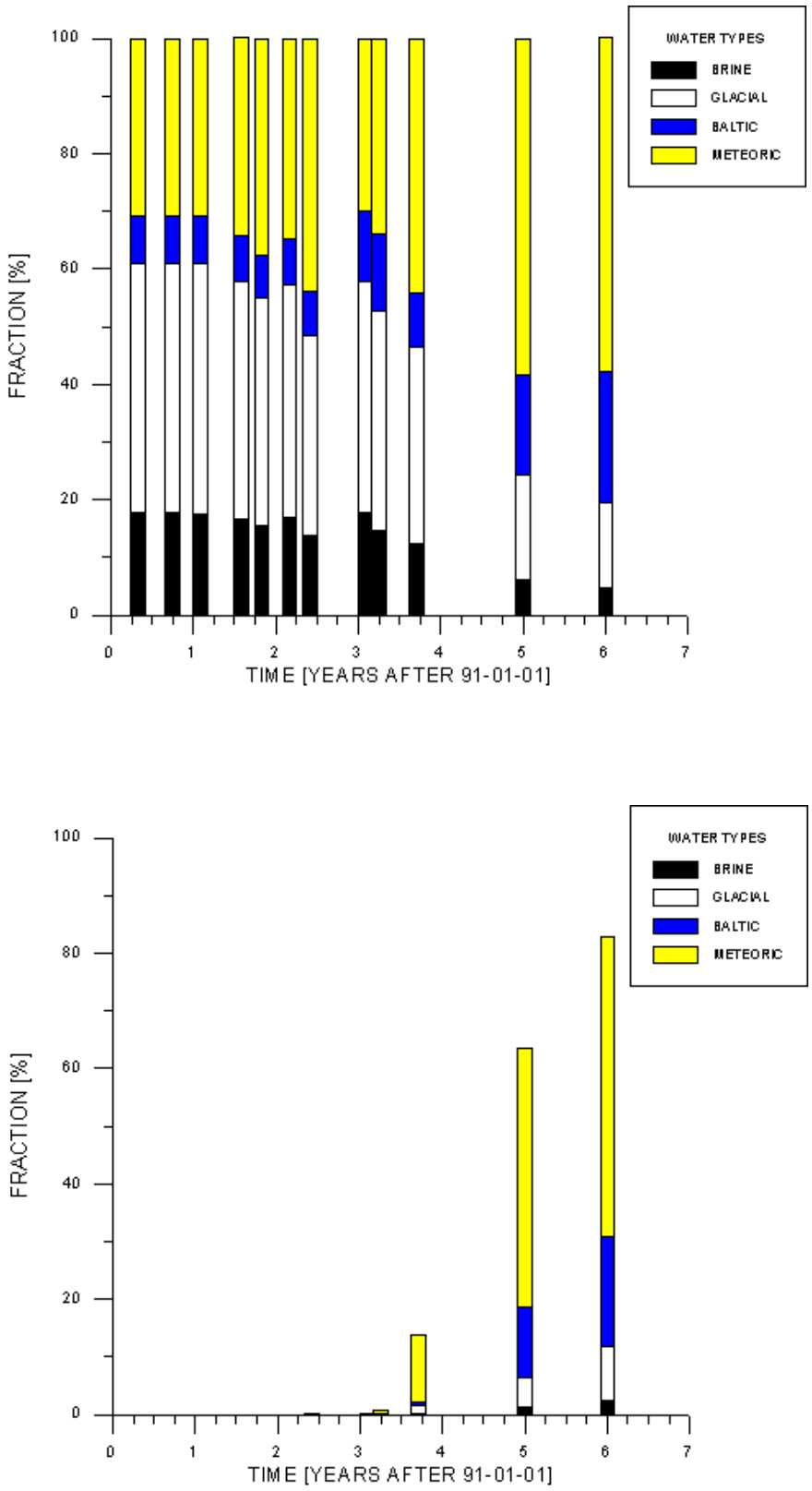

Figure 6-26. *Model99. Water composition in control point SA2783 as a function of time (top) and fraction coming from the domain boundaries. Time for tunnel passing the point: 3.03.*

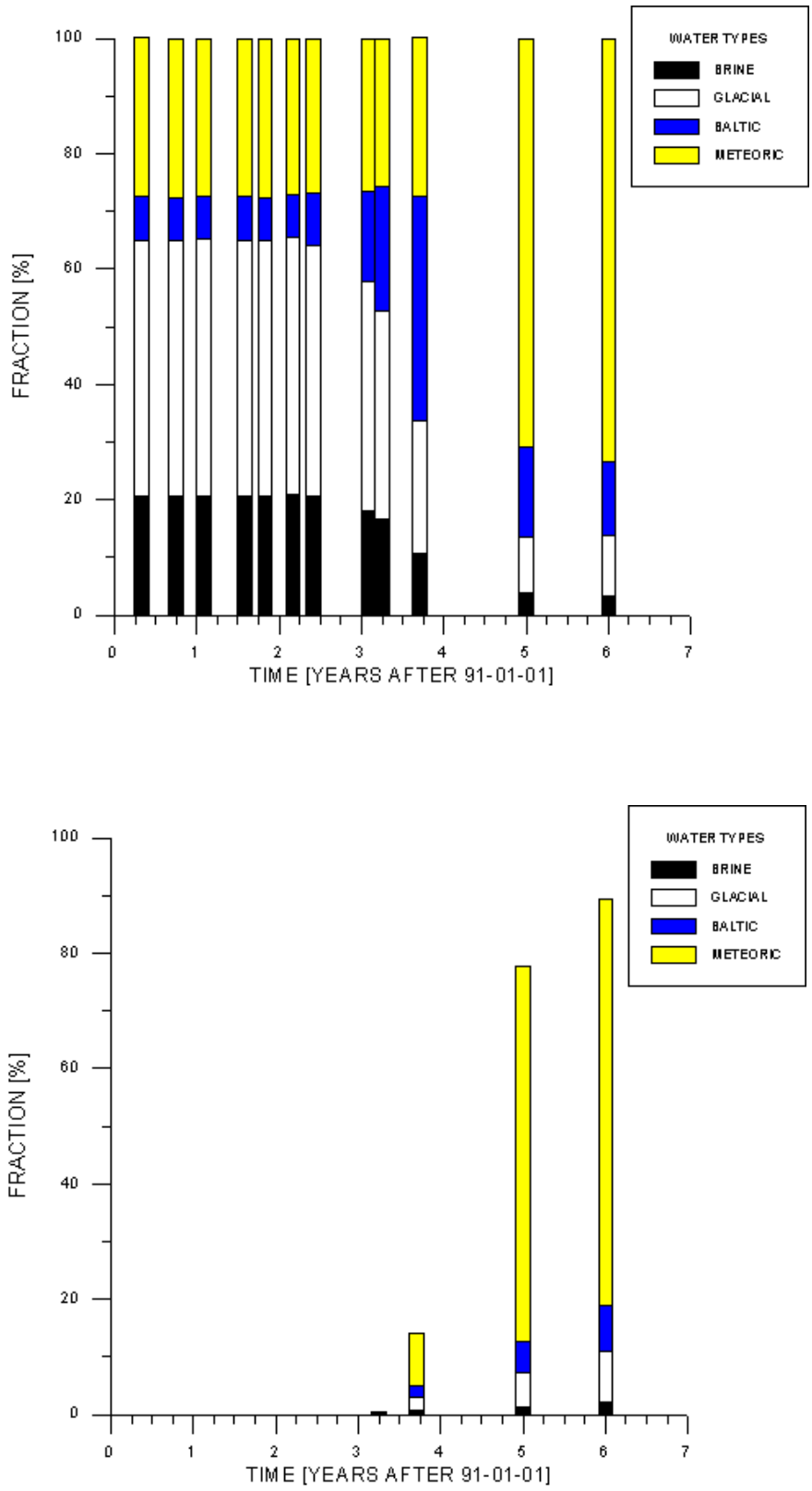

Figure 6-27. *Model99. Water composition in control point KA3005 as a function of time (top) and fraction coming from the domain boundaries. Time for tunnel passing the point: 3.13.*

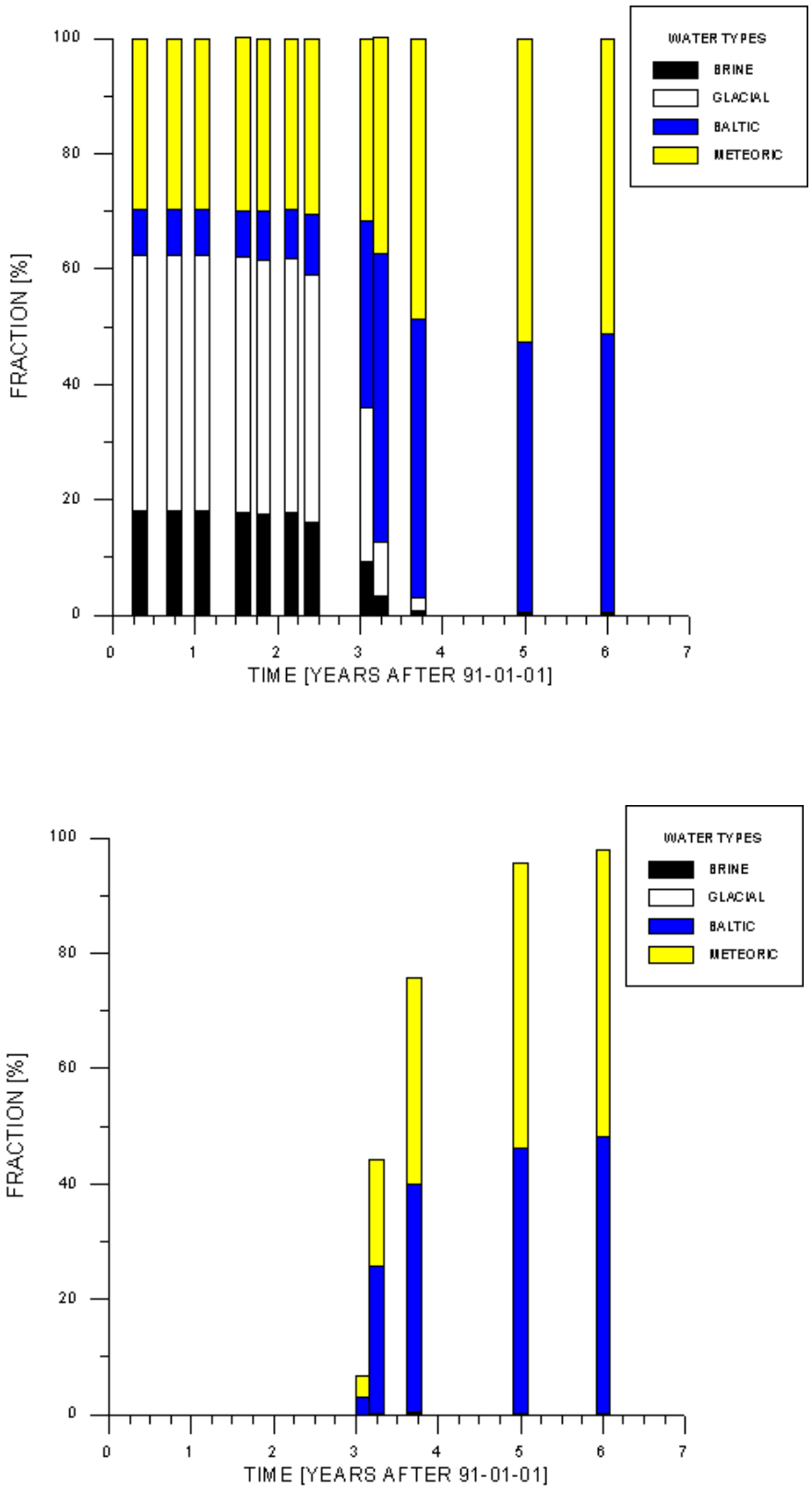

Figure 6-28. *Model99. Water composition in control point KA3110 as a function of time (top) and fraction coming from the domain boundaries. Time for tunnel passing the point: 3.20.*

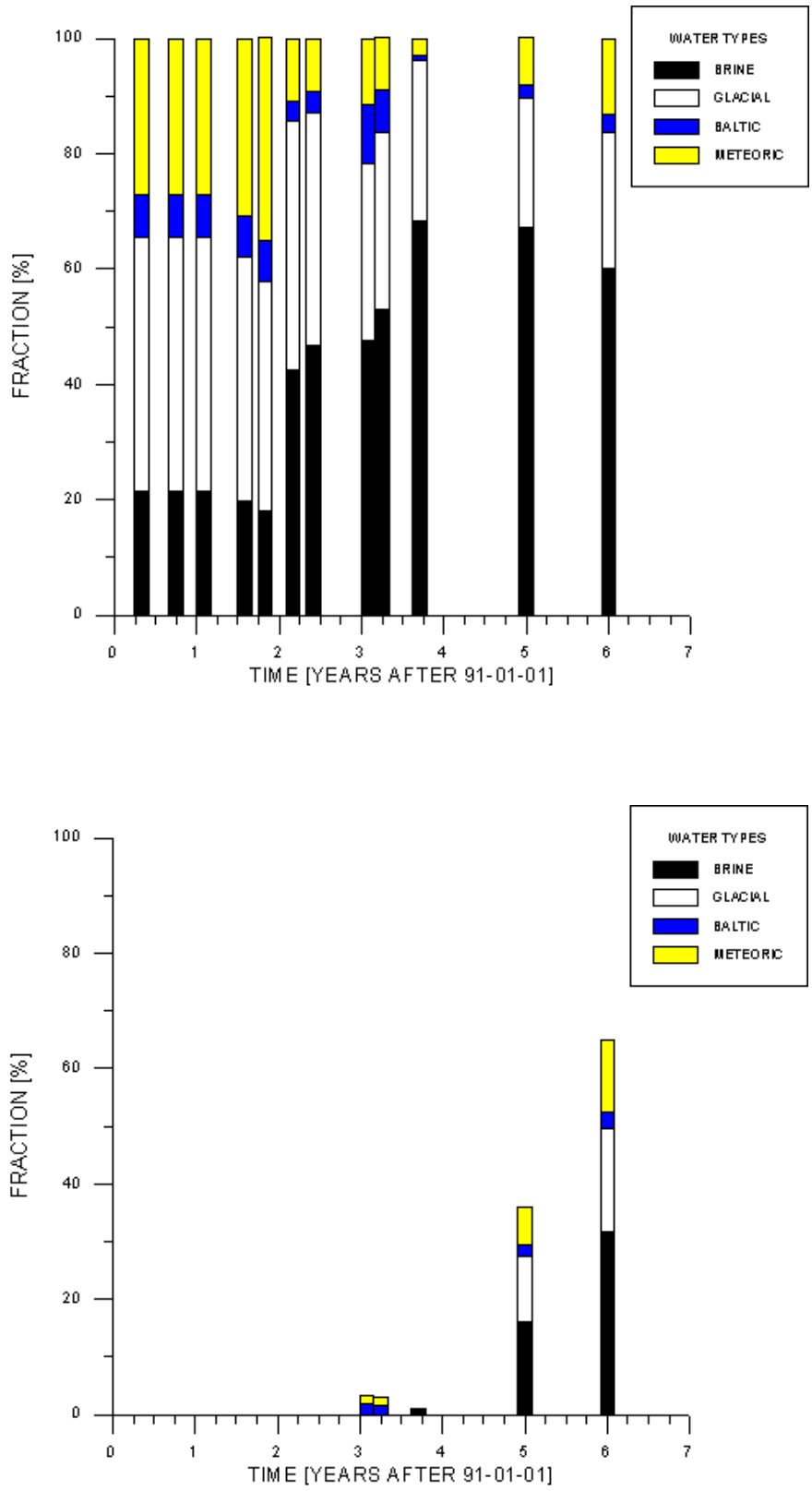

Figure 6-29. *Model99. Water composition in control point KA3385 as a function of time (top) and fraction coming from the domain boundaries. Time for tunnel passing the point: 3.60.*

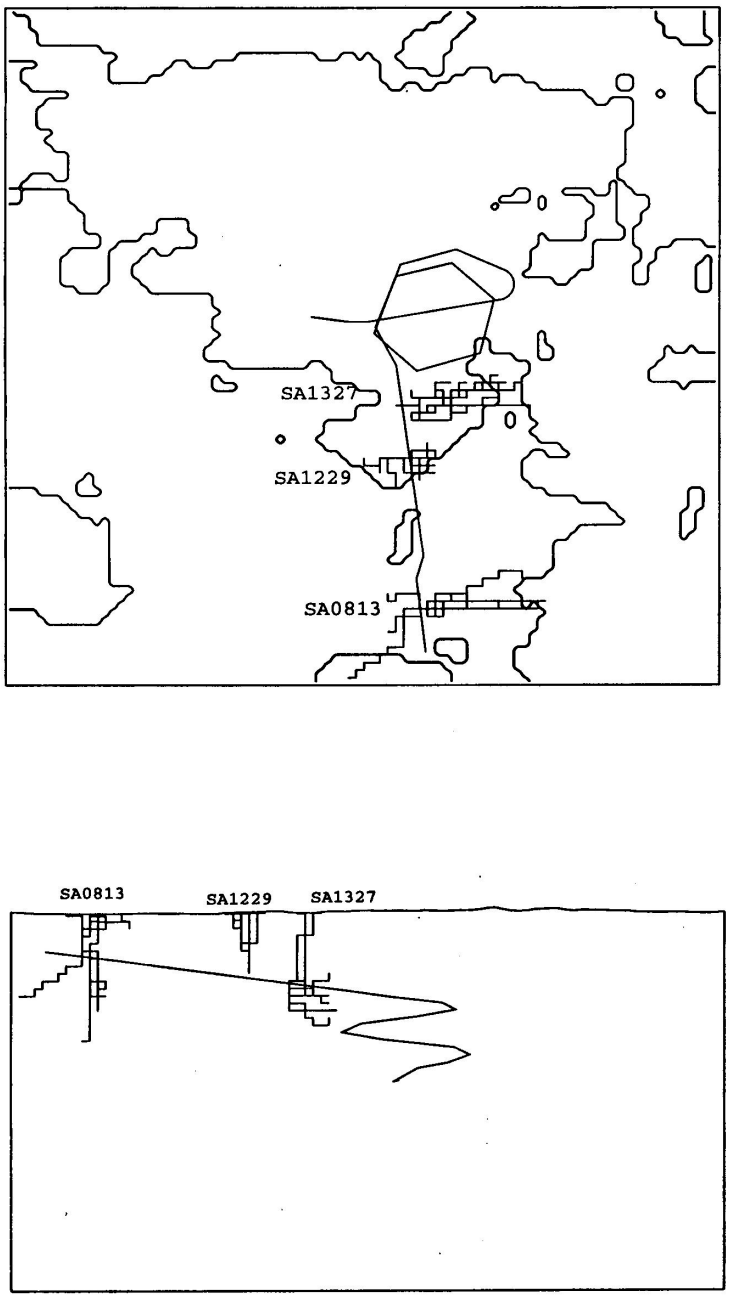

Figure 6-30. *Model99. Flow paths for water in control points SA0813, SA1229 and SA1327. Horizontal view (top) and view from east. Tunnel front at: 1 400 metres.*

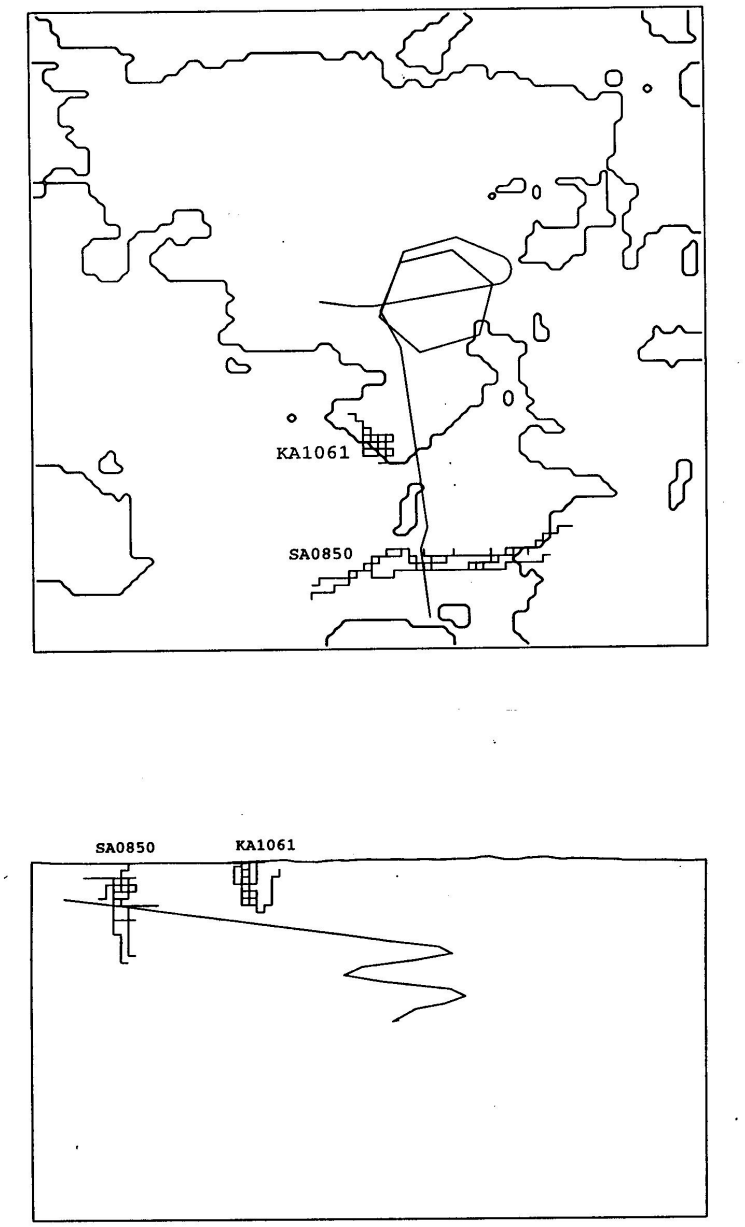

Figure 6-31. *Model99. Flow paths for water in control points SA0850 and KA1061. Horizontal view (top) and view from east.*
Tunnel front at: 1 400 metres.

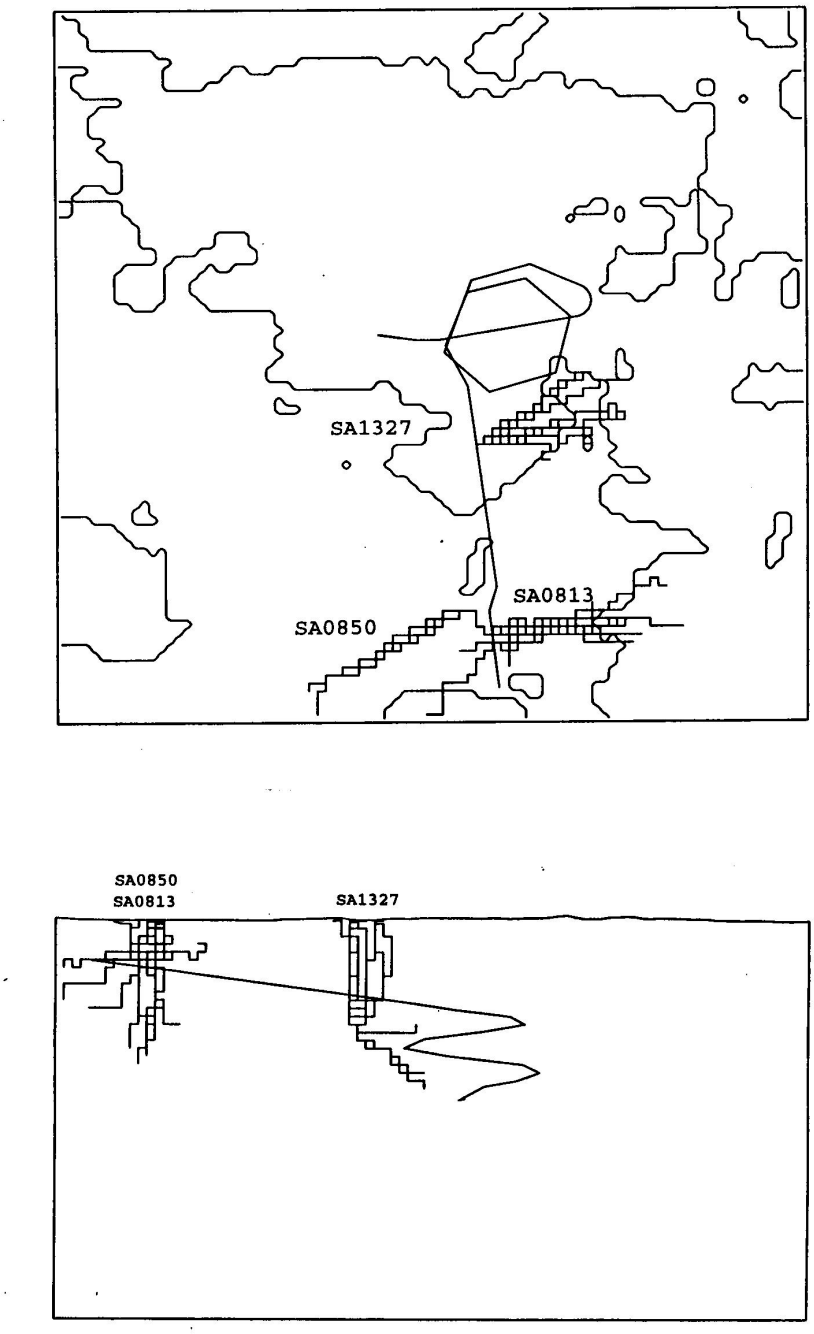

Figure 6-32. *Model99. Flow paths for water in control points SA0813, SA0850 and SA1327. Horizontal view (top) and view from east. Tunnel front at: 2 100 metres.*

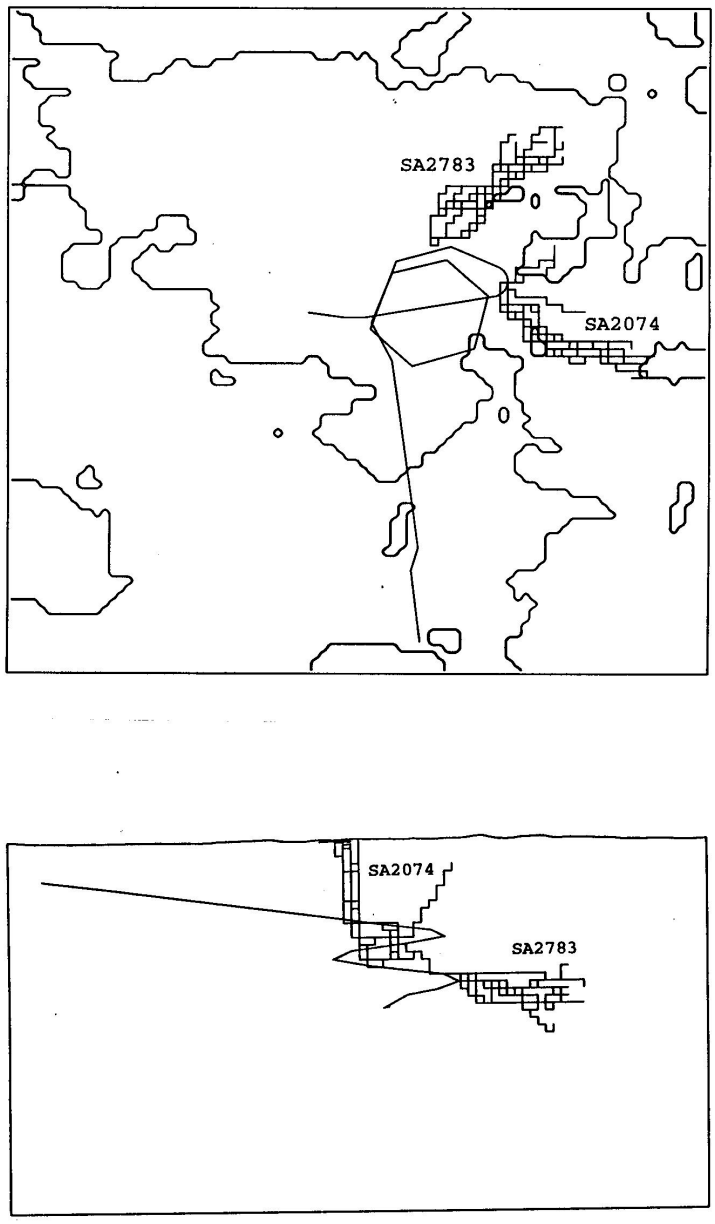

Figure 6-33. *Model99. Flow paths for water in control points SA2074 and SA2783. Horizontal view (top) and view from east.*
Tunnel front at: 3 000 metres.

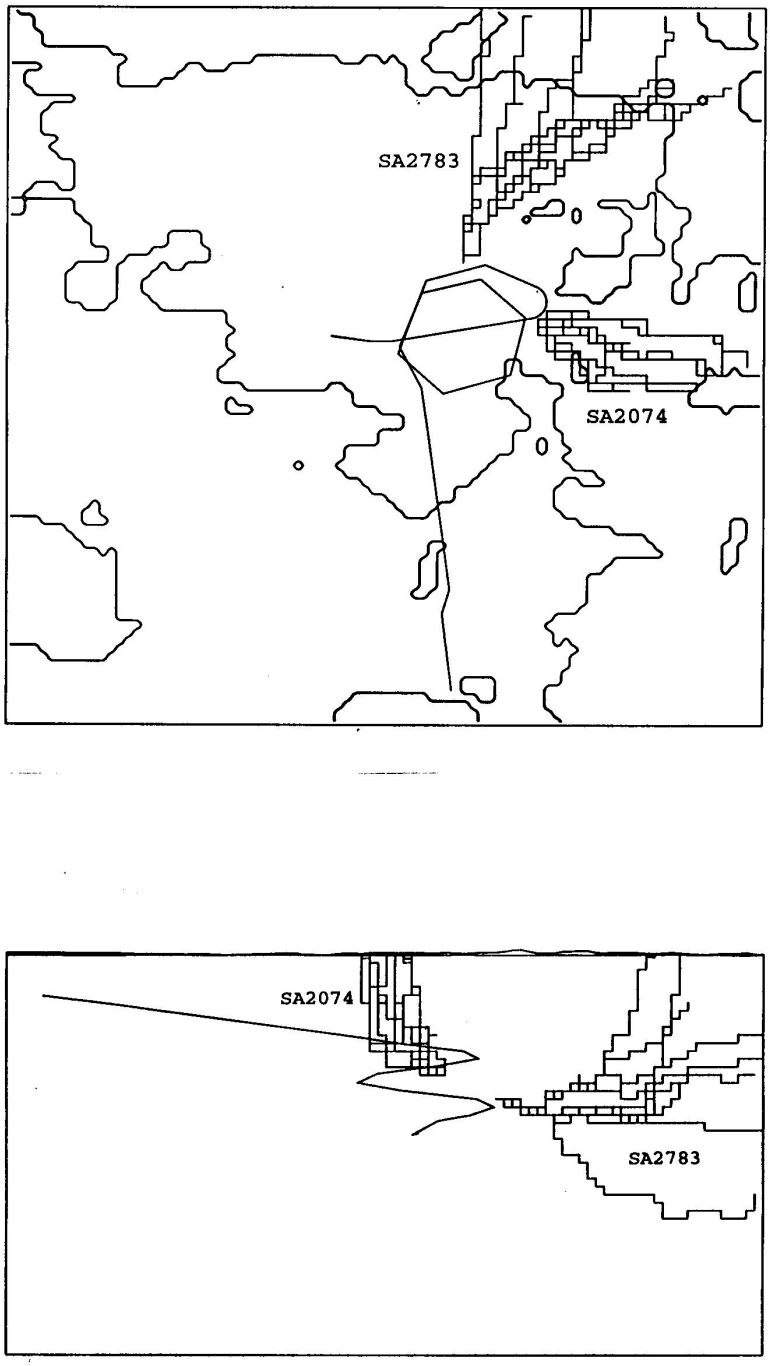

Figure 6-34. *Model99. Flow paths for water in control points SA2074 and SA2783. Horizontal view (top) and view from east.*
Tunnel front at: 3 600 metres.

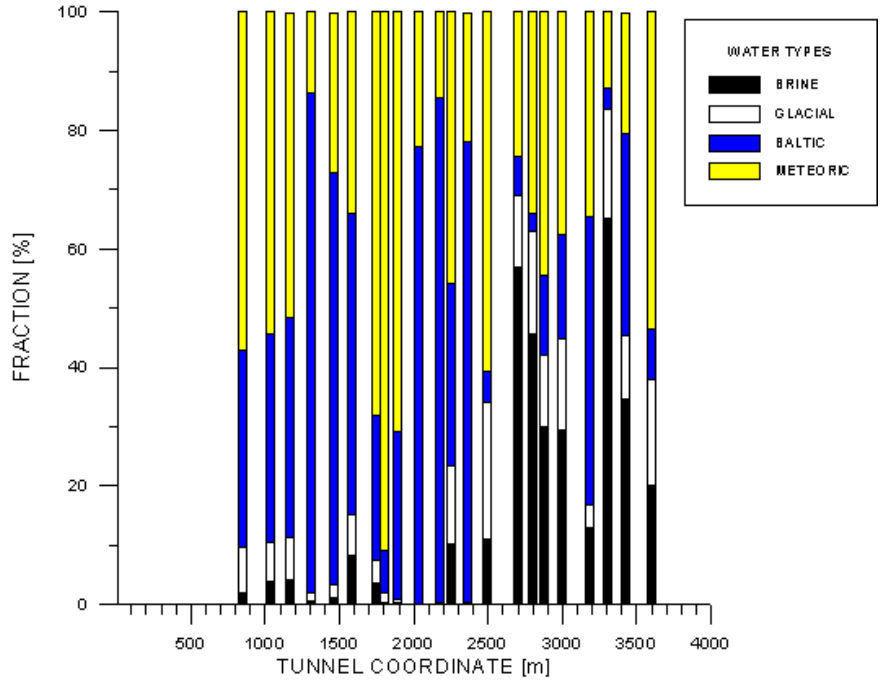

***Figure 6-35**. Model99. Water composition of inflows to tunnel 1997-01-01*

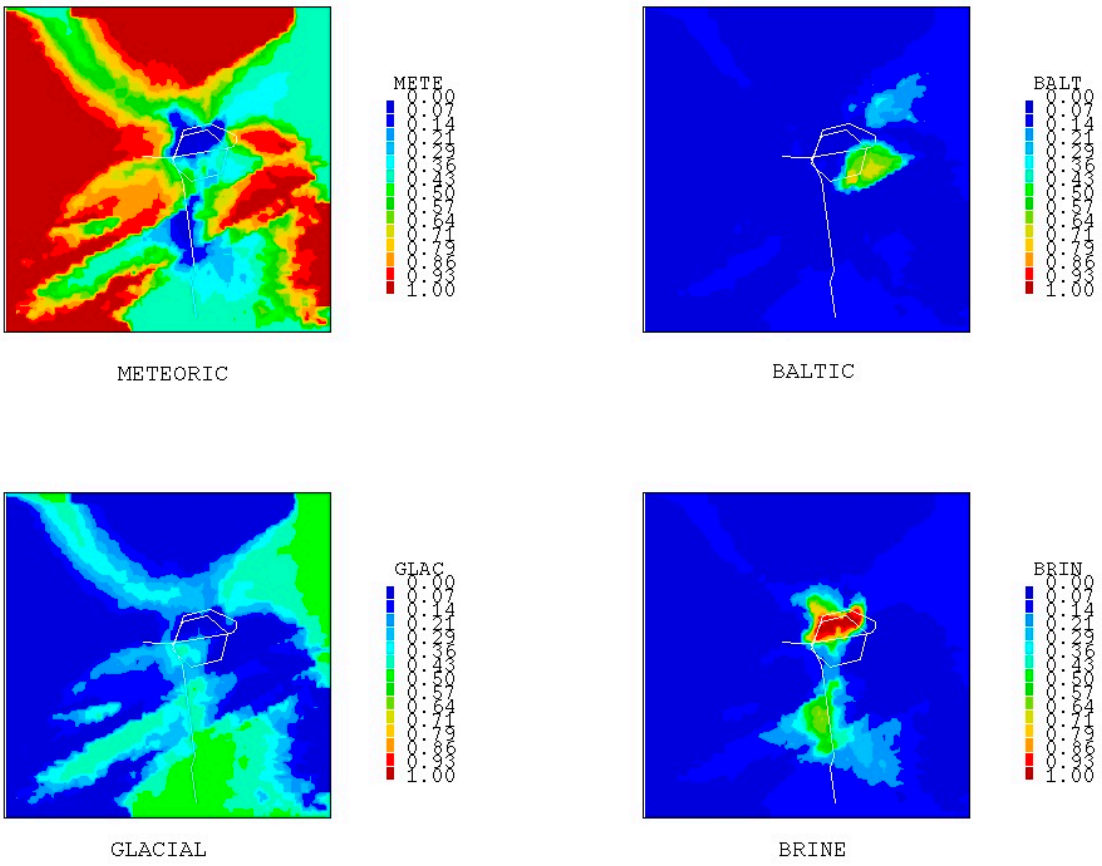

Figure 6-36. *Model99. Water composition 1997-01-01 at a depth of 450 metr*

7 SENSITIVITY STUDIES

7.1 SELECTION OF TOPICS

In complex simulations, like the present ones, it is possible to test the sensitivity of the results to a number of parameters (boundary conditions, material properties, numerical resolution, etc). One striking feature of the present simulations, see for example Figure 6-18, is the high variability in the predicted water composition. This makes every comparison with field data uncertain and one may question if point to point comparisons is the correct approach. In order to shed some light on this question, the following sensitivity studies will be carried out:

- Use different realisations of the background fracture network (given in Table 5-1) and study how this affects the calculated water comparison. Presumably the variability is related to the connectivity of the fracture network. Note that the different realisations of the conductivity field will also generate new porosity fields.

- Study the sensitivity to the discretization by comparing the measured composition also to the neighbouring cells. In the comparisons discussed in this report the coordinates of the measuring point has been used to locate the corresponding cell in the computational grid. Depending on the local fractures, it may however be more relevant to compare with a neighbouring cell. This test will show how sensitive the comparison is to the exact location selected for the comparison.

Both tests will be carried out for tunnelfront position 3170 metres and Table 5-3 can thus serve as a reference case.

7.2 RESULTS

Simulated water compositions for tunnel front position 3170 metres, using three different realisations of the background fracture network, are in Table 7-1 compared to field measurements. As can be seen (SA1420, SA1641, SA2074, etc) the water composition is very sensitive to the various realisations. In Table 7-2 the sensitivity to the point chosen for the comparison is given. The four values in each column represent the measured value (top), the simulated values in the neighbouring cell to the east, the correct cell and the neighbouring cell to the north, respectively. The distance to a neighbouring cell centre is 20 metres. Also for this case, see for example SA1420 and SA1696, a significant sensitivity can be demonstrated.

7.3 CONCLUDING REMARKS

The tentative conclusion from this very limited sensitivity study is:

- If the control, or studied, point is located in a major fracture zone, the composition is stable with respect to different realisations or small (i.e. grid neighbour) displacements.
- If the point is located outside these zones a strong sensitivity to different realisations and a small displacements is found. The explanation to this is that the point will be connected to the major zones in different ways and may also be subjected to different flow rates in different realisations.

Table 7-1. Sensitivity to realisation of background fracture network. In each group of four values the top one gives the measured fraction, while the three below represent realisation 1, 2 and 3, respectively, of the conductivity field. Tunnelfront: 3170 m.

Borehole depth [m]	Measured (top) and simulated water composition			
	Meteoric	Baltic	Glacial	Äspö Brine
KAS09	35.0	57.0	4.0	4.0
100 m	12.9	87.1	0.0	0.0
	17.9	82.0	0.1	0.0
	15.2	84.7	0.0	0.0
KAS14	32.0	64.0	2.0	2.0
100 m	19.2	79.6	0.9	0.3
	21.7	77.3	0.8	0.3
	20.2	78.0	1.3	0.4
SA0813	48.0	41.0	5.5	5.5
100 m	32.7	64.0	2.5	0.8
	30.6	66.0	2.5	0.8
	35.9	58.3	4.3	1.5
SA1229	40.0	51.0	4.5	4.5
160 m	18.1	81.6	0.2	0.1
	18.9	80.2	0.7	0.2
	17.0	82.6	0.3	0.1
SA1420	54.0	28.0	9.0	9.0
200 m	34.1	29.6	25.1	11.1
	21.2	40.1	25.6	13.2
	28.0	52.5	13.6	6.0
KAS07	60.0	32.0	4.0	4.0
200 m	16.7	82.3	0.6	0.3
	18.2	81.2	0.4	0.2
	17.5	69.2	8.6	4.6
SA1641	48.0	16.0	20.0	16.0
220 m	46.5	18.4	24.9	10.2
	32.1	14.6	37.3	16.0
	27.9	58.6	9.3	4.2
SA1696	35.0	18.0	29.0	18.0
220m	45.9	21.5	22.3	10.2
	45.5	21.8	22.6	10.0
	45.3	17.7	25.0	12.0
SA1828	46.0	28.0	13.0	13.0
240 m	71.0	15.6	9.7	3.6
	70.1	14.4	10.7	4.9
	82.0	12.1	4.4	1.6
SA2074	47.0	29.0	12.0	12.0
280 m	56.3	18.1	18.0	7.5
	25.4	17.0	41.6	16.0
	34.3	52.3	9.8	3.6
SA2175	39.0	39.0	11.0	11.0
280 m	26.6	70.8	1.9	0.7
	23.3	75.8	0.6	0.2
	21.3	78.3	0.3	0.1
SA2273	41.0	41.0	9.0	9.0
300 m	22.7	68.4	6.2	2.8
	26.2	61.9	8.2	3.8
	21.9	73.3	3.3	1.5
SA2600	32.0	19.0	29.0	20.0
340 m	13.5	12.3	44.8	29.4
	13.1	12.3	45.0	29.7
	22.4	13.3	43.3	21.1
SA2783	20.0	20.0	39.0	21.0
360 m	17.6	13.1	44.7	24.6
	17.7	12.9	44.4	25.1
	21.9	13.4	42.5	22.1
SA2834	19.0	19.0	37.0	25.0
360 m	20.7	13.7	44.6	21.0
	20.5	13.2	44.0	22.4
	22.4	13.3	42.0	22.4
KAS08	37.0	29.0	17.0	17.0
440 m	18.9	13.8	43.5	23.8
	25.6	20.4	36.8	17.2
	21.5	14.7	42.1	21.6
KAS07	27.0	18.0	37.0	18.0
460 m	16.5	13.0	45.0	25.5
	15.8	12.9	45.0	26.3
	17.8	13.3	45.0	23.9
KAS05	16.0	16.0	45.0	23.0
480 m	13.3	12.3	45.0	29.4
	13.0	12.2	45.0	29.7
	14.8	12.6	45.0	27.5
KAS03	25.0	23.0	49.0	13.0
560 m	24.4	14.8	44.9	16.0
	23.5	14.6	44.9	16.9
	23.1	14.5	44.9	17.4
Average	36.9	30.9	19.8	12.9
	27.8	38.4	22.4	11.4
	25.3	38.5	24.0	12.3
	26.9	42.8	20.3	10.1

Table 7-2. Sensitivity to selected point for comparison. In each group of four values the top one gives the measured fraction, while the three below give the values in the neighbouring cell to the east, the correct cell and the neighbouring cell to the north, respectively.
Tunnel front: 3170 m.

Borehole depth [m]	Measured (top) and simulated water composition			
	Meteoric	Baltic	Glacial	Äspö Brine
KAS09	35.0	57.0	4.0	4.0
100 m	15.6	84.4	0.0	0.0
	17.9	82.0	0.1	0.0
	17.6	82.4	0.1	0.0
KAS14	32.0	64.0	2.0	2.0
100 m	22.2	76.5	0.9	0.3
	21.7	77.3	0.8	0.3
	21.8	77.9	0.2	0.1
SA0813	48.0	41.0	5.5	5.5
100 m	38.7	60.1	0.9	0.3
	30.6	66.0	2.5	0.8
	35.5	60.8	2.7	0.9
SA1229	40.0	51.0	4.5	4.5
160 m	20.8	79.1	0.0	0.0
	18.9	80.2	0.7	0.2
	19.2	79.4	1.0	0.4
SA1420	54.0	28.0	9.0	9.0
200 m	19.0	66.2	9.6	5.2
	21.2	40.1	25.6	13.2
	23.1	25.1	34.6	17.1
KAS07	60.0	32.0	4.0	4.0
200 m	18.2	81.2	0.5	0.2
	18.2	81.2	0.4	0.2
	19.2	60.8	13.3	6.7
SA1641	48.0	16.0	20.0	16.0
220 m	28.3	13.7	39.7	18.2
	32.1	14.6	37.3	16.0
	27.3	13.9	40.8	18.1
SA1696	35.0	18.0	29.0	18.0
220m	20.8	65.8	8.6	4.7
	45.5	21.8	22.6	10.0
	58.2	15.7	18.7	7.3
SA1828	46.0	28.0	13.0	13.0
240 m	57.7	24.2	12.5	5.6
	70.1	14.4	10.7	4.9
	84.5	7.8	5.8	2.0
SA2074	47.0	29.0	12.0	12.0
280 m	23.5	14.7	44.8	17.1
	25.4	17.0	41.6	16.0
	25.4	15.2	42.7	16.7
SA2175	39.0	39.0	11.0	11.0
280 m	23.8	75.1	0.8	03
	23.3	75.8	0.6	0.2
	21.1	78.5	0.3	0.1
SA2273	41.0	41.0	9.0	9.0
300 m	25.5	73.2	1.0	0.4
	26.2	61.9	8.2	3.8
	23.9	55.1	14.1	6.9
SA2600	32.0	19.0	29.0	20.0
340 m	13.1	12.3	44.9	29.8
	13.1	12.3	45.0	29.7
	13.2	12.3	44.9	29.6
SA2783	20.0	20.0	39.0	21.0
360 m	24.6	13.4	42.9	19.2
	17.7	12.9	44.4	25.1
	24.7	13.4	42.9	19.0
SA2834	19.0	19.0	37.0	25.0
360 m	21.0	13.2	43.7	21.1
	20.5	13.2	44.0	22.4
	22.4	13.3	43.4	20.9
KAS08	37.0	29.0	17.0	17.0
440 m	30.3	19.9	34.9	15.0
	25.6	20.4	36.8	17.2
	25.6	20.4	36.8	17.2
KAS07	27.0	18.0	37.0	18.0
460 m	15.5	12.8	45.0	26.8
	15.8	12.9	45.0	26.3
	15.3	12.8	45.0	27.0
KAS05	16.0	16.0	45.0	23.0
480 m	12.9	12.2	45.0	29.9
	13.0	12.2	45.0	29.7
	12.9	12.2	45.0	29.9
KAS03	25.0	23.0	49.0	13.0
560 m	23.3	14.6	45.0	17.2
	23.5	14.6	44.9	16.9
	20.6	14.0	45.0	20.4
Average	36.9	30.9	19.8	12.9
	23.9	42.8	22.1	11.2
	25.3	38.5	24.0	12.3
	26.9	35.3	25.1	12.6

8 DISCUSSION

8.1 GENERAL

The objective of Task #5 is to integrate hydrochemical and hydrogeological data and to develop modelling techniques for this integration. From a technical point of view this has been achieved in this report. A more difficult question to answer is whether a useful model for site analysis has been developed. Before we try to give an answer to this question, a number of arguments and observations that should be considered when the simulations are evaluated will be listed:

- Two basic conceptual problems were identified in Chapter 2; why do we find large fractions of Glacial water below Äspö?, and what water composition should we assume for water that originates from outside the computational domain? If we accept field measurements, i.e. water have been stored for 12 000 years at a depth of a few hundred metres, we have a modelling problem. The porosity field needs to have large volumes with only weak contact with the major flow paths. In Svensson (2001a), (see also Appendix A), it is demonstrated that the technique used in the present model has the potential to store water for very long times. However, the present "state of affairs" is that the presence of Glacial water close to ground suggests that topics like connectivity and storage volumes need further attention in continuum models.

- Three water types Mixed Water High (MWH), Mixed Water Low (MWL) and Mixed Water Bottom (MWB) were introduced to solve the problem with water from outside the domain. The compositions of these were assumed, based on borehole data from Laxemar. It should however be noted that these compositions were used for all vertical boundaries. One may argue that the vertical boundary facing the Baltic should bring in water with a composition that is different from that facing Laxemar.

- The present model gives a strong spatial variability in the water composition, see for example Figure 6.18. As demonstrated in the sensitivity studies, this makes all point by point comparisons with field data uncertain. Task #5 is to a large extent centred on comparisons in a number of control points. If we accept the high variability given by the present model, it may not be a good idea to use point by point comparisons.

- Task #5 considers a transient problem. The transport of a certain property is then linearly related to the kinematic porosity. In the present study some attention to the specification of the kinematic porosity has been given (based on flow aperture and considered in the calibration process). However, in the author's view we have very little "hard facts" from field data to base a realistic kinematic porosity field on.

These are some of the major uncertainties that need to be considered in the evaluation of this modelling task and they may also serve as suggestions for further studies.

The results presented do however give a certain description of the evaluation of the groundwater composition during the construction of the Äspö HRL. The main features of this description will now be given.

- The atmospheric pressure in the tunnel generates high pressure gradients close to the tunnel with an inflow of water as a result. The low pressure around the tunnel is reflected at ground level, see Figure 6-1. However, on a regional scale the Äspö HRL is perhaps best considered as a "point sink" that draws water from all directions.

- Starting with water from above, one can show that the Meteoric water from Äspö is not enough to explain the fraction of Meteoric water in the inflows to the tunnel. Probably, Meteoric water from the Laxemar area is providing a substantial part, see Figure 6-18.

- The horizontal flow towards the tunnel can be expected to follow the selective withdrawal principle, meaning that water from a certain density interval is mainly contributing to the inflow. This suggestion was given in Svensson (1997a), where also an illustration can be found. The withdrawn water is replaced with water from above. This leads us to expect that the Glacial water in the domain should steadily be replaced by Meteoric and Baltic waters. The decrease in Glacial water can be found in both measurements and simulations, see Tables 5-3 and 5-5.

- Water with higher salinity, than is found at the level of Äspö HRL under natural conditions, is found in the central part of the tunnel spiral. This is an indication of a transport of water from below the tunnel level, the so called upconing process. Field data of the salinity variation with time at tunnel position 2 800 metres can be found in Figure 5-2, where also simulation results are presented. It is interesting to note that the simulated maximum salinity continues to rice also after the tunnel was completed, which is at time 3.7 years in Figure 5-2. The salinity field is hence not in a steady state at time 97-01-01, which is the date the simulation was carried out to. The upconing can also be seen in Figure 6-18, where it is found that water with a high fraction of Äspö Brine is found in the spiral part of the tunnel.

8.2 MODEL99 VERSUS THE FINAL MODEL

From the results of the two models, it is not possible to say that the final model is more accurate than the Model99. However, from the discussion above, and the sensitivity study, it is not obvious how the "accuracy of a model" should be determined.

When Model99 was evaluated, it was hence concluded that all results were in "fair agreement with field measurements" and did not call for any major revisions of the model. The basic concepts and assumptions of the model were also discussed and a major conceptual problem was found:

- A traditional stochastic continuum model can not be expected to have the ability to store a certain water type (like Glacial water) for very long time periods, i.e. thousands of years. The reason for this is, loosely speaking, that all points in the domain are too well connected.

The main objective for the second step of the hydrological model development was therefore to improve the conductivity, porosity and connectivity structures in the model, see Chapters 3 and 4. As this will change the hydrological model in a fundamental way, it was further decided that the calibration of the model should be more extensive in the second step. In other projects, see Svensson (2001a), it has been demonstrated that the new concepts do result in a model that can store water with certain characteristics for very long time periods.

In summary, the final model differs from the Model99 in the concepts used to generate conductivity, porosity and connectivity fields and in the way the model was calibrated.

9 CONCLUSIONS

An attempt has been made to integrate hydrochemical and geohydrological data and modelling concepts. From the results presented the following conclusions are drawn:

- The task has been carried out technically, meaning that all the requested information has been produced. This is not a minor achievement as the task is a real challenge computationally (3D, transient, transport, backtracking, etc).
- The presentation of the hydrochemistry as four water types (Meteoric, Baltic, Glacial and Äspö Brine) is a convenient way to bridge the gap between geohydrologists and hydrochemists.
- The main uncertainty about the four water types concerns the boundary conditions (Note that initial conditions were generated in the present study). It was assumed that the same boundary conditions apply to all four vertical boundaries; this can certainly be questioned.
- The hydrochemical data points to some shortcomings in the hydrological model. Field data indicates that Glacial water has been stored for 12 000 years at a depth of a few hundred metres below Äspö. The method to generate the porosity field used in the present study has the potential to store water for long time periods, (Svensson, 2001a), but more work is needed before any firm claims can be made. Also the kinematic porosity ought to be better founded on field data, than has been possible in the present study.
- All results presented do however give a plausible and consistent description of the evolution of the groundwater chemistry; trends are in fair agreement with field data.

Appendix A

A HYPOTHESIS CONCERNING THE PRESENCE OF OLD WATER TYPES.

A1 BACKGROUND

Field data indicates that Glacial water (which is melt water from the inland ice) is present close to ground level, i.e. at a depth of a few hundred metres. The last inland ice left the area about 12 000 years ago and it is not clear why this water has not been replaced by younger water types. Up to about 4 000 years before present (BP) Äspö was under the Baltic Sea and exposed to various stages, with varying salinity, of the Baltic. The period with the highest salinity, around 1.2%, is the Litorina period about 7 000 years BP.

A2 SUGGESTED EXPLANATION

A possible explanation to why old water types remain in the fracture system can be based on gravitational effects. If the two fractures in Figure A1 are initially filled with Glacial water, which has freshwater density, and then exposed to a water with a varying salinity the following will happen.

- As long as salinity is increasing, the inflowing water will replace the water in the lower half of the vertical fracture. The upper half will not be affected as the density of the incoming water is higher than the freshwater density.
- When the salinity has reached its maximum value the replacement in the lower half will stop.
- When the salinity of the incoming water is decreasing it is expected that the flow is centred at the level of the horizontal fracture, i.e. no replacement of water in the vertical fracture takes place.

The final result is thus that Glacial water will remain in the upper half of the fracture and the lower half will be occupied with the water with the highest salinity during the period considered, i.e. the Litorina water.

A3 NUMERICAL SIMULATIONS

In order to evaluate this idea some numerical simulations will be carried out. We choose to study the water exchange in the vertical fracture as a two-dimensional problem, see Figure A2. The following assumptions are made:

- The fracture is exposed to a pressure difference between inflow and outflow of 1 000 *Pa*, with no variation in time.
- The salinity of the inflowing water varies according to Figure A2. This is a simplified view of the salinity variation in the Baltic Sea during the last 10 000 years. Diffusion and dispersion of salt is neglected.
- The conductivity is put to 10^{-7} m/s and the kinematic porosity to 4×10^{-3}. These are values believed to be typical for the Äspö area.
- The dimension of the fracture, which also specifies the computational domain, is $100\times100\times1$ m^3 and the total integration time is 10 000 years. A grid spacing of 1 metre was used. The inflow and outflow sections are 2 metres high.

A4 RESULT

The final salinity distributions for two conductivities can be found in Figure A3. The area with zero salinity represents Glacial water as it entered the fracture more than 9 000 years, see Figure A2. Water with a salinity of 1.2%, which we may call Litorina water, entered the fracture 7 000 to 5 000 years ago and is now found in the lower part of the fracture.

It was found that the ability of the fracture to keep old water types depends on the conductivity; the lower the conductivity the higher fractions of old water. This is clearly seen in Figure A3. If the conductivity was put to 10^{-6} m/s, the fracture lost its ability to keep the old waters for long time periods. Some test simulations indicate that a fractures ability to keep old water types can be characterised by a time scale nL/K, where n is the kinematic porosity, L the dimension of the fracture and K the conductivity. A longer time scale means a higher ability to keep old water types and one may thus interpret the time scale as an exchange time. More work is however needed to fully explore this suggestion.

It may be added that this idea about storage of old water types has also been evaluated in a realistic fracture network, see Svensson (2001a). It was found that old water types can be stored for 10 000 years, also in this system.

A5 CONCLUSION

The simple generic simulations suggest that gravitational effects may arrest old water types in a fracture for very long time periods. A vertical fracture was investigated but the only difference to a fracture with a certain dip is that the gravitational force will be reduced by $\sin\alpha$, where α is the deviation from 90°. Many fractures in the rock volume below Äspö should thus have the ability to arrest old water types.

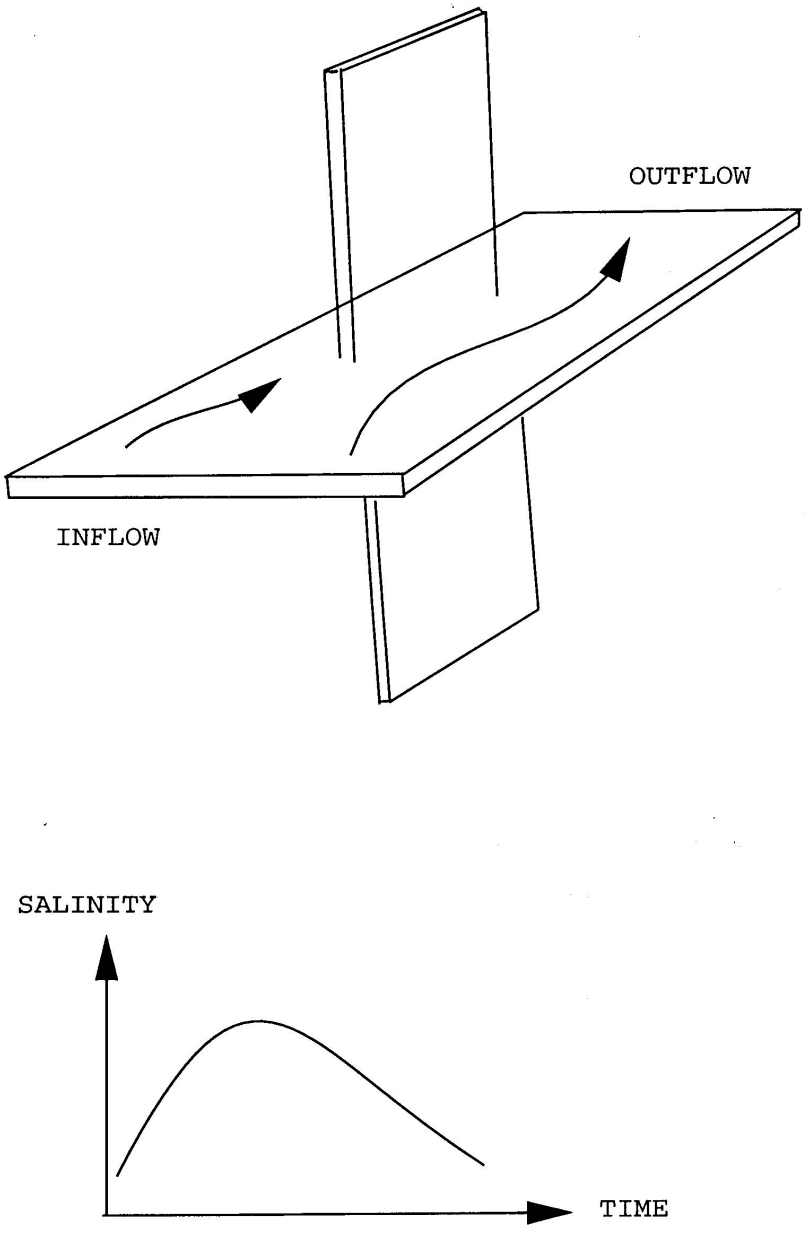

Figure A1. *Schematic outline of the problem studied.*

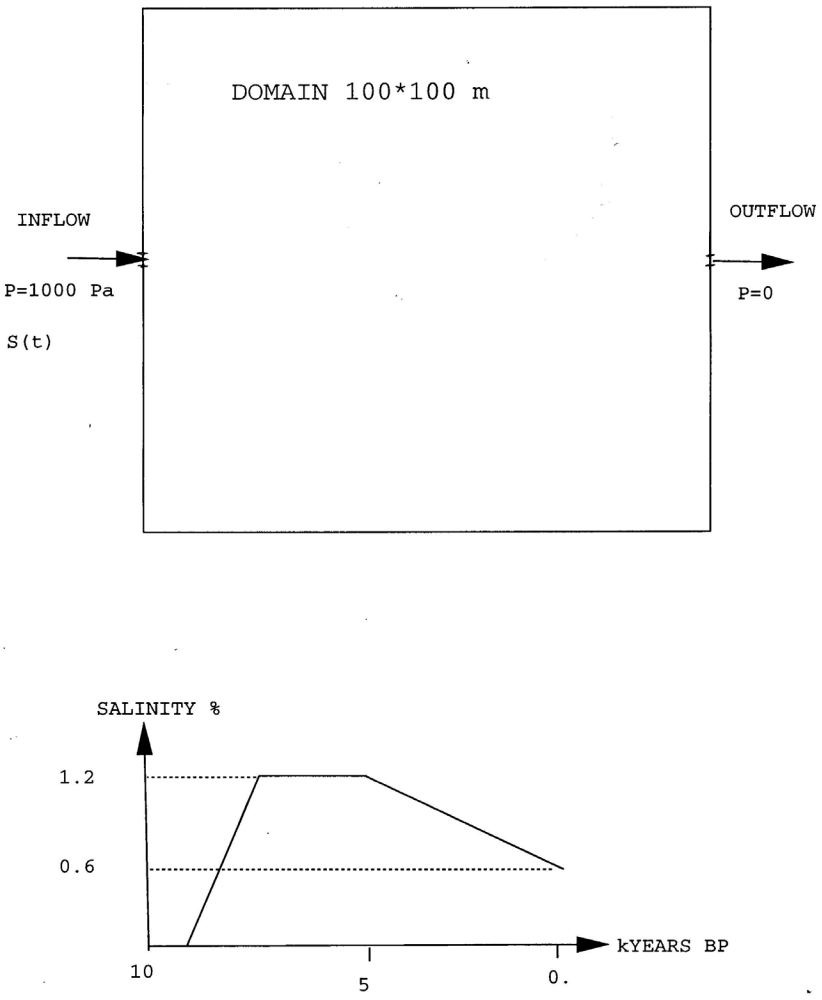

Figure A2. *Specification of computational domain and boundary conditions.*

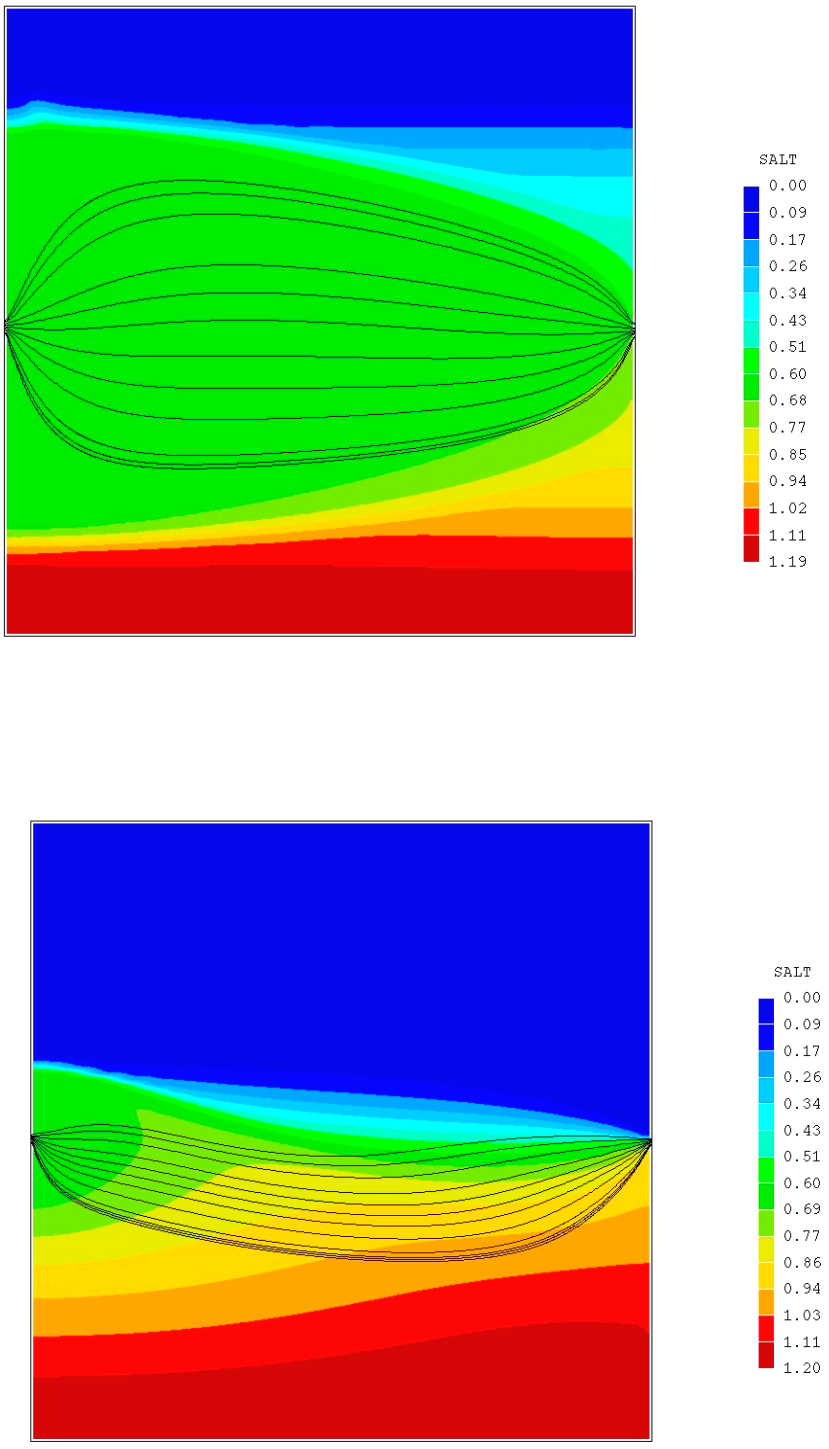

Figure A3. *Simulated salinity distribution after 10 000 years for a conductivity of* 10^{-7} m/s *(top) and* 10^{-8} m/s.

Part IV

MODELLING QUESTIONNAIRE FOR TASK #5, ACKNOWLEDGEMENTS AND REFERENCES

Urban Svensson* and Marcus Laaksoharju**

*Computer-aided Fluid Engineering AB, **GeoPoint AB

MODELLING QUESTIONNAIRE FOR TASK 5

worked October 1999

This is a Modelling Questionnaire prepared by SKB based on discussions within the Task Force group. It should be answered when reporting Task 5 in order to simplify the evaluation process of the modelling exercise. Preferably, include this response in an appendix to your forthcoming report.

This questionnaire is prepared by Urban Svensson concerning the PHOENICS modelling and by Marcus Laaksoharju concerning the M3 modelling.

1. SCOPE AND ISSUES

a) What was the purpose for your participation in Task 5?
As we performed the task for SKB, the objectives conform exactly with the ones stated in the Task #5 description.

b) What issues did you wish to address through participation in Task 5?
See 1a); applies also to issues.

2. CONCEPTUAL MODEL AND DATA BASE

a) Please describe your models using the tables 1-3 in the appendix.
b) To what extent have you used the data sets delivered? Please fill in Table 4 in the appendix.
c) Specify more exactly what data in the data sets you actually used? Please fill in "Comments" in Table 4
d) What additional data did you use if any and what assumptions were made to fill in data not provided in the Data Distributions but required by your model? ? Please add in the last part of Table 4.
2a)-2d), see Tables 1-4.
e) Which processes are the most significant for the situation at the Äspö site during the simulation period?
Hydrology: The excavation of the tunnel changes the flow, pressure and salinity distributions significantly (upconing, lowering of groundwater table, etc.) and is hence the most important factor during the simulation period. Hydrochemistry: The changes in groundwater composition due to changes in mixing proportions.

3. MODEL GEOMETRY/STRUCTURAL MODEL

a) How did you geometrically represent the ÄSPÖ site and its features/zones?
A model size of 1.8 x 1.8 x 1.0 km^3 was chosen. The top of the grid follows the topography. Conductivity and porosity fields were generated from a fracture network. Deterministic fracture zones were represented as planar features with a given transmissivity.
b) Which features were considered the most significant for the understanding of flow and transport in the ÄSPÖ site, and why?
The major deterministic fracture zones were found to govern the drawdown calculations (in the calibration process).
c) Motivate selected numerical discretization in relation to used values of correlation length and/or dispersion length.
The grid was made as fine as possible; the gridspacing used was 20 metres. The dispersion coefficient for salt was assumed to represent "subgrid effects" and was hence made proportional to the grid spacing. The correlation length in the conductivity and porosity fields are not related to the grid as these are generated from a fracture network.

4a. MATERIAL PROPERTIES - HYDROGEOLOGY

a) How did you represent the material properties in the hydraulic units used to represent the ÄSPÖ SITE?
All material properties are due to the fractures in the fracture network, except for a thin layer close to ground, for which conductivities were found in the calibration process.

b) What is the basis for your assumptions regarding material properties?
Deterministic fracture zones were given transmissivities from field data. Other fractures and zones were assumed to have a transmissivity proportional to their linear size (see report for details). The transport aperture was assumed to be proportional to transmissivity. With transport aperture and thickness of a fracture given, the kinematic porosity was estimated.

c) Which assumptions were the most significant, and why?
The assumptions regarding the kinematic porosity are crucial as they determine the transport velocity.

4b. CHEMICAL REACTIONS - HYDROCHEMISTRY

a) What chemical reactions did you include? ***Effects from major reactions such as: organic decomposition, organic redox reactions, dissolution/precipitation of calcite, ion exchange, sulphate reduction.***

b) What is the basis for your assumptions regarding the chosen chemical reactions?
Major reactions are the main modifiers of the groundwater composition.

c) Which reactions were the most significant, and why? ***Biogenic reactions (i.e gain of HCO_3 which***
can indicate organic decomposition) can control the redox state of the groundwaters.

5a. BOUNDARY CONDITIONS FOR HYDROGEOLOGICAL MODEL

a) What boundary conditions were used in the modelling of the ÄSPÖ site tests?
Top boundary: Given recharge on Äspö, fixed pressure and salinity below the Baltic Sea. Vertical and bottom boundaries: From a regional model.

b) What was the basis for your assumptions regarding boundary conditions?
Top boundary: Estimated precipitation minus evaporation for the area. Below the Baltic Sea: "Seems correct". Vertical and bottom boundaries: Best possible estimates available.

c) Which assumptions were the most significant, and why?
No sensitivity tests were performed. However, it seems important that more Meteoric water should infiltrate when the tunnel is present. The top boundary condition used, and the algorithm for the unsaturated zone, ensures this.

5b. BOUNDARY/INITIAL CONDITIONS FOR HYDROCHEMICAL MODEL

a) What boundary conditions were used in the modelling of the ÄSPÖ site tests?
Geographical
locations of the reference waters.

b) What was the basis for your assumptions regarding boundary conditions? ***Field observations.***

c) Which assumptions were the most significant, and why? ***Glacial water is a historical water type which is not reproduced and should therefore not increase during the tunnel construction. The observations confirmed this assumption.***

6. MODEL CALIBRATION

a) To what extent did you calibrate your model on the provided hydraulic information? (Steady state and transient hydraulic head etc.)
Groundwater table for natural conditions and drawdowns for tunnel front position 2 875 m.

b) To what extent did you calibrate your model on the provided "transport data"? (Breakthrough curves etc.)
The time history of the upconing.

c) To what extent did you calibrate your model on the provided hydrochemical data? (Mixing ratios; density/salinity etc.)
Water composition in borehole section for natural conditions, tunnel front at 3 170 metres and completed tunnel (96-05).
d) What parameters did you vary?
Transmissivities, conductivities of layers close to ground, kinematic porosity and water compositions at vertical and bottom boundaries.
e) Which parameters were the most significant, and why?
Most of the parameters are significant, but for different aspects (conductivity of layers close to ground are for example important for ground water table).
f) Compare the calibrated model parameters with the initial data base – comments?
Mostly minor changes. For conductivity of layers close to ground no initial data were available.

7. SENSITIVITY ANALYSIS

Identify the sensitivity in your model output to:
a) the discretization used
The point to point comparisons of water composition were found to be sensitive to the discretisation. Using a neighbouring cell gives a different result.
b) the transmissivity/hydraulic conductivity (distribution) used
Different realisations of the background fracture networks were found to be significant for the point to point comparisons.
c) transport parameters used
The kinematic porosity was found to be important for the correct time history of the upconing.
d) chemical mixing parameters used ***To test the feasibility and sensitivity of the selected reference waters.***
e) chemical reaction parameters used ***To test the feasibility and sensitivity of the selected mixing model.***

8. LESSONS LEARNED

a) Given your experience in implementing and modelling the ÄSPÖ site, what changes do you recommend with regards to:
- Experimental site characterisation?
Site characterisation: As we are dealing with a transport problem more information about the kinematic porosity is needed. More information is needed concerning chemical time series. The sampling should be simultaneously from several or all boreholes at a site only then the chemical dynamics of a site can be modelled.
- Presentation of characterisation data?
Presentation OK.
- Performance measures and presentation formats?
Performance measures: The present study indicates that point by point comparisons is not the best approach (see report). Overall similarities/differences in the site description is of greater importance and interest than accuracy of predictions at selected sampling points.
b) What additional site-specific data would be required to make a more reliable prediction of the tracer experiments?
Boundary conditions (different for all vertical boundaries) of water composition. Kinematic porosities. Better time series.
c) What conclusions can be made regarding your conceptual model utilised for the exercise?
The model used in stage one (called Model99 in the report) was too simple, the model of stage two is a major improvement conceptually. The introduction of MWH, MWL and MWB (see report) was very useful. For M3, the conceptual paleohydrolological model of Äspö seems to be supported by observations.

d) What additional generic research results are required to improve the ability to carry out predictive modelling of transport on the site scale?

- ***It needs to be demonstrated that the numerical model used can simulate transport in a single fracture (comparison with analytical solutions) and in a fracture network of a simple kind (changing kinematic porosity, assumptions at intersections, etc)***
- ***Show how storage volumes and other stagnant volumes affect transport.***
- ***Show and test the uncertainties of different models.***

9. RESOLUTION OF ISSUES AND UNCERTAINTIES

a) What inferences did you make regarding the descriptive structural-hydraulic model on the site scale for the ÄSPÖ site?
The descriptive model is good.

b) What inference did you make regarding the active hydochemical processes, hydrochemical data
provided and the hydrochemical changes calculated? ***Helpful in understanding the complexity of***
the site in terms of flow and reactions affecting the obtained groundwater composition.

c) What issues did your model application resolve?

- ***It is technically possible to carry out a simulation like this (not a trivial task!)***
- ***The integration of hydrology and chemistry as manifested in the mixing proportions of the four water types is very useful.***
- ***Mixing proportions summarise the groundwater composition and offers the tool for integration with the hydromodel.***
- ***A hydromodel can be used to predict an operational groundwater composition at any point by using the mixing proportions of the reference waters.***

d) What additional issues were raised by the model application?
Pointed to weaknesses in the continuum model used, i.e. storage of water for long time periods. The mixing portions should be used more effectively to calculate an operational turnover time for the water, and the results from the chemical modelling could be presented as flow lines for easier integration/comparison with the hydrogeological modelling.

10. INTEGRATION OF THE HYDOGEOLOGICAL AND HYDROCHEMICAL MODELLING

a) How did you integrate the hydrogeological and hydro chemical work?
Through the mixing portions of the four water types.

b) How can the integration of the hydrogeological and hydrochemical work be improved?
The task #5 approach is a good one, it seems. No suggestions for improvements at this stage (wait for the evaluation of Task #5). The results of the chemical modelling should be presented as flow lines and pressure lines (if possible).

c) Hydrogeologist: How has the hydrochemistry contributed to your understanding of the hydrogeology around the Äspö site?
Pointed to the improvement of the porosity and connectivity fields. All exchanges of matter by stagnant volumes of various types need to be considered (on a variety of time and length scales).

d) Hydrochemist: How has the hydrogeology contributed to your understanding of the hydrochemistry around the Äspö site? ***An independent model that can be used for comparison and correction of the selected chemical reference waters and conceptual model.***

Table 1 Description of model for water flow calculations

TOPIC	Example	Our Model
Type of model	Stochastic continuum model	Continuum model based on a fracture network
Process description	Darcy´s flow including density driven flow. (Transport equation for salinity is used for calculation of the density)	- Darcian flow including density effects - Adv/Diff equation for salinity - Mass conservation - Density function of salinity
Geometric framework and parameters	Model size: 1.8x1.8x1 km^3 . Deterministic features: All deterministic features provided in the data set. Rock outside the deterministic features modelled as stochastic continuum, based on a fracture network.	Model size: 1.8 x 1.8 x i km^3 Deterministic features: All deterministic features provided in the data set. Rock outside the deterministic features modelled as stochastic continuum, based on a fracture network.
Material properties and hydrological properties	Deterministic features: Transmissivity (T), Kinematic Porosity, Thickness Rock outside deterministic features: Hydraulic conductivity(K), Specific storage (Ss)), Kinematic Porosity, Thickness	Deterministic features: Transmissivity (T), Kinematic Porosity, Thickness Rock outside deterministic features: Hydraulic conductivity(K), Kinematic Porosity, Thickness
Spatial assignment method	Deterministic features: Constant within each feature (T,S). No changes due to calibration. Rock outside deterministic features: (K,Ss) lognormal distribution with correlation length xx. Mean, standard deviation and correlation based on calibration of the model	Deterministic features: Constant within each feature. Minor modifications due to calibration. Rock outside deterministic features. Transmissivities of background fracture network related to size of fracture.
Boundary conditions	Surface: Constant flux. Sea: Constant head Vertical-North: Fixed pressure based on vertical salinity distribution. Vertical-East: Fixed pressure based on vertical salinity distribution. Vertical-South: Fixed pressure based on vertical salinity distribution. Vertical-West: Fixed pressure based on vertical salinity distribution. Bottom: No flux. Linear change by time based on regional simulations for undisturbed conditions and with Äspö tunnel present.	Top: Specified flux on land specified pressure and salinity below Baltic Sea. Vertical and bottom: From a regional model. Linear change by time based on regional simulations for undisturbed conditions and with Äspö tunnel present.
Numerical tool	PHOENICS	PHOENICS
Numerical method	Finite volume method	Finite volume method
Output parameters	Head, flow and salinity field.	Head, flow and salinity field.

Table 2 Description of model for tracer transport calculations

TOPIC	EXAMPLE	Our model
Type of model	Stochastic continuum model	Continuum model based on a fracture network.
Process description	Advection and diffusion, spreading due to spatially variable velocity and molecular diffusion.	Advection, spreading due to spatially variable velocities in the fracture network.
Geometric framework and parameters	Model size: 1.8x1.8x1 km^3 . Deterministic features: All deterministic features provided in the data set. Rock outside the deterministic features modelled as stochastic continuum.	Model size: 1.8 x 1.8 x i km^3 Deterministic features: All deterministic features provided in the data set. Rock outside the deterministic features modelled as stochastic continuum, based on a fracture network.
Material properties	Flow porosity (ne)	Kinematic porosity, based on the porosities assigned to the fractures in the network.
Spatial assignment method	ne based on hydraulic conductivity value (TR 97-06) for each cell in model, including deterministic features and rock outside these features.	See above.
Boundary conditions	Mixing ratios for endmembers as provided as initial conditions in data sets.	Initial conditions calculated as Steady State Solution. Top: 100% Meteoric on land, 100% Baltic below the Baltic Sea. Vertical and botttom: Mixing ratios from assumptions and calibration.
Numerical tool	PHOENICS	PHOENICS
Numerical method	Particle tracking method or tracking components by solving the advection/diffusion equation for each component	Solving the advection/diffusion equation for each component. Backtracking, using particle tracking, for analysis of flow paths.
Output parameters	Breakthrough curves	Mixing ratios for all points at all times.

Table 3 Description of model for chemical reactions calculations

TOPIC	EXAMPLE	Our model
Type of model	xxx	M3 (Mixing and Massbalance Modell) and Voxel 3D interpolation
Process description	Mixing. Reactions: Xx, Yy,Zz,Dd…..	Construction of an ideal mixing model for the site based on measured groundwater composition. Calculated deviations from the ideal model for the constituents is used as an indicator of reactions. The data was used as background information for other modelling teams within TASK#5 and for M3 predictions and reporting.
Geometric framework and parameters	Modelling reactions within one fracture zone, NE-1.	Modelling transport and reactions at the whole site. Modelling mixing proportions in fracture network that is fairly conductive.
Reaction parameters	Xx: a=ff, b=gg,… Yy: c=. Zz: d=...	Effects from major reactions such as organic decomposition, organic redox reactions, inorganic reactions such as sulphide oxidation, dissolution and precipitation of calcite, ion exchange and sulphate reduction.
Spatial distribution of reactions assumed	Xx: seafloor sediments Yz: Bedrock below sea, superficial Dd: Bedrock ground surface, superficial Yz: Bedrock below sea, at depth Zz: Bedrock ground surface, at depth Yy, Zz: near tunnel	Whole site
Boundary/initial conditions for the reactions	Xx: aaa… Yy: bbb…	Calculated in relation to the selected reference waters
Numerical tool	Phreeque	M3
Numerical method	xx	Multivariate statistics
Output parameters	xx	Mixing proportions and deviations (used for chemical massbalance calculations) for sampling points and mixing proportions within the modelled volume.

Table 4a Summary of data usage

Data del. No	**Data**	**Importance of data (see notes)**	**Comment**
1	*Hydrochemical data 1*	***P***	*Used in M3 to calculate the background information concerning mixing and reactions used within TASK#5. The data was used for M3 predictions and Voxel 3D interpolations used for visualisation of the data distribution.*
1a	*Surface bore holes- undisturbed conditions, Äspö-Laxemar*	***P***	*Used within M3 calculations*
1b	*Surface bore holes- disturbed conditions (by tunnel excavation), Äspö*	***P***	*Used within M3 calculations*
1c	*Surface bore holes- undisturbed conditions, Ävrö*	***M***	*Used within M3 calculations*
1d	*Surface bore holes- sampled during drilling, Äspö*	***P***	*Used within M3 calculations*
1e	*Data related to the Redox experiment*	***P***	*Used within M3 calculations*
1f	*Tunnel and tunnel bore holes- disturbed conditions*	***P***	*Used within M3 calculations*
2	*Hydogeological data 1*		
2a1	*Annual mean air temperature*	***-***	
2a2	*Annual mean precipitation*	***M***	
2a3	*Annual mean evapotranspiration*	***M***	
2b1	*Tunnel front position by time*	***P***	
2b2	*Shaft position by time*	***P***	
2c1	*Geometry of main tunnel*	***P***	
2c2	*Geometry of shafts*	***P***	
2d	*Hydrochemistry at weirs (Cloride, pH, Electrical conductivity, period: July 1993- Aug 1993)*	***-***	
2e	*Geometry of the deterministic large hydraulic features (Most of them are fracture zones)*	***P***	

Table 4b Summary of data usage

Data del. No	**Data**	**Importance of data (see notes)**	**Comment**
3	*Hydrogeological data 2*		
3a	*Monthly mean flow rates measured at weirs. Tunnel section 0-2900m, period May 1991 – January 1994*	***P***	*Used for prescribed tunnel inflows*
3b	*Piezometric levels for period June 1st 1991 – May 21st 1993. Values with 30 days interval (Task 3 data set)*	***P***	
3c	*Salinity levels in bore hole sections for period -Sept 1993. (Task 3 data set)*	***M***	
3d	*Undisturbed piezometric levels*	***P***	*Used in calibration*
3e	*Co-ordinates for bore hole sections*	***P***	
3f	*Piezometric levels for period July 1st 1990 – January 24st 1994. Daily values.*	***p***	
4	*Hydochemical data 2*		*Used in M3 for predictions of the future groundwater changes.*
4a	*Chemical components, mixing proportions and deviations for all bore hole sections used in the M3 calculations*	***P***	*Calculated by using M3*
4b	*Bore holes with time series, > 3 samples (part of 4a)*	***P***	*Used for M3 predictions*
4c	*Bore holes sections interpreted to intersect deterministic large hydraulic features (Most of them are fracture zones) (part of 4a)*	***P***	*Used in M3 modelling*
4d	*Chemical components, mixing proportions and deviations. Grid data based on interpolation. Undisturbed conditions*	*m* ***P*** (in M3)	*Calculated initial conditions and compared mainly with borehole data. Calculated by using M3. Grid data calculated by using Voxel analyst.*
4e	*Chemical components, mixing proportions and deviations. Grid data based on interpolation. Disturbed conditions (by tunnel excavation)*	*m* ***P***(in M3)	*Mainly used borehole data. Calculated by using M3. Grid data calculated by using Voxel analyst.*
4f	*Boundary and initial conditions. Chemical components, mixing proportions and deviations (1989). Grid data for vertical boundaries based on interpolation. Undisturbed conditions*	*m* ***P***(in M3)	*Mainly used borehole data. Calculated by using M3 and Voxel analyst.*
4g	*Boundary conditions after tunnel construction (1996) Chemical components, mixing proportions and deviations. Grid data for vertical boundaries based on interpolation. Disturbed conditions (by tunnel excavation)*	*m* ***P****(in M3)*	*Mainly used borehole data. Calculated by using M3 and Voxel analyst.*

Table 4c Summary of data usage

Data del. No	**Data**	**Importance of data (see notes)**	**Comment**
5	*Geographic data 1*		
5a	*Äspö coast line*	***P***	*Used as boundary conditions in chemical interpolation by Voxel.*
5b	*Topography of Äspö and the nearby surroundings*	***P***	*Upper boundary for hydrological model*
6	*Hydro tests and tracer tests*		
6a	*Large scale interference tests (19 tests)*	***P***	
6b	*Long time pump and tracer test, LPT2*	***-***	
7	*Hydochemical data 3, update of data delivery 4 based on new endmembers. Recommended to be used instead of 4.*	***-*** p (in M3)	*Calculated by using M3*
7a	*Chemical components, mixing proportions and deviations for all bore hole sections used in the M3 calculations*	***P***	*Calculated by using M3*
7b	*Bore holes with time series, > 3 samples (part of 7a)*	***P***	
7c	*Bore holes sections interpreted to intersect deterministic large hydraulic features (Most of them are fracture zones) (part of 7a)*	***P***	
7d	*Chemical components, mixing proportions and deviations. Grid data based on interpolation. Undisturbed conditions*	***P***	*Calculated by using M3 and Voxel 3D interpolation.*
7e	*Chemical components, mixing proportions and deviations. Grid data based on interpolation. Disturbed conditions (by tunnel excavation)*	*m*	*Calculated by using M3 and Voxel 3D interpolation.*
7f	*Boundary and initial conditions. Chemical components, mixing proportions and deviations (1989). Grid data for vertical boundaries based on interpolation. Undisturbed conditions*	*m*	*Calculated by using M3 and Voxel 3D interpolation.*
7g	*Boundary conditions after tunnel construction (1996) Chemical components, mixing proportions and deviations. Grid data for vertical boundaries based on interpolation. Disturbed conditions (by tunnel excavation)*	*m*	*Calculated by using M3 and Voxel 3D interpolation.*

Table 4d Summary of data usage

Data del. No	**Data**	**Importance of data (see notes)**	**Comment**
8	*Performance measures and reporting 1*		
8a	*Performance measures*		
8b	*Suggested control points. 6 points in tunnel section 0-2900m and 3 point in tunnel section 2900-3600m.*	***P***	*Used in M3 predictions.*
8c	*Suggested flowchart for illustration of modelling*	*m*	*Used in reporting.*
9	*Hydrogeological data 3*		
9a	*Monthly mean flow rates measured at weirs. Tunnel section 0-3600m, period: May 1991- Dec 1996.*	***P***	
10	*Geographic data 2*		
10a	*Topography of Äspö and the nearby surroundings (larger area than 5b)*	***P***	
10b	*Co-ordinates for wetlands*	***-***	
10c	*Co-ordinates for lakes*	***-***	
10d	*Co-ordinates for catchments*	***-***	
10e	*Co-ordinates for streams*	***-***	
10f	*Co-ordinate transformation Äspö system- RAK*	***-***	
11	*Boundary and initial conditions*		
11a	*Pressure before tunnel construction, from the regional SKB model (TR 97-09)*	***P***	*Used as boundary condition for hydrological model*
11b	*Salinity before tunnel construction, from the regional SKB model (TR 97-09)*	***P***	*Used as boundary condition for hydrological model*
11c	*Pressure after tunnel construction, from the regional SKB model (TR 97-09)*	***P***	*Used as boundary condition for hydrological model*
11d	*Salinity after tunnel construction, from the regional SKB model (TR 97-09)*	***P***	

Table 4e Summary of data usage

Data del. No	Data	**Importance of data (see notes)**	**Comment**
12	*Performance measures and reporting 2*		
12a	*Suggested control points. 6 points in tunnel section 0-2900m and 3 point in tunnel section 2900-3600m (same as 8b) and 2 outside the tunnel.*	***P***	*Used in M3 predictions*
13	*Transport parameters compiled*		
13a	*LPT2 tracer tests*	***-***	
13b	*Tracer test during passage of fracture zone NE-1*	***-***	
13c	*Redox tracer tests*	***-***	
13d	*TRUE-1 tracer tests*	***-***	
14	*Hydrochemical data 4*		
14a	*Groundwater reactions to consider within TASK5 modelling (Description of how M3 calculates the contribution of reactions and identifying dominating reactions based on the M3 calculations.*	***P (in M3)***	*Used in M3 modelling*
15	*Co-ordinates for the test sections defining the control points*	***P***	
16	*Co-ordinates for bore holes drilled from the tunnel*	***P***	

Table 4f Summary of data usage

Data del. No	**Data**	**Importance of data (see notes)**	**Comment**
17	*Hydogeological data - prediction period*		
17a	*Hydrochemistry at weirs (Cloride, pH, Electrical conductivity, period: July 1993- Dec 1995)*	***-***	
17b	*Piezometric levels for period July 1st 1990 – Dec 1996. Daily values.*	*m*	
18	*Hydochemical data - prediction period.*		
18a	*Chemical components, mixing proportions and deviations for all bore hole sections used in the M3 calculations. Data for tunnel section 2900-3600m.*	***P***	*Used in M3 predictions*
18b	*Bore holes with time series, > 3 samples (part of 18a)*	***P***	*Used in M3 predictions*
18c	*Bore holes sections interpreted to intersect deterministic large hydraulic features (Most of them are fracture zones) (part of 18a)*	***P***	
	Other data (part of data to Task 1, 3 and 4)		
	Fracture orientation, fracture spacing and trace length – tunnel data	***P***	*Used for generating the fracture network (see report for ref.)*
	Fracture orientation, fracture spacing– mapping of cores	***P***	
	Fracture orientation, fracture spacing and trace length – mapping of outcrops	***P***	

P = data of great importance for quantitative estimation of model parameters
p = data of less importance for quantitative estimation of model parameters
M = data of great importance used qualitatively for setting up model
m = data of less importance used qualitatively for setting up model
X = data useful as general background information
- = data not used

ACKNOWLEDGEMENTS

The authors are indebted to the project leaders of Task #5, Peter Wikberg, Ingvar Rhén and John Smellie, for their technical input and reviews. We should also like to acknowledge the constructive comments from the external reviewers, Peter Jackson and Adrian Bath.

REFERENCES

Alley W M (ed.), 1993. Regional groundwater quality. ISBN 0-442-00937-2. Van Nostrand Reinhold, New York, USA, pp634.

Banwart S, Gustafsson E, Laaksoharju M, Nilsson A-C, Tullborg E-L, Wallin B, 1993. The large scale Redox experiment: Redox processes in a Granitic coastal aquifer. SKB Progress Report PR 25-93-03, Stockholm, Sweden.

Banwart S (ed), Laaksoharju M, Skårman C, Gustafsson E, Pitkänen P, Snellman M, Landström O, Aggeryd I, Mathiasson L, Sundblad B, Tullborg E-L, Wallin B, Pettersson C, Pedersen K, Arlinger J, Jahromi N, Ekendahl S, Hallbeck L, Degueldre C, Malmström M, 1995. Äspö Hard Rock Laboratory. The Redox Experiment in Block Scale. Final reporting of results from the three year project. SKB Progress Report PR 25-95-06, Stockholm, Sweden.

Bear J, Verruijt A, 1987. Modelling groundwater flow and pollution. D.Reidel Publishing Company, Dordrecht, Holland.

Gurban I, Laaksoharju M, Andersson C, 1998. Influences of the tunnel construction on the groundwater chemistry at Äspö. SKB IPR-02-58. (in press)

Laaksoharju M, Skårman C, 1995. Groundwater sampling and chemical characterisation of the HRL tunnel at Äspö, Sweden. SKB-Progress report PR 25-95-29, Stockholm, Sweden.

Laaksoharju M, Smellie J, Nilsson A-C, Skårman C, 1995. Groundwater sampling and chemical characterisation of the Laxemar deep borehole KLX02. SKB Technical Report TR 95-05, Stockholm, Sweden.

Laaksoharju M, Wallin B (eds.), 1997. Evolution of the groundwater chemistry at the Swedish Äspö Hardrock Laboratory site. Proceedings of the second Äspö international geochemistry workshop. SKB International Cooperation Report 97-04, Stockholm, Sweden.

Laaksoharju M, Tullborg E-L, Wikberg P, Wallin B, Smellie J, 1999a. Hydrogeochemical conditions and evolution at Äspö HRL, Sweden. Applied Geochemistry Vol. 14, #7, 1999, Elsevier Science Ltd., pp835-859.

Laaksoharju M, Skårman C, Skårman E, 1999b. Multivariate Mixing and Mass-balance (M3) calculations, a new tool for decoding hydrogeochemical information. Applied Geochemistry Vol. 14, #7, 1999, Elsevier Science Ltd., pp861-871.

Laaksoharju M, 1999c. Groundwater Characterisation and Modelling: Problems, Facts and Possibilities. Dissertation TRITA-AMI-PHD 1031; ISSN 1400-1284; ISRN KTH/AMI/PHD 1031-SE; ISBN 91-7170-. Royal Institute of Technology, Stockholm, Sweden.

La Pointe P R, Cladouhos T, Follin S, 1999. Calculation of displacements on fractures intersecting canisters by earthquakes: Aberg, Beberg and Cberg examples. SKB Technical Report TR-99-03.

Nilsson A-C, 1995. Compilation of groundwater chemistry data from Äspö 1990-1994. SKB Progress Report PR 25-95-02, Stockholm, Sweden.

Rhén I, Danielsson P, Forsmark T, Gustafson G, Liedholm M, 1993. Äspö Hard Rock Laboratory. Geohydrological evaluation of the data from section 700-1475m. SKB Progress Report PR 25-93-06, Stockholm, Sweden.

Rhén I, Stanfors R, 1993. Passage through water-bearing fracture zones. Evaluation of investigations in fracture zones NE-1, EW-7 and NE-3, SKB Progress Report PR 25-92-18, Stockholm, Sweden.
Rhén I, Danielsson P, Forsmark T, Gustafson G, Liedholm M, 1994. Äspö Hard Rock Laboratory. Geohydrological evaluation of the data from section 2265-2874m. SKB Progress Report PR 95-94-20, Stockholm, Sweden.

Rhén I (ed.), Gustafson G, Stanfors R, Wikberg P, 1997. Äspö HRL Geoscientific evaluation 1997/5. Models based on site characterisation 1986-1995. In: SKB Technical Report TR 97-06, Stockholm, Sweden.

Smellie J, Laaksoharju M, 1992. The Äspö Hard Rock Laboratory: Final evaluation of the hydrogeochemical pre-investigations in relation to existing geological and hydraulic conditions. SKB Technical Report TR 92-31, Stockholm, Sweden.

Smellie J, Laaksoharju M, Wikberg P, 1995. Äspö, SE Sweden: A natural groundwater flow model derived from hydrogeochemical observations. Journal of Hydrogeology 172 (1995) 147-169.

Spalding D.B, 1981. "A general purpose computer program for multi-dimensional one- and two-phase flow". Math. Comp. Sim., 8, 267-276. See also: http://www.cham.co.uk.

Stanfors R, Gustafson G, Munier R, Olsson P, Stille H, Wikberg P, 1992. Evaluation of geological predictions in the access ramp 0-700m. SKB Progress Report PR 25-92-02, Stockholm, Sweden.

Stanfors R, Liedholm M, Munier R, Olsson P, Stille H, 1993a. Geological-structural evaluation of data from section 700-1475m. SKB Progress Report PR 25-93-05, Stockholm, Sweden.

Stanfors R, Liedholm M, Munier R, Olsson P, Stille H, 1993b. Äspö Hard Rock Laboratory. Geological-structural evaluation of data from tunnel section 1475-2265m. SKB Progress Report PR 25-93-10, Stockholm, Sweden.

Stanfors R, Liedholm M, Munier R, Olsson P, Stille H, 1994. Äspö Hard Rock Laboratory. Geological-structural evaluation of data from tunnel section 2265-2874m. SKB Progress report PR 25-94-19, Stockholm, Sweden.

Svensson U, 1995. Modelling the unsaturated zone at Äspö under natural conditions and with the tunnelfront at 2874 metres. SKB Progress Report 25-95-24.

Svensson U, 1997a. A regional analysis of groundwater flow and salinity distribution in the Äspö area. SKB Technical Report 97-09.

Svensson U, 1997b. A site scale analysis of groundwater flow and salinity distribution in the Äspö area. SKB Technical Report TR-97-17.

Svensson U, 1999a. Representation of fracture networks as gridcell conductivities. SKB Technical Report TR-99-25.

Svensson U, 1999b. A laboratory scale analysis of groundwater flow and salinity distribution in the Äspö area. SKB Technical Report TR-99-24.

Svensson U, 2001a. Representation of porosity and connectivity in a continuum model described in: **Svensson U, Kuylenstierna H-O, Ferry M, 2002 (in prep).** DarcyTools – Concepts, Methods, Equations and Tests. Version 2.0. SKB TRxxx.

Svensson U, 2001b. Unsaturated zone. described in: **Svensson U, Kuylenstierna H-O, Ferry M, 2002 (in prep).** DarcyTools – Concepts, Methods, Equations and Tests. Version 2.0. SKB TRxxx.

Wikberg P, 1998. Äspö Task Force on modelling of groundwater flow and transport of solutes. SKB progress report HRL-98-07.